Evaluating the adaptability of chimeric protein switch biosensors

By
Emma Elisabeth Campbell

Submitted in Accordance with the Requirements for the Degree of Doctor of Philosophy

The University of Leeds

School of Biomedical Sciences
Faculty of Biological Sciences

October 2023

Declaration

The candidate confirms that the work submitted is her own, except where work which has formed part of jointly authored publications has been included. The contribution of the candidate and the other authors to this work has been explicitly indicated below. The candidate confirms appropriate credit has been given within this thesis where reference has been made to the work of others.

Jointly Authored publications:

Sections 1.3 and 1.4 were used in the following jointly authored book chapter: Emma Campbell, Timothy Luxton, Declan Kohl, Sarah A. Goodchild, Christoph Wälti, and Lars J.C. Jeuken. Chimeric Protein Switch Biosensors. *Springer*. The writing of which was carried out by myself and Timothy Luxton, and edits carried out by co-authors.

"Chapter 2" was used to write a jointly authored publication: Campbell, E. (EC), Adamson, H. (HA), Kohl, D. (DK), Tiede, C. (CT), Wälti, C. (CW), Tomlinson, D. C. (DT), & Jeuken, L. J. C. (LJ) (2023). Enzyme - Switch sensors for therapeutic drug monitoring of immunotherapies. *Biosens bioelec*, **237**, 115488. I carried out all experimental work, data analysis and writing. HA assisted with sensor cloning and DK assisted with SPR experiments. CT completed the initial Affimer phage display screen to select the Affimer proteins against each target analyte. CW and LJ assisted with writing edits and conceptualisation. Some initial data from this chapter was included in a MBiol Pharmacology Master's dissertation written by myself.

The data presented in "Chapter 3" was used in the curation of a co-authored manuscript that has been accepted for publication: Campbell, E. (EC), Adamson, H. (HA), Luxton, T. (TL), Tiede, C. (CT), Wälti, C. (CW), Tomlinson, D. C. (DT), & Jeuken, L. J. C. (LJ) (2023). Therapeutic drug monitoring with novel Affimer-NanoBiT sensor constructs. *Sens diagn.* Sensor cloning was completed by HA, TL assisted with optimisation experiments. I completed all other experimental work, all data analysis and writing. CW and LJ assisted with writing edits and conceptualisation.

Acknowledgements

This research has been carried out by a team which has included: Christoph Wälti, Lars Jeuken, Sarah Goodchild, Timothy Luxton, Hope Adamson, Christian Tiede, Darren Tomlinson, Iain Mansfield, Declan Kohl. Their contributions have been as follows: Christoph Wälti, Lars Jeuken and Sarah Goodchild, project conception and supervision; Timothy Luxton, initial rituximab NanoBiT sensor optimisation; Hope Adamson, conceptualisation, cloning of TmAb-BLA-BLIP and TmAb-NanoBiT constructs; Christian Tiede, TmAb Affimer phage display and selection; Darren Tomlinson, supervision of Affimer phage display; Iain Mansfield, supervision of SPR experiments; Declan Kohl, assisted with SPR experiments.

I would first like to express my thanks to all of those that have supervised me throughout this work. Lars for supporting through my academic journey. Christoph for accompanying me across the world and for encouraging me through it all. Sarah for the expert opinions on expression and for the yearly Eurovision gossip. I also must give thanks to all the past and present members of the Jeuken group: Tim, Rosa, Declan, Hope, Huijie, Gordon, and Darren, who have been good friends over the years. Thank you to my sponsors who made this project possible; BBSRC White Rose DTP and DSTL for the financial support and providing external training opportunities.

I would like to thank my family for supporting me through the entirety of my education, even when they thought I was insane at times. A special thankyou to my Mum and Dad for their love and encouragement, for cheering me up when things went wrong, and constantly reminding me how proud they are. I'd also like to thank Julie, Jim, and Jenny for being there to give me a morale boost when needed.

I extend my deepest thanks to my friends who have been my pillars of support and my source of sanity throughout this journey. To Maria and Sarah, I want to express my heartfelt gratitude for being unwavering constants, for being my science sounding boards, providing comfort and distraction, and being the best cheerleaders I could ask for.

Above all, my profound appreciation is reserved for Jack, who has been my rock and who's love, and encouragement has fuelled my motivation. I dedicate this thesis to you as a thank you for standing by me, cheering me on and believing in me, even when I doubted myself.

Abstract

Standard methods of analyte detection for disease diagnosis and management have limitations that prevent their use in a point-of-care (PoC) setting. Chimeric protein switch biosensors provide an alternative to traditional laboratory tests with the potential for PoC implementation. These biosensors combine the reporter and recognition elements into a single design. Recognition elements are vital to biosensor performance, so far nanobodies have been underutilised for this purpose despite their valuable characteristics.

In this work, I used two chimeric protein switch biosensor designs to develop sensors for therapeutic drug monitoring (TDM) of four therapeutic monoclonal antibodies (TmAbs). Affimer proteins, specifically selected for each TmAb, were used to create: a one-component modular allosteric switch sensor utilizing a ß-lactamase – ß-lactamase inhibitor protein (BLA-BLIP) reporter complex and a two-component proximity switch using the NanoBiT split luciferase technology. The performance of the TDM sensors were compared. The same sensor designs were used to evaluate the feasibility of using nanobody proteins as the recognition elements within chimeric protein switch biosensors. The expression, purification, and performance of these nanobody biosensors was assessed.

The two-component NanoBiT design outperformed the one-component BLA-BLIP design in all aspects. With a rapid 10-minute run time, these sensors had low pM limit of detection and a wide quantifiable range. This effectively covered the clinical ranges of the TmAbs, aligning with existing TDM gold standards.

While the introduction of nanobodies into the one-component BLA-BLIP sensor design encountered insurmountable expression challenges, the application of denaturation and dilution-mediated refolding proved to be a successful approach for extracting and purifying nanobody NanoBiT sensor constructs. The resulting proof-of-concept sensor displayed high sensitivity and specificity, with a low pM limit of detection and a broad quantifiable range. This research established the groundwork for the development of rapid, cost-effective, and clinically relevant nanobody NanoBiT biosensors, with the potential to transform protein detection in healthcare applications.

Table of Contents

List of Figures

List of Tables

1 Chapter 1: Introduction

1.1 Analyte Detection

Rapid detection of relevant analytes – biomarker proteins, DNA and metal ions – are valuable techniques with applications in environmental monitoring (1), food safety (2), disease diagnosis (3, 4) and drug discovery (5) among many others. These rapid detection techniques facilitate timely decision making to improve outcomes. Specifically in the field of medicine, the detection of protein biomarkers and relevant DNA sequences have become a central aspect of disease diagnosis, monitoring, and management. Laboratory based tests including enzyme linked immunoassays (ELISA), polymerase-chain reaction (PCR) and western blotting have historically been first choice methods for detection and quantification of specific proteins (6, 7).

1.1.1 Polymerase chain reaction

The polymerase chain reaction (PCR) involves the denaturation of DNA, the annealing of specifically designed primers to target DNA sequences and the extension of DNA fragments, resulting in the amplification of specific DNA sequences (8). PCR has revolutionised molecular biology techniques, with the general principles unchanged since the process was first introduced (9). The advances in this field come from the further application of PCR to diagnostic areas. Real time PCR, also known as quantitative PCR (qPCR) can detect, characterise, and quantify nucleic acids using fluorescence labelling. It can be dye-based qPCR or probe-based qPCR. Dye-based methods use double stranded-DNA (dsDNA) binding dyes for labelling and the fluorescence intensity is measured after each cycle to quantify the number of amplicons. This method of qPCR tends to bind to any dsDNA present in a sample which causes background binding and issues with test specificity. Alternatively, probe-based qPCR involves designing labelled DNA oligos that will bind a specific nucleotide sequence. This oligo probe has a fluorophore at one end and a quencher at the other.

Whilst intact, the quencher prevents any fluorescence emission. However, during the extension step of PCR cycling, the probe is hydrolysed resulting in an amplification-dependent signal from the fluorophore (**Figure 1**). Probe-based methods are much more specific than dye-based methods and allow for simultaneous labelling of multiple probes if well designed and optimised. Probe-based qPCR is most commonly used in clinical diagnostics (10).

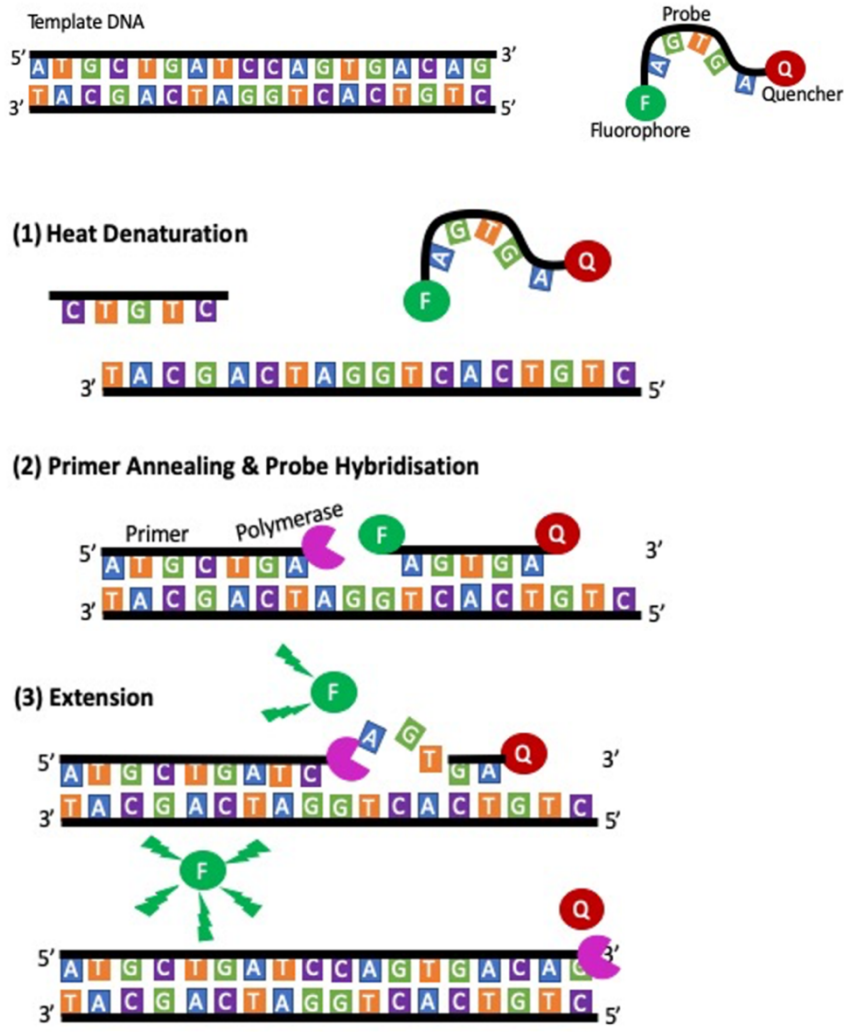

Figure 1. Schematic of quantitative PCR (qPCR) using a fluorescent DNA probe. *(1) Heat denaturation, usually at 98°C, unravels double stranded DNA so that the template strand is accessible. (2) The annealing temperature of the forward primer and the fluorescent probe is calculated prior to PCR. The primer annealing allows binding of the polymerase to begin to generate a complementary DNA strand and the hybridisation of the probe acts as a detection of target DNA. (3) Extension of the DNA strand generated through the activity of the polymerase. This essentially removes the probe and frees the fluorophore which emits a fluorescent signal in the absence of the quencher, resulting in an amplification-dependent increase in fluorescence.*

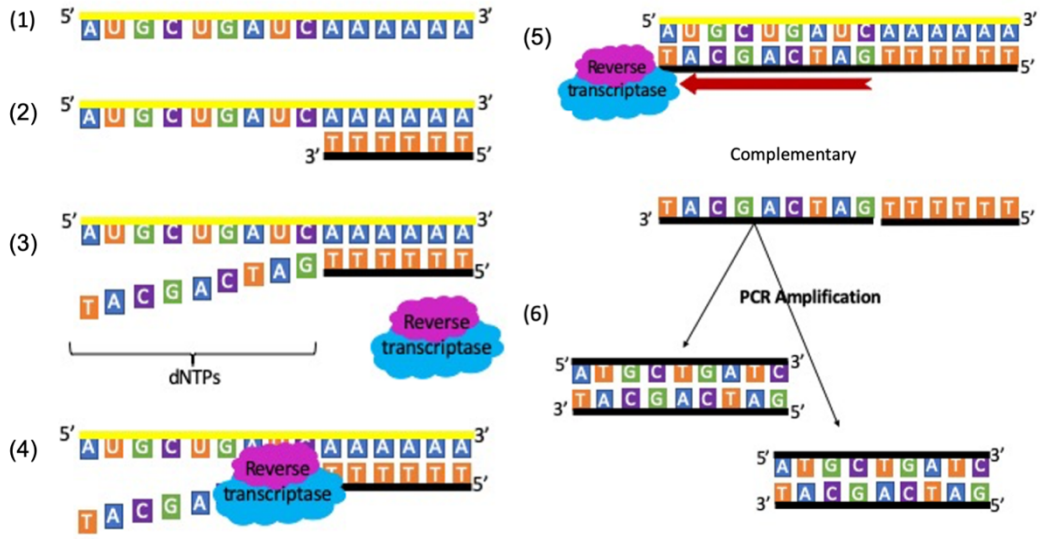

Figure 2. Schematic diagram of reverse transcriptase polymerase chain reaction, *which can be used in virology diagnostics to identify viral RNA in clinical samples as well as having research and development applications. (1) RNA begins with a start codon, AUG, and ends with a poly adenosine tail. (2) An oligo deoxythymine primer (dT) binds to the poly-A tail of RNA. (3) The dT primer catalyses the binding of reverse transcriptase and deoxyribonucleotide triphosphates (dNTPs) are recruited. (4-5) Reverse transcriptase catalyses the generation of complimentary DNA (cDNA) using free dNTPs. (6) The cDNA produced can then be amplified via PCR as double stranded DNA using specifically designed primers or quantified using qPCR.*

Another diagnostic advancement in PCR was the development of reverse transcriptase PCR (RT-PCR). This technique generates complementary DNA strands (cDNA) from RNA (**Figure 2**). RT-PCR is a valuable tool for the accurate diagnosis of viral infections. Many viruses store their genomic information as viral RNA (vRNA), which can be isolated from biological samples of an infected host. The cDNA generated from RT-PCR can then be quantified via qPCR, collectively known as RT-qPCR. The level of fluorescence signal produced in response to denaturation of the probe (**Figure 1**) is measured against a ‘no template DNA’ control to calculate the quantity of vRNA in the sample (11). Viruses that store their genome as DNA (DNA viruses) can be detected and quantified without the use of reverse transcriptase.

The wide range of genomic sequences available to the scientific community makes developing primers against numerous disease biomarkers possible, and therefore, qPCR is easily applied to a vast range of clinical diagnostic. For diagnosis of many viral infections, qPCR (DNA viruses) and RT-qPCR (RNA viruses) are still the best diagnostic method available (12). qPCR is highly specific; however, the full process from obtaining the clinical sample, extracting the RNA, and running RT-qPCR is long and laborious, which could be critical in a pandemic situation. However, it is still the simplest way of detecting relatively unknown virus strains and so is still in use today (13).

1.1.2 Western Blot

A well-known method of direct protein detection is the western blotting (WB) technique (14). This involves the separation of denatured proteins, by molecular weight, in a sample using gel electrophoresis. The separated proteins are then transferred onto a suitable membrane and the protein of interest can be detected with a specific primary antibody. A secondary antibody conjugated to an enzyme with colourimetric, luminescent or fluorescent activity can then be used to visualise the protein of interest (**Figure 3**). WB is commonly used in biological research laboratories to confirm the presence of protein in tissue and cell lysates (15).

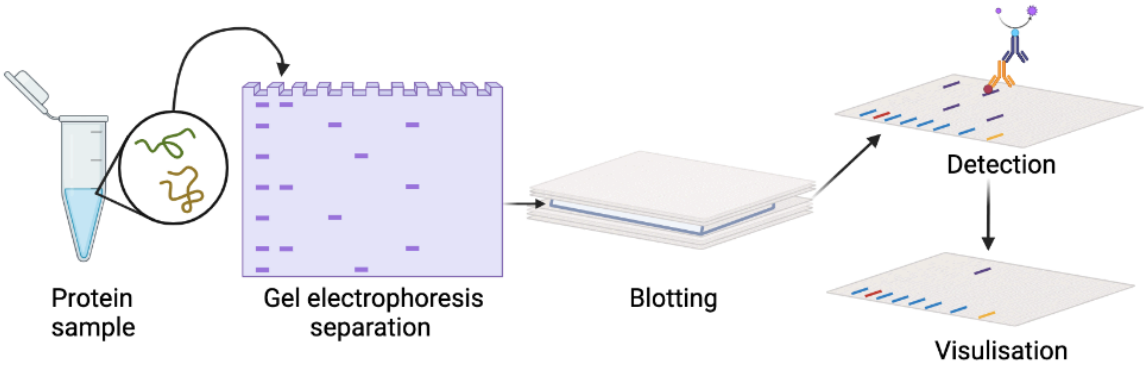

***Figure 3. The general workflow of a western blot**. Initially a sample in need of analysis is loaded onto an agarose gel for separation by gel electrophoresis. The resultant gel is transferred onto a blotting membrane which in turn is blocked and incubated with a specific primary antibody known to bind to the protein of interest. Successful binding of the primary antibody is determined with a conjugated secondary antibody allowing visualisation via colourimetric, luminescent or fluorescent methods. Created with Biorender.com.*

The sensitivity of WB made it a valued diagnostic technique in clinical settings. It is not a quantitative method of protein detection and so has typically been used as an aid to confirm diagnoses in a clinical setting. Historically, WB has been used in the diagnosis of a few diseases including hepatitis C virus (HCV), Lyme disease and human immunodeficiency virus (HIV) (16-18). Issues with false-positive results have limited the applicability of WB as a one-tier test and are more commonly used in combination with other protein detection methods to confirm a diagnosis (19). WB testing for HIV has generally been superseded by rapid antibody or antigen tests, including enzyme immunoassays (EIAs) and molecular tests developed for high throughput screening large quantities of blood bank products (20) and point-of-care (PoC) immunoblot self-test kits for use in community settings (21). WB are still routinely used as a confirmatory test after a positive PoC test (22, 23).

1.1.3 Enzyme Linked Immunosorbent Assay

The enzyme linked immunosorbent assay (ELISA) is a molecular method which provides quantitative results on the presence of a specific protein analyte. As an immunoassay, the key component of an ELISA are antibodies, both monoclonal and

polyclonal (24, 25), for specific detection of a protein analyte. These specially raised antibodies work as a detection mechanism within the assay as they bind to highly specific targets. For example, in an indirect ELISA, monoclonal antibodies raised against the target analyte are used as the primary antibody and secondary antibodies are raised in a different animal against the primary antibody, with the addition of chemiluminescent or fluorescent labelling for quantification (**Figure 4**). The most used labelling is horseradish peroxidase (HRP), which catalyses the oxidation of the substrate 3,3′,5,5′-Tetramethylbenzidine (TMB) causing a change in colour from clear to blue (26).

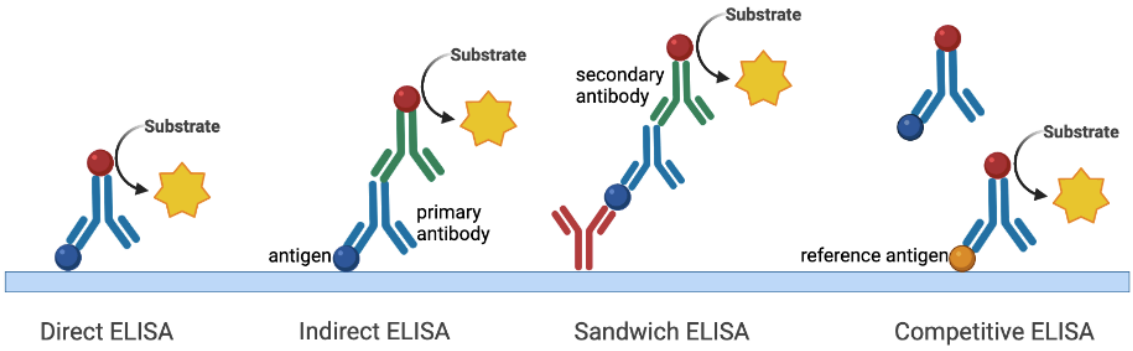

Figure 4. Schematic diagram of ELISA techniques (direct, indirect, sandwich and competitive). *All ELISA formats use the standard method of adsorbing an analyte to a surface, usually a multi-well plate, and detecting with a labelled antibody raised against the analyte. There are a variety of steps involved in each method that distinguish them from one another.* ***Direct ELISA*** *detect the antigen with one conjugated antibody that can both bind to the analyte and produce a signal.* ***Indirect ELISA*** *utilise a secondary conjugated antibody raised against the primary antibody to produce a signal.* ***Sandwich ELISA*** *add an extra step by first coating the plate with an antibody and subsequently incubating the analyte to bind followed by the standard indirect (or direct) method.* ***Competitive ELISA*** *involves coating a reference antigen to the plate and pre-incubating the sample antigen with labelled antibodies, addition of the antigen-antibody mix results in the reference and sample antigens competing for the antibody. After washing the less signal produced the more sample antigen present. Adapted from "ELISA overview", by BioRender.com (2023). Retrieved from https://app.biorender.com/biorender-templates*

There are a variety of ELISA techniques (**Figure 4**) in addition to the indirect ELISA, which work along the same principles. A direct ELISA uses a primary antibody conjugated to HRP so absorbance can be visualised directly from detection of the analyte. This is beneficial as it saves time on incubation and wash steps and limits the chance of cross-reactivity with a secondary antibody. However, there is a higher potential of background signal from the antibody conjugate binding to the surface (27). The sandwich ELISA depends on there being two different antibodies raised against different epitopes of the analyte, as a matched antibody pair. In this case, one of the antibody pair is adsorbed to the surface, which the analyte then binds to. The second of the pair then takes on the role of the primary antibody. Similarly, the sandwich ELISA can be direct or indirect, with the indirect approach using a secondary antibody-conjugate. Like the indirect ELISA, the indirect sandwich ELISA has the limitations of long, laborious techniques and secondary antibody cross-reactivity. The direct sandwich ELISA omits the cross-reactivity and reduces steps. Sandwich ELISAs are limited by the discovery or design of matched-pair antibodies, but the reward of this is a highly specific and selective detection method (28).

In a clinical setting, ELISAs are routinely used for the detection of antigens, biomarkers, and antibodies in biological samples (29-31). One of the most notable advances in diagnostic ELISAs is the improvement of HIV diagnostics since the development of the first HIV ELISA in 1985. This ELISA was not approved to diagnose patients, only to screen blood products to prevent transmission. Since then, 5 generations of HIV ELISA tests have been developed, each improving with sensitivity and selectivity (22). These ELISAs were originally seen to produce numerous false positives, relying on WB confirmation, which lead to unnecessarily lengthy processes. The sensitivity and specificity of these assays has improved and the fifth generation ELISA can quantify both antibodies and antigens associated with HIV (32). In addition to aiding infectious disease diagnosis, ELISA methods have been routinely used to

monitor therapeutic drug levels during treatment (33-35) and screen for anti-drug antibodies (36) in the pursuit of personalised medicine.

Despite their long-standing performance as a standard test for detection and quantification of protein analytes, ELISAs do have major drawbacks which have become more pronounced in present times (37). The multiple incubation and wash steps necessary make ELISA a long and laborious method even with automated equipment. They also lack multiplicity, require large (>100 μL) volumes and rely on the development of antibodies against each new target. These factors mean that conventional ELISAs are not a suitable method for rapid and affordable protein detection which is desirable in many situations. There is on-going research adapting ELISA formats to improve on the limitations aforementioned (37-40).

1.1.4 Point of Care Diagnostics

Current laboratory-based methods of protein detection are highly sensitive and selective, but they are limited by the need for multiple steps and long incubation periods which prevent use in a point-of-care setting. The recent COVID-19 pandemic caused by severe acute respiratory syndrome coronavirus 2 (SARS-CoV-2) illustrated the failures of relying on laboratory-based testing when trying to triage a global population. The successful identification and isolation of infected individuals in a pandemic relies on rapid screening which ELISA, WB and PCR methods cannot deliver. The capacities of available testing facilities were quickly overwhelmed due to the reliance on trained personnel to run diagnostic tests, which delayed effective isolation methods (41). Further to this, the lack of global co-operation led to low-income and middle-income countries being denied access to the facilities necessary to effectively screen patients and respond to the COVID-19 pandemic (42). These shortcomings throughout the pandemic have revealed the crucial need for rapid and widespread diagnostics as a countermeasure to the spread of disease in epidemic and pandemic circumstances.

Point-of-care (PoC) diagnostic testing refers to any test, assay or device that can provide a result in the same place the patient sample was collected. The aim of point-of-care testing (PoCT) is to provide a rapid result in settings such as general practice (GP) clinics, accident and emergency (A&E) departments, intensive care units (ICU) and mobile clinics without the need for centralised testing where samples are analysed in a laboratory. These tests are designed to be used by health care staff with basic training (43) and in some instances at home by the public.

The most prominent examples of PoCT are those intended for home use, which are generally lateral flow devices (LFDs). LFDs are made using porous paper which permits spontaneous fluid transport via capillary action. A series of strips are spaced out along the paper with freeze dried binding reagents on them. The first strip is known as the conjugation strip, this usually contains a target-specific primary antibody conjugated to a fluorescent or chromogenic dye. The antigen-antibody complexes continue to flow along the paper where there are two more strips, known as the test strip and the control strip. These have immobilised antibodies specific to the target antigen (test strip) or specific to the primary antibody (control strip) (**Figure 5**). Binding of the antigen-antibody complexes at the test and control strips immobilises the dye allowing visualisation of the result. LFDs are a qualitative test that can provide a positive or negative result.

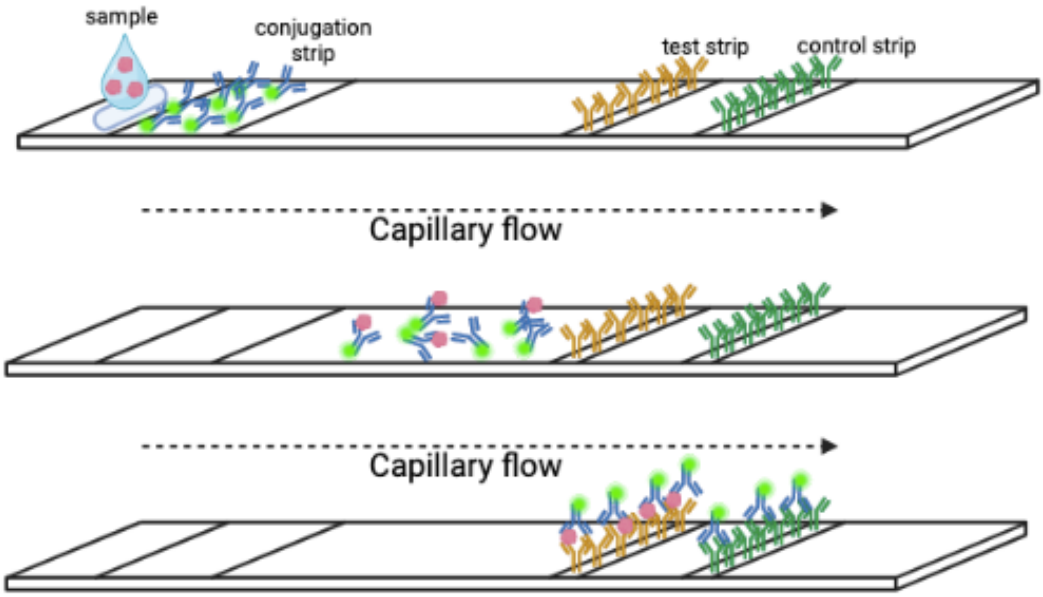

Figure 5. Schematic diagram of a standard lateral flow device*. Sample is loaded and transported along the test paper via capillary action. As the sample encounters the conjugation strip any antigen present will bind to the labelled antibodies. Antibody – antigen conjugates then flow along to the test and control strip.*

The home pregnancy test is a notable LFD developed in 1976 (44). There are many variations of this home test now available over the counter. These LFDs detect human chorionic gonadotropin (hCG) in urine (44-46). Concentrations of hCG in urine raise from 0 milli-international units per millilitre (mIU/ml) prior to conception to around 100 mIU/ml 14 days after, and surge up to ~ 50,000 mIU/ml at 40 days post conception (44). On average, the sensitivity of home pregnancy tests falls around 25 mIU/ml which accounts for the > 99% accuracy after day 10. Inaccurate test results usually occur in very early pregnancy due to inadequate hCG concentrations, causing false negative results. Due to most analyses of home pregnancy test specificity and sensitivity being conducted in a laboratory setting, there have been reports that the real-life accuracy is < 99% due to user error or difficulties reading the result correctly (47, 48).

More recently, the COVID-19 pandemic led to an influx of LFD research and development to provide a cost-economical solution to mass screening of the population (49). The SARS-CoV-2 antigen LFDs that have become routine home-tests use

conjugated antibodies that bind to spike, or nucleocapsid SARS-CoV-2 viral proteins (50, 51). The nucleocapsid protein is more commonly detected in COVID-19 LFDs as higher concentrations per virion are available in the samples used for LFD assays (nasal swab and saliva) compared to spike protein concentrations (52, 53). The current COVID-19 LFDs are highly specific but have variable sensitivity which prevents their sole use as a primary diagnostic test (49), They have however, demonstrated the value of swift and convenient screening of symptomatic and asymptomatic infection.

1.1.5 Disease diagnosis

The emergence of the COVID-19 pandemic in 2020 was a major factor in the growth of the LFD market. An increase in capacity throughout the supply chain of reagents necessary for LFD design and development has led to more interest into PoC LFD for infectious disease diagnosis (54). There are rapid tests on the market for SARS-CoV-2 (55), Hepatitis (56, 57), HIV (58) and malaria (59). PoCT are also applicable for rapid diagnosis of non-infectious diseases including certain cancers (60, 61) and cardiac diseases (62). Further to initial diagnosis, PoCT can be utilised for disease monitoring or drug monitoring to aid treatment efforts.

1.1.6 Disease monitoring

There are PoCT that do not use the lateral flow format, the most successful example is the glucometer, with widespread application and recent advances in continuous monitoring (63). Glucometers are the main platform for disease monitoring of diabetes mellitus, a group of metabolic diseases that are defined by impaired glucose metabolism due to insufficient insulin production or resistance to insulin (64). Vigilant monitoring of glucose levels allows patients to prevent hypo- and hyperglycaemic episodes by tailoring insulin administration or glucose intake. Unlike LFDs that use an optical readout, glucometers are unique in their utilisation of glucose oxidase (GOx) to produce an electrochemical signal. The enzyme GOx catalyses the oxidation of

glucose molecules into gluconic acid and hydrogen peroxide (H_2O_2), the latter of which can be further oxidised on an electrode surface. The transfer of electrons from the H_2O_2 molecule to the electrode creates a measurable electrical current. The rate at which the H_2O_2 is oxidised and subsequent electrical current generated is proportional to the concentration of H_2O_2 which can be used to calculate the concentration of glucose in a sample (65, 66).

The global prevalence of diabetes mellitus is estimated at 9.3% of the population (> 450 million) as of 2019, with another 7.5% (>350 million) with pre-diabetes (67). With diabetes mellitus affecting a large percentage of the population, a lot of research has gone into advancing the technologies used for disease management. In recent years there has been a move from the self-monitoring of blood glucose (SMBG), like finger prick glucometers, to continuous glucose monitoring (CGM). CGM devices are usually minimally invasive, implantable or wearable devices that can provide semi-continuous glucose measurements and set up alarms for hypo- and hyperglycaemic states (68). They use samples of interstitial fluid (ISF) which has a high level of correlation with blood in terms of glucose concentrations as well as other biomarkers (69, 70). Creating continuous monitoring systems is a major goal for future health monitoring and maintenance. Current attempts have focused on biomarkers that can be directly oxidised by an oxidase enzyme to maintain the same format as CGM (71). This approach restricts possible applications to measuring analytes such as lactate, alcohol, and cholesterol (72).

1.1.7 Drug monitoring

Monitoring of drug concentrations in a PoC setting has the potential to aid treatment regimens for individuals undergoing chemotherapies. This is especially pertinent for medications with narrow therapeutic windows or possible severe adverse reactions (SAR) due to inter- and intra-patient disparities. Currently, monitoring of these drug types, such as immunosuppressive drugs (ISD), is limited by centralised, laboratory-

based testing, because no quantitative PoCTs for therapeutic drug monitoring (TDM) are available on the market (73). PoCT for detection of drugs are qualitative in their ability to detect the presence or the absence of a drug in a biological sample. These are widely used for illicit drug detection in oral fluid (OF) and rely on lateral flow technology (74, 75). Low sensitivity, specificity issues and in-field variables such as insufficient sample collection mean that subsequent centralised testing is necessary, after positive PoCT results, to confirm the presence of the analyte (76).

1.2 Biosensors

Sensors are defined as devices that have the capability to measure biological or chemical reactions by generating a proportional signal which correlates with the concentration of analyte. The introduction of a biological component into a sensor is what defines a biosensor (77, 78). Many aspects of biosensors make them suitable to be adapted into PoCTs. The reduced sample volume, ease of use and cost-effectiveness associated with biosensors makes portability and miniaturisation possible which are important features of PoCTs. Further to this, the possibility of customising biosensors whilst maintaining their sensitivity, specificity and speed also make them good candidates for integration into PoC settings. Typically, biosensors consist of a biorecognition element, such as an antibody or enzyme, which detects an analyte and transduces a reaction into a measurable signal. An electronic component can then transmit the signal into a readable format (**Figure 6**). Classification of biosensors is generally based on either the recognition (sensing) element or transduction method.

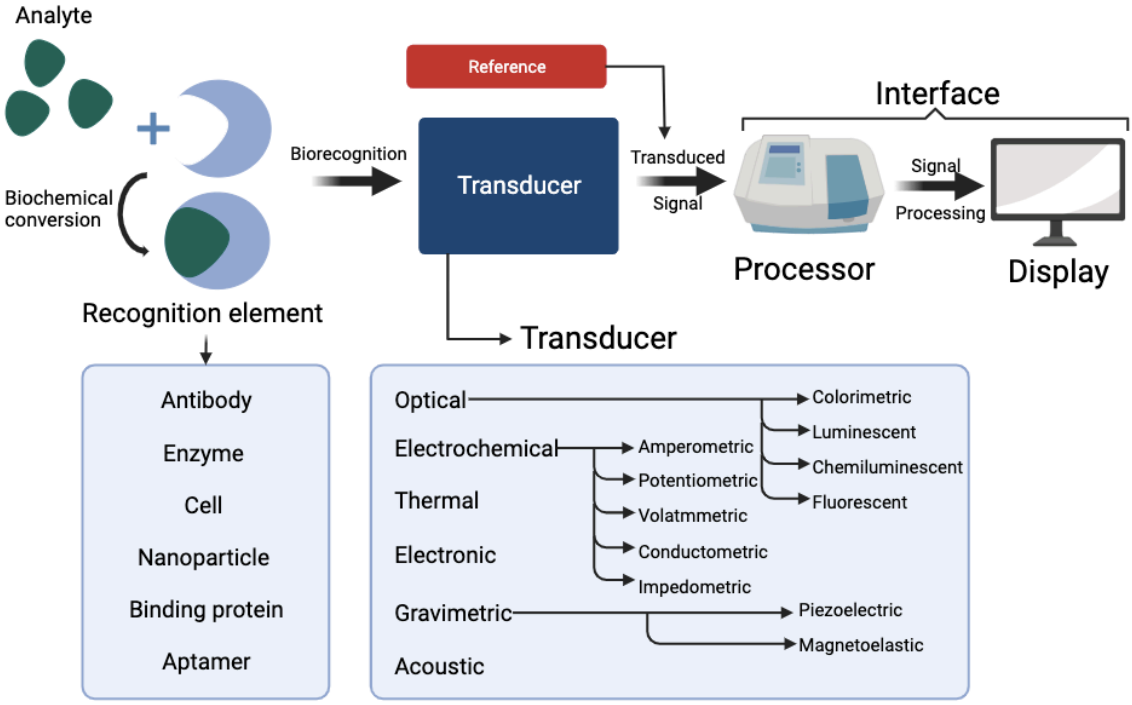

Figure 6. Schematic diagram of the typical components of a biosensor *consisting of a suitable recognition element, a transducer and an interface which processes and displays the signal in a user-friendly format. Adapted from (79) Copyright 2021 according to CC-BY license. Created with Biorender.com.*

1.2.1 Recognition element classification

1.2.1.1 Enzymatic biosensors

The direct catalysis of a reaction via an available enzyme integrated or intimately associated with the recognition elements of a biosensor defines the classification of enzyme-based biosensors. Within this type of biosensor design, the analyte is a specific substrate for the enzymatic recognition element, whereby detection of the analyte results in a new biochemical reaction product (78). During an enzymatic reaction, certain biochemical changes occur, or by-products are formed which can be exploited as a measurable factor. These factors include changes in proton concentration (H+ ions), the release or uptake of gases (CO_2, O_2, etc.), heat emission, light emission, or absorption. The most relevant measurable change then informs the choice of transducer used to convert it into a readable signal (80). Glucose sensors serve as a prime example of enzyme-based biosensors. Enzyme-based glucose

sensors typically utilize the enzyme glucose oxidase (GOx) or glucose dehydrogenase (GDH) immobilized on a sensor surface. When glucose molecules encounter the enzyme, a chemical reaction occurs, resulting in the conversion of glucose into gluconic acid and the generation of electrons. The flow of these electrons produces an electrical current that can be quantified by the biosensor. The magnitude of the current is directly proportional to the concentration of glucose present in the sample.

1.2.1.2 Immunosensors

Biosensors that incorporate antibodies as their recognition elements can be split into two distinct types; labelled and label-free immunosensors. Both types of immunosensors require immobilisation of the recognition element (usually an antibody) onto a sensor surface. In label-free immunosensors, the surface must be an active surface with characteristics that can sensitively detect the formation of an immunocomplex (antibody-antigen complex). Electrodes, membranes, and optically active surface materials are all possible transducers for label-free immunosensors (**Figure 7A**) (81-83). Surface plasmon resonance (SPR) is an extensively used technique for the detection of protein interactions. The exploitation of this method to create optical, SPR immunosensors enables the direct, label-free, and real-time quantification of interactions between immobilised antibodies and the antigen of interest. This is achieved through the measurement of refractive index changes occurring at or near a thin gold film surface on which the antibody recognition element is covalently bonded (84, 85). The rapid and real-time analysis capable with label-free immunosensors has made them a good option for clinical use as a PoCT. Label-free immunosensors are more prone to false positives due to non-specific binding of the antigen and other proteins to the antibody or sensor surface and producing a signal when immunocomplex formation has not occurred. To mitigate this, the use of a blocking solution is necessary to prevent any negative impact on specificity (86, 87).

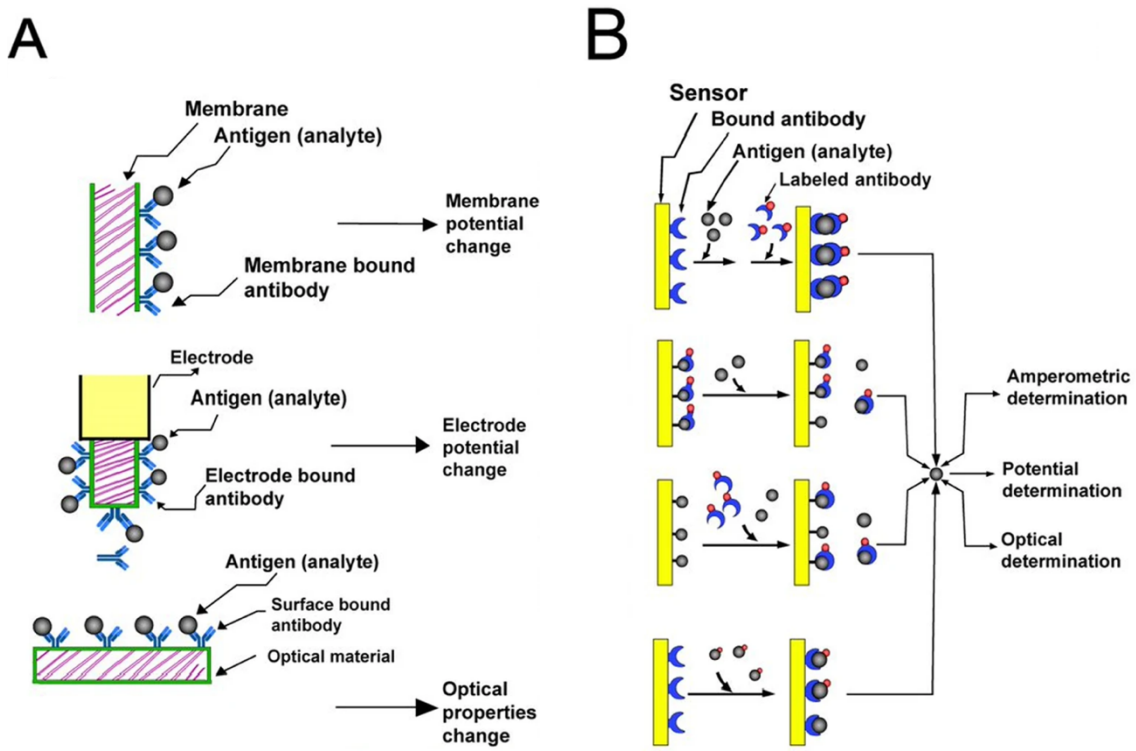

Figure 7. Label-free (A) and labelled (B) immunosensors. *Adapted from (88) Copyright © 2021, Dina M. El-Sherif et al, under exclusive licence to Springer-Verlag GmbH Germany, part of Springer Nature.*

Alternatively, labelled immunosensors generate their signal from indirect measurement of label activity. The labels are usually enzymes alongside an electrochemically active compound to act as a mediator such a ferrocene or Prussian blue (**Figure 7B**) (89, 90). The use of an electrochemical mediator in labelled immunosensors is necessary as antigens and antibodies are not typically electroactive. Labelled immunosensors incorporate the sensitivity of the labels they are tagged with which can improve the overall sensitivity of the immunocomplex detection compared to label-free immunosensors (91). The use of labels also reduces the negative impact of non-specific adsorption onto the sensor surface. However, in some instances the introduction of labels can affect the binding capabilities of the antibody, as it is difficult to control the position of labels with certain coupling reactions (92).

1.2.1.3 DNA Sensors

Due to the robust biochemical properties, thermal stability, and customisability of DNA it has become an attractive recognition element within biosensors in recent years (93, 94). The versatility of DNA provides the opportunity to detect a wide range of target analytes, including, but not limited to, proteins; metal ions; small molecules and nucleic acids (95-104).

Various types of DNA-based biosensors exist, encompassing functional DNA strand-based biosensors, DNA template-based biosensors, and DNA hybridization-based biosensors. Functional DNA strand-based biosensors employ functional DNA strands to recognize specific targets, such as aptamer biosensors (95, 100) and DNAzyme biosensors (99). DNA nanopore biosensors use nanopores embedded in a membrane, which can be functionalized with specific DNA sequences that interact with target molecules. When a target molecule passes through the nanopore, it causes characteristic changes in electrical current, which can be detected and used for molecular analysis. This DNA sensor design is commonly used for single molecule detection (105, 106). DNA template-based biosensors feature a DNA template decorating the biosensor, often in the form of supra-molecular DNA assembly structures with programmable anchoring points, as seen in biosensors based on DNA origami (107). DNA hybridization-based biosensors, on the other hand, utilize enzyme-free nucleic acid amplification strategies to enhance their responses, examples of which include biosensors based on DNA hairpin structures, and catalytic hairpin assembly (101). Detailed reviews are available which explore the different types of DNA-based biosensors (108, 109).

1.2.1.4 Cell based biosensors.

Living cells, possessing a wide range of biomolecular mechanisms, provide an intriguing alternative to molecular bioreceptors like DNA, enzymes, and antibodies. Using whole cells means that enzymes, receptors, and other molecules used in the

sensing mechanism are in their native environment, so they display optimal activity and specificity for their targets. (110-119). Both prokaryotic and eukaryotic cell types have been utilised in the development of whole cell biosensors (120-125). The transduction method used is dependent on the cell type used and the functional strategy employed. Optical and electrochemical readouts are more common as a change in metabolism within the cell (or cell death) can directly impact electron generation and colourimetric or fluorescent signal output. Other readouts are also possible as a change in electrical activity can be measured eukaryotic cells. Published reviews explore that recent advances and challenges in cell-based biosensor development for both eukaryotic and prokaryotic cell types (126, 127).

1.2.2 Transducer classification

Transduction methods are the methods involved in producing a signal upon binding of the target analyte to the recognition elements. These can be used to categorise biosensors into various classifications, including: electrochemical sensors, such as potentiometric, amperometric, and impedimetric; optical sensors, such as colourimetric, spectrophotometric, luminescent, and fluorescent; thermal sensors, such as calorimetric, and thermometric; and mass-based sensors, including magnetoelectric, and piezoelectric sensors (128). Optical biosensor classifications will be further explored here, other classifications are covered in referenced reviews (129-134).

1.2.2.1 Optical biosensors

Optical biosensors utilise light to detect a change in chemical or physical properties of a biological sample. The detected signal can be an increase or decrease in light transmission, reflectance, fluorescence, or luminescence. Optical biosensors are common due to the low manufacturing cost and the ease of use, especially when considering the potential for PoC applications (135). Common optical detection methods including surface plasmon resonance (SPR) and fluorescence spectroscopy have been developed from the fundamentals of light emission or light – matter

interactions and can be employed in biosensing mechanisms (136). Lateral flow tests (LFTs) are immunodetection devices that typically produce an optical signal upon protein detection, beneficial for testing that requires a positive or negative result without quantification. These optical sensors are beneficial in PoC settings due to the ease of signal read-out, in that the signal is visible to the naked eye usually as a colour change. As mentioned, they have a long history of use in home pregnancy testing and have been widely adopted over the course of the COVID-19 pandemic, due to their low cost, ease of use and utility in low resource settings. Despite their broad uptake, LFTs are semi-quantitative, and often have limited sensitivity that may not be sufficient for some applications (137).

1.2.2.1.1 Colourimetric

Colourimetry is the technique of measuring a colour change that is dependent on the concentration of the target analyte (138). Colourimetry has been used extensively as a transduction method in biosensor development. The integration of an enzyme as a reporter within a biosensor system can promote the production of H_2O_2 when a catalytic reaction occurs, H_2O_2 production can be easily detected as a colourimetric reaction with the addition of 3,3′,5,5′-tetramethylbenzidine (TMB), resulting in a naked-eye-observed colour change from clear to blue. This colour change can be used to determine the presence of H_2O_2 and subsequently activity of the precursing enzyme which can in turn quantify the target analyte by measuring the level of absorption at a particular wavelength (139).

Nanoparticles can be used as colorimetric probes to develop versatile biosensors. This is based on the unique optical properties of gold nanoparticles (AuNPs) that can cause colour changes. Alternatively, they can be utilised as labelling dyes which can be visible to the naked eye or quantitatively measured with an optical detector. This is due to a surface plasmon resonance (SPR) effect, where the dispersion or aggregation of the nanoparticles is mediated by the presence or absence of analyte and the addition

of salt, which shifts the plasmonic absorption of the solution and causes a colour change (140). In some instances, the presence of viral RNA can cause coagulation of AuNPs, so unmodified AuNPs can work as a biosensor for virus detection (141-143), however this is not a specific method. Nanoparticles functionalised with antibodies or other highly specific binding proteins improve the specificity of AuNP colourimetric biosensors. AuNPs functionalised with influenza A virus (IAV) antibodies created a sensitive and specific biosensor whereby AuNPs aggregated in the presence of IAV causing a colour change from red to purple (144).

1.2.2.1.2 Luminescent

When developing biosensors, chemiluminescence, the emission of light as a result of a chemical reaction, or bioluminescence, the emission of light biologically, can be used as transduction methods. Luciferase enzymes are an example of bioluminescent proteins that turn over a substrate to produce light (145). Although more sensitive than colourimetric transduction, luminescence is not visible and therefore requires equipment to read the output signal. Whole cell luminescence sensors have been developed to test the antibacterial effects of carbon nanomaterials. The introduction of an inducible luminescence gene into *E. coli* has produced a recombinant strain of *E. coli* that luminesces when under oxidative stress, termed Lux biosensors, which can be used to determine antibacterial activity of reagents and materials (146).

Resonance energy transfer (RET) is a photophysical phenomenon that describes the transfer of energy from an excited-state donor chromophore to an acceptor chromophore through a nonradiative dipole–dipole coupling process. When this transfer of energy occurs in the context of bioluminescent reactions, it is referred to as Bioluminescence Resonance Energy Transfer (BRET). The efficiency of BRET is inversely proportional to the sixth power of the distance separating the donor and acceptor molecules. As a result, BRET serves as a valuable technique for monitoring subtle changes in distance between donors and acceptors (147). This BRET

phenomenon has led to a wide range of applications in the fields of protein-protein interaction studies, biosensing, and functional imaging (148, 149). Luciferases are frequently employed as BRET donors, while fluorescent proteins serve as BRET acceptors. These components can be fused with various sensing elements to create diverse bioluminescent biosensors. Photoluminescent quantum dots (QDs) are a popular choice for use as BRET acceptors in biosensing. QDs are appealing acceptors due to their high photostability, continuous absorption spectra, and size-dependent fluorescence (150, 151). Two DNA probes complementary to sections of the target sequence that are in proximity (15 nucleotides apart) can be used as recognition elements in a BRET based sensor. By conjugating one DNA probe to a QD and the other to a Renilla luciferase (RLuc), the probes anneal adjacent to each other which brings the QD and RLuc into close proximity and increases the BRET signal to indicate analyte presence within the sample (152). A major benefit of BRET based sensors is that BRET does not require an excitation source which permits the use of simple reading equipment such as smart phones (153) or digital cameras (154).

1.2.2.1.3 Fluorescent

Stable fluorescent molecules can be easily attached to recognition elements or linkers to produce sensitive signals in fluorescent biosensors (155). For instance, chemical modification of recognition elements can facilitate fluorescent labelling and numerous diagnostics have been published using fluorophores and quenchers in sensor design. For example, a DNA sensor using DNA aptamers as the recognition elements exploits a conformational change in the aptamer as a result of binding to the target that is then transduced into a measurable signal due to positions of the fluorophore and quencher (156, 157).

Similar to BRET, incorporating fluorescent molecules into sensors also allows for Förster resonance energy transfer (FRET)-based techniques. FRET occurs through energy transfer between two dipoles (dipole-dipole coupling). When the two dipoles are

within appropriate proximity and spectral overlap, energy is transferred from an excited state donor fluorophore to an acceptor, a ground state fluorophore or a quencher (A) (158). FRET produces a stronger signal than BRET and does not require the addition of a substrate. There are several well documented FRET pairs in literature whereas only a few BRET donors have been identified to date (159). However, FRET requires an excitation source. The donor fluorophore molecule must first be excited by absorbing light photon of suitable frequency at a specific wavelength. Once excited, the donor can then transfer some of its energy to the acceptor molecule if in proximity. This leads to an increase in fluorescence emission from the acceptor molecule and a decrease in fluorescence emission from the donor molecule (160). FRET based immunosensors generally involve labelling the capture antibody and detection antibody with the fluorescent donor and acceptor respectively, this results in FRET signal production upon binding of the target analyte (160, 161). Using a FRET label instead of a simple fluorescent label can increase the sensitivity of a sensor as FRET measures the transfer of energy and does not rely on the level of light emitted.

1.3 Chimeric Protein switch biosensors

The majority of the biosensors reviewed so far in this introduction rely on immobilisation techniques and interactions between molecules and sensor surfaces. Chimeric protein switch biosensors, which are the focus of the work here, are an alternative biosensor format. Chimeric protein switch biosensors are defined as sensors in which the reporter and recognition element are fused in a single design (**Figure 8**). They can be grouped into (a) domain-inserted allosteric switches, (b) modular allosteric switches, and (c) proximity switches (137, 162). Protein or enzyme switches enable highly sensitive quantitative analyte detection at the point-of-need, while retaining the benefits of LFT such as low cost, simplicity for the user and application at the point-of-need.

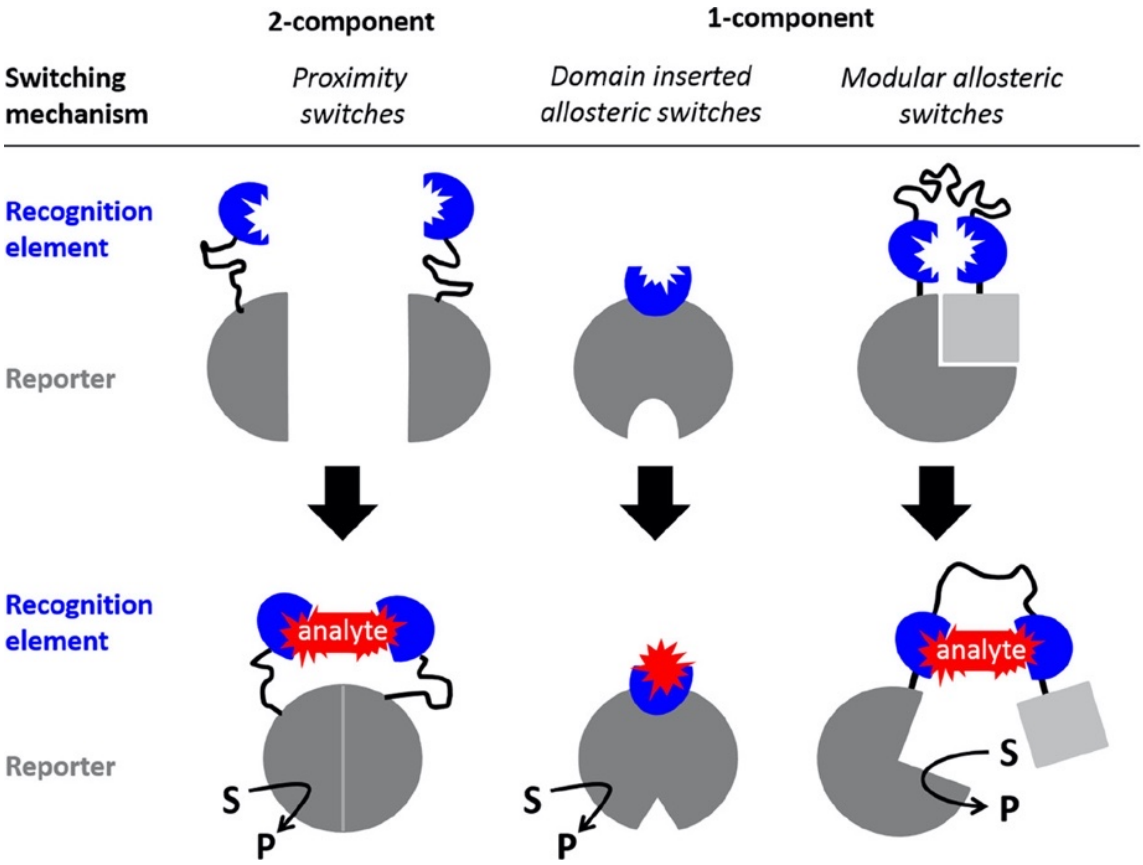

Figure 8. Switching mechanism classifications of chimeric protein switches. *Reprinted from ref* (137) *Copyright 2020 according to CC-BY license.*

Like all biosensors, chimeric protein switch biosensors need to be specific to the target of interest, so that a signal is not produced in the presence of molecules other than the analyte. Specificity to the target comes from the recognition elements, a range of recognition elements are described in detail in section 1.4. As well as specificity, the biosensor needs to be sensitive enough to produce a measurable signal in the presence of the analyte within the desired concentration range. In chimeric protein switch biosensors, lack of sensitivity might result from an inability of the target binding event to drive the switching mechanism. Less specific but highly sensitive recognition elements can produce a high background signal. Control of sensor component concentrations can typically reduce background binding when using recognition elements with good specificity. Aside from analyte affinity to the recognition elements, sensitivity can be affected by the transduction method and sensor design. Largely, biosensors can be split

into “switch-off” and “switch-on” designs (**Figure 9**). Switch-off sensors produce a signal in the absence of their target, and when the target is present the signal is inhibited. This sensor design is common for measuring small molecules. Typically, the signal is generated by a tagged target homologue that binds to the recognition element. When the target is present in a sample, it competes for binding with the tagged homologue and the signal decreases. This sensor design only requires one recognition element and hence is more frequently used for small analytes that have less chemical ‘space’ for two simultaneous recognition elements to bind. However, at low analyte concentrations, differences in the signal compared to the blank become harder to confidently detect, resulting in lower sensitivity and increase in error. Switch-off sensors thus typically have a lower sensitivity than switch-on sensors. Switch-on sensors produce a signal in the presence of the target of interest. Generally, two recognition elements specific to non-overlapping target epitopes are needed for a switch-on sensor. This allows for capture and detection of the target, such as in a sandwich ELISA. As a signal is produced in the presence of the target, switch-on sensors tend to be more sensitive as differences in signal compared to the background can be measured even at low analyte concentrations. Switch on sensors can, however, be difficult to validate when they exhibit high background signal as this must be accounted for in limit of detection and limit of quantification calculations (163).

The mechanism by which a reporter, within a chimeric protein switch biosensor, recovers its activity to transduce a signal in response to analyte binding is known as the switching mechanism. The design of this mechanism aims to maximise the signal-noise ratio (S/N) to obtain a large signal change in response to an analyte. Besides “switch-on” vs “switch-off”, the switching mechanism can be determined as one-component or multi-component. Here the difference between one-component and multi-component chimeric protein switch biosensors will be explored.

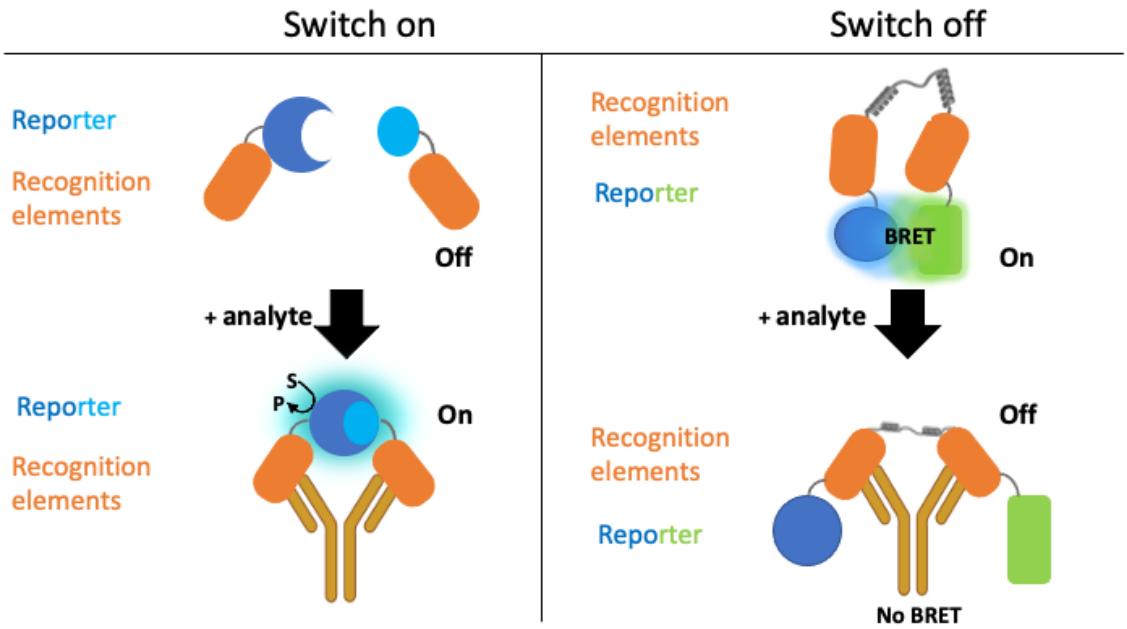

Figure 9. Schematic examples of "switch on" and "switch off" sensor mechanisms. *Defined by an increase in signal from baseline (switch on) or a decrease in signal from baseline (switch off).*

1.3.1 One-component switching mechanisms

In some instances, all recognition and reporter components of a protein switch are designed and purified as one multimeric polypeptide and can utilise peptide linker regions to connect multiple domains. These are known as one component, or allosteric, protein switches (137, 162). Generally allosteric switches are modelled on naturally occurring protein switches that control biomolecular signalling pathways.

Allosteric switches can be categorised as having either a domain inserted or a modular design (**Figure 8**). To transduce input to output, domain inserted switches rely on conformational change within the reporter to switch its activity on (or off). Modular switches limit the conformational change to linker regions which drive the change in reporter activity. Recombinantly engineering a multidomain protein with the ability to recognise analytes and transduce a signal in a single protein has advantages. It limits the number of steps necessary in the resulting detection assay, typically creating a 'one-pot' assay. It also decreases the number of proteins to be expressed and purified for the

assay. Still, there are challenges posed by the expression of multidomain proteins. The multidomain structure these switches possess can end up as large (>80 kDa) proteins, each domain of which must be correctly folded to generate a functional product. The host expression system must also navigate the correct folding of the overall structure, with the possibility of adjacent domains sterically hindering one another. The lack of machinery available in bacterial expression systems to aid in correctly folding such large and complex proteins can result in formation of unfolded, or aggregated, insoluble protein.

1.3.1.1 Domain inserted switches

Domain inserted protein switches depend on direct fusion of a recognition element to a reporter protein. The reporter protein undergoes a conformational change in response to the target analyte binding to the fused recognition element (**Figure 8**). The development of these switches requires allosteric coupling of the recognition and reporter elements to allow transduction through residues that are adjacent in the tertiary protein structure (137, 162, 164, 165). Direct fusion of a recognition element to a reporter can be challenging and ultimately detrimental to reporter activity or binder affinity. Most successful accounts of domain insertion require the inserted domain to be paralogous to the protein in which it is being inserted (166). β-lactamase (BLA) is a reporter enzyme readily used throughout the field of synthetic biology and bioengineering, and has been successfully inserted into periplasmic binding proteins (PBPs) to create domain inserted protein switches (164). The binding of PBPs to their target analyte causes a conformational change which in turn creates a change in conformation and enzymatic activity of BLA. A similar mechanism has been observed with the insertion of calmodulin into the reporter glutamate dehydrogenase (GDH) (165). Domain inserted protein switches have been largely limited to specific, naturally occurring binding proteins that are designed with one target analyte in mind and can be restricted in application to other analytes. In this sense, domain inserted protein switches are often not modular in design.

The use of a modular approach in which a single switch system can measure a range of analytes by replacing the recognition domain is more challenging. There have been accounts of insertion of binding domains from non-paralogous species such as heavy chain variable domains (V_HH nanobodies) into the solvent-exposed loop of BLA whilst preserving the functionality of both proteins (167). However, to create the conformational response necessary to make it a protein switch, the reporter protein usually needs to be inserted into the recognition element. Attempts at this with non-immunoglobulin binding proteins, such as Designed Ankyrin Repeat Proteins (DARPins) and monobodies, led to diminished binding affinity, limiting the sensitivity and ability to trigger switching activity (168). Domain inserted designs have been complemented by more modular designs to improve adaptability to a range of analytes.

1.3.1.2 Modular allosteric switches

With few protein families exhibiting conformational changes powerful enough to be exploited for signal transduction, engineering of allosteric regulation has taken precedent with more modular designs (**Figure 8**). The use of generic reporters that are structurally separated from recognition elements by polypeptide linkers reduces the risk that either the enzyme switch or the recognition domains are affected by the chimera protein design. Such modular style thus proposes easy adaptability with interchangeable recognition elements (**Figure 8**). Interdomain peptide linkers produce a loosely structured conformation to the sensor in its unbound “off” state. A large conformational change is driven by ligand binding, the bound “on” state can cause linkers to become rigid, which in turn shifts the conformation of the reporter element(s). In contrast to domain inserted designs, where the conformational change typically occurs within one protein domain, these modular designs exploit the disruption of an interaction such as an enzyme-inhibitor complex, a fluorophore and quencher or the distance between donor and acceptor fluorophores.

One such successful modular allosteric switch design exploits enzyme autoinhibition, whereby the “on-off” state of the switch is controlled by the inhibited and non-inhibited state of the enzyme. The wealth of information available on enzymes, their inhibitors and the biophysical properties of their interactions makes these switches easier to design (162). TEM-1β-lactamase (BLA) can be used for enzyme autoinhibition with its naturally occurring β-lactamase inhibitor protein (BLIP). The BLA-BLIP complex has been engineered into a modular allosteric switch whereby the enzyme and inhibitor are tethered via a long flexible linker containing two recognition elements (**Figure 10**). The use of a long, glycine-serine rich linker between the two recognition elements provides the flexibility for the two recognition elements, raised against non-overlapping epitopes, to bind the analyte in a sandwich (capture-detection) format. In contrast, the short rigid linkers that anchor BLA and BLIP to the recognition elements ensures that binding to the analyte disrupts the enzyme-inhibitor complex (**Figure 10**).

This action activates BLA activity so that its hydrolytic activity can be measured with the addition of a colourimetric substrate. The modular aspect of this switch allows for different recognition elements to be used for a range of targets. This has been demonstrated with peptide epitope sequences (**Figure 10A**) (169) and Affimer reagents (**Figure 10B**) (170). The design of this chimeric protein switch biosensor is favourable for the detection of large protein analytes, including antibodies and the multimeric protein biomarker C-reactive protein (CRP).

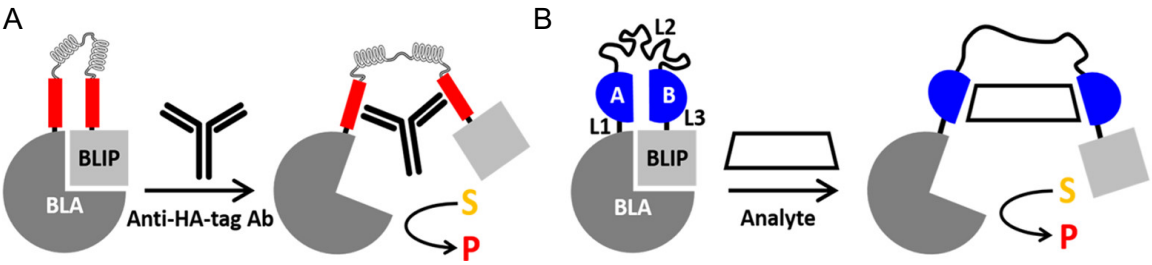

Figure 10. Chimeric protein switch biosensor design of the BLA-BLIP modular allosteric enzyme switch. *(A) Original design with peptide epitope sequence recognition elements for the detection of monoclonal antibodies. (B) Adapted design with Affimer reagent recognition elements for the detection of multiple protein analytes. Adapted from Ref (170) Copyright 2019 according to CC-BY* license.

The BLA-BLIP reporter system has also been adapted for the detection of viral DNA in a single component modular biosensor (171). Here, the presence of viral DNA controls BLA inhibition. BLA and BLIP are conjugated to oligonucleotide strands, either side of a region that is complementary to the target viral DNA. In the absence of the target viral DNA, BLIP binds to BLA, inhibiting nitrocefin hydrolysis. When viral DNA is present in the sample, the formation of dsDNA disrupts the BLA-BLIP interaction, resulting in signal generation and viral DNA detection as low as 2 fmol DNA.

Introducing a new reporter, a single component BRET system was created to measure titres of antibodies – LUMABS (LUMinescent AntiBody Sensor) (**Figure 11**). Here, the NanoLuc bioluminescent enzyme was used as the donor and the green fluorescent protein mNeonGreen was used as the acceptor, with both proteins fused together by a semi-flexible peptide linker with two peptide recognition elements, specific to the target antibody, included at either end of the peptide linker. In the absence of the antibody target the NanoLuc and mNeonGreen donor and acceptor are held in proximity by a helper domain. The SH3-proline-rich peptide (Sp1) interaction was used as the helper domain, whereby the SH3 protein was fused to the N- terminus of the mNeonGreen protein and the Sp1 peptide was fused to the C- terminus of the NanoLuc. SH3 and Sp1 interact, bringing NanoLuc and mNeonGreen together, allowing BRET from NanoLuc to mNeonGreen. When the target antibody is present in a sample, the antibody binds to the

specific peptide epitopes which disrupts the SH3-Sp1 interaction. This separates NanoLuc and mNeonGreen, consequently inhibiting BRET, giving a measurable signal that is dependent on the concentration of the target antibody. The ratiometric BRET signal produced by the change permits measurements in whole blood, ideal for PoC testing (153).

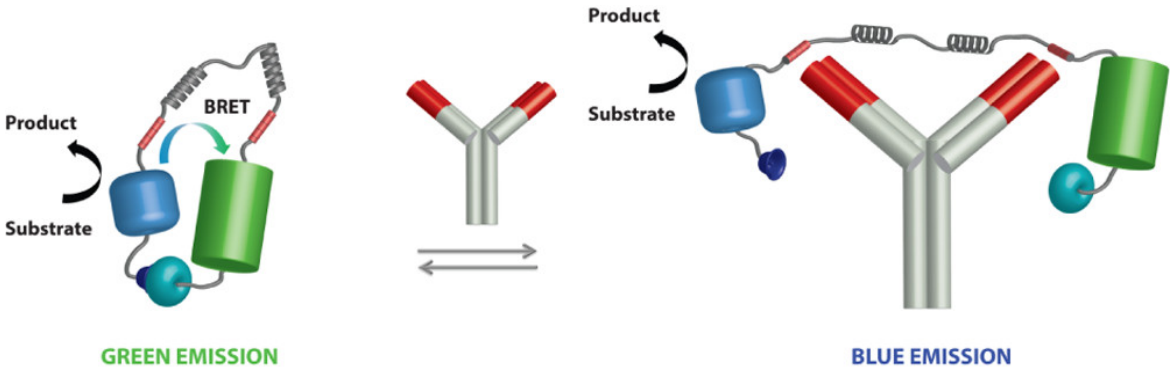

Figure 11. LUMABs sensor design for antibody detection. *Reprinted with permission from Ref (153) Copyright 2016 American Chemical Society.*

Another one component modular allosteric switch that uses BRET as a transduction method are the LUCID sensors (luciferase-based indicators of drugs), designed for therapeutic drug monitoring (TDM) in PoC settings. LUCID sensors use only one recognition element and do not rely on binding of non-overlapping epitopes to activate the protein switching mechanism. Instead, displacement of a fluorescent-tagged competitor ligand from the recognition element by the target analyte causes a conformational change within the linker regions of the sensor. Binding of the analyte therefore disrupts BRET between the blue NanoLuc luciferase and red fluorophore, shifting the colour from red to blue in a concentration dependent manner (**Figure 12**). The signal produced permits the quantification of drugs by spotting samples onto paper, followed by analysis with a digital camera. This requirement for non-specific equipment allows these tests to be used in a low resource environment, often where PoC testing is most needed (154).

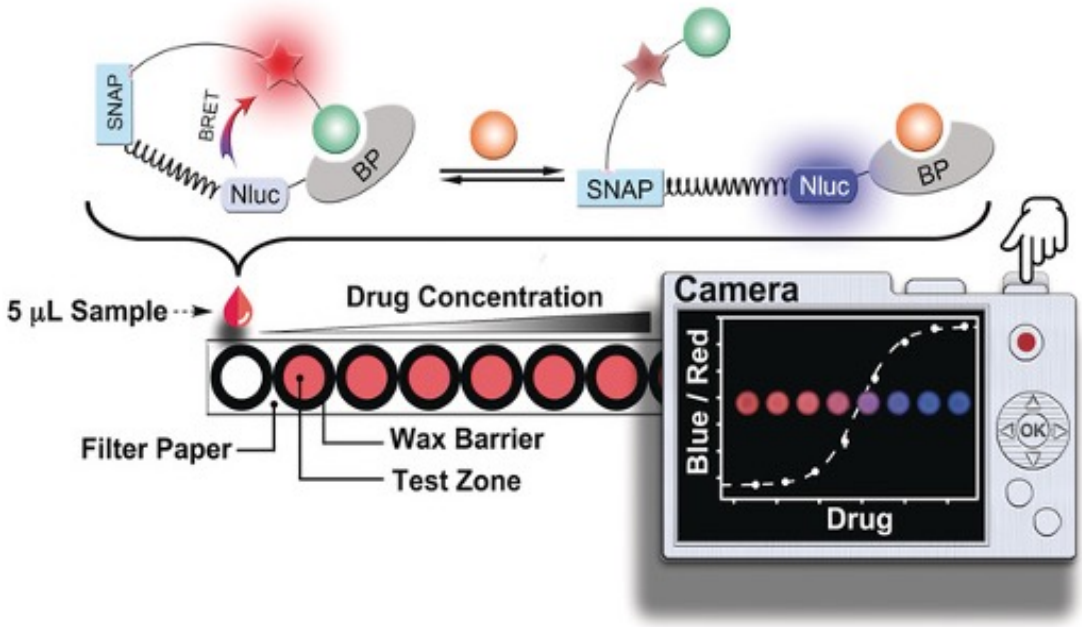

Figure 12. LUCID sensor design for small molecule drug detection. *The LUCID sensor is a fusion protein of NanoLuc luciferase (NLuc), SNAP-tag, and a binding protein (BP). SNAP-tag is labelled with a fluorophore containing molecule (red star) and a synthetic ligand (green ball) that binds to BP. Wax printed filter paper is used in the paper-based format and the resulting signal collected using a digital camera. Adapted from ref (154) Copyright 2017 according to CC-BY license.*

1.3.2 Multi-component switching mechanisms.

Multicomponent switching mechanisms usually rely on the re-complementation of a reporter, as shown in the 2-component panel of **Figure 8**. The reporter, most commonly an enzyme, is split into two inactive fragments that produce no signal when separated (172-175). It is also possible to exploit the polymerisation process of a multimeric enzyme by modifying the affinity of the associated sub-domains (monomers) (176, 177). As with most protein switches, the recognition elements selected must bind non-overlapping epitopes of the target analyte to ensure co-localisation of reporter fragments (173, 177-180). Binding of fused recognition elements to the analyte increase the effective concentration of the reporter fragments, prompting enzyme re-assembly. This results in an increase in signal that is dependent on the concentration of the target analyte; providing that the affinity of the target to the recognition elements is stronger than the

consolidation of the reporter enzyme components, so not to drive spontaneous reporter complementation.

Within early examples, two component proximity switches relied on the split reporter being fused to two proteins that directly interact with one another to drive re-complementation (181, 182). The system was developed for the analysis of protein–protein interactions (PPI), with an evolution into high-throughput screening (HTS) through the introduction of inhibitors and measurement of the “off” state of the switch (181). More recently, improvements in design and development of high affinity binding proteins, such as antibody fragments, antibody mimetics and DNA binders, have opened the possibility of indirect protein detection.

The concept of protein fragment recomplementation to yield active molecules was first observed in β-galactosidase (β-Gal) and ribonuclease (183, 184). Splitting of a protein for the purpose of measuring its reassembly to monitor PPI was introduced by a split ubiquitin sensor in 1994 (185), however successful reconstitution of ubiquitin was determined by visualisation of ubiquitin-mediated cleavage using blotting methods. Enzymes such as β-Gal have since been split for use in PPI studies. The enzymatic catalysis that produces a fluorescent dye after reconstituting the split parts of the enzyme allows for much easier measurement of PPI and permits such chimeric proteins to work as a tracer of direct PPI within live cells (182). Chimeric protein biosensors can utilise enzyme complementation for several read-out signals depending on the enzyme and substrate used (175-179, 186, 187).

One development in chimeric protein biosensors exploited the proximity switching mechanism for the detection of small molecules. Isolated variable (V_H and V_L) domains of a Fab fragment raised against 4-hydroxy-3-nitrophenylacetyl (NP) have been genetically fused to dimerised subunits of the homotetrameric enzyme β-glucuronidase (GUS) to function as a proximity switch (177). This style of proximity switch relies on high

effective concentrations of the chimeric protein driving polymerisation of the dimerised monomers of GUS to produce the fully active homotetrameric enzyme.

Improvement of enzyme complementation has largely been focused on luciferases due to their luminescent output and subsequent low background signal, making them highly sensitive in a proximity switch mechanism (179). A variety of organisms emit light via luciferases which catalyse light-producing reactions, these range from bacteria and fungi to marine life and insects (188). The splitting of *Renilla* luciferase (189), *Gaussia* luciferase (190) and firefly luciferase (191) have successfully been used for protein-protein interaction (PPI) studies.

To be successfully implemented into a PoC setting for *in vitro* detection of proteins, chimeric biosensor components need to be purified as stable isolated protein. The aforementioned enzyme complementation sensors have been exclusively used in *in vivo* settings where the sensor components have no need to be extracted from the expression environment. There have been noted issues with the stability of split enzymes *in vitro,* with the reconstituted activity not reaching that of the wild-type enzyme or high residual activity in the isolated fragments resulting in large background signals and loss of sensitivity (174, 176, 177, 192, 193).

Efforts to optimise a luciferase system resulted in the isolation of an engineered catalytic subunit of the deep sea shrimp (*Oplophorus gracilirostris*) termed NanoLuc (179, 194). The high stability and small size of this subunit permitted splitting into two inactive fragments to create a proximity switch system known as the NanoLuc Binary Technology (NanoBiT) (**Figure 13**) (195, 196). Initially the NanoBiT system was attached to two interacting proteins to monitor how two related proteins were interacting with one another. An example of NanoBiT utility within a PPI study is in the screening of inhibitors, in this instance the presence of an effective inhibitor can result in diminished interactions between the proteins and therefore limiting the re-complementation of NanoLuc and subsequent emitted luminescence (197).

The replacement of interacting proteins with recognition elements has developed the NanoBiT system into a tool for analyte quantification. The large and small NanoBiT fragments (LgBiT and SmBiT) have been genetically fused to immune and mimetic binding proteins, expressed in *E. coli,* and successfully purified as fully functional chimeric proteins. The NanoBiT system is diverse in its applications with proximity switch assays developed for the detection of large (~270 kDa) and small (~14 kDa) protein biomarkers (195, 196). An ongoing issue with two-component biosensors is that they are much less sensitive to the orientation of the recognition element binding domains and the analyte. Although this makes their construction easier, the concentration driven nature means activity is reliant on absolute and relative component concentrations (198). There is a trade-off between background activity from spontaneous fragment re-complementation and limits to the concentration range that is detectable, as fragment concentrations must be kept below the residual K_d (137). Component concentrations must also be controlled to limit hook effects at high analyte concentrations: this is where the two sensor components start binding to two different analyte molecules, omitting the co-localisation of fragments, and diminishing the response.

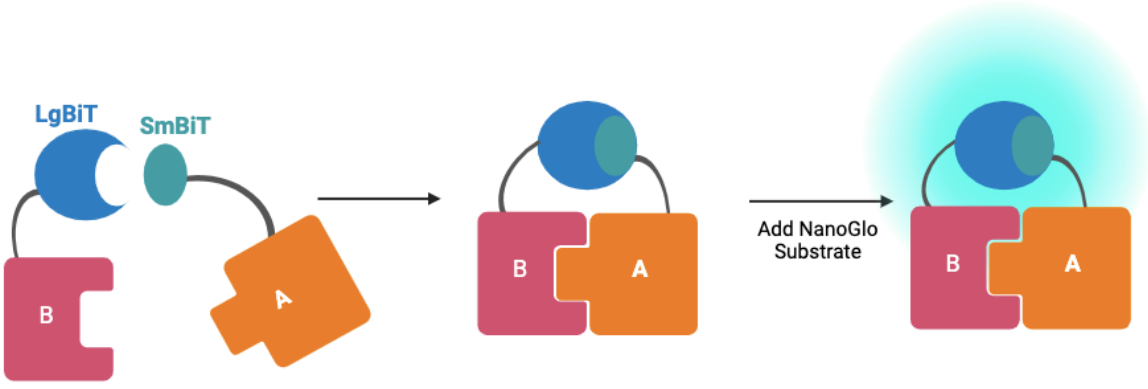

Figure 13. Schematic diagram of the NanoBiT proximity switch, *where target driven co-localisation of the SmBiT and LgBiT fragments results in complementation of the NanoLuc enzyme which emits luminescence with addition of the substrate.*

NanoLuc has also been split into three fragments to create a tri-part split luciferase (179, 186, 192). This involves splitting of NanoLuc into two 11 amino acid β-strand peptides to be fused to recognition elements as chimeric proteins. The use of two smaller peptide reporter fragments improves upon the expression, purification and storage issues commonly seen when creating chimeric proteins with larger more complex reporter proteins. The remainder of the NanoLuc makes up the third component of the switch as a detector protein, or co-operative binder, to limit the hook effect and promote co-localisation (**Figure 14**). Split enzyme systems have the capacity to be used as chimeric protein biosensors with a range of recognition elements facilitating the detection of diverse analytes with diagnostic value.

Figure 14. Schematic of Target Engaged Complementation (TEC) split reporter system for the detection of HER2. *Reprinted from ref (179). Copyright 2017 according to CC-BY license.*

Fluorescent reporter proteins can also be used in proximity switches: this mechanism is known as biomolecular fluorescence complementation (BiFC) (199). Two fragments of a fluorescent protein are inactive apart, therefore do not produce a fluorescent signal. Co-localisation of the two inactive fragments permits reassembly of the fluorescent protein resulting in a readable signal. However, as with enzyme re-assembly, spontaneous self-association of the reporter must be considered as background signal. The use of reporters from the green fluorescent protein (GFP) family in BiFC can be slow and result in irreversible complex formation (200, 201), which make them less suitable for rapid analyte detection. However, other fluorescent proteins have been used for BiFC more successfully.

A protein tag derived from apo photoactive yellow protein (PYP) of *Halorhodospira halophila* has been engineered. The protein tag coined FAST (Fluorescence-Activating and absorption-Shifting Tag) forms fluorescent complexes with 4-hydroxybenzylidene rhodanine (HBR) derivatives (202). FAST was spilt into two inactive loops which maintained some affinity for one another in the presence of HBR derivatives. Fusion of two mammalian binding proteins which interact in the presence of rapamycin resulted in a proximity switch able to image, and measure the presence of rapamycin *in vivo* (203).

A multi-component biosensor to measure aflatoxin B_1 (AFB_1), a small molecule, using a competitive FRET based system has been published (204). Here, two different sized quantum dots (QD) were used. In proximity, energy transfer occurs from the donor QD (emission: 530nm) to the acceptor (emission: 650nm). On the donor QD, multiple AFB_1 molecules were conjugated to the surface. The antibody against AFB_1 was then monovalently conjugated to the acceptor QD. With no AFB_1 present in a sample, the AFB_1 molecule on the donor QD would bind the antibody attached to the acceptor QD, resulting in high FRET and a higher 650nm emission spectrum. If a sample contained AFB_1, less of the donor QD would be in proximity to the acceptor QD, as the monovalent antibody would be bound by AFB_1 in the sample, resulting in a higher 530 nm emission spectrum and a lower 650nm emission spectrum (204).

Small molecule toxins, microcystin and nodularin, have been detected in a capture-detection format using single chain variable fragments (ScFv) recognition elements. A ScFv labelled with Alexa Fluor 680 and a monoclonal antibody labelled with europium enabled the FRET process to occur in the presence of microcystin or nodularin, within a sandwich binding format (205).

1.4 Recognition elements

Recognition elements serve as the molecular recognition component in a biosensor and are a fundamental component of biosensors, playing a pivotal role in their ability to selectively detect and identify specific analytes. These elements are typically biomolecules, such as antibodies, enzymes, nucleic acids (DNA or RNA), or receptors, that possess a high affinity for the target analyte of interest.

The key functions of recognition elements in biosensors include binding to the target analyte with high specificity and affinity, facilitating a transduction event upon binding, and enabling the biosensor to discriminate between the target analyte and other interfering substances present in the sample (78). The choice of recognition element is critical and is determined by the nature of the analyte being detected and the overall design and purpose of the biosensor (206). In conclusion, the binding interaction between the recognition element and the target molecule forms the basis for the biosensor's selectivity and sensitivity, making it a crucial element in the successful operation of the biosensor. A variety of antibody-based and non-immunoglobulin binding proteins will be introduced here, including antibody fragments, nanobodies, Affimer proteins and monobodies, referring particularly to their application within chimeric protein switch biosensors. Other recognition elements such as enzymes and DNA binders – like aptamers – will not be explored in depth as they are outside of the scope of this project.

1.4.1 Antibody based binding proteins.

Antibody-based or immune-based binding proteins are proteins that are derived from the immune system and have the capability to specifically bind to other molecules, often antigens or pathogens that the immune system has been exposed to. There are a variety of antibody-based binding proteins that have diagnostic value as recognition

elements. The characteristics of the most prominent binding proteins within this class are compared in **Table 1**.

Table 1. Overview of the characteristic of antibody-based binders with documented use in chimeric protein biosensors. *Adapted from ref* (207) *Copyright 2021 according to CC-BY license.*

Antibody- based binder	Size	Production	Refs
Antibody	~150 kDa	Hybridoma or recombinant DNA technology & mammalian cell expression	(208, 209)
Fragment Antibody Binding (Fab)	~50 kDa	Proteolysis (e.g., with papain, IdeS, or GingisKHANTM) or recombinant DNA technology and mammalian, yeast, or bacterial cell expression	(210, 211)
Single Chain Variable Fragment (ScFv)	~25 kDa	Recombinant DNA technology and yeast or bacterial cell expression	(212-214)
Nanobodies	~ 15 kDa	Recombinant DNA technology and plant, mammalian, yeast, or bacterial cell expression	(215, 216)

1.4.1.1 Antibodies.

The antibody was first referenced in 1890 by Emil Von Behring and Shabasabura Kitasato who observed that serum transfer between an animal immunized against diphtheria and an animal suffering from it could in effect cure the disease (217). The diagnostic potential of antibodies was introduced in 1896 by George Fernand Isidore Widal who observed the phenomenon of agglutination between antibodies in serum and antigens in bacteria. From this, he devised a test where exposing a patient's blood sample to a suspension of typhoid bacilli could indicate either current infection or prior exposure by visualisation of agglutination with the naked eye (218). Since the late 19th century, a magnitude of data has been obtained on the structure and functions of

antibodies, including the isolation of monoclonal antibodies from polyclonal antibody serum and the Nobel prize winning development of hybridoma cell lines (219). Antibodies are produced from B-cells and are complementary to one antigen (220). Hybridoma cells are a fusion of B-cells, which are short lived, and immortal myeloma cells, resulting in an immortalised antibody producing cell line and, therefore, a maintained source of the selected antibodies (221). Being able to produce antibodies that are highly specific and highly reproducible has paved the way for tests that are both reliable and accurate, revolutionising diagnostic technologies (222).

Antibodies were the first and are still the most utilised recognition elements in immunoassays and biosensors. Antibodies are characteristically ‘Y’ shaped and are approximately 150 kDa in size. Their structure is made up of four chains, two identical heavy chains and two identical light chains, with disulphide bonds linking a light chain to each heavy chain and the two heavy chains together (**Figure 15**) (223). The heavy chains are composed of four regions, three constant regions, and one variable region. The sequences of the heavy chain constant regions determines the class of the Immunoglobulin (Ig) as, IgG, IgD, IgM, IgA or IgE (222). The light chains can be divided into two regions, a constant and a variable region. The antigen binding sites of an antibody lie in the complementarity-determining regions (CDRs). The CDRs dictate the antibody's specificity and are situated in both the variable regions of the heavy and light chains (222). In contrast, the constant regions play a role in influencing the immune response upon antigen binding, referred to as effector functions (224).

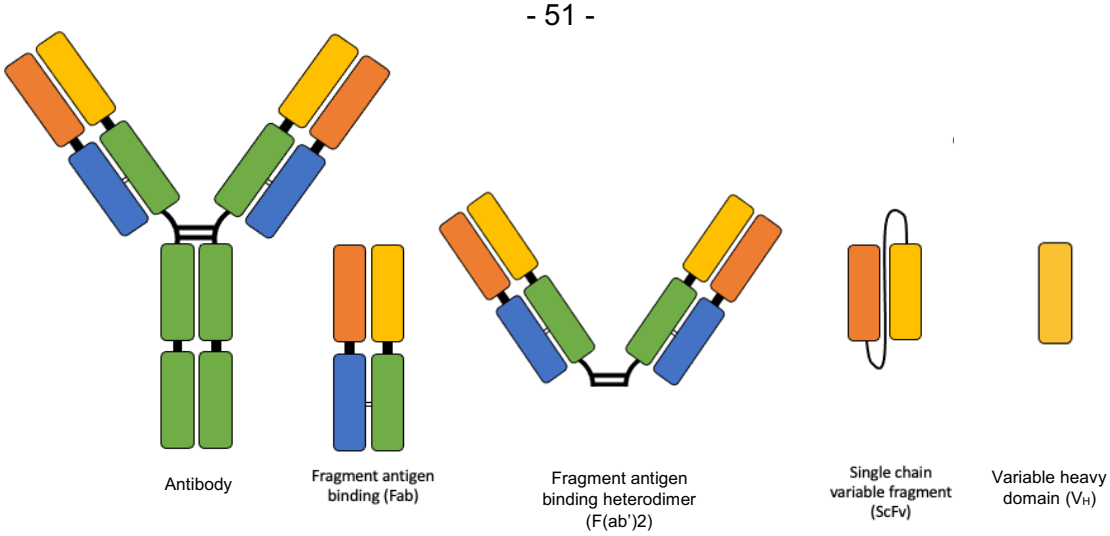

Figure 15. Antibodies and their fragments used as recognition elements for chimeric protein biosensors. *Heavy chain constant domains are depicted in green; light chain constant domains are depicted in blue; heavy chain variable domains are depicted in yellow; light chain variable domains are depicted in orange. Inter-domain disulphide bonds are depicted as double lines between constant regions.*

As the name suggests, the sequences of the constant regions are generally conserved, while the variable regions exhibit significant sequence variability. This diversity in the variable region is essential for specific binding to a wide range of analytes and is a consequence of somatic hypermutation and gene recombination, which are immune processes which occur during the development of B cells in response to foreign antigen exposure (223). This capacity for sequence diversity is what enables the adaptive immune system to effectively react to countless threats to the host organism (225), an ability that is exploited by the biotechnology industry for numerous applications. Antibodies have been used extensively in the development of biosensors, which has been previously reviewed (223, 226-228).

Biosensors rely on the high affinity and specificity of antibodies to the target of interest. These targets include large macromolecules, such as proteins, larger units such as bacteria, or even small molecules (229). Although antibodies serve as the most commonly employed binding proteins, there are constraints and challenges associated with both their utilization and production. Antibodies are typically heat sensitive and for

their stability they require disulphide bonds and glycosylation (230). This complex macromolecular structure makes whole antibodies difficult to express in bacteria, so production is often expensive, requiring the use of mammalian cell culture or animal immunisation (230). Additionally, there are several factors that can result in poor antibody production, including mixed hybridoma cultures, poor downstream testing, or antibodies not working well together in an assay. Poor quality antibodies then raise questions about the reproducibility of antibodies, where researchers have struggled to reproduce results of published papers (231). Thus although the applications for antibodies are vast, an antibody is only as good as the target it is raised against, as well as the validation carried out subsequent to its selection (232).

1.4.1.2 Antibody fragments.

As mentioned, when looking for highly specific and sensitive recognition elements, antibodies have been the gold standard, but have numerous limitations that impede them as effective recognition elements in biosensors, particularly chimeric protein switch biosensors. Chimeric proteins can be engineered at the genomic level or by chemical conjugation of the antibody with the reporter protein. However, as mentioned, bacteria are unable to produce antibodies, and thus chimeric proteins engineered at the genomic level would need to be expressed in mammalian cell cultures. Their large size means that when chimeras are formed by chemical conjugation, a heterogenous chimera sample is obtained, affecting the biosensor's performance. The modularity of antibodies allows for the uncoupling of the domains via genetic or biochemical means, enabling the engineering of simplified custom binders. The uncoupling of antibody domains produces antibody fragments with a variety of domain combinations (**Figure 15**).

The most obvious method of antibody engineering is the separation of the antigen binding fragment (Fab) from the fragment crystallisation (Fc) region to decrease the size of the immunoprotein. Whole antibodies require mammalian expression systems, whereas antibody fragment proteins can be produced using lower-level organism

expression systems, because glycosylation is only necessary when expressing the Fc region. The use of lower-level organism expression systems significantly reduces the manufacturing cost (211). In the wake of antibody engineering, multiple domain combinations have produced an array of immunoglobulin-based binders.

The manipulation of the Fab region of one or more antibodies can create mono- or bi-specific F(ab)'2 which are disulphide-linked dimers of the two light chain dimers. Fabs contain the CDRs of antibody but remove the immune cell recruiting section of them, which is much less relevant in diagnostic and research applications.

Singular Fab regions can be obtained from IgG mAbs via enzymatic digestion with papain. Papain is a nonspecific, thiol-endopeptidase with a sulfhydryl group in the active site which must be reduced for enzymatic activity. Papain digests the upper peptide bonds within the hinge region of IgG, producing three fragments – two Fabs and an Fc region – which can then be separated using protein A resin to isolate the Fabs. In addition to singular Fab regions, monospecific F(ab')2 proteins can also be isolated from IgGs by enzymatic digestion. Pepsin is a nonspecific endopeptidase active in acidic environments; when incubated with an IgG, pepsin degrades the lower peptide bonds of the hinge region producing a single F(ab')2 fragment and numerous small Fc peptides due to extensive degradation of the Fc region. These Fc peptides can be separated from the F(ab')2 by dialysis, ion exchange chromatography or gel filtration (233, 234).

However, these methods do not achieve sufficient purity or yield of monospecific F(ab')2 proteins from all subtypes of IgG molecules for large scale production. An alternative method was developed using papain digestion to produce a mix of Fab, F(ab')2 and whole antibody fragments and then purifying F(ab')2 fragments using Fast Protein Liquid Chromatography (FPLC) on DEAE-Sepharose-FF. This attained F(ab')2 purity of 78% in large-scale production (235).

Further antibody fragments can be obtained from Fabs. Single chain variable fragments (ScFv) contain the heavy chain (V_H) and light chain (V_L) variable domains linked by a flexible amino acid (AA) linker, most commonly glycine and serine rich and ~15 residues long (212) (**Figure 15**). Singular V_H and V_L domains can also be isolated, although producing these as soluble proteins can be difficult due to the naturally occurring hydrophobic interface between the V_H and V_L domains. The introduction of hydrophilic residues into the V_H/V_L interface has shown improvements in solubility and stability of isolated human V_H or V_L domains (236). Many of these fragments can be efficiently selected via affinity selection techniques such as with the construction of phage display libraries, using synthetic, naïve, or immune libraries. Synthetic libraries are built on the genetic framework of an antibody fragment with the introduction of randomised sequences into the CDRs and naïve libraries are constructed with the B-cells of unimmunised donors, both of which do not require animal immunisation. However immune libraries, which require animal immunisation, tend to be more reliable in the generation of high affinity reagents (237-240). Molecular display techniques are discussed in more detail in section 1.4.2.

Production of Fab, ScFv and V_H fragments eliminates the need for glycosylation and therefore removes the need for mammalian expression systems (211). Additionally, the reduced size of the binding protein makes the process of creating a chimeric protein biosensor by genetic fusion easier, as antibody fragments might be easier to express recombinantly with a reporter protein. Despite this simplified structure, Fab fragments, ScFvs and V_H domains still contain disulphide bonds (Fab: 5-6, ScFv: 2, V_H: 1), therefore, an oxidising environment is needed to facilitate native folding of the proteins. Yeasts (*Saccharomyces cerevisiae* and *Pichia pastoris*) are regularly used for the expression of Fab and ScFv fragments. They are the simplest organism that contain an endoplasmic reticulum which aids post translational modifications, such as the formation of disulphide bonds (241).

Production in bacterial systems (*Escherichia coli*) is advantageous during the research stage as it enables fast production of many different biosensing constructs. However, the reducing environment of the cytoplasm prevents intradomain disulphide bonds from forming, meaning antibody fragments produced in the cytoplasm must frequently be refolded from inclusion bodies under oxidising conditions *in vitro* (214). Antibody fragment production can also be directed to occur in the periplasm of *E. coli*, where the environment is oxidising. The volume of the periplasm is much smaller than the cytoplasm and the pathways that secrete proteins from the cytoplasm for folding have a limited capacity, which can become overloaded. This results in lower yields of correctly folded proteins (242). When expressing chimeric protein biosensors that include multiple ScFvs alongside reporter proteins, *E. coli,* in our experience, is not a reliable host for producing soluble, correctly folded proteins. However, the K-12 type strain RV308 (DE3) expresses insoluble protein as inclusion bodies, and demonstrates less degradation of soluble protein compared to *E. coli* strain BL21(DE3) (243). The RV308 host strain provides a cheaper alternative for the expression of antibody fragments as inclusion bodies in the cytoplasm with high-yield expression (213). This does, however, require the development of a successful refolding procedure when expressing genetically fused chimera proteins.

Antibody fragments have shown promise as recognition elements within one component and multi-component protein switch biosensors, with success sensing a range of analytes. One research group has focused on utilising Fab fragments for the detection of the transmembrane protein HER2, an epidermal growth factor receptor (EGFR) overexpressed in HER2+ breast cancer (244). Dixon *et al.* selected a pair of Fab fragments from two monoclonal antibody therapies that target two separate epitopes of HER2 (178). Fab fragments were genetically fused to a “BiT” of the split NanoLuc® luciferase enzyme (Promega) and expressed recombinantly in SHuffle T7 (NEB) competent *E. coli* cells. SHuffle T7 *E. coli* is a commercial strain of *E. coli* which has been

engineered to be deficient in trxB and gor reductases, and contain DsbC in the cytoplasm which creates an oxidising environment, aiding correct disulphide bond formation inside the cell (245). ScFvs have also been used as recognition elements to enable the detection of HER2 in a concentration dependent manner. ScFvs were fused to firefly luciferase fragments and expressed in a cell-free system (193), however, this proved to be less successful for other targets in the same expression system due to the issues with folding of ScFvs.

Alongside detecting large (~185 kDa), multidomain proteins like HER2, the unique binding properties of Fab fragments make them attractive candidates for detecting small molecules. Structural observations of antigen-antibody interactions demonstrate a binding pocket or groove between the variable domains of the light and heavy chain to accommodate small molecular weight haptens or short peptides (246, 247). Xue *et al.* validated the modularity of their Fab based, one component, allosteric switch sensor by targeting three small molecule drugs (154). These luciferase-based indicators of drugs (LUCID) biosensors measure the disruption of bioluminescent resonance energy transfer (BRET) to quantify the analyte at sub micromolar to sub millimolar concentration ranges.

The combination of the V_H and V_L domains in a ScFv permit a binding pocket formation between the domains, also seen within a Fab fragment and whole antibodies. ScFvs are therefore, a good candidate recognition element for detecting small molecules. Within a GUS proximity switch, the sandwich binding pocket created by the V_L and V_H domains of an antibody binding to an analyte allows for the detection of small molecules such as 4-hydroxy-3-nitrophenyl acetyl (NP) and caffeine (176). A time-resolved Förster resonance energy transfer (TR-FRET) proximity switch sensor combines a typical monoclonal antibody with an isolated ScFv raised against the haptotoxin targets nodularin and microcystin. In this instance the ScFv was expressed in *E. coli* K-12 type strain RV308(DE3) with alkaline phosphatase attached (205).

The detection of viruses in clinical samples has also been demonstrated using a chimeric ScFv. Two ScFv fragments, raised against non-overlapping epitopes of the monomeric subunits of avian influenza virus (AIV) nucleoproteins, were conjugated to lanthanide-doped nanoparticles (LnNP) using thiol-maleimide “click” reactions. With both a dual emitting LnNP as a doner and absorbing LnNP, the ScFv-LnNPs create a luminescence resonance energy transfer (LRET) system wherein AIV nucleoprotein can be detected (248). Kang *et al.* also tested the same LRET system with ScFv-Fc conjugates, to determine how the size of antibody fragments effect the activity of the sensor. The addition of the Fc region to the recognition elements, increases the distance between the doner and acceptor which resulted in a 2.57-fold decrease in quenching efficiency, demonstrating the appeal of smaller recognition elements.

Although less commonly used due to the challenges presented during expression, isolated human V_H and V_L have been introduced into protein switch sensors. To detect Osteocalcin a small protein (5.8 kDa) biomarker, V_H and V_L genes derived from an anti-osteocalcin antibody were recombinantly expressed with a tri-part split NanoLuc® luciferase in SHuffle T7 Express lysY *E. coli*. In addition to the recombination of the NanoLuc® enzyme when the components are in proximity, the presence of analyte (osteocalcin) increases the affinity of the V_H and V_L for one another, stabilising the complex (192). Demonstrating that the binding pocket between the variable domains of antibodies is exploitable across antibody fragments.

1.4.1.3 Nanobodies.

Heavy-chain-only antibodies (HcAb) were discovered in 1993 in the sera of camelid species (249). Compared to the standard mammalian immunoglobulin, HcAbs structurally lack any kind of light chain and only have two of the usual three heavy chain constant domains (**Figure 16**). The variable domain of each heavy chain contains three CDRs for antigen recognition. Although they contain only 50% of the binding loops found in IgGs, HcAbs have comparable affinity (250). Not long after their discovery, the variable

domains of HcAbs were isolated and coined V_HH (**Figure 16**). HcAbs have also been observed in the sera of elasmobranchs, known as the immunoglobulin new antigen receptor (IgNAR) (251). These homodimeric HcAbs differ from the camelid HcAbs by three extra constant domains on each chain of the native immunoglobulin (**Figure 16**). The isolated variable domains (V_{NAR}) also differ slightly, with 2 CDRs (CDR1 and CDR3), and two smaller hypervariable regions (HV2 and HV4) in place of CDR2. V_{NAR} domains can be further categorised into four isotypes based on the position and number of non-canonical cysteine residues (252). The collective term for V_HH and V_{NAR} domains is nanobodies or single domain antibodies (SdAbs). Alongside the high affinity binding and small size (12-15 kDa), the lack of a hydrophobic V_H/V_L domain interface makes them more soluble, another desirable trait for protein engineering. Nanobodies are commonly selected through immune libraries. This involves the immunisation of camelid or shark species, followed by the removal of peripheral blood lymphocytes, extraction of RNA from B-cells, and subsequent synthesis of cDNA. Further selection and affinity maturation of nanobodies can then occur via phage display, see section 1.4.2. Yeast and bacterial display have also been used for this purpose (253). Nanobodies have been championed for their expression in bacterial systems, however, reports of chimeric proteins involving nanobodies typically use mammalian or yeast expression systems to aid proper folding (216). In our experience, bacterial hosts do not have the machinery necessary to produce soluble proteins when working with multi-domain chimeric proteins containing V_HH or V_{NAR} domains. Bacterial expression of chimeras with nanobodies is possible, but may need to rely on refolding from inclusion bodies to successfully produce pure proteins (215).

The stability and size of nanobodies has made them versatile tools in developing biosensors. Two V_HHs raised against non-overlapping epitopes of the ectodomain of EGFR (~190 kDa dimer) have been conjugated to semiconductor quantum dot nanocrystals (QD) or terbium (Tb) via bioconjugation techniques. Due to the distance

dependence of this detection system, the use of small V_HH domains is advantageous compared to conventional antibodies. V_HH domains can also be used in protein switch biosensors for small molecule recognition. Dimerised V_HH domains form a binding pocket for small molecules, as seen in ScFvs and Fab fragments. Hapten-induced dimerization of V_HHs provides a 2:1 binding stoichiometry for small molecules, demonstrated in a sensor for caffeine (176, 254).

So far there is little published research utilising V_{NAR} domains as chimeric protein biosensors, with most work focusing on their binding properties in analytical assays such as ELISAs, *in vivo* diagnostic imaging, and their potential as therapeutic agents. But their potential value in PoC diagnostic settings has been well documented in reviews (252).

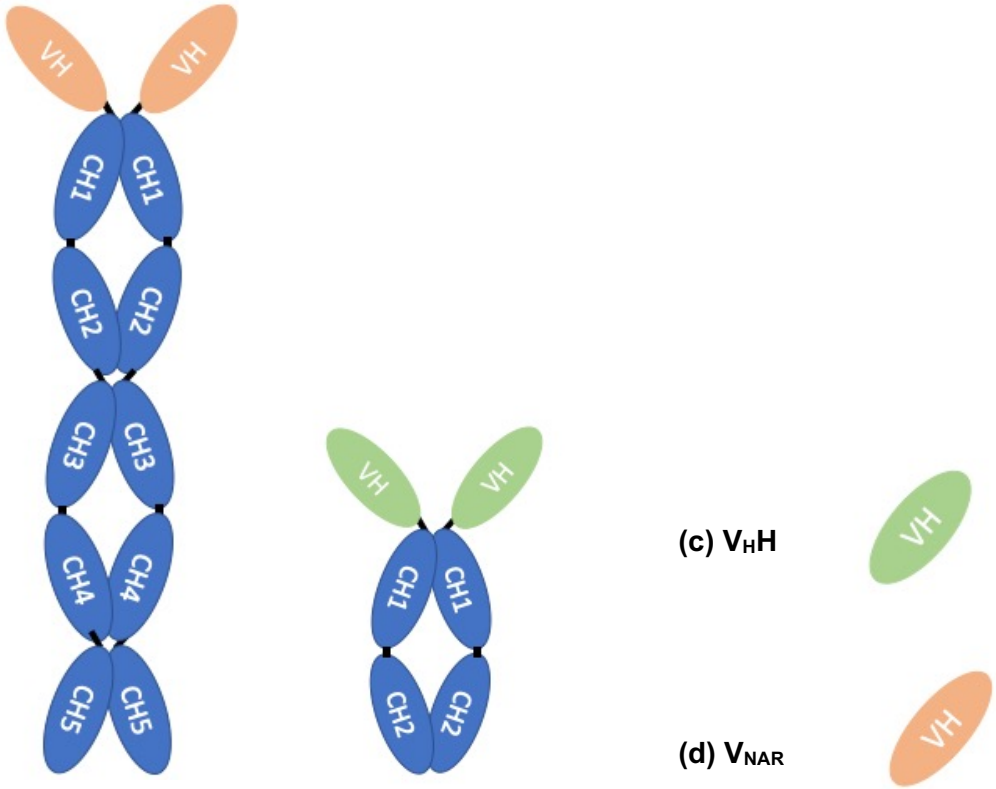

Figure 16. Single domain antibodies (sdAb) can be isolated from shark and camelid single chain antibodies. *(a) Heavy chain-only shark antibody consisting of 5 heavy constant domains and 1 variable domain per chain, also known as an Immunoglobulin new antigen receptor (IgNAR). (b) Heavy chain-only camelid antibody consisting of 2 constant domains and 1 variable domain per chain. (c) Isolated camelid variable fragment, coined V_HH. (d) Isolated variable fragment of the shark antibody known as a V_{NAR}.*

1.4.2 Non-immunoglobulin binding proteins

Antibody mimetics or non-immunoglobin binding proteins are small, single domain binding proteins that are made up of a conserved scaffold region and a synthetically engineered variable region. Without the natural immune system to rely upon, antibody mimetics with high specificity for analytes need to be selected from protein libraries in the lab with display methods (255, 256). There are several display methods available for selecting proteins with the desired affinity to analytes of interest. Display methods refer

to the presentation of recognition element variants, most commonly proteins, to select binders against a target analyte. The most commonly used display method, phage display, uses bacteriophages that contain the recognition element as a fusion with a coat protein, thus presenting the recognition element on the coat of the phage, while retaining the genetic information that encodes that protein within the phage genome. Where in antibody production diversity is produced through somatic hypermutation and gene recombination, diversity in libraries of other protein scaffolds is introduced synthetically. DNA plasmid libraries coding phage containing different recognition element variants are transformed into *E. coli,* which then produce the phage library. The analyte of interest is immobilised onto a surface and the phage library is introduced. Phages presenting recognition elements that bind to the target analyte are identified through panning. Non-binders are washed away, whilst binders are eluted, transformed into *E. coli* and the process is repeated over a number of rounds of affinity selection known as “panning” rounds (**Figure 17a**). Binders are then sequenced, produced, and characterised, before introduction into a biosensor detection system. Other display methods utilise cell surface expression of the target analyte in yeast and bacterial cells, and more recently methods that use RNA-templates, such as ribosome display, have been developed that work completely *in vitro*. They all follow the general concept of converting genetic material into the protein phenotype to select proteins with affinity to a target analyte (**Figure 17b**). There are in-depth reviews of the molecular display techniques available for selecting binding proteins (257, 258).

The standard scaffold structure of mimetic binding proteins allows for genetic randomisation of the variable regions, providing a diverse selection of binding proteins with target specificity and high affinity. In addition, desirable protein scaffolds can be selected based on other criteria that ensure downstream utility is optimal. Lower molecular weight, cysteine-free, structures are typically selected to try to ensure that binding reagents are easy to manufacture recombinantly in simple heterologous

expression systems (137, 256, 259). Many non-immunoglobulin binding proteins have been developed (255), and only a selection will be further explored here as recognition elements in chimeric protein switch biosensors. The characteristics of these non-immunoglobulin binding proteins are compared in **Table 2**.

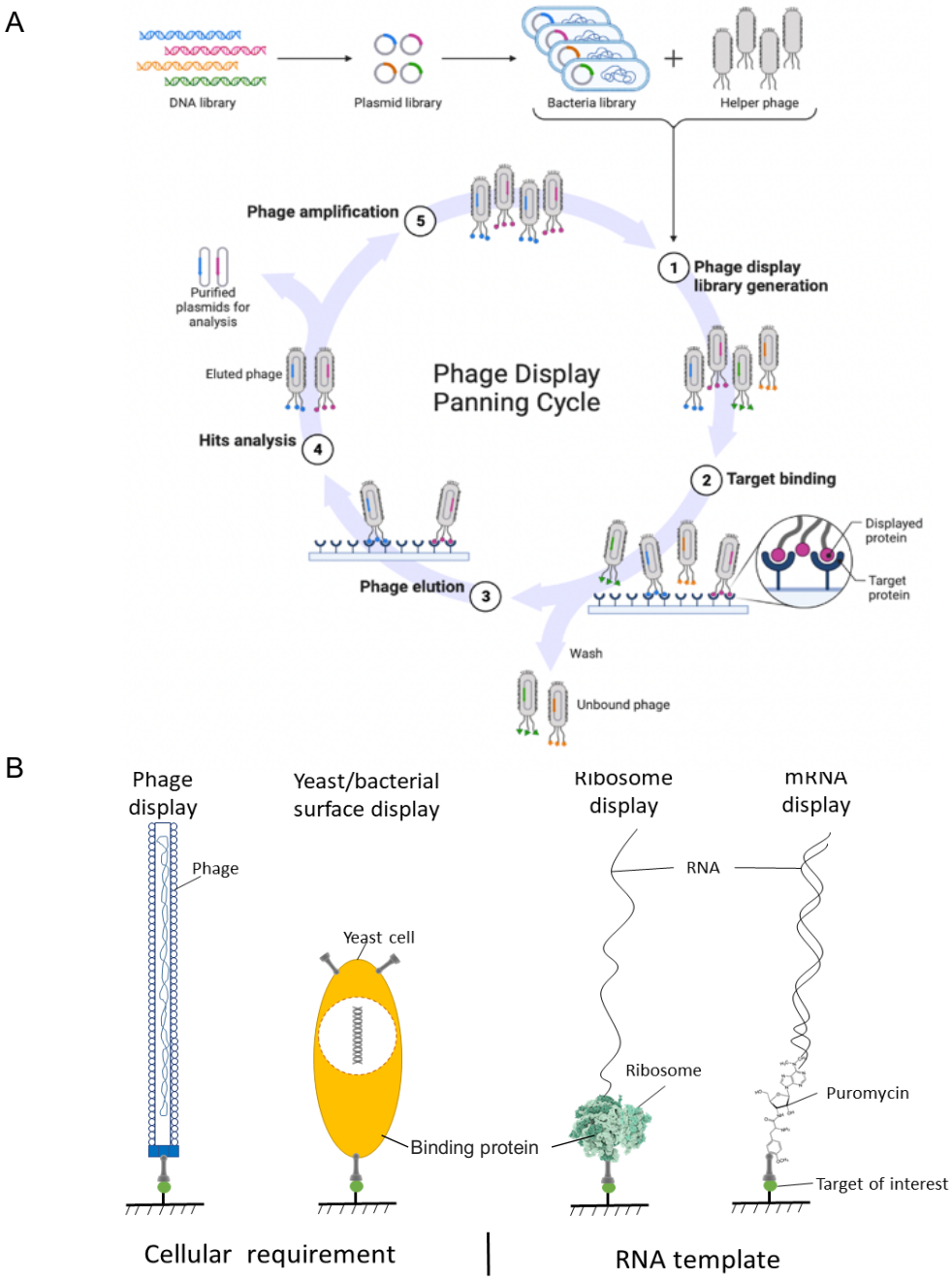

Figure 17. Panning methods for the selection of binding proteins. ***A****: Example phage display panning cycle. Phage libraries presenting recognition element variants are introduced to the immobilised target analyte, high-affinity binders are kept, whilst low-affinity and non-binders are washed away. Binders are eluted and amplified, and the panning cycle is repeated. Image from BioRender.com.* ***B****: Example molecular display methods used for peptide selection. Phage display is the most well-known and commonly used technique. Other display techniques such as cell surface display and RNA-based display are being developed for the discovery of new binding proteins.*

Table 2. Overview of the characteristics of a small selection of non-immunoglobulin binders that have been used as recognition elements in chimeric protein biosensors. *Adapted from ref (207) Copyright 2021 according to CC-BY*

Non-immunoglobulin binder	Size	Scaffold	Production	Refs
Affimer	~12-14 kDa	Cystatin	Phage display and bacterial expression	(260-262)
DARPins	~14-18 kDa	Ankyrin repeats	Phage or Ribosome display and bacterial expression	(263, 264)
Monobodies	~10 kDa	Human fibronectin type III domain	Phage or yeast display and bacterial expression	(265, 266)

1.4.2.1 DARPins.

One such mimetic protein type is designed ankyrin repeat proteins (DARPins) which are derived from the naturally occurring binding proteins – ankyrin repeat proteins (263). Randomisation of the 7 variable amino acids per repeat unit results in large DARPin libraries for selection purposes (267). The small size of DARPins (14-18 kDa) alongside the absence of disulphide bonds make them ideal candidates for bacterial expression with limited aggregation (264), more so than those derived from immune proteins. This, together with high affinity binding properties, make DARPins an ideal candidate for the design of chimeric protein biosensors.

The value of DARPins as recognition elements in chimeric protein switch platforms has been displayed in a combinatorial use with Fab fragments by Dixon *et al.* to detect Human Epidermal Growth Factor 2 (HER2) with a split enzyme proximity switch (**Figure 14**) (179). Further work by this group included screening of several pair combinations of V_HH, Fab and DARPin proteins raised against EGFR and HER2 to determine which two recognition elements could best detect EGFR-HER2 dimerisation (187). A DARPin pair against separate epitopes of the EGFR-HER2 dimer outperformed all other binding protein pairs in the tri-split NanoLuc proximity switch. However, another chimeric protein

switch sensor designed with ß-lactamase as a reporter and DARPin proteins as the recognition element noted that the affinity of the DARPin for its analyte decreased by 1000-fold when fused to a reporter (168).

1.4.2.2 Monobodies.

Another example of antibody mimetic binders with the potential to be implemented as recognition elements are monobodies. Monobodies are built on a scaffold of human fibronectin 10th type III domain, which function as ligand binding domains in nature (265, 266). With display-based selection processes, monobodies have been developed against several target analytes such as kinase domains implicated in human health and disease (268, 269), the SARS-CoV2 spike protein (270), tumour biomarkers (271) and monoclonal antibodies (272). The majority of work surrounding the use of monobodies has so far been focused on therapeutics and *in vivo* diagnostics as imaging probes (271). However, monobodies possess the desirable properties to be used as recognition elements within chimeric protein biosensors. Recently they have been implemented into a domain inserted one-component protein switch sensor for multiplexed live-cell imaging of proteins involved in cell division pathways and indicated in cancer. Three distinct monobodies were inserted into the surface loop of fluorescent proteins to create Adaptable, Turn-On Monobody (ATOM) fluorescent biosensors (273). Monobodies have also been developed into allosteric protein switches using the Alternate Frame Folding (AFF) technique. AFF involved duplicating a fraction of the monobody sequence at either the carboxy (C) or the amino (N)-terminus. This provides the opportunity for the monobody to fold into its native structure or an alternative structure to bind the analyte of interest (274). By attaching donor and acceptor fluorophores to the N and C-terminus respectively, FRET measurements can be used to determine if the alternative folding (no analyte) or the native folding (analyte bound) has occurred (**Figure 18**) (275).

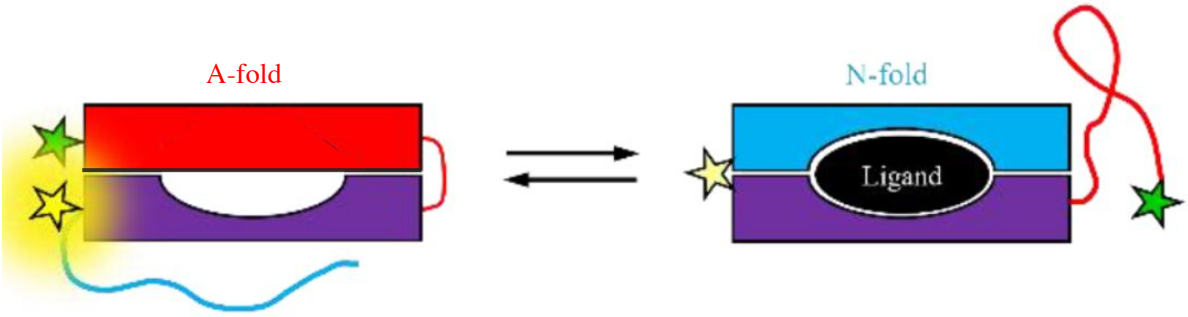

Figure 18. Design of monobody – AFF protein switch sensors. *Binding of the ligand (black oval) shifts the population from the A-fold (alternative fold) to the N-fold (native fold), resulting in a loss of FRET efficiency as the donor fluorophore (green star) and acceptor fluorophore (yellow star) move apart. Adapted from Ref (275) Copyright 2022 according to CC-BY-NC-ND 4.0 International license.*

1.4.2.3 Affimers

Affimer binding proteins are another group of antibody mimetic binders based on a cystatin scaffold, with two hypervariable loops for high affinity binding (262). The 'consensus concept' (276) was used to improve the thermostability of the cystatin to produce the synthetic Adhiron scaffold, resulting in a scaffold thermal stability of Tm=101˚C (262). Affimer proteins are selected against specific targets through phage display (260, 261), with numerous examples published (262, 277-280). Affimer proteins are small proteins (~12 kDa) without cysteines or disulphide bridges in the scaffold structure. Like DARPins, this makes them easy to express in *E. coli* and allows for both site-specific labelling (262), and inclusion in large multi-domain protein switches without misfolding and aggregation complications (170). Although Affimers can be raised against small molecules (262), Affimers against macromolecules typically have a higher affinity. Affimers have been implemented into both one component and multicomponent biosensors for the detection of antibodies, protein biomarkers and viral proteins (170, 195).

1.5 Project Aims

The main aim of this project is to explore the use of different recognition elements and switching mechanisms within chimeric protein switch biosensors fused at the genomic level. To achieve this, I will:

- Compare switching mechanisms in the context of chimeric protein switch biosensors for therapeutic drug monitoring (TDM) of monoclonal antibodies (TmAb).
- Use Affimer proteins to develop one-component and multi-component chimeric protein switch biosensors and analyse their suitability as a platform for TDM of TmAb.
- Investigate the practicality of using antibody fragments, specifically nanobodies, as recognition elements within chimeric protein switch biosensors.

Overall, this study will aid the understanding of chimeric protein switch biosensor development and explore the challenges faced when introducing novel binding proteins into biosensor systems.

2 Chapter 2: One component modular allosteric enzyme-inhibitor switch biosensor for therapeutic drug monitoring of immunotherapies.

2.1 Abstract

Therapeutic monoclonal antibodies (TmAb) have emerged as effective treatments for a number of cancers and autoimmune diseases. However, large interpatient disparities in the pharmacokinetics of TmAb treatment requires close therapeutic drug monitoring (TDM) to optimise dosage for individual patients. Here we demonstrate an approach for achieving rapid, sensitive quantification of two monoclonal antibody therapies using a previously described enzyme switch sensor platform. The enzyme switch sensor consists of a β-lactamase – β-lactamase inhibitor protein (BLA-BLIP) complex with two anti-idiotype binding proteins (Affimer proteins) as recognition elements. The BLA-BLIP sensor was engineered to detect two TmAbs (trastuzumab and ipilimumab) by developing constructs incorporating novel synthetic binding reagents to each of these mAbs. Trastuzumab and ipilimumab were successfully monitored with sub-nM sensitivity in up to 1% serum, thus covering the relevant therapeutic range. Despite the modular design, the BLA-BLIP sensor was unsuccessful in detecting two further TmAbs (rituximab and adalimumab), an explanation for which was explored. In conclusion, the BLA-BLIP sensors provide a rapid biosensor for TDM of trastuzumab and ipilimumab with the potential to improve therapy. The sensitivity of this platform alongside its rapid action would be suitable for bedside monitoring in a point-of-care (PoC) setting.

2.2 Introduction

Detection of antibodies has high diagnostic value and can indicate many disease states including autoimmune disorders, allergies and infectious disease (281-283).

Furthermore, the growing market of immunotherapies has provided a new purpose to antibody detection: therapeutic drug monitoring (TDM). This type of monitoring is usually seen alongside any drug treatments that have severe adverse reactions (SARs) and a narrow therapeutic window (284). Anticoagulant, immunosuppressive and cytotoxic drugs are among those that need vigilant monitoring (285-287). Monoclonal antibody (mAb) therapies are generally used as immunosuppressive or immune targeting agents in the treatment of autoimmune diseases and certain cancers (288-290). Although therapeutic mAbs (TmAbs) are generally well tolerated, SARs have been observed (**Table 3**) – attributed to their promiscuous pharmacological profile and the abundance of target receptors throughout the body (291, 292). Interpatient variability of TmAb pharmacokinetics plus an association between inadequate serum mAb concentration and lack of therapeutic response means that TDM is necessary (293). Monitoring of trough concentrations of ipilimumab between dosages has improved survival of metastatic melanoma patients by preventing drug concentrations from dropping too low (294).

Table 3. Profiles of four mAb therapies and their associated side effect.

Trastuzumab – a recombinant IgG1 kappa, humanized monoclonal antibody that binds to the extracellular domain of HER-2. Used to prevent excessive activation of proliferation pathways (Ras/Raf/mitogen-activated protein kinase (MAPK)) which lead to tumour growth. Adalimumab is a fully human, recombinant IgG1 kappa monoclonal antibody that inhibits TNF-α interacting with p55 and p75 cell surface TNF receptors, inhibiting downstream inflammatory pathways overly activated in autoimmune disorders. Rituximab is a chimeric human/murine IgG1 kappa monoclonal antibody which mediates B-cell lysis via complement dependent cytotoxicity (CDC) and/or antibody dependent cell-mediated cytotoxicity (ADCC). The exact mechanism is still unclear (295). Ipilimumab is a fully human, recombinant IgG1 kappa monoclonal antibody that inhibits CTLA4 which activates anti-tumour immunity and sustains T-cell activity (289).

TmAb name (Brand Name)	***Target***	***FDA approval***	***Indications for use***	***Adverse effects***	***Ref***
trastuzumab (Herceptin)	Human epidermal growth factor receptor 2 (HER2)	1998	HER2-positive breast carcinoma	Cardiotoxicity with anthracycline Pulmonary toxicity Hypomagnesaemia	(244)
adalimumab (Humira)	Tumour necrosis factor-α (TNF- α)	2002	Rheumatoid arthritis Ankylosing spondylitis Crohn's disease Ulcerative colitis	Anaemia, leukopaenia & thrombocytopaenia Malignancy, lymphoma & lymphoproliferative disorders	(296)
rituximab (Rituxan)	CD20 on B cells	1997	Follicular non-Hodgkin's lymphoma CD20 diffuse large B cell non-Hodgkin's lymphoma	Cytokine release syndrome Tumour lysis syndrome Serum sickness Progressive multifocal leukoencephalopathy	(295)
ipilimumab (Yervoy)	Cytotoxic T lymphocyte antigen 4 (CTLA4)	2011	Advanced renal cell carcinoma Metastatic melanoma Metastatic colorectal cancer	Enterocolitis Erythematous Pruritus Inflammatory hepatitis Hypophysitis	(289)

The most commonly used methods of TDM currently in clinical use are the fluorescence polarization immunoassay (FPIA), liquid chromatography–tandem mass spectrometry (LC-MS/MS), enzyme immunoassay (EIA), and enzyme linked immunosorbent assay

(ELISA) (297-299). Although highly sensitive and specific techniques, the lengthy time to results (>2.5 hours) makes them inadequate platforms for frequent TDM. A rapid point-of-care (PoC) platform would facilitate constant monitoring of therapeutic mAb titres so dose adjustments can be made to improve efficacy and quality of life (300).

Allosteric enzyme switches provide a rapid platform for enzyme linked detection of clinically relevant proteins (137, 168, 170, 301, 302). A protein switch incorporating ß-Lactamase (BLA) and its inhibitor protein (BLIP) has previously been shown to produce a readable signal within 15 minutes, in response to target driven disruption of a linked enzyme-inhibitor complex, where binding of both recognition elements results in a conformational change within the sensor (**Figure 19**). Initial BLA-BLIP designs used anti-Haemagglutinin mAb peptide epitopes as binding moieties (169). Linker 1 (L1) and linker 3 (L3) anchor the two recognition elements to BLA or BLIP, respectively. These linkers need to be short enough to aid the disruption of the enzyme-inhibitor complex, but long enough to not impair folding of the protein domains. Linker 2 (L2), in contrast, needs to be sufficiently long to allow the recognition elements to bind both variable regions of the TmAb. Point mutations were made at the interface of BLA (E104D) and BLIP (E31A) to weaken their interaction (170), facilitating dissociation of the complex in response to binding of both recognition elements. The addition of a chromogenic compound, hydrolysed by BLA, allows the activity of the enzyme to be determined by measuring light adsorption at 551 nm, which directly corresponds to the concentration of analyte.

Utilising the modular design of the BLA-BLIP enzyme switch sensor, it was recently shown that biomarker proteins can be detected down to pM concentrations when using non-immunoglobin binding proteins, Affimer proteins, as recognition elements (170). Affimer proteins (~12 kDa) are a class of non-immunoglobulin binders built on a cystatin scaffold with two highly variable regions that mediate molecular recognition (262). These are particularly well suited to use in this type of system due to their small size and

stability, making them easy to express within a multidomain construct. Affimers were introduced in detail in section 1.4.2.3.

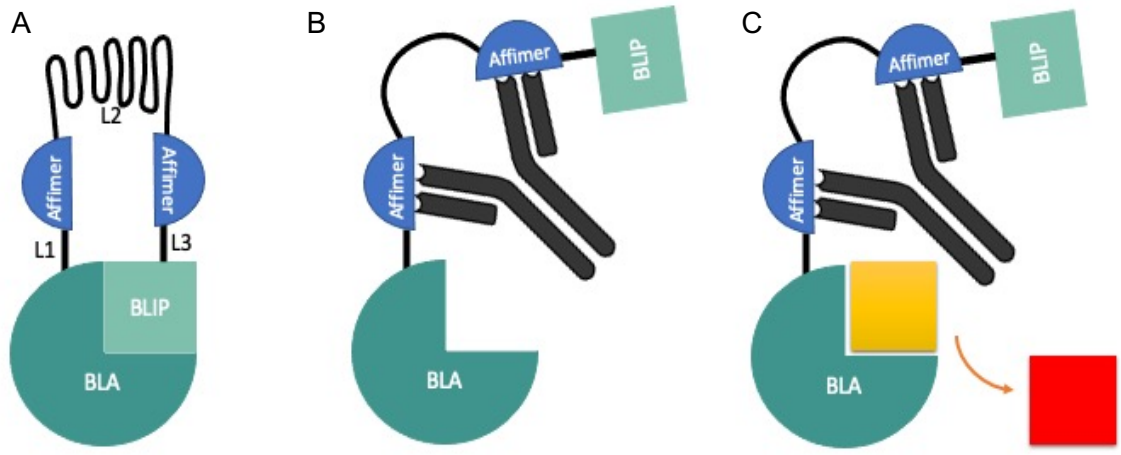

Figure 19. The mechanism of detection by which BLA-BLIP senses monoclonal antibodies in a 1-pot, wash free assay. *(A) The BLA-BLIP sensor in its closed state with ß-lactamase inhibitor protein (BLIP) associated with the enzyme (BLA). Affimer proteins are attached to the enzyme and inhibitor via rigid (L1 & L3) and semi-flexible (L2) peptide linkers. (B) Introduction of the analyte to the assay allows specific binding of the recognition elements to the mAb paratopes causing a conformational change in the enzyme switch sensor. BLA and BLIP dissociate from one another and the active site of BLA is free. (C) Nitrocefin is added to the assay solution and hydrolysed by the active BLA causing a colorimetric reaction from yellow to red. The change in absorbance measurement directly corresponds to the amount of free BLA and ergo the concentration of analyte.*

Trastuzumab (Herceptin), a TmAb used in the treatment of HER2+ breast carcinoma, has previously been detected using the BLA-BLIP enzyme switch sensor with anti-idiotypic (anti-ID) Affimer proteins (244). Here, this work was expanded by determining technical challenges when this platform is adapted to other TmAb, providing a critical understanding of the requirements when this approach is more broadly applied (303). Including trastuzumab, all four TmAbs targeted (trastuzumab, ipilimumab, rituximab & adalimumab) are currently in clinical use for a range of treatments (**Table 3**).

2.3 Methods

2.3.1 Materials

All restriction enzymes, buffers and cloning reagents were purchased from New England Biolabs LTD (NEB, Hitchin, UK), unless otherwise specified. All chemicals and reagents used were of analytical grade and purchased from Melford Biolaboratories Ltd. (Ipswich, UK) or Sigma Aldrich (Missouri, USA) unless otherwise specified.

2.3.2 Generation of TmAb specific BLA-BLIP enzyme switch constructs

All primers (Integrated DNA Technologies) used for cloning can be found in **Appendix A: Primer tables**. Anti-idiotype Affimer® proteins raised against trastuzumab, ipilimumab, adalimumab and rituximab have been reported (303). Restriction cloning was used to introduce these anti-ID binding reagents into the sensor construct vector (based on the expression vector pET28a), as described previously by Adamson *et al.* (170). All DNA was purified using the Illustra GFX PCR DNA and Gel Band Purification Kit (GE Healthcare). Subcloned vectors were transformed into competent *Escherichia coli* XL-1 cells (Agilent Technologies) (genotype: recA1 endA1 gyrA96 thi-1 hsdR17 supE44 relA1 lac [F´ proAB lacIq ZΔM15 Tn10 (Tetr)). Charge Switch Pro Plasmid Miniprep Kit (Invitrogen) was used for all plasmid DNA purification and successful sub-cloning was confirmed by gene sequencing of the full sensor constructs (GeneWiz) (sequences available **in Appendix C: DNA and Protein Sequences**).

2.3.3 Expression and purification of TmAb specific BLA-BLIP sensor constructs

All sensor constructs were expressed and purified using the protocol previously detailed (170). Briefly, plasmids containing the sensor constructs were transformed into *E. coli* BL21 (DE3) competent cells (Genotype: fhuA2 [lon] ompT gal (λ DE3) [dcm] ΔhsdS λ DE3 = λ sBamHIo ΔEcoRI-B int:⍉lacI::PlacUV5::T7 gene1) i21 Δnin5.). 500 mL LB media (with 50 μg mL^{-1} kanamycin) was inoculated with a 10 mL starter culture and

grown at 37°C, 220 rpm. At OD_{600} ~0.6, cultures were induced with 0.3 mM isopropylβ-D-thiogalactoside (IPTG) and grown overnight at 15°C, 150 rpm. Cells were harvested at 4000 *g* for 10 minutes and the periplasmic protein extracted by osmotic shock. The cell pellet was resuspended in 15 ml TSE buffer (30 mM Tris, 20 % w/v sucrose, 1 mM EDTA, pH 8) and placed on a roller mixer at 4°C for 15 min. Cells were pelleted at ca. 17000 ×*g* for 20 min and the supernatant retained as periplasmic fraction 1 (P1). The pellet was resuspended in 15 ml of ice cold 5 mM $MgSO_4$ and placed on a roller mixer at 4°C for 20 min. Cells were pelleted at ca. 17000 ×*g* for 20 min and the supernatant retained as periplasmic fraction 2 (P2). Fractions P1 and P2 were combined, adjusted to 50 mM Tris, 150 mM NaCl, 20 mM imidazole, pH 7.4 by addition of small amounts of concentrated stock solution. The sensor construct was batch purified with Super Ni-NTA resin (Generon) via the N-terminal 6xHis tag. The resin was washed thrice with 20 ml wash buffer (50 mM Tris, 150 mM NaCl, 20 mM imidazole, pH 7.4) and protein eluted with 4 X 500 µl elution buffer (50 mM Tris, 150 mM NaCl, 250 mM imidazole, pH 7.4). Eluates were pooled and further purified via the C-terminal Strep-II tag using the Strep-Tactin spin column kit (IBA). The double tag purified protein was buffer exchanged into storage solution (50 mM Tris, 150 mM NaCl, pH 7.4) using Zeba spin desalting columns (Thermofischer). Protein concentration was determined by BCA assay and purity checked via 12.5% SDS-PAGE (**Figure 21**). Aliquots were stored at -80°C.

2.3.4 Characterisation of sensor functionality

2.3.4.1 Targets

mAb biosimilars (Invivogen) that the anti-ID Affimer® proteins were raised against were used as antibody targets, as follows: Anti-HER2Tra-hIgG4 (trastuzumab), Anti-hTNF-a-hIgG1 (adalimumab), AntihCTLA4-hIgG1 (ipilimumab) and Anti-hCD20-hIgG4 (rituximab). For the purposes of this work, they will be referred to by name of the TmAb.

2.3.4.2 ELISA

40 µl of 20 µg mL^{-1} mAb in PBS (137 mM NaCl, 2.7 mM KCl, 8 mM Na_2HPO_4, 2 mM KH_2PO_4, pH 7.4) was adsorbed onto a Nunc Maxisorb microtiter plate for 1 h at 20°C. After washing thrice with PBST (137 mM NaCl, 2.7 mM KCl, 8 mM Na_2HPO_4, 2 mM KH_2PO_4, 0.1%Tween-20, pH 7.4), wells were blocked with casein blocking buffer (Sigma-Aldrich) diluted 1:10 in PBST for 1 h and washed thrice with PBST. 40 µl of 10 µg mL^{-1} sensor (diluted in casein block) was applied to the plate for 1 h and washed with PBST before adding 25 µl 1 µg mL^{-1} Streptactin-HRP (IBA) in casein block for 1 h. Wells were washed 6 times before adding 50 µl 3,3′,5,5′-Tetramethylbenzidine (TMB) (Sigma-Aldrich) to the plate and incubated for 15 minutes at 20°C. Absorbance was measured at 650 nm on a plate reader (MultiSkan FC, Thermo Scientific).

2.3.4.3 BLA-BLIP Assay

For all enzyme activity assays, non-binding-surface 96-well plates (Corning) were used, with a final volume of 200 µl assay buffer (50 mM sodium phosphate, 100 mM NaCl and 1 mg mL^{-1} BSA, pH 7). 2 nM of sensor were incubated with serial dilutions of their TmAb target for 15 minutes. Nitrocefin (Merck) was added at 50 µM and absorbance measured at 551 nm on a plate reader (MultiSkan FC, Thermo Scientific) after 10 minutes. Sensor and substrate concentrations, and incubation times were identical for all nitrocefin assays performed. A four-parameter logistic (4PL) regression was fitted to dose response curves using GraphPad Prism 9 software. Limit of detection (LoD) was calculated using the equation:

$$LoD = mean\ blank + 1.645(SD\ blank) + 1.645(SD\ low\ conc.test) \quad (163).$$

SD blank refers to the standard deviation calculated when no analyte is present and *SD low conc. Test* refers to the standard deviation calculated at the lowest concentration of analyte tested, in this instance 1 pM.

When measuring the activity of an enzyme, correcting background interference is commonplace with a no-analyte measurement used as a baseline (304). The fold-activity gain of the sensor with target compared to without was calculated using:

$$\frac{\mathrm{A}_{551}(target, t = 10) - \mathrm{A}_{551}(target, t = 0)}{\mathrm{A}_{551}(zero\ target, t = 10) - \mathrm{A}_{551}(zero\ target, t = 0)} = \frac{\Delta\mathrm{A}_{551}(\mathrm{target})}{\Delta\mathrm{A}_{551}(\mathrm{zero\ target})}$$

where A_{551}(target) refers to absorbance measured at each concentration of analyte, A_{551}(zero target) refers to the absorbance when no analyte is present, and *t* refers to the time (minutes) of the measurement.

For experiments testing stability in serum, pooled human serum (Clinical Trials Laboratory Services Ltd) diluted in assay buffer to the following: 0%, 1% or 10% (v/v), was spiked with serial concentrations of trastuzumab or ipilimumab.

2.3.5 Cloning of cysteine residues onto anti-ID Affimer® proteins

Cysteine residues were cloned onto the C-terminus of all anti-ID binding reagents for maleimide biotinylation to facilitate Streptavidin HRP detection within the bridge ELISA format. Anti-ID Affimer® protein DNA was amplified with primers to introduce C-terminal cysteine residues (**Table A 4**) as previously described (305) and transformed into competent BL21Star™ (DE3) (genotype: F- ompT hsdSB (rB-mB-) gal dcm rne131).

2.3.6 Production and purification of anti-ID Affimer® proteins

Affimer® proteins were produced as previously described (303). Cells from a 50 mL culture were harvested by centrifugation at 4000 $\times g$ for 15 minutes re-suspended in 1 mL lysis buffer (50 mM NaH_2PO_4; 300 mM NaCl; 30 mM Imidazole; 10% Glycerol; pH 7.4) supplemented with 0.1 mg mL^{-1} Lysozyme (Sigma-Aldrich, USA); 1% Triton X-100; 10 U mL^{-1} Benzonase® Nuclease (Merck, Germany); 1x Halt protease inhibitor cocktail. The solution was transferred to a microcentrifuge tube and incubated at 20°C for one hour on a Stuart SB2 fixed speed rotator. The lysate was heat-treated at 50°C for 20

minutes in a water bath and centrifuged at 16000 ×*g* for 20 minutes to remove cell debris and insoluble, heat denatured proteins. For each Affimer® protein, the supernatant from the lysed cells was incubated with Ni-NTA resin for 1 hour on a rotator at 20°C. The resin was washed with wash buffer (50 mM NaH_2PO_4; 500 mM NaCl; 20 mM Imidazole; pH 7.4). Affimer® protein was eluted from the resin with elution buffer (50 mM NaH_2PO_4, 500 mM NaCl; 300 mM Imidazole; 20% Glycerol; pH 7.4). All eluted samples were run on a 15% SDS-PAGE gel to monitor the purity of the protein (**Figure 27**).

2.3.7 Biotinylation of anti-ID Affimer® proteins

Prior to biotinylation of the Affimer® proteins, they were desalted and exchanged into PBS using Zeba Spin Desalting Columns, 7K MWCO (Thermo Fisher) according to the manufacturer's instructions and then diluted down to 0.5 mg mL^{-1} in PBS. Potential disulphide bonds were reduced with TCEP disulphide-reducing gel according to manufacturer's instruction (ThermoFisher Scientific). Cys-Affimer® proteins were then biotinylated as previously described (305), final concentration of the biotinylated Affimer® proteins were determined using the adsorption at 280 nm (A_{280}) using a DS-11 Nanodrop spectrophotometer and using a BCA protein assay (306).

2.3.8 Bridge ELISA

A Nunc Maxisorb 96-well plate was first coated with capture Affimer® protein (1 µg mL^{-1}) and incubated for 1 hour at 20°C. After washing thrice with PBST (0.2% Tween-20), 50 µL casein blocking buffer (1:10 in PBST) was incubated in each well for 1 hour at 20°C, followed by washing thrice with PBST. Increasing concentrations from 10 ng mL^{-1}– 30 µg mL^{-1} of each of the TmAb were incubated in each well for one hour at 20°C followed by washing thrice with PBST. The biotinylated detection Affimer® protein was then added to the plate (2 µg mL^{-1}) and incubated for 1 hour at 20°C, followed by washing thrice with PBST. Streptavidin HRP (1 µg mL^{-1}) was then added to the wells and incubated at 20°C for 30 minutes. This step was followed by washing 6x with PBST and

incubation with 50 µL of TMB for 15 minutes, the plate was then read at 650 nm using a plate reader.

2.3.9 Surface plasmon resonance (SPR)

Affimer affinities for their TmAb analyte were determined by surface plasmon resonance (SPR) using a BIAcore 3000 (GE Healthcare Europe GmbH). Trastuzumab, ipilimumab, adalimumab and rituximab were covalently immobilized on separate channels of a CM5 sensor chip with amine-coupling chemistry. The chip was activated with 200 mM 1-Ethyl-3-(3-dimethylaminopropyl) carbodiimide (EDC) and 50 mM N-Hydroxysuccinimide (NHS) before target injection under optimised conditions (trastuzumab, 5 µg mL^{-1} in 10 mM acetate pH 5.5; ipilimumab, 5 µg mL^{-1} in 10 mM acetate pH 5.5; rituximab, 5 µg mL^{-1} in 10 mM acetate pH 5.5; adalimumab, 5 µg mL^{-1} in 10 mM acetate pH 4.5). Remaining reactive groups were capped with ethanolamine (1 M, pH = 8.5). BIAcore experiments were performed at 25°C in PBST buffer (PBS pH 7.4, containing 150 mM NaCl and 0.2% Tween 20). Affimers were injected at 1.56 3.13, 6.25 and 12.5 nM at a flow rate of 5 µL min^{-1}, followed by 12 minute dissociation. The on- and off- rates and Kd parameters were obtained from a global fit to the SPR curves using a 1:1 Langmuir model, using the BIAevaluation software. Quoted Kd values are the mean ± Standard Error of the Mean (SEM) of three replicate runs, unless specified otherwise.

2.3.10 Data analysis

All data were presented as the mean of at least 3 biological repeats with error bars representing ± SEM. To determine the significance of data, one-tailed, student's t-tests were used. Significance was shown by $p<0.05$.

The quantifiable ranges of the sensors were determined based on parameters set by the food and drug administration (FDA) for validation of new bioanalytical methods (307), including percentage recovery values between 80 – 120% and the coefficient of variation (% CV) < 25%.

2.4 Results

2.4.1 Selection and characterisation of binding proteins

An Affimer reagent phage display library was screened against target antibodies trastuzumab, rituximab, adalimumab, and ipilimumab, as described previously (260, 303). Briefly, the binding reagents selected for in three rounds of phage panning were subject to ELISA validation, and a lead candidate was chosen for each target TmAb and further characterised (303). Surface plasmon resonance (SPR) was used to determine the affinity of each anti-idiotypic Affimer protein. TmAb biosimilars were covalently immobilised onto an SPR chip and titrated with serial dilutions of respective Affimer reagents. Nanomolar affinities were confirmed for all antibody – Affimer reagent complexes (**Figure. 20, Table 4**).

2.4.2 Optimisation of signal change in anti-trastuzumab BLA-BLIP sensor

To create the anti-ID sensor constructs, two copies of the selected anti-ID Affimer proteins were attached to TEM1–ß-lactamase (BLA) and ß-lactamase inhibitor protein (BLIP) using recombinant DNA technology. pET28a(+) plasmids containing the BLA-BLIP sequences were expressed in BL21(DE3) *E.coli* and purified via a two-step affinity chromatography protocol detailed in the methods section 2.3.3

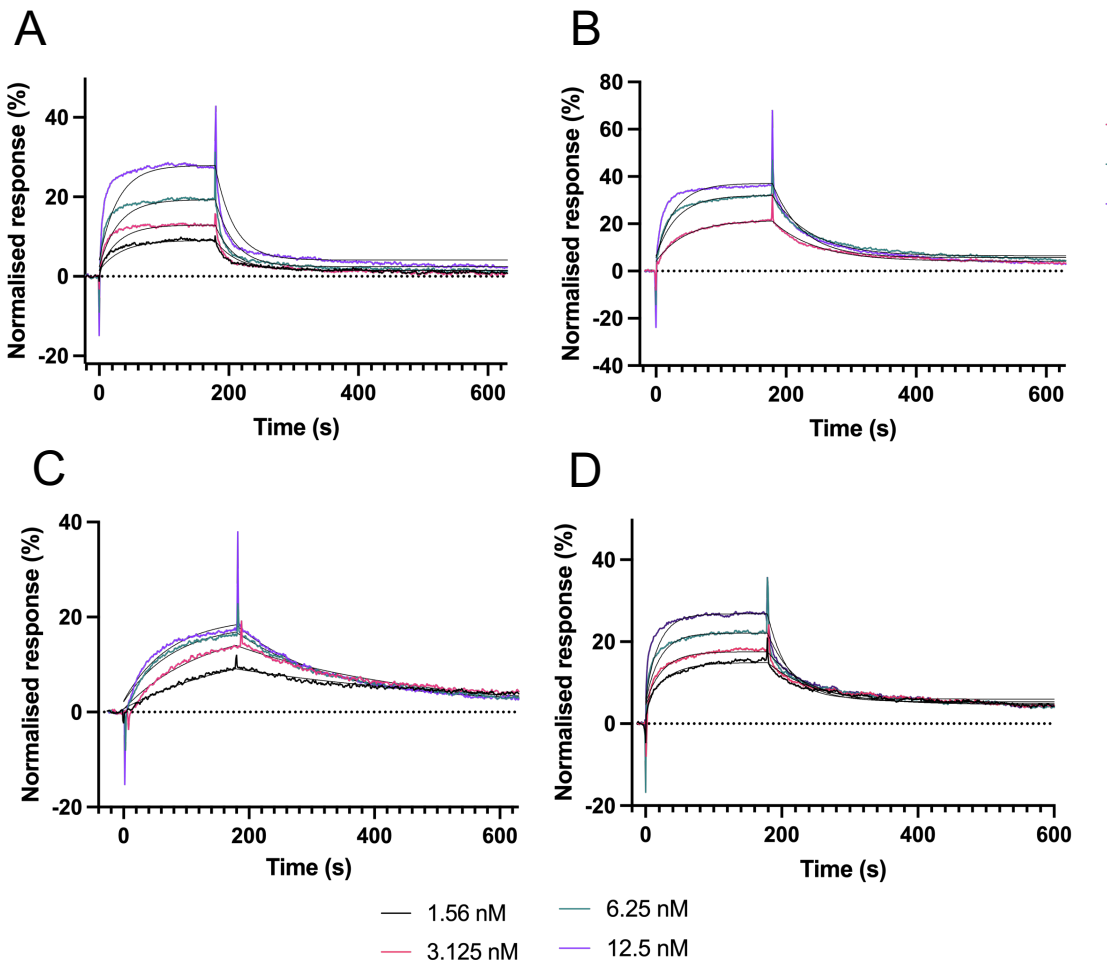

Figure. 20 Surface Plasmon Resonance (SPR) curves plotted for each anti-idiotype Affimer to analyse binding to their respective TmAb. *Aff-Ada and adalimumab (**A**), Aff-Ipi and ipilimumab (**B**), Aff-rit and rituximab (**C**) and Aff-trast and trastuzumab (**D**). SPR plots are shown between TmAb concentrations of 1.56 nM and 12.5 nM. Langmuir model fits are plotted alongside each concentration for each TmAb-Affimer binding study. SPR experiments were conducted in triplicate (duplicate for Aff-Ipi) however only replicate one has been included for clarity. Evaluation of SPR data and Langmuir model fits were conducted on BIAevaluation software. Data for all plots and fits were then extracted from BIAevaluation and re-plotted on GraphPad to improve visualisation of data.*

Table 4. K_D values calculated from evaluation of Langmuir model fits of SPR curves. *All anti-idiotypic Affimer proteins have nM affinity for their respective TmAb analytes and are within ~ 12-fold of one another. K_D values were calculated with BIAevaluation software and are presented as a mean of three replicates ±SEM. (Aff-Ipi – ipilimumab n=2).*

	K_D (nM)	SEM (nM)
Aff-Trast – trastuzumab	0.75	± 0.12
Aff-Ipi – ipilimumab (n=2)	7.8	± 0.8
Aff-Ada – adalimumab	9.77	±2.54
Aff-Rit – rituximab	4	±0.75

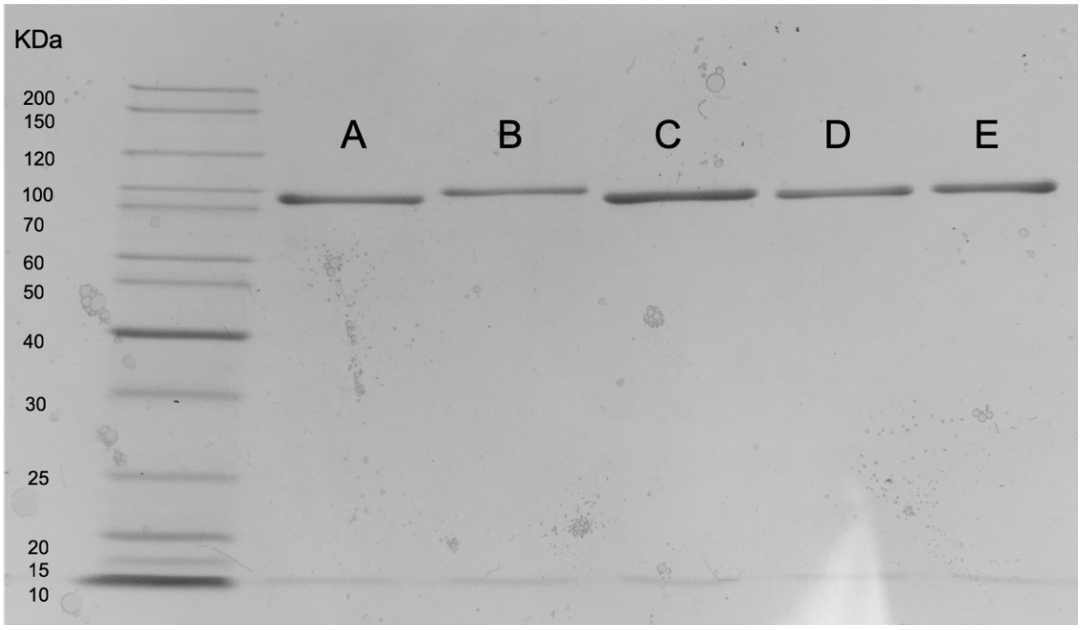

Figure 21. SDS-PAGE of 5 BLA-BLIP constructs purified. *A: BB_Trast2, B: BB_Trast3, C: BB_Ipi, D: BB_Rit, E: BB_Ada. All constructs came out at ~80 kDa. Construct B however, had a slightly higher KDa (~83) due to the longer middle linker cloned in for linker optimisation.*

The mechanism of target-driven disruption employed by BLA-BLIP to produce a signal is largely dominated by recognition element affinity and the three peptide linkers between the four protein domains (**Figure 19** and **Figure 22A**). It has previously been reported that the use of two specific recognition elements within this sensor design that are able

to bind to the analyte is essential for enzyme-inhibitor disruption, with only one recognition element unable to produce a signal (170). As detailed in the introduction to this chapter (section 2.2), the linker regions are integral to the functionality of the BLA-BLIP sensor.

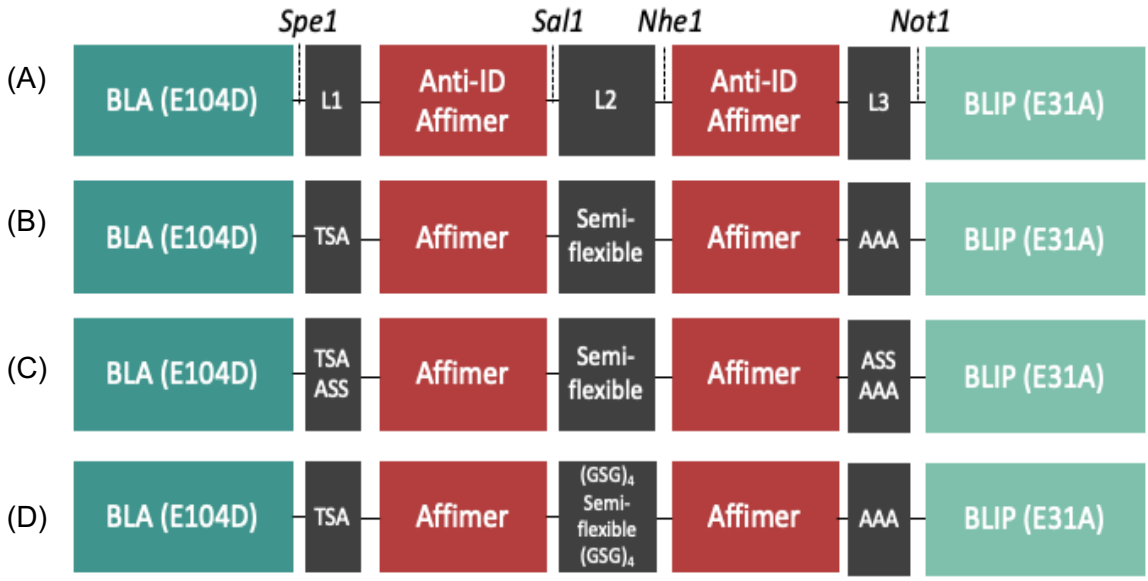

Figure 22. Schematic diagrams of sensor components. (A) *The general BLA-BLIP sensor construct (BB_anti-ID)* ***(B)*** *BB_Trast as previously reported (170)* ***(C)*** *BB_Trast2 with Longer L1 and L3 linkers* ***(D)*** *BB_Trast3 with additional $(GSG)_4$ encompassing the semi flexible linker - $(GSG)_6A(EAAAK)_6A(GSG)_6A(EAAAK)_6A(GSG)_6$.*

Prior to this work, a proof-of-principle anti-trastuzumab BLA-BLIP sensor was developed (170), but the linkers (L1, L2 and L3, **Figure 22**) were not optimised for sensor performance. Linker optimisation has previously helped improve sensor activity when adapting to new targets, especially when Affimer binding sites on the target analyte are unknown, as is the binding orientation and distance between them. To optimise the overall signal change, three constructs were designed against trastuzumab (BLA-BLIP_Trast) with varying linker lengths (BB_Trast, BB_Trast2 and BB_Trast3; **Figure 22**). BB_Trast has short, rigid L1 and L3 linkers (three amino acid residues) along with a semiflexible L2 linker known to span the approximately 100 Å distance between the variable regions of mAbs (169, 170). The hinge region of antibodies does, however, allow

for flexibility in the distance between variable regions, dependent on the antigen it is binding to (308). The exact positioning of the antigen binding regions of the TmAbs used here is unknown, therefore trials with differing linker lengths allowed us to determine the best performing sensor design for TmAb quantification using BLA-BLIP. BB_Trast2 introduced longer L1 and L3 linkers (six amino acid residues) with the same semiflexible L2 linker while BB_Trast3 (**Figure 22D**) has a longer semiflexible L2 linker - $(GSG)_{10}A(EAAAK)_6A(GSG)_6A(EAAAK)_6A(GSG)_{10}$.

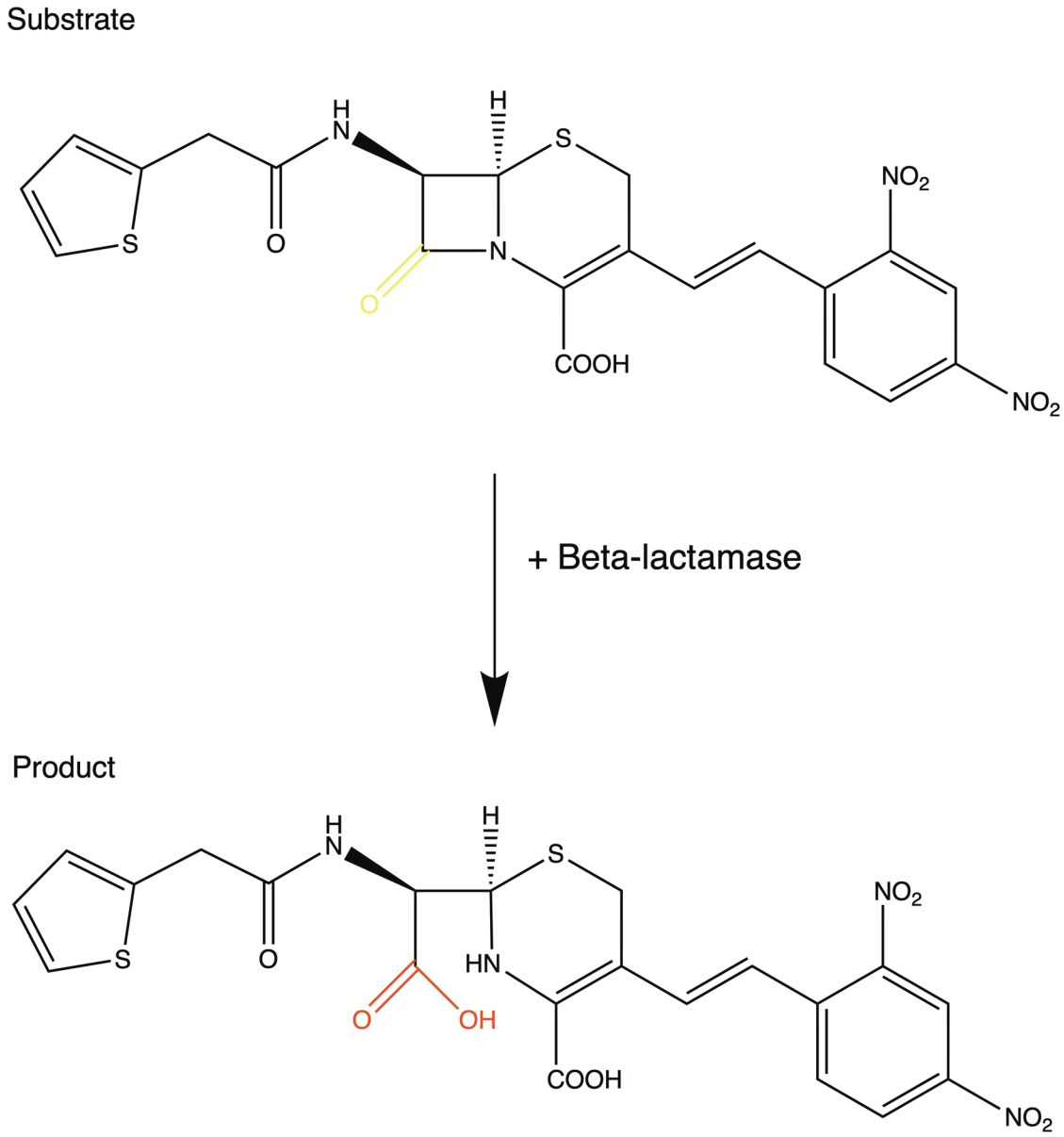

Figure 23. The hydrolysis of nitrocefin mediated by the presence of beta-lactamase causes a colourimetric reaction changing the solution from yellow to red. *Chemdraw (RRID:SCR_016768) software was used to draw chemical structures.*

The activity of BB_Trast, BB_Trast2 and BB_Trast3 in response to trastuzumab were measured as BLA activity using a homogenous assay where the turnover of nitrocefin can be measured. As a cephalosporin compound, nitrocefin contains a beta-lactam ring which is susceptible to beta-lactamase mediated hydrolysis (**Figure 23**). The extent of nitrocefin hydrolysis can be determined by the extent of colour change from yellow to red which allows us to measure the presence and activity of beta-lactamase as a change in light absorbance at 551 nm (A_{551}) (**Figure 24**). BB_Trast outperformed BB_Trast3 in terms of fold-activity gain measured at A_{551} ($p \leq 0.05$). Additionally, the calculated LoD for BB_Trast3 was significantly increased at 3 nM compared to 300 pM for BB_Trast. BB_Trast2 has a calculated LoD of 300 pM, but a very low signal gain.

After careful consideration, the optimal performance of the BLA-BLIP sensor for TmAb detection was found to include rigid linker 1 and linker 3 regions consisting of three amino acid residues to anchor the recognition elements close to the switching mechanism of the enzyme and inhibitor. The optimal composition of the semiflexible linker 2, found between the enzyme and the inhibitor, consisted of three flexible blocks of six GSG repeats and two 45 Å alpha-helical blocks ($(GSG)_6A(EAAAK)_6A(GSG)_6A(EAAAK)_6A(GSG)_6$) to effectively bridge the distance between the antigen binding sites and maintain specific and sensitive activity. Linker optimisation is tailored to the size and shape of the analyte, as monoclonal antibodies have a uniform shape all anti-ID BB_sensors from this point onwards were designed in the same format as BB_Trast (**Figure 22B**).

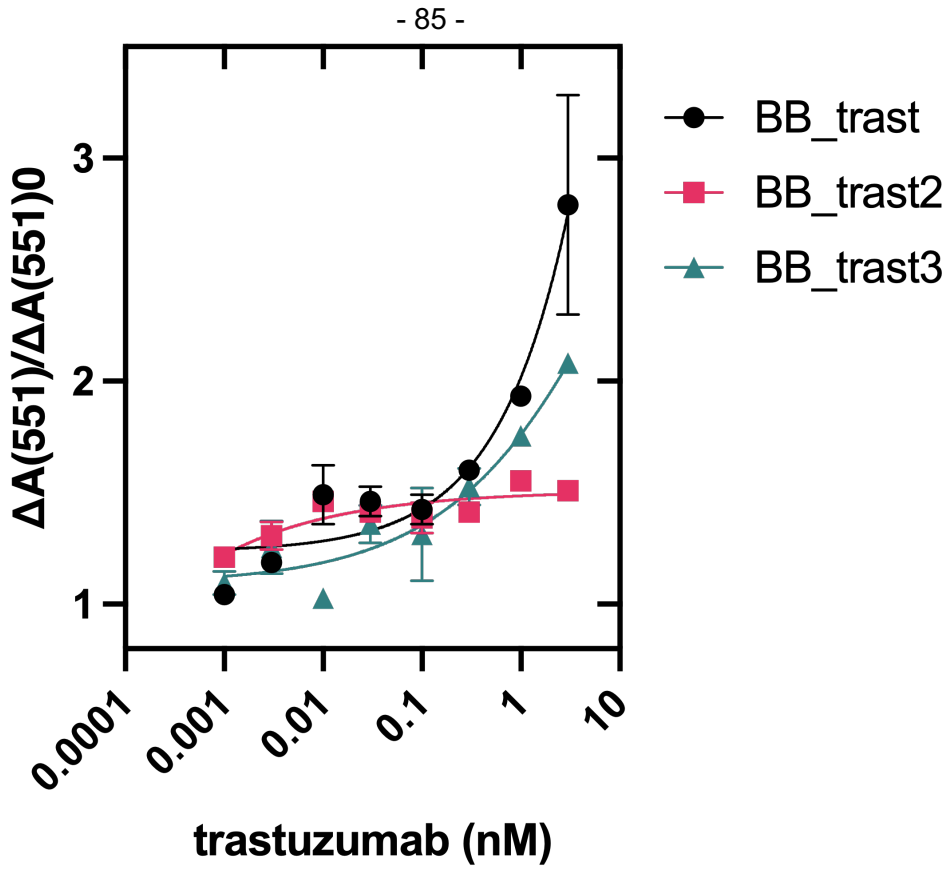

Figure 24. Length of linkers affects the BLA activity of the biosensor construct. *Activity of sensors: BB_Trast (TSA Trast Semi Trast AAA), BB_Trast2 (TSAASS Trast Semi Trast ASSAAA) and BB_Trast3 (TSA Trast $(GSG)_4$ Semi $(GSG)_4$ Trast AAA) were measured as absorbance at A_{551} and presented as fold activity gains ΔA_{551} (x nM Ab)/ΔA_{551} (0 nM Ab). All data are presented as a mean of at least three repeats with error bars representing ±SEM. Where error bars are not visible, they are situated within the symbol plot.*

2.4.3 Therapeutic monoclonal antibody detection

The recognition elements of BLA-BLIP sensors are easily exchanged genetically using the restriction sites flanking position A (SpeI & SalI) and position B (NheI & NotI). This allowed us to create three anti-ID BLA-BLIP sensors with the anti-ID Affimer proteins against rituximab, adalimumab and ipilimumab (303) to produce the BLA-BLIP sensors BB_Rit, BB_Ada and BB_Ipi, respectively, alongside BB_Trast.

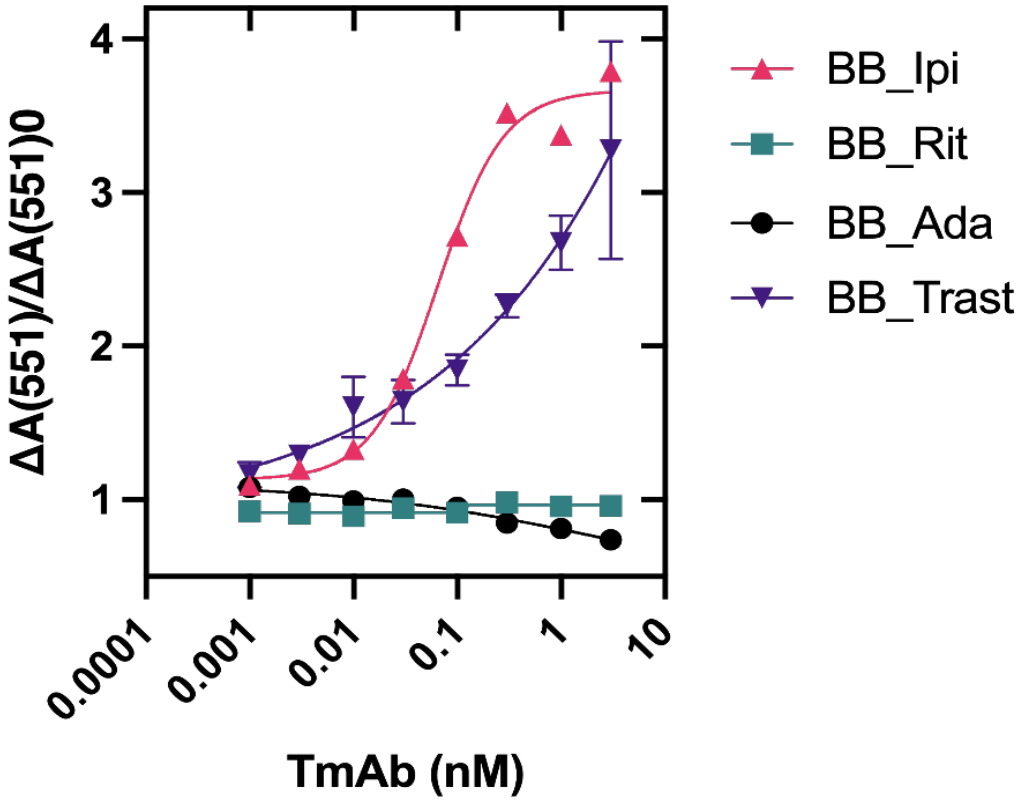

Figure 25. The BLA-BLIP sensor construct can be applied to the detection of ipilimumab when anti-idiotype Affimer proteins against the mAb are inserted*. Activity of BB_Trast, BB_Rit, BB_Ada and BB_Ipi when incubated with 0.001 – 10 nM of their respective TmAb analyte and presented as fold activity gain from the baseline (no analyte). All data are presented as a mean of at least three repeats and error bars represent ±SEM. Where error bars are not visible, they are situated within the symbol plot.*

The dose response of BB_Trast, BB_Rit, BB_Ada and BB_Ipi were measured using the homogenous BLA-BLIP assay (**Figure 25**). A pronounced “switch on” effect was displayed by BB_Trast and BB_Ipi when incubated with varying concentrations of TmAb. BB_Trast showed a 3.3-fold increase in activity in response to 3 nM trastuzumab, similar to the 2.8-fold increase previously reported (170). BB_Trast activity never reaches saturation across this concentration range (1 pM – 3 nM). The use of TmAb concentrations >3 nM was avoided as a sensor concentration of 2 nM was tested and a “hook” effect would likely be seen at higher concentrations. This occurs when sensor components bind multiple analyte molecules, preventing disruption

of the enzyme-inhibitor complex. BB_Ipi responded to 3 nM ipilimumab with a 3.5-fold increase in activity. The LoD of BB_Ipi was calculated to be 30 pM, whereas the LoD of BB_Trast was calculated to be 300 pM. BB_Ipi outperformed BB_Trast, both in terms of fold-activity gain at the highest drug concentration tested (C_{max}) and LoD. BB_Trast and BB_Ipi showed high specificity to their individual TmAbs. When incubated with 10 nM non-specific TmAbs in the BLA-BLIP assay (**Figure 26A**), there was no significant ($p>0.05$) response compared to the response generated in the presence of buffer only. Specificity of sensor binding was further demonstrated with direct ELISA (**Figure 26C**).

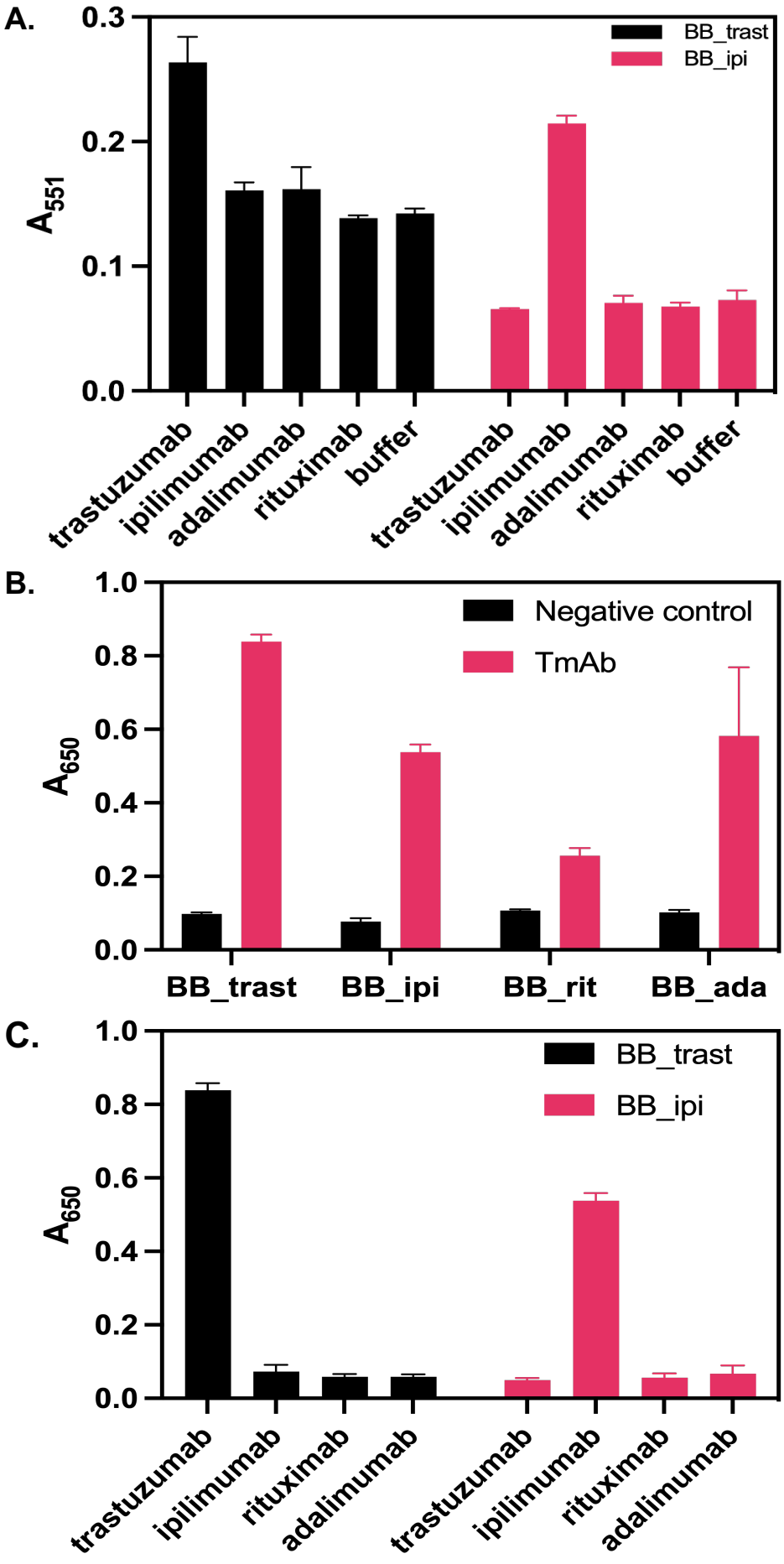
A.
0.3
0.2
0.1
0.0
A551
BB_trast
BB_ipi
trastuzumab
ipilimumab
adalimumab
rituximab
buffer
trastuzumab
ipilimumab
adalimumab
rituximab
buffer
B.
1.0
0.8
0.6
0.4
0.2
0.0
A650
Negative control
TmAb
BB_trast
BB_ipi
BB_rit
BB_ada
C.
1.0
0.8
0.6
0.4
0.2
0.0
A650
BB_trast
BB_ipi
trastuzumab
ipilimumab
rituximab
adalimumab
trastuzumab
ipilimumab
rituximab
adalimumab

***Figure 26. TmAb BLA-BLIP sensors are specific to their target analyte**. **(A)** 2 nM of the BLA-BLIP sensor constructs were incubated with 10 nM of specific TmAb, non-specific TmAb or blank buffer. BB_Trast and BB_Ipi both displayed significant ($p \leq 0.05$) absorbance at A_{551} compared to non-specific TmAb analytes and blank buffer. **(B)** ELISA data demonstrating the binding characteristics of each specific BLA-BLIP construct towards the appropriate target and a non-immunoglobulin negative control, C. difficile toxoid B. 10 µg mL^{-1} (125 nM) of the sensor construct were incubated with 20 µg mL^{-1} of target TmAb (135 nM) or toxoid B (74 nM). **(C)** Direct ELISAs were performed on BB_Trast and BB_Ipi to determine their specificity. 10 µg mL^{-1} (125 nM) of the sensor constructs were incubated with 20 µg mL^{-1} of specific or non-specific TmAb (135 nM). Data of biosensors binding to their respective targets and non-specific analytes are presented as a mean of three repeats and error bars represent ±SEM.*

2.4.4 Affimer protein – TmAb binding

No enzymatic response was observed from BB_Rit or BB_Ada in the presence of their respective TmAb target (**Figure 25**). One explanation for this could be that the synthetic binding reagents against rituximab and adalimumab no longer bind to their targets once incorporated into the BLA-BLIP sensor constructs. To test whether the recognition elements were compromised in the BB_Rit and BB_Ada sensors, direct ELISAs were performed on the BLA-BLIP sensor constructs (**Figure 26B**) using the C-terminal strep-II tag for detection.

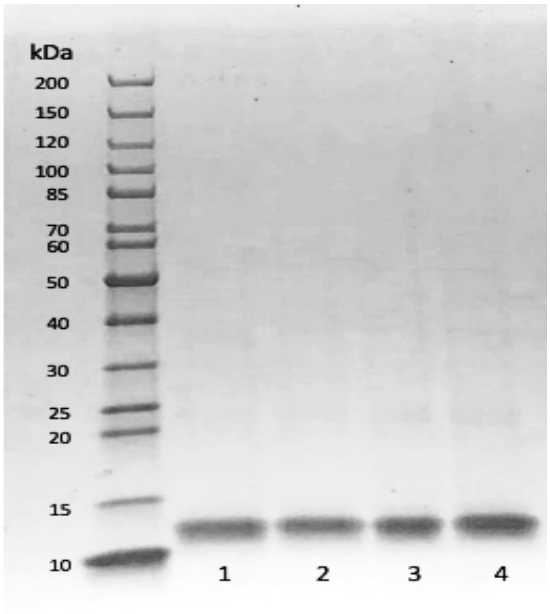

Figure 27. 15% SDS PAGE of purified Cysteinated anti-ID Affimers: 1: *Aff_Trast,* ***2:*** *Aff_Ada,* ***3:*** *Aff_Ipi and* ***4:*** *Aff_Rit.*

The direct ELISAs confirmed that BB_Rit and BB_Ada bound to their targets, even though the responses of the homogenous enzyme assay indicate that binding to their respective TmAbs does not result in the disruption of BLA-BLIP complex. This could be due to only one Affimer protein binding the TmAb instead of two as required to switch on the enzyme activity (see **Figure 19**). To test whether the two Affimer proteins can bind, a bridge ELISA was performed using cysteinated Affimer proteins (**Figure 27**, **Figure 29**; see **Figure 28** for a schematic of a bridge ELISA) (303, 309). Typically a pharmacokinetic (PK) assay, bridge ELISAs utilise anti-ID antibodies and take advantage of the two identical binding sites on IgG Abs to measure the concentrations of mAbs (310). As expected, the bridge ELISA confirms that two Affimer proteins can simultaneously bind to trastuzumab, whereas the binding reagents against rituximab or adalimumab were unable to detect their respective TmAbs in the bridge ELISA (**Figure 29**). The latter could indicate that only one Affimer protein can bind to rituximab or adalimumab, preventing the switching mechanism to function as intended. The lack of response from the binding reagents against ipilimumab in this format is unexpected and is discussed below.

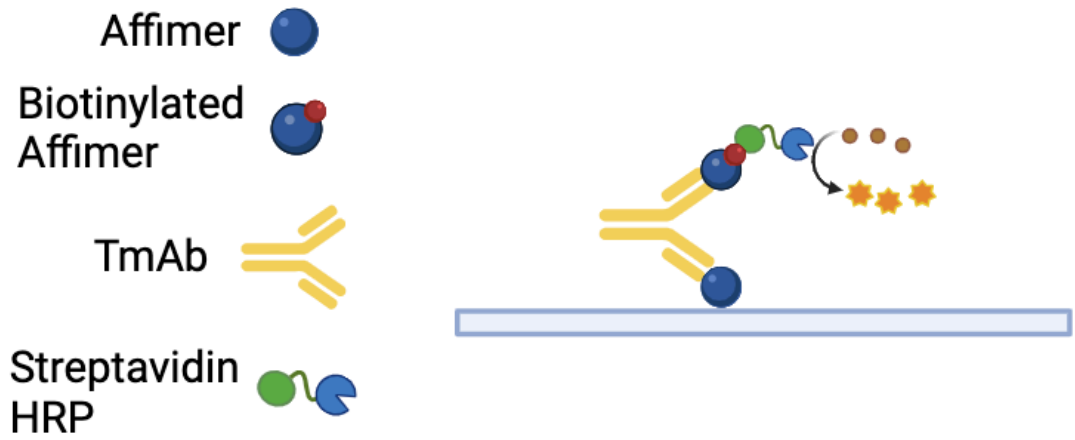

Figure 28 . Diagram of Bridge ELISA. *In the Bridge ELISA, unlabelled anti-TmAb Affimer are first immobilised on the surface of the plate, incubated with the TmAb which are subsequently detected using a biotin-labelled version of the anti-TmAb Affimer. Streptavidin-HRP can then bind to the biotinylated detection Affimer, and the catalysis of TMB by HRP can be used to measure the quantity of TmAb successfully detected with this method. The symmetrical conformation of an IgG should allow for the binding of two anti-ID Affimers should they bind to the variable domain of the antibody.*

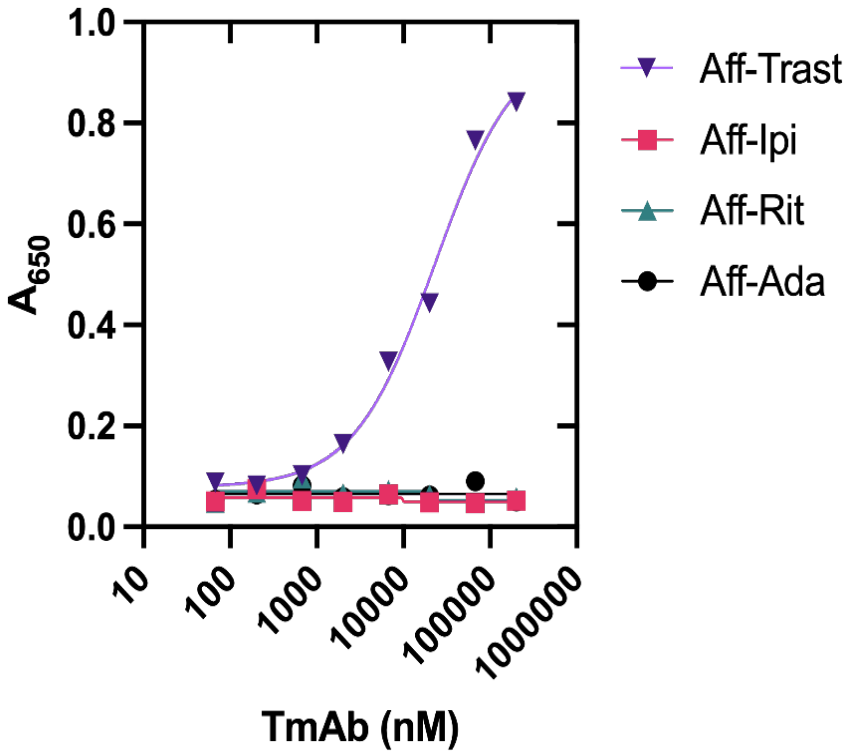

Figure 29. Bridge ELISA of four anti-ID Affimer proteins *with their respective mAb targets presented as absorbance at 650 nm as a measurement of TMB turnover by HRP. All data are presented as a mean of three repeats with error bars representing ±SEM. Where error bars are not visible, they are within the symbol plot.*

2.4.5 BLA-BLIP enzyme switch sensor performance in serum

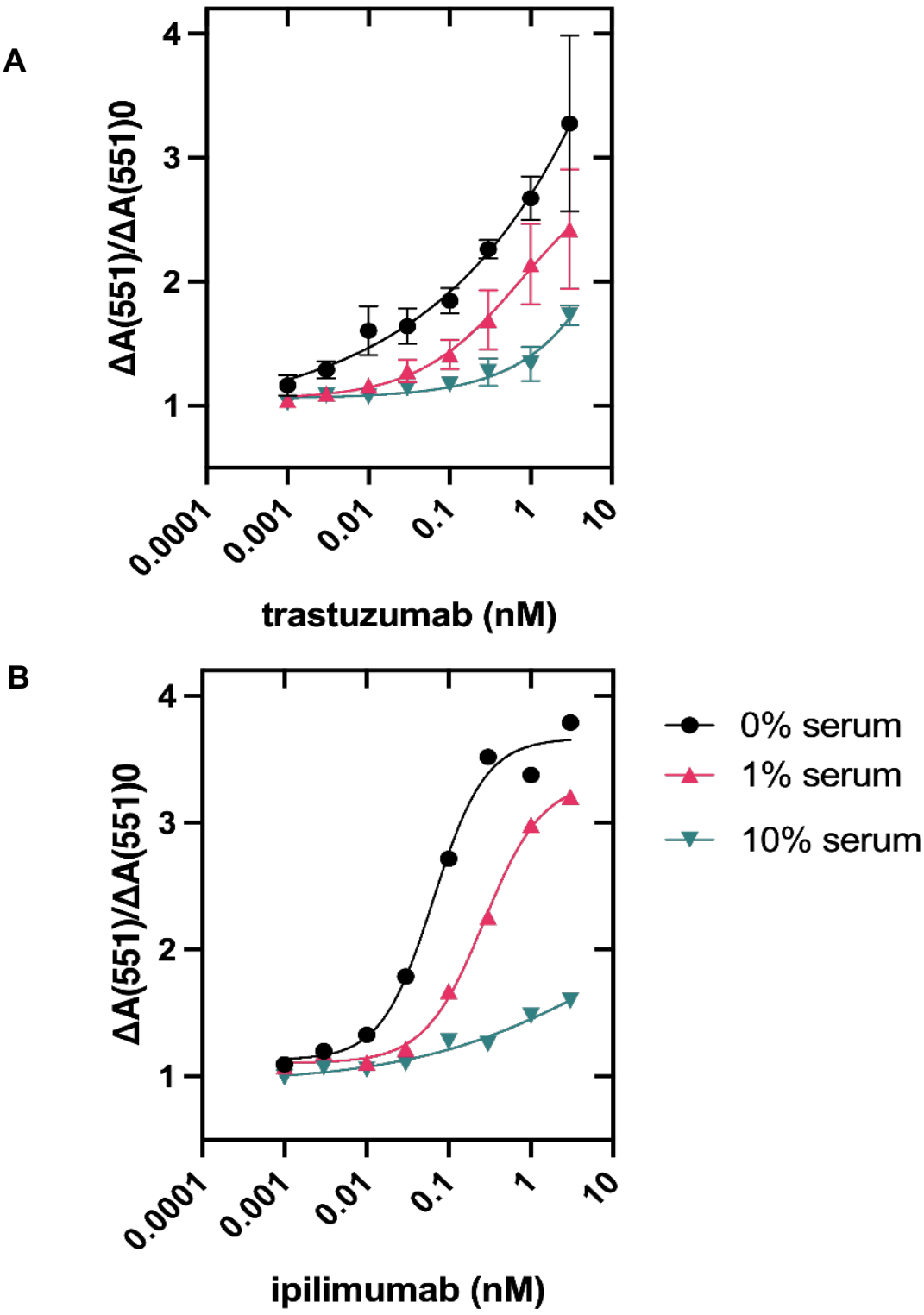

***Figure 30. BB_Trast and BB_Ipi maintain activity in 1% serum**. Serial dilutions of trastuzumab **(A)** and ipilimumab **(B)** were made up in 0%, 1% or 10% pooled human serum and incubated with the enzyme-switch sensors. Data plotted as fold activity gain from baseline measurements, as a mean of at least three repeats with error bars representing ±SEM. Where error bars are not visible, they are within the symbol plot.*

The activity of BB_Trast and BB_Ipi were tested in the BLA-BLIP assay in varying percentages of pooled human serum (**Figure 30**). The activity of BB_Trast in response to trastuzumab (**Figure 30A**) was maintained when incubated in up to 1% serum, there were no significant ($p \leq 0.05$) changes in fold-activity gain, however, the calculated LoD dropped from 100 pM in buffer to 300 pM in 1% serum. The stability in serum seen with BB_Trast was mirrored by BB_Ipi (**Figure 30B**), at C_{max} there were no significant ($p \leq 0.05$) changes in fold-activity gain however, significant differences were apparent around the LoD. Despite the drop in activity at lower concentrations, a LoD of 30 pM was retained. Quantifiable ranges for BB_Trast and BB_Ipi were calculated in 1% human serum as 30 pM – 3 nM and 30 pM – 300 pM respectively (See **Table 5** for details). BB_Trast and BB_Ipi were unresponsive to increasing concentrations of their respective analytes when in 10% serum. This is thought to be due to the breakdown of nitrocefin and inhibition of BLA by the variety of serum proteins including IgG and IgE antibodies present (311, 312).

Table 5 Interpolated standard curves for BB_Trast and BB_Ipi provided quantifiable ranges based on accuracy and precision of the sensors in spiked 1% human serum. *Percentage recovery and percentage coefficient variance (%CV) values for BB_Trast and BB_Ipi were used to determine the quantifiable range of each sensor based on recovery values between 80 – 120% and % CV < 25%.*

	BB_Ipi	**BB_Trast**
Quantifiable Range	30 – 300 pM	30 pM – 3 nM
% recovery	94 – 101%	81 – 119%
% CV	2.7 – 12%	12.3 – 22%

2.5 Discussion

One of the challenges when designing biosensors for clinical diagnostics is performance in biological fluids. The complex composition of biological fluids, be that blood, saliva, or faeces, poses the problem of interference from nonspecific proteins. This is especially apparent with enzyme-based biosensors with many biological components able to interfere with enzymatic activity (313, 314). The implementation of TDM for mAb therapies has, so far, been affected by the difficulties presented when detecting mAbs in serum. Furthermore, with BB_Trast and BB_Ipi, the recognition elements are specific to humanised IgG1 kappa monoclonal antibodies (244, 315), the antibody type most abundant in human sera (316). TmAb titres have been successfully monitored using PoC platforms where 1:100 dilutions of patient samples were necessary (317). Clinically relevant serum concentrations of trastuzumab are between 70-2000 nM and ipilimumab trough concentrations range between 30-230 nM (318, 319). BB_Trast and BB_Ipi can detect TmAb spiked buffer at concentrations 100x lower than the clinically relevant values. Furthermore, in 1% serum there is no significant loss of activity for either sensor. This allows for dilution of patient serum to prevent matrix effects whilst maintaining the required sensitivity, thus both sensors presented here can measure clinically relevant concentrations of TmAbs within 30 minutes without the need for pre-treatment or washing steps such as those required in ELISAs. In HER2+ breast cancer, tumour shedding of the extracellular domain (ECD) of HER2 in exosomes can occur, especially in advanced disease (320). These exosomes can bind circulating trastuzumab with an inhibitory effect, which should be accounted for in TDM methods (321). Free (unbound) drug concentrations are the most essential measurement for TDM as these are available for distribution and pharmacodynamic action (322). The recognition elements implemented in BB_Trast target the variable regions of trastuzumab and therefore it can be speculated that exosome-bound trastuzumab would not be measured in this system, but HER2+ patient serum should be tested to confirm this hypothesis.

These enzyme-switch sensors have the capacity to be implemented into a doctor's surgery or at a patient's bedside for single measurements of trough concentrations before dose administration, to ensure maintenance of the minimal effective concentration (MEC) and allow dosing to be adjusted accordingly (293). For both trastuzumab and ipilimumab this would occur on a weekly, three-weekly, or monthly regimen (323-325).

Current ELISA methods used for measurement of ipilimumab and trastuzumab have a lower limit of quantification LLOQ of 2 nM (325) and 1 nM (35, 326) respectively. These ELISA methods require 1/100 dilutions of serum equivalent to the BLA-BLIP assay. The BLA-BLIP assays can detect ipilimumab and trastuzumab at concentrations as low as 30 pM in 1% serum, which is an improvement on the sensitivity of current ELISA methods. Additionally, the much shorter, 30-minute timeframe of the BLA-BLIP assay, compared to the 3-4 h timeframe of ELISA detection methods (327) make the BLA-BLIP assay a prospective alternative to current TDM methods. Designing a homogenous assay with a colourimetric reporting system, like BLA-BLIP, has well established benefits in relation to PoC devices. The colour change signal provides a simple visual read-out without the requirement of specialised equipment. This makes for a user-friendly, cost-effective diagnostic platform, ideal for low-resource settings to provide on-site analyte detection. These benefits, however, are more applicable to the development of qualitative tests, whereas this specific project requires quantitative analysis of serum drug concentrations for effective TDM of immunotherapies. By utilising a plate reader to measure changes in absorbance (A_{551}) this sensor can be used for quantitative measurements of TmAb titres.

The BLA-BLIP sensor presented here is classified by its switching mechanism as a modular allosteric switch. Unlike proximity switches, also known as split enzyme systems, allosteric switches maintain the full activity and stability of their reporter both in an active and inactive state (169, 170). Therefore, they do not suffer from the consequences of incorrect reassembly and subsequently compromised activity recovery

(174, 177). This does, however, increase overall background activity, which must be accounted for. Other modular systems, similar to the one presented in this study, have also suggested a binding-induced conformational change as the driving force for sensor functionality (302, 328, 329). Allosteric switch biosensors require special attention to the linker lengths, specifically the distance between the recognition elements. When using linkers to span IgG mAb variable regions, linker lengths significantly shorter or longer than the distance between these regions (10 – 12 nm) impacts the signal output. Using a consistent linker design between mAb targets has previously yielded versatile sensors (329), hence the decision to replicate this.

Based on the data produced for BB_Rit and BB_Ada, showing a lack of signal in response to their respective TmAb analytes, it can be speculated that there are issues with the binding of the recognition elements when incorporated into the BLA-BLIP enzyme switch, preventing them from functioning as intended. The schematic model of the enzyme – inhibitor switch sensor (**Figure 19**) implies that the affinity of the recognition elements must be above the threshold necessary to successfully disrupt the BLA-BLIP interaction (K_i = 2.1μM) (169). SPR analysis showed low nM affinity values for all four anti-ID binding reagents (**Table 4**). The calculated K_D are all within 12-fold of one another and well above the threshold needed to disrupt the enzyme switch. The lack of correlation between affinity and sensor activity suggest that low affinity is not the primary cause of BB_Rit and BB_Ada inactivity.

The successful disruption of the enzyme inhibitor complex could be dependent on exact binding geometries of the recognition elements, which is a difficult factor to control and likely varies between targets. The binding sites on trastuzumab of Aff-Trast have since been determined with hydrogen–deuterium exchange mass spectrometry (HDX-MS) (330), and were as expected. Structural data on the binding of Aff-Rit and Aff-Ada to their respective targets could help explain the lack of activity from BB_Rit and BB_Ada. Previous work has confirmed that the BLA-BLIP switch mechanism requires two anti-ID

binding proteins that interact with the variable regions of a TmAb to activate the reporter enzyme (170). The lack of response from BB_Rit and BB_Ada could thus be due to the inability of two Affimer proteins to bind simultaneously to the TmAb variable regions. Indeed, the negative bridge ELISA responses for rituximab and adalimumab are in line with this hypothesis. However, the bridge ELISA was also negative for the anti-ipilimumab binding proteins, while the BB_Ipi sensor is functional. It can be speculated that in the latter bridge ELISA, non-optimal orientation of the Affimer protein and ipilimumab on the polystyrene plate, which is known to affect sensitivity of immunodiagnostic procedures (331), prevents the assay from working adequately. Still, no conclusive correlations between bridge ELISA activity and successful BLA-BLIP sensors can be made and it is possible that BB_Ipi functions in an alternative, unknown mechanism. Either way, a screening method that directly tests whether two binding reagents can bind simultaneously would stimulate the development of BLA-BLIP sensor constructs, as current screening methods for high affinity binders do not always translate to binding proteins that are suitable for sensor development (137, 256).

2.6 Conclusion

The simple “one pot” set up of the BB_Trast and BB_Ipi assays, which require no washing steps like those necessary in ELISAs, means the assay can easily be adapted into a diagnostic device for a point-of-care setting. This is in contrast to the standard tests currently used for measuring TmAb concentrations such as LC-MS/MS and ELISA which require skilled personnel and take multiple hours to produce results with LoD values in the low nM range (33, 35, 299, 332). Comparatively, the sub-nM LoD and < 45-minute timeframe of the BLA-BLIP assay would allow for the immediate action needed for successful implementation of TDM.

The accurate monitoring of drug therapies with narrow therapeutic windows opens the door to personalisation of dosage, which can improve treatment success and quality of

patient life (73). Due to the universal shape of TmAbs alongside the BLA-BLIP sensor mechanism of target driven disruption, easy adaptation of BB_Trast to three other TmAbs was hypothesised. A 50% yield of successful implementation suggested that the adaptation of BLA-BLIP to multiple TmAb targets is not as simple as expected, and optimisation of each sensor would be recommended. Overall, two BLA-BLIP sensors have been presented here that could detect clinically and therapeutically relevant TmAb concentrations with comparable sensitivity to current ELISA methods in 1% serum and significantly shorter run times, opening the opportunity for implementation in TDM.

3 Chapter 3: Proximity switch biosensors for therapeutic drug monitoring of immunotherapies.

3.1 Abstract

Concentration–therapeutic efficacy relationships have been observed for several therapeutic monoclonal antibodies (TmAb), where low circulating levels can result in ineffective treatment and high concentrations can cause adverse reactions. Rapid therapeutic drug monitoring (TDM) of TmAb drugs would provide the opportunity to adjust an individual patient's dosing regimen to improve treatment results. However, TDM for immunotherapies is currently limited to centralised testing methods with long sample-collection to result timeframes. Here, four point-of-care (PoC) TmAb biosensors are developed by combining anti-idiotypic Affimer proteins and NanoBiT split luciferase technology at a molecular level to provide a platform for rapid quantification (< 10 minutes) for four clinically relevant TmAb (rituximab, adalimumab, ipilimumab and trastuzumab). The rituximab sensor performed best with 4 pM limit of detection (LoD) and a quantifiable range between 8 pM – 2 nM with negligible matrix effects in serum up to 1%. After dilution of serum samples, the resulting quantifiable range for all four sensors falls within the clinically relevant range and compares favourably with the sensitivity and/or time-to-result of current ELISA standards. Further development of these sensors into a PoC test may improve treatment outcome and quality of life for patients receiving immunotherapy.

3.2 Introduction

In the previous chapters, issues with current therapeutic drug monitoring (TDM) methods were explored with a focus on the lengthy processes and need for large laboratory-based equipment operated by trained personnel, making them unsuitable for rapid dose adjustment (297, 333). The introduction of a rapid point-of-care (PoC) dose monitoring platform for TmAbs provides a feedback mechanism so drug concentrations

can be maintained within the therapeutic range with the potential of improving treatment efficacy and patient quality of life (300). To overcome the lengthy processes (>> hour) of detection methods like enzyme linked immunoassays (ELISA), homogenous immunoassays, also known as mix-and-read assays, are being developed for diagnostic applications (169, 170, 177, 195, 196, 334). These simple assays forgo the need for immobilisation or wash steps, making them ideal candidates for implementation into PoC settings.

A one-component, colourimetric sensor design was first used to create a sensitive, selective and rapid therapeutic drug monitoring platform for immunotherapies which is explored in detail in Chapter 2: One component modular allosteric enzyme-inhibitor switch biosensor for therapeutic drug monitoring of immunotherapies. Although this design provided an effective detection method for ipilimumab and trastuzumab, it was less modular than expected and could not be easily adapted for the detection of rituximab and adalimumab. Developing an adaptable platform that can be used for the detection of a range of targets was a major aim of this project, to this end, the one-component modular protein switch was unsuitable so a decision to explore alternative protein switch sensor designs was made. In order to keep the chapters of this thesis as self-contained as possible, repetition of some relevant points will occur throughout this chapter due to the similar aims of the work conducted in the previous chapter.

One potential homogenous assay method is the split enzyme system, commonly referred to as a proximity switch (145). These systems rely on splitting a reporter, usually an enzyme, into two inactive fragments which produce no signal individually or when mixed at concentrations well below the binding affinity of the two fragments (172-174). The inactive split enzyme fragments are each genetically or chemically fused to a recognition element that bind non-overlapping epitopes of the target analyte. Binding of the recognition elements co-localises the two inactive reporter fragments, increasing

their effective concentration and prompting re-assembly of the active enzyme, the activity of which can be measured (177, 180, 195, 196).

As discussed earlier, monoclonal antibodies (mAb) are valuable therapeutic agents with widely employed immunotherapies for autoimmune disorder management and cancer treatment (288, 290). Therapeutic monoclonal antibody (TmAb) treatments are predominantly immunosuppressive or immune targeting agents (285, 287), and although TmAbs are generally well tolerated, there have been instances of severe adverse reactions (SARs) due to their promiscuous pharmacological profiles (**Table 3**) (244, 289, 291, 292, 295, 296). Moreover, an association between inadequate serum mAb concentration and lack of therapeutic response, alongside interpatient variability of TmAb pharmacokinetics suggest that regular TDM would be beneficial (293). An inverse relationship between serum levels of rituximab, and the quantity of circulating B-cells has been observed in individuals with B-cell lymphoma. Additionally, elevated tumour burden is linked with diminished concentrations of rituximab in the serum (33, 335). Case studies of TDM of rituximab in B-cell lymphoma treatment have suggested a strong correlation between treatment response and higher trough concentrations as well as improved survival rates, showcasing the benefits of TDM in immunotherapy (336, 337). Similarly, maintaining a trough concentration > 1.5 μg mL^{-1} of TmAb therapy in Crohn's disease management can improve the remission rate of patients by 76% (338).

Here, the development of a homogenous split enzyme assay for the detection of the four routinely used TmAb treatments (adalimumab, ipilimumab, rituximab and trastuzumab) introduced in the previous chapter is described. The sensor combines the same Affimer proteins utilised earlier as recognition elements with an established split-luciferase, NanoLuc® Binary Technology (NanoBiT) (145, 195, 196). The NanoBiT fragments reassemble into the functional luciferase which, in the presence of molecular oxygen, oxidises coelenterazine (CTZ), an imidazopyrazinone containing luciferin, into

a coelenteramide (CEI), in a cofactor-independent decarboxylating reaction to generate blue light. Further optimisation of the NanoLuc system found superior activity when oxidising the novel imidazopyrazinone substrate furimazine (FMZ) into furimamide (FMA) (**Figure 31**) (339, 340). The commercial substrate sold by Promega, and used throughout this chapter, is known as Nano-Glo and contains approximately 20 μM of furimazine. Affimers are non-immunoglobulin-binding proteins and offer the benefit of being small, stable, and easily expressed as recombinant proteins when fused genetically to split-enzyme fragments (170, 195, 262, 303). TmAbs, like all mammalian monoclonal antibodies, contain two identical variable regions and thus only one Affimer needs to be selected, as two copies can be used to target non-overlapping epitopes (**Figure 32**).

With previous work supporting the NanoBiT system as a method of detecting proteins in biological fluids (195), the Affimer-NanoBiT system presented here was expected to provide a rapid and sensitive alternative for TDM of TmAb levels that could be implemented into a PoC setting.

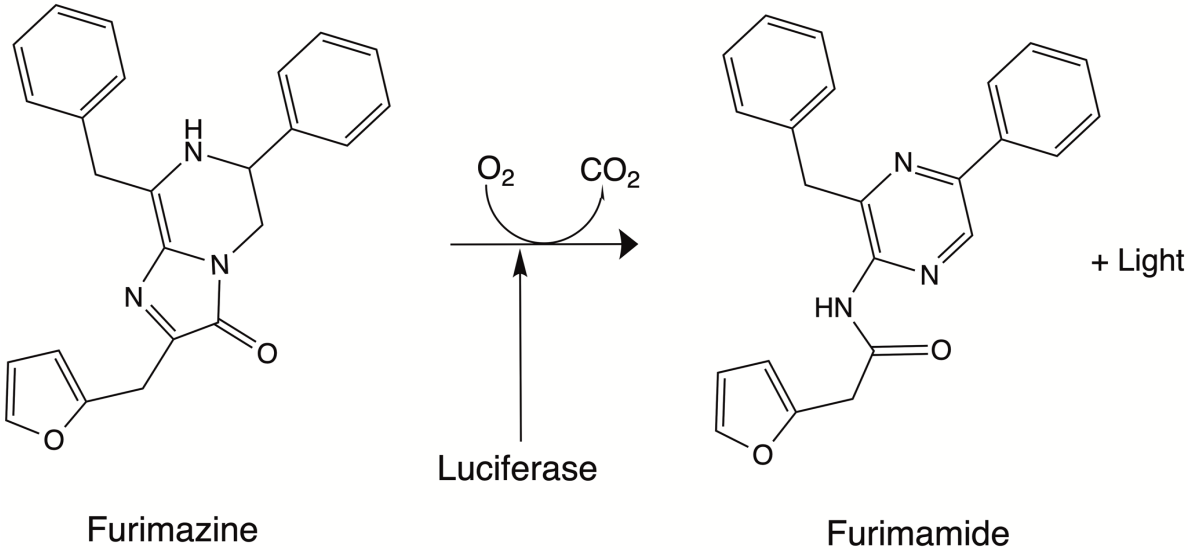

Figure 31. Bioluminescence from the NanoBiT system relies on the reaction between the reconstituted NanoLuc luciferase enzyme and the substrate furimazine commercially known as Nano-Glo*. In the presence of molecular oxygen, NanoLuc reacts with furimazine to produce furimamide and a luminescent output. Chemdraw (RRID:SCR_016768) software was used to draw chemical structures.*

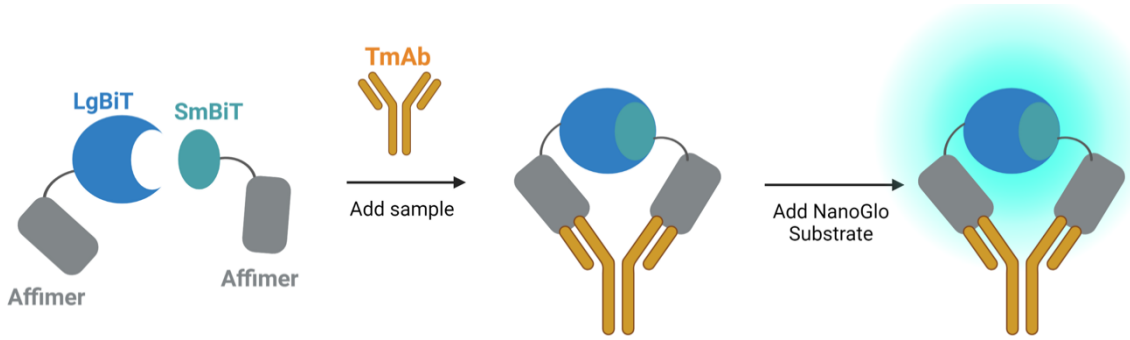

Figure 32. Schematic diagram of Affimer – NanoBiT mechanism of sensing monoclonal antibodies. *The luciferase fragments LgBiT and SmBiT101 are attached to the binding reagents via short GSG linkers to create two separate sensor components. Antibody binding colocalizes the LgBiT and SmBiT, promoting reconstitution of the enzyme and bioluminescence upon addition of Nano-Glo substrate.*

3.3 Experimental Methods

3.3.1 Sensor Cloning

The DNA and primers (Integrated DNA Technologies) used in this method are detailed in the **Appendix C: DNA and Protein Sequences** and **Appendix A: Primer tables** sections, respectively. All sensor constructs were generated in a pET28a vector containing NheI, NotI, SpeI and SalI restriction sites between the NcoI and XhoI sites of the vector, with an in-frame 6xHis-tag sequence and stop-codon following XhoI. Sequential restriction enzyme cloning was used to insert DNA encoding LgBiT, SmBiT (101) or Affimer sequences between NheI/NotI and SpeI/SalI and a $(GSG)_7$ linker sequence between NotI and SpeI. The vector was digested with appropriate restriction enzymes (NEB), dephosphorylated with antarctic phosphatase (NEB), separated on an 0.7% agarose gel, and then purified. All DNA was purified using the Illustra GFX PCR DNA and Gel Band Purification Kit (GE Healthcare). The synthetic DNA encoding LgBiT was purchased from Genscript in pUC57 vector. Affimers were encoded in a previously described pEtLECTRA vector (303). This insert DNA was PCR amplified with primers encoding appropriate restriction sites, then treated with DpnI (NEB) to remove parental vector DNA. Insert DNA encoding SmBiT101 and $(GSG)_7$ linker sequences were generated by PCR of overlapping primers encoding appropriate restriction sites. Amplified insert DNA was purified, digested with appropriate restriction enzymes (**Table 6**) and then re-purified. The digested vector and insert were ligated with T4 DNA ligase (NEB) and transformed into *E. coli* XL-1 competent cells (Agilent Technologies) (genotype: recA1 endA1 gyrA96 thi-1 hsdR17 supE44 relA1 lac [F´ proAB lacIq ZΔM15 Tn10 (Tetr)). Plasmid DNA was purified using the ChargeSwitch Pro Plasmid Miniprep Kit (Invitrogen) and successful generation of constructs was confirmed by sequencing (Genewiz) with T7 / T7term primers.

Table 6. Restriction sites flanking N- or C-terminal recognition elements used for sub-cloning of sensors.

Restriction Sites	*Sensor Position*
NheI and NotI	N-terminal recognition element
SpeI and SalI	C-terminal recognition element

3.3.2 Sensor Expression and Purification

The pET28a vectors with sensor constructs were transformed into *E. coli* BL21* (DE3) cells (genotype: F- ompT hsdSB (rB-mB-) gal dcm rne131). A 1 mL starter culture was added to 50 mL LB media (with 50 µg mL^{-1} kanamycin) and grown at 37°C, 220 RPM before induction at OD_{600} ca. 0.6 with 0.3 mM isopropyl-β-D-thiogalactoside (IPTG) and grown overnight at 16°C, 180 RPM. Cells were harvested at 4000 ×*g* for ca. 20 min, resuspended in 4 mL lysis buffer (pH 7.4, 50 mM Tris, 300 mM NaCl, 10 mM imidazole, 0.1 mg mL^{-1} lysozyme, 1X cOmplete EDTA-free protease inhibitor (Merck), 0.001% v/v benzonase nuclease (Merck)) and incubated on a roller mixer for 1 hour at 4°C. Cells were lysed by sonication (UP50H, Hielscher) for 2 min (5s on / 5s off) at 100% amplitude then pelleted at 17000 ×*g* for 20 min. The supernatant was added to 250 µL Super Co-NTA resin (Generon) that had been pre-equilibrated with wash buffer (pH 7.4, 50 mM Tris, 300 mM NaCl, 10 mM imidazole) and was then incubated on a roller mixer for 1 hour at 4°C. The resin was washed thrice with 5 mL wash buffer and protein eluted with 3 x 0.5 mL elution buffer (pH 7.4, 50 mM Tris, 300 mM NaCl, 300 mM imidazole). Pure fractions (as assessed by 15% SDS-PAGE) were buffer exchanged into storage buffer (50 mM Tris, 150 mM NaCl, pH 7.4) using Zeba spin desalting columns (ThermoFisher). Protein concentration was determined by BCA assay and aliquots stored at -80°C.

3.3.3 Sensor Characterisation

3.3.3.1 Target mAbs

Target analytes were obtained as described in section 2.3.4.1.

3.3.3.2 NanoBiT assay (in buffer)

Assays were performed in PBSB (pH 7.4, PBS + 1 mg mL^{-1} BSA) dilution buffer. 10 µL LgBiT sensor (5x final conc.), 10 µL SmBiT sensor (5x final conc.) and 5 µL mAb (InvivoGen) (10x final conc.) were added to a well of a white no-bind 384-well plate (Corning) and incubated for 30 mins, 25°C, shaking. Then 25 µL of 1:500 Nano-Glo was added to give a final dilution of 1:1000. Luminescence was read (500 ms integration) on a Tecan Spark plate reader. Parameter changes for optimisation are depicted in the results section. Unless otherwise specified in figure legends, these assays were performed with 30 min. incubation between Affimer-constructs and TmAb, followed by addition of 1:1000 NanoGlo and bioluminescence read after 2 min.

3.3.3.3 NanoBiT assay (with serum)

For experiments in 0 – 1% serum, assays were performed in PBSB (pH 7.4, PBS + 1 mg mL^{-1} BSA) dilution buffer. 10 µL 10 nM LgBiT + 10 nM SmBiT in PBSB (2 nM each final conc.) and 5 µL mAb (InvivoGen; 10x final conc.) in PBSB were added to 10 µL human serum (Clinical Trials Laboratory Services) at 5x the final concentration (in PBSB) in a white no-bind 384-well plate (Corning) and incubated for 30 mins, 25°C, shaking.

For experiments in 5 and 50% serum, assays were performed by first preparing stock solutions (LgBiT, SmBiT, mAb) in either 10% human serum with PBSB or 100% human serum. 10 µL of 10 nM LgBiT sensor (5x final conc.), 10 µL of 10 nM SmBiT sensor (5x final conc.) and 5 µL mAb (InvivoGen; various concentrations at 10x the final conc.) were added together in a well of a white no-bind 384-well plate (Corning) and incubated for 30 mins, 25°C, shaking.

For all assays, bioluminescence was initiated by addition of 25 µL of 1:500 Nano-Glo to give a final dilution of 1:1000. Luminescence was read (500 ms integration) on a Tecan Spark plate reader. Parameter changes for optimisation are depicted in the results section.

3.3.4 Data analysis

All data analysis was performed using GraphPad, Prism software version 9.0. Graphs presented as fold gain refer to:

$[RLU\ (X\ nM\ TmAb)\ /\ RLU\ (0\ nM\ TmAb)]$.

Optimisation experiments presented as the mean of at least 2 repeats ± SEM unless specified otherwise. Intra- and inter-assays presented as n=3 or N=3 ± SEM. Statistical significance was determined as $P<0.05$, using one-tailed homoscedastic t-tests.

The four-parameter logistic (4PL) non-linear curve fits were used. This is a mathematical model commonly used to describe dose-response or concentration-response relationships. It employs four key parameters: the bottom plateau representing the minimum response, the top plateau representing the maximum response, the Hill slope indicating the steepness of the curve, and the EC50 (Effective Concentration 50) signifying the concentration that produces a response halfway between the minimum and maximum.

Limit of detection (LoD) was defined as the lowest concentration of analyte that produced a reading above a minimal value (RLU_{min}):

$$RLU_{min} = RLU_{blank} + 1.645\ (SD_{blank}) + 1.645(SD_{low\ conc.})$$

in which RLU_{blank} is the average reading without analyte, SD_{blank} is the standard deviation of samples without analyte and $SD_{low\ conc.}$ is the standard deviation of samples with analyte at the lowest concentration for which a signal above baseline is produced (163).

Accuracy of assay performance was measured as percentage recovery:

$$\%\ \text{recovery} = (\text{mean interpolated concentration}/\text{nominal concentration}) \times 100\%$$

And precision measured as percentage coefficient variation:

$$\%\ \text{CV} = (\text{SD interpolated concentration}/\text{mean interpolated concentration}) \times 100\%$$

3.4 Results

3.4.1 Selection and characterisation of binding proteins

The selection of the Affimer proteins is detailed in section 2.4.1. The same Affimer proteins selected against target antibodies trastuzumab, rituximab, adalimumab, and ipilimumab are used as recognition elements throughout this section.

3.4.2 Split Luciferase sensor development

Luciferase enzymes are commonly used in split enzyme proximity switches with successful recombination seen from multiple luciferases (189, 191, 341). An engineered catalytic subunit of a luciferase from the deep-sea shrimp (*Oplophorus gracilirostris*) was isolated and termed NanoLuc (145, 194). The small size and high stability of this luciferase subunit allows for splitting of NanoLuc into two inactive fragments that recover their enzymatic activity with reassembly, known as the NanoBiT system (145, 195, 196). Here the 18 kDa LgBiT and 11 amino acid SmBiT101 peptide (VTGYRLFEKES) were used as the reporter fragments. The LgBiT and SmBiT101 fragments were genetically fused to either the N-terminus or C-terminus of the anti-idiotypic binding reagents to produce four pair combinations for each TmAb. A $(GSG)_7$ peptide linker was inserted between the NanoBiT fragment and the binding reagent. One letter codes for the LgBiT (**L**) and SmBiT101 (**S**) fragments will be used, as well as for the four Affimers raised against the four TmAbs (adalimumab, **A**; ipilimumab, **I**; rituximab, **R**; and trastuzumab, **T**). The order of the one-letter codes represents N-terminal vs C-terminal constructs with, for instance, **L-A** denoting an Affimer against

adalimumab with an N-terminal LgBiT fragment, connected via a $(GSG)_7$ linker. Full protein sequences are given in the **Appendix C: DNA and Protein Sequences**. All 16 possible combinations were constructed and expressed in *E. coli* and purified via a C-terminal 6xHis-tag (**Figure 33**).

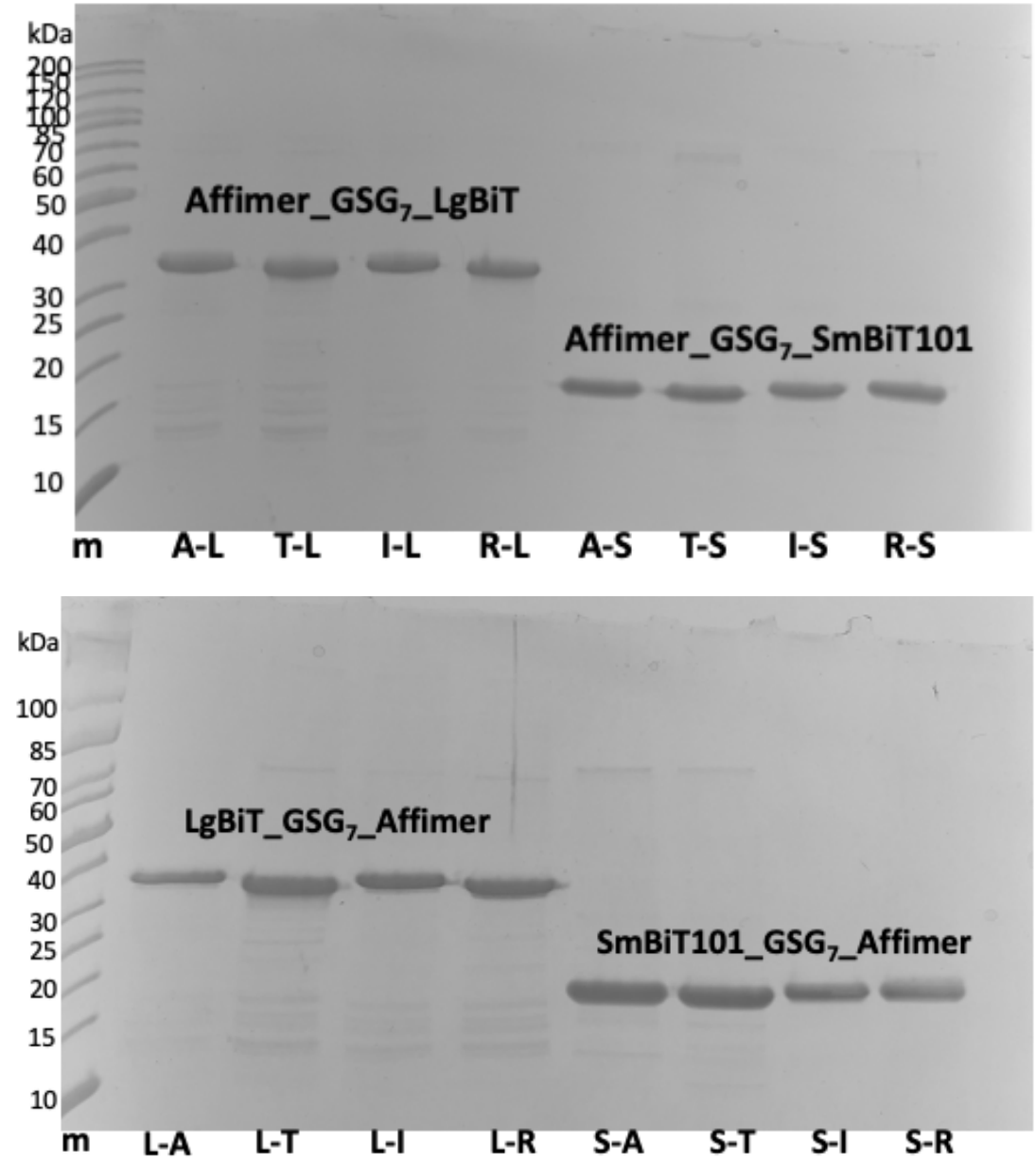

Figure 33. 15% SDS-PAGE of purified Affimer-NanoBiT sensors. Top: *visualisation of anti-ID Affimer NanoBiT construct where the luciferase fragment has been attached to the C-terminus of the Affimer protein with a polypeptide linker.* ***Bottom:*** *visualisation of anti-ID Affimer NanoBiT construct where the luciferase fragment has been attached to the N-terminus of the Affimer protein with a polypeptide linker.*

To determine the optimal sensor pair combinations for TmAb quantification, 2 nM of each sensor pair was incubated with a range of 0 – 100 nM respective TmAb, and after addition of substrate, bioluminescence was measured (**Figure 34**). A 2 nM component concentration was chosen as a starting point for initial experiments due to previous success when detecting other biomarkers (195). Sensor pairs displayed responses ranging from 5-fold to 170-fold gain in bioluminescence. An obvious hook effect is observed at > 10 nM TmAb titres, which is likely due to the excess of TmAb relative to the split enzyme-Affimer constructs (2 nM). When TmAb is in excess, it is stochastically likely only one Affimer binds to each TmAb (**Figure 35**). Even without excess it is possible that two SmBiT or two LgBiT fragments bind to the same TmAb, which should reduce the ensemble signal. Still, the binding affinity between the SmBiT101 and LgBiT fragments will provide a slight thermodynamic advantage to the formation of a SmBiT101-LgBiT-TmAb complex.

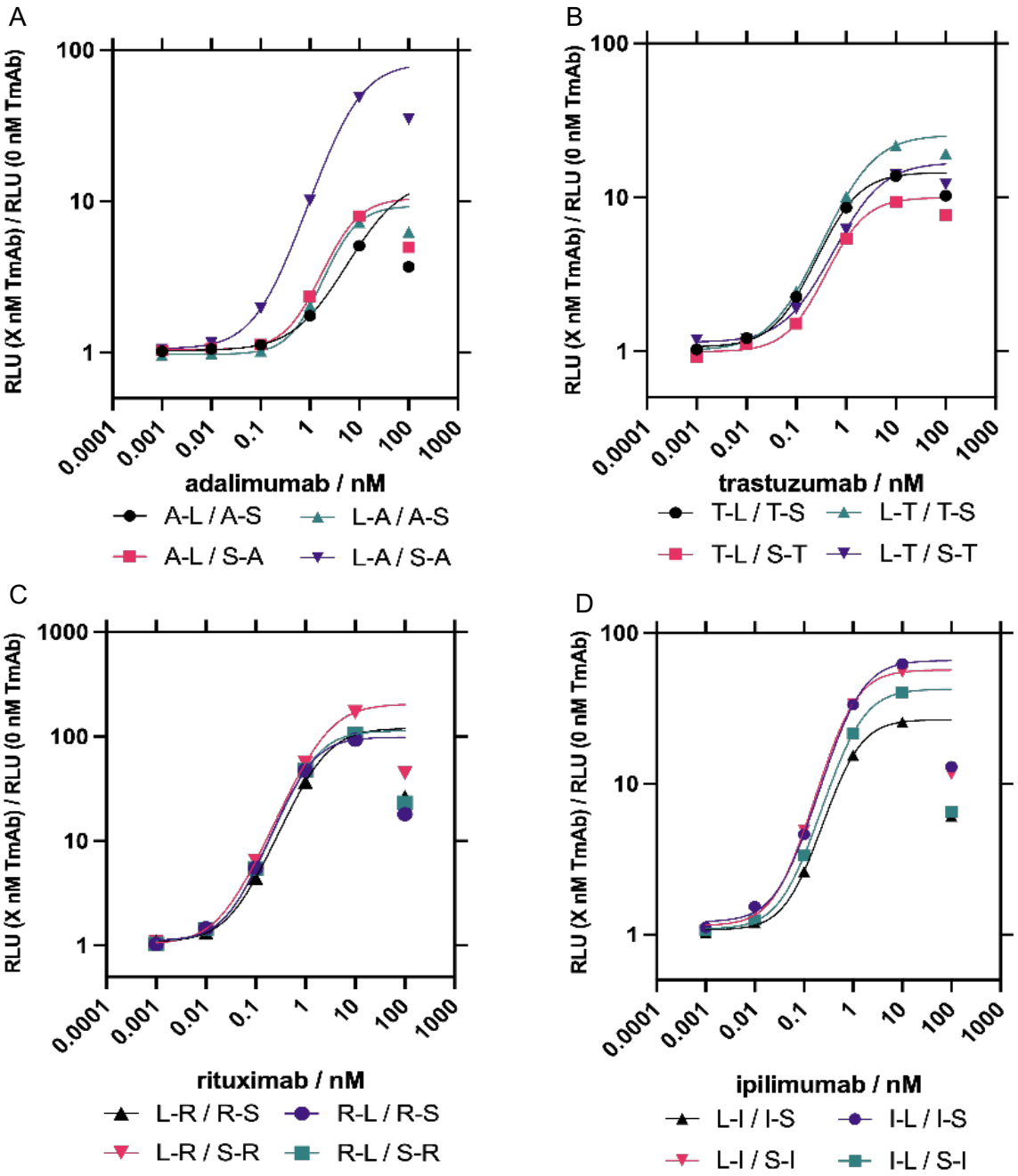

Figure 34. selection of best LgBiT / SmBiT101 NanoBiT sensor combinations for each TmAb target. *A: anti-adalimumab sensor pairs, B: anti-trastuzumab sensor pairs, C: anti-rituximab sensor pairs, D: anti-ipilimumab sensor pairs. 10 µL of each sensor, to a final concentration of 2 nM, were incubated with 5 µL of target TmAb at final concentrations ranging from 0.001 – 100 nM. Plates were incubated at 25ºC, shaking for 30 minutes. 25 µL of NanoGlo diluted 1:500 was then added, and luminescence readings taken immediately (t = 0). Sigmoidal, 4 parameter logistic (4PL) fits were used on data points up to a concentration of 10 nM. Due to the evident hook effect at 100 nM, these data points were not included in the fit and the curve was extrapolated for these points. n = 1.*

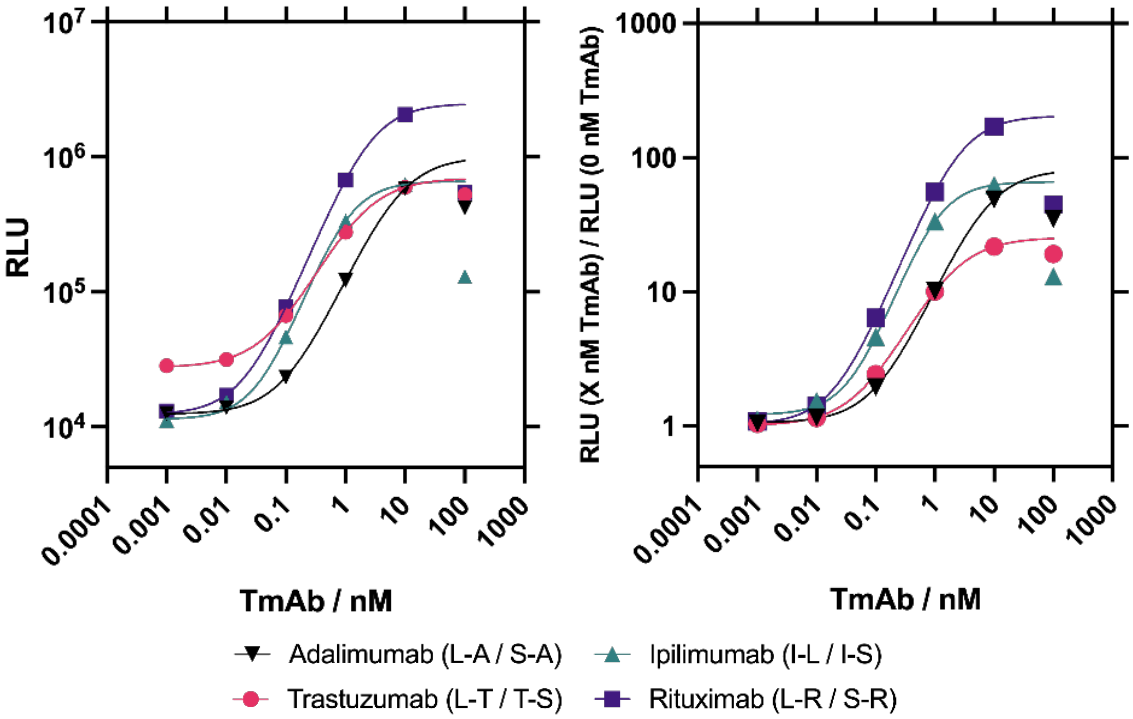

Figure 35. Four sensor combinations were trialled for each target TmAb, and the optimal pair chosen for each. *Raw luminescence data (**Left**) and fold gain data (**Right**) from NanoBiT assays performed on the best performing LgBiT / SmBiT101 pairs selected for each target TmAb. Sigmoidal, 4 parameter logistic (4PL) fits were used on data points up to concentrations of 10 nM. Due to the evident hook effect at concentrations of 100 nM, these data points were not included in the fit and the curve was extrapolated for these points. n = 1.*

The best sensitivity and activity fold gain was seen by the L-R / S-R sensor pair against rituximab and thus this rituximab sensor was chosen to further optimise the assay conditions (**Figure 36 – Figure 41**). First, the ideal sensor concentration was determined (**Figure 36**). Higher concentrations of LgBiT and SmBiT components resulted in a larger relative light unit (RLU) response but also contributed to much higher background complementation. In contrast, the lowest concentration had much lower background, but reduced the maximum analyte-driven reconstitution. To account for both extremes a mid-range concentration of 2 nM for each sensor component was

selected to maximise the ratio of analyte-induced to background bioluminescence signal.

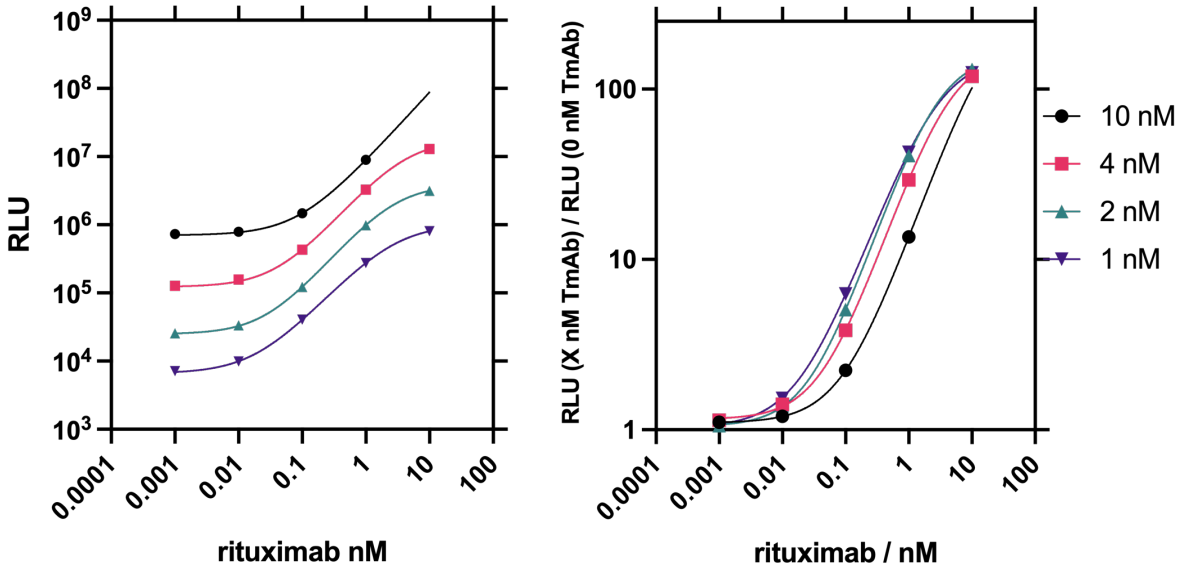

Figure 36. Assay optimisation: The higher the concentration of sensor components, the less sensitive the assay. *RLU (left) and Fold gain (right) data from NanoBiT assays performed on the selected optimal LgBiT / SmBiT101 pair for rituximab with varying sensor concentrations. Measurements taken 2 minutes after substrate incubation. Sigmoidal, 4 parameter logistic (4PL) fits were used on data points up to X = 10 nM. Due to RLU measurements of the 10 nM sensor pair at X = 10 nM being over the limit of RLU measurement of the Tecan, the fits were extrapolated for these points, but no data points were plotted. n = 2, data is plotted as a mean of 2 repeats with ±SEM, where error bars are not visible, they are within the symbol.*

Optimal substrate concentration and incubation time before taking readings were then established (**Figure 37** and **Figure 38**). Increasing substrate concentration increases the RLU, but also the time required before maximum activity is observed (**Figure 37B**). After an initial rise between 2 to 5 min, the signals slowly decayed over time (**Figure 37B** and **Figure 38**). When analysed in terms of fold-gain, differences were significant but very small (**Figure 39** and **Figure 37A**). To optimise the assay for speed and sensitivity, bioluminescence was recorded 2 minutes after addition of the substrate (NanoGlo) at a dilution factor of 1:1000 in the final assay.

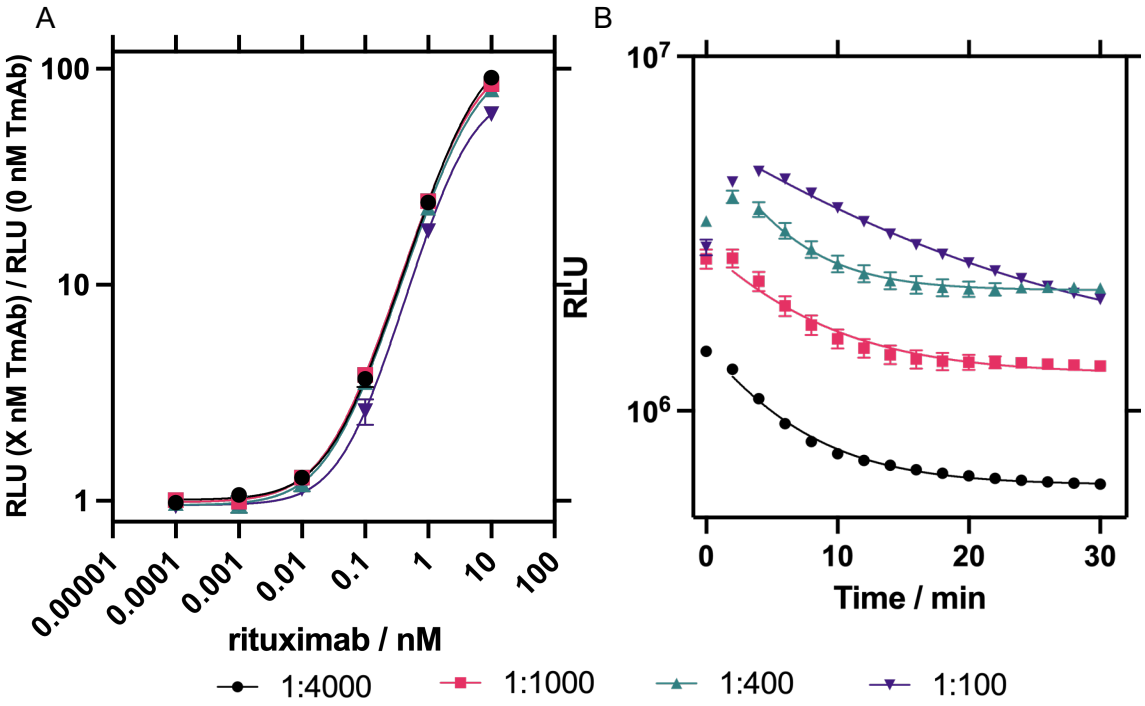

Figure 37. Assay optimisation: Use of higher concentrations of substrate (1:50) can affect the sensitivity of the assay. ***A:*** *The fold-gain luminescence signal of anti-rituximab sensor (L-R/S-R) in response to increasing concentrations of rituximab, using varying dilutions of the NanoGlo substrate. Luminescence measurements were taken 2 minutes after substrate addition. Sigmoidal, 4 parameter logistic (4PL) fits were used.* ***B:*** *Signal decay is more rapid at lower concentration of substrate (1:2000). Change in fold-gain luminescence signal of anti-rituximab sensor (L-R/S-R) in response to 10 nM rituximab, plotted against time for four dilutions of NanoGlo substrate. RLU readings were taken every 2 minutes from 0-30 minutes post substrate incubation. Non-linear regression curves were fitted to the data using a one phase exponential decay equation:*

$$Y = Span \cdot e^{-K \cdot X} + Plateau$$

starting at X = 2 minutes for 1:4000 and 1:1000 and at X = 4 minutes for 1:400 and 1:100. Data points were plotted as n = 3 with error bars representing ±SEM.

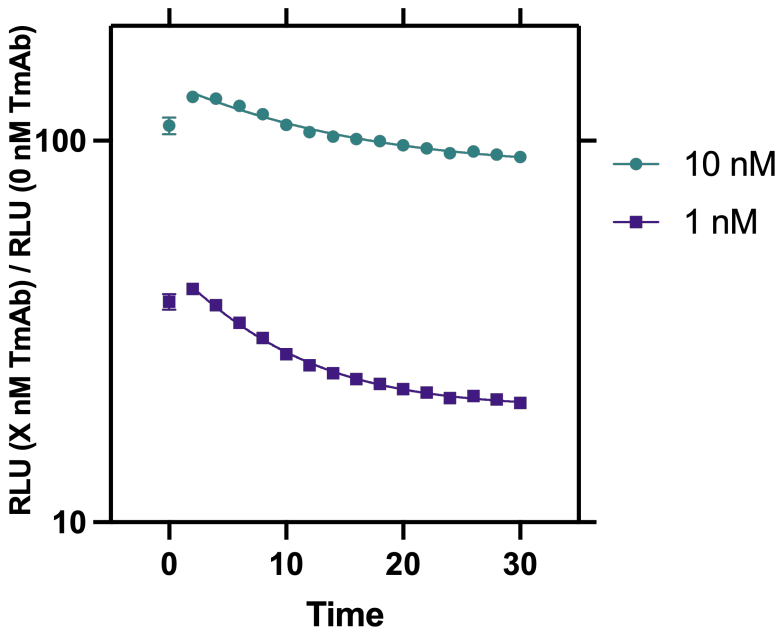

Figure 38. Assay optimisation: Luminescence signal decay begins 2 minutes after substrate addition. *Change in fold-gain luminescence signal of anti-rituximab sensor (L-R/S-R) in response to 10 nM and 1 nM rituximab, plotted against time. RLU readings were taken every 2 minutes from 0-30 minutes post substrate incubation. Non-linear regression curves were fitted to the data using a one phase exponential decay equation* $Y = Span \cdot e^{-K \cdot X} + Plateau$ *starting at X = 2 minutes. Data points were plotted as n = 2 with error bars representing ±SEM.*

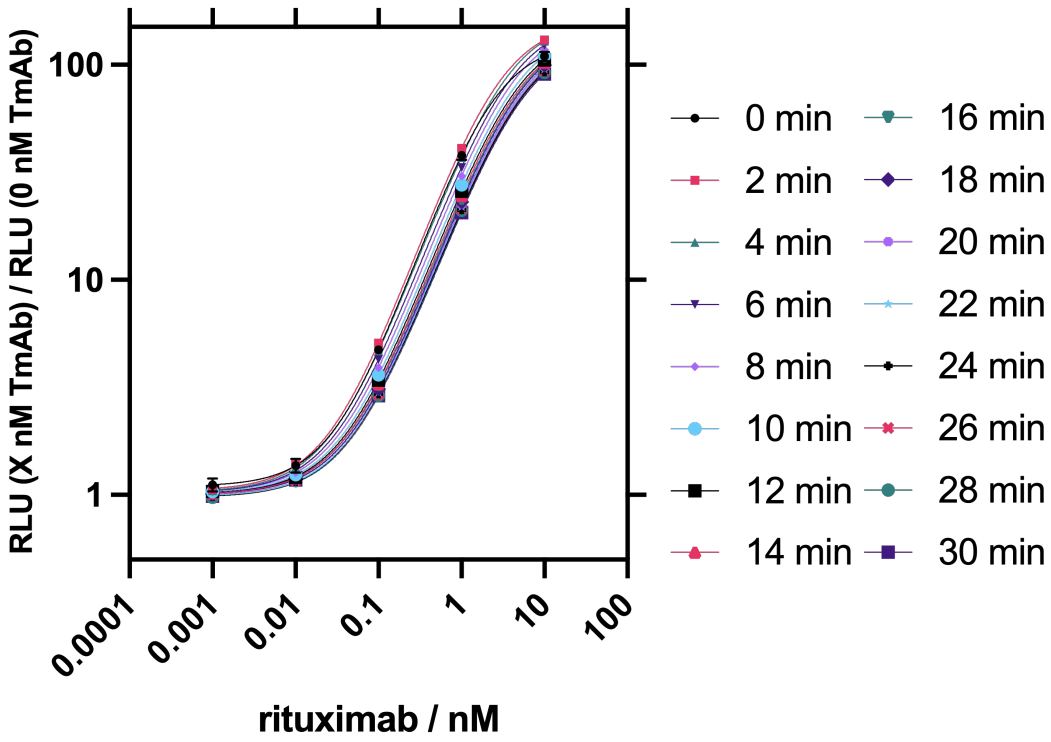

Figure 39. Assay optimisation: RLU measurements are highest 2 minutes after substrate addition. *Fold gain measurements in response to 0.001 – 10 nM rituximab measured every 2 minutes from t = 0 to t = 30 minutes. Sigmoidal, 4 parameter logistic (4PL) fits were used with data points plotted as n = 2 with error bars representing ±SEM.*

Another aspect of the NanoBiT assay that could be optimised was the incubation time between the Affimer constructs and TmAb (at 25°C) prior to substrate addition (**Figure 40**). Maximum activity was already observed within 2.5 min, with the signal remaining stable thereafter. Therefore, and to allow time to prepare multiple tests at once, a 25°C incubation step of ≥ 2.5 minutes should be used before adding the substrate. Importantly, when all reagents are prepared in advance, the time-to-results of the optimised assay is under 10 minutes.

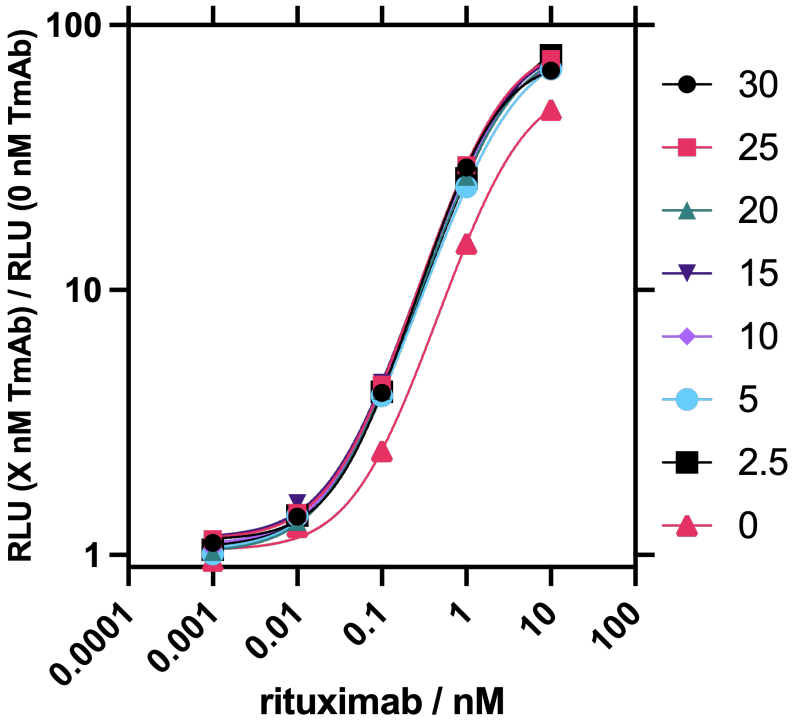

Figure 40. Assay optimisation: The shaking incubation time does not impact the sensitivity of the assay*. Fold gain data from NanoBiT assays performed on the selected optimal LgBiT / SmBiT101 pair for rituximab (L-R/S-R) with varying shaking incubation time at 25°C. Measurements taken 2 minutes after substrate incubation. Sigmoidal, 4 parameter logistic (4PL) fits were used. Data points were plotted as n = 1.*

The functionality of the NanoBiT sensor assay in pooled human serum was tested to establish its feasibility as a PoC TDM test. No significant difference in maximum fold gain of bioluminescence signal was detected in up to 1% pooled human serum ($P>0.05$) (**Figure 41**). However, sensor activity was significantly diminished in 50% serum. The serum sample dilution was optimised so that the therapeutic range of rituximab was within the linear range of the interpolated curve. The therapeutic range of rituximab is approximately 150-500 nM (342). In 0.1% serum the LOD of the rituximab NanoBiT assay is ~ 8 pM (see below), therefore, a 1000x dilution of serum samples would result in TmAb concentrations quantifiable in this assay.

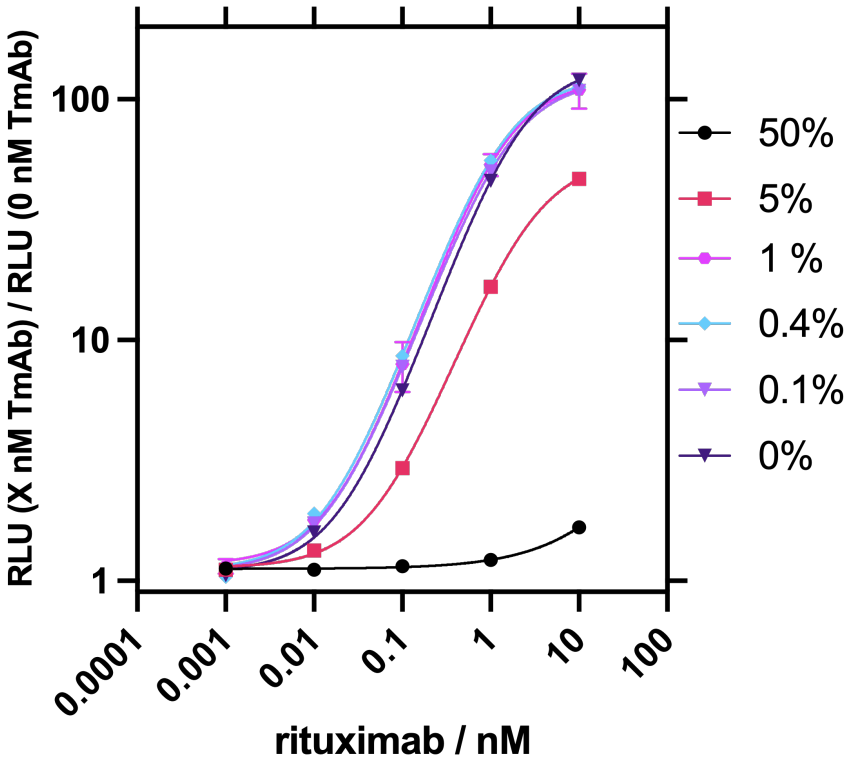

Figure 41. Assay optimisation: L-R/S-R is functional in up to 10% pooled human serum. *The fold-gain luminescence signal of anti-rituximab sensor (L-R/S-R) in response to increasing concentrations of rituximab, in varying dilutions of pooled human serum. Luminescence measurements were taken 2 minutes after substrate addition. Sigmoidal, 4 parameter logistic (4PL) fits were used. Data points were plotted as n = 3 (0%, 0.1%, 0.4%, 1%) or n = 2 (5%, 50%), error bars represent ±SEM.*

Before applying the optimised protocol to the other three sensor pairs, the specificity of each sensor was tested against the four TmAbs and blank buffer as a measurement of bioluminescence (**Figure 42**). All sensors are highly specific to their target TmAb, with no response to non-specific TmAb targets significantly higher than buffer (P>0.05).

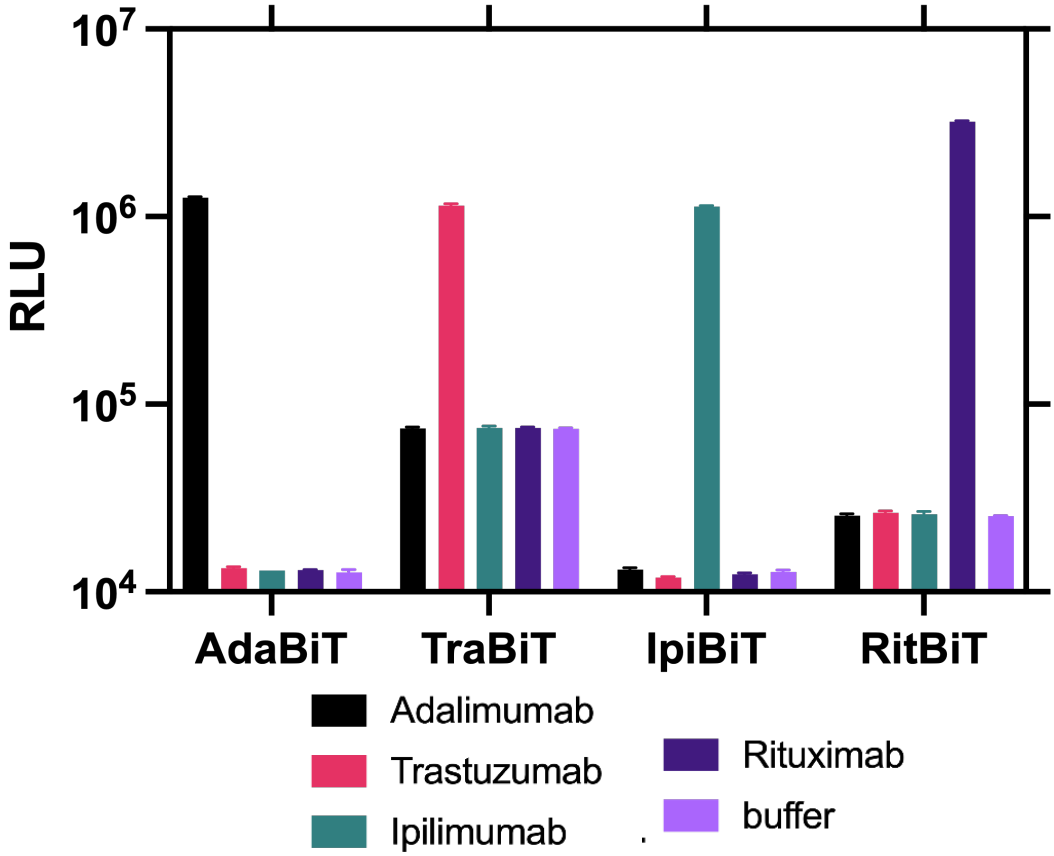

Figure 42. The four best performing sensor combinations for each target TmAb are highly specific for their respective TmAb. *Raw luminescence from NanoBiT assays performed on the selected optimal LgBiT / SmBiT101 pairs for all four target TmAb. A final concentration of 2 nM LgBiT and SmBiT were used with 5 µg mL^{-1} (35 nM) of each TmAb. Data are presented as a mean of 3 repeats with error bars representing ±SEM.*

Finally, performance and intra-assay and inter-assay variability were determined for the four best-performing sensor combinations for each of the TmAb. In the final optimised assay, 10 µL of 10 nM (2 nM final concentration) SmBiT101 and 10 nM LgBiT was incubated with 10 µL 0.5% pooled human serum (0.1% final concentration) and 5 µL of varying TmAb concentration from 0.005 – 2500 ng mL^{-1} (~ 16 fM – 17 nM) for 5 minutes shaking at 25°C. 25 µL 1:500 dilution of NanoGlo substrate (final dilution 1:1000) was then added and bioluminescence readings were taken after 2 minutes. For intra-assay assessment, measurements were taken as n = 3 performed on the same

plate (**Figure 43A, Figure 44A**) and to determine inter-assay variation, 3 independent measurements were taken on separate dates for each target analyte, N = 3 (**Figure 43B, Figure 44B**). Concentrations from 0.005 – 2500 ng mL^{-1} (~ 16 fM – 17 nM) were used to create a standard curve and concentrations interpolated back to determine percentage recovery and percentage coefficient of variance (CV) to assess accuracy and precision respectively. Quantifiable ranges were subsequently calculated by percentage recovery between 80% and 111% and percentage CV < 20% (or < 25% at limit of quantification) (307).

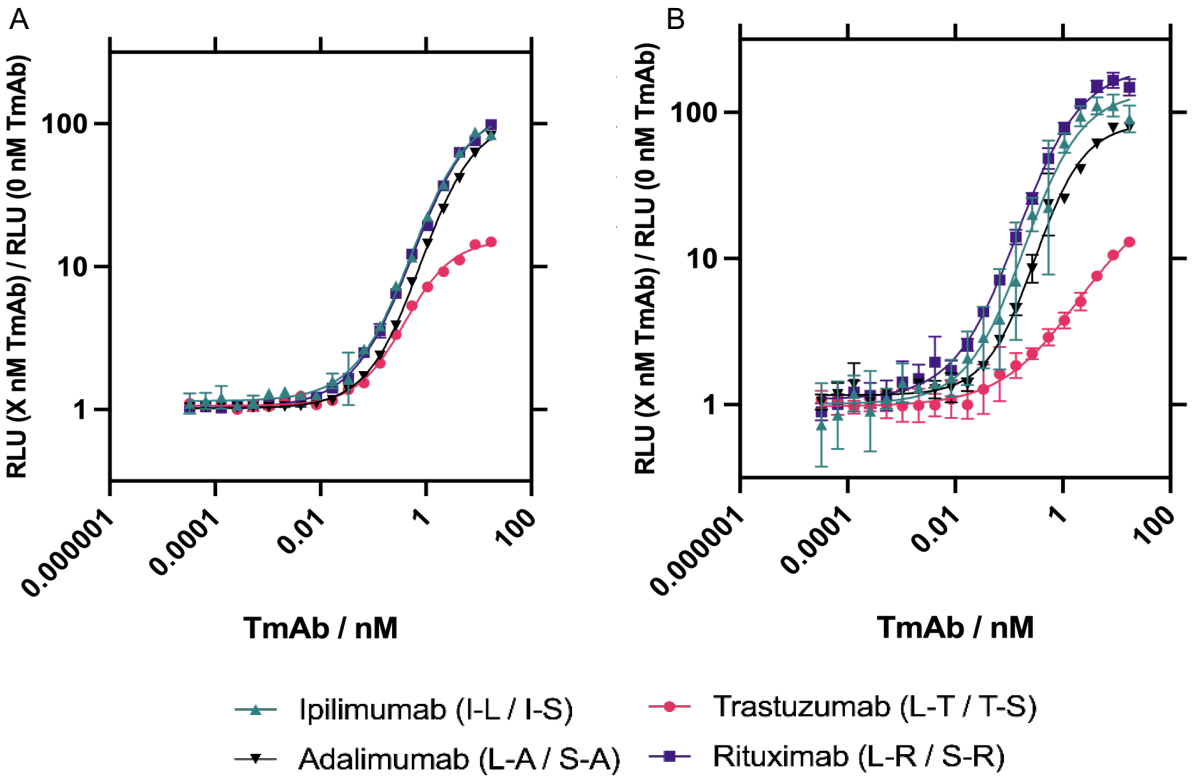

Figure 43. All four TmAb NanoBiT sensors have similar quantifiable ranges. *Data on all sensors at 2 nM in response to increasing concentrations of their respective TmAb. Assays were performed in 0.1% pooled human serum, incubated for 5 minutes shaking at 25°C, and RLU measurements taken after 2 minutes. Standard curves were interpolated for all four sensors using sigmoidal, 4 parameter logistic (4PL) fits.* ***A*** *n = 3, performed on the same day with the same reagents.* ***B*** *N = 3, performed on separate days, using fresh reagents. Data is presented as fold gain activity and error bars represent ±SD.*

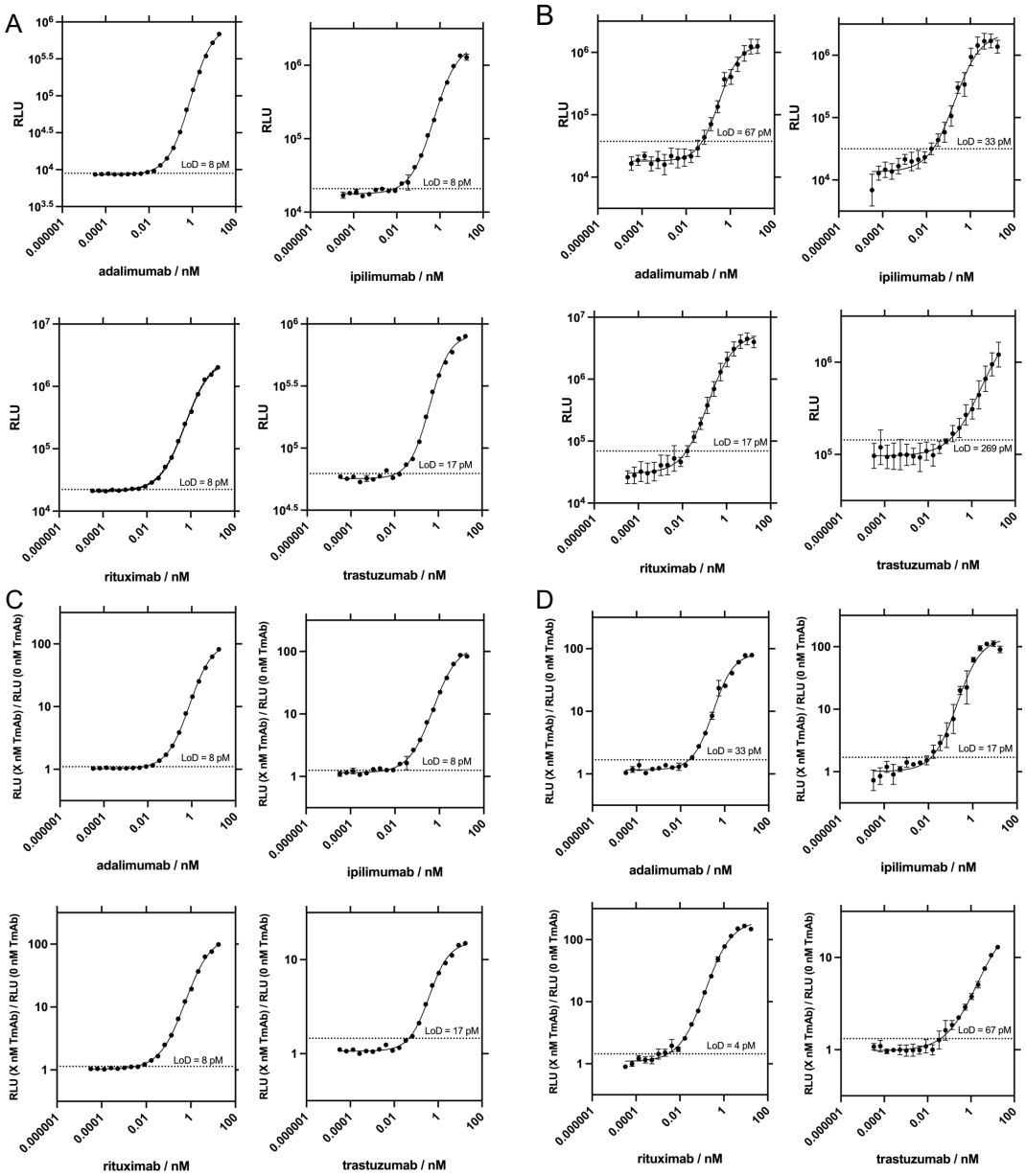

Figure 44 .Standard curves of all four TmAb sensor pairs depicting LoD values*. Data on all sensors at 2 nM in response to increasing concentrations of their respective TmAb (0.005 – 2500 ng mL^{-1}). Assays were performed in 0.1% pooled human serum, incubated for 5 minutes shaking at 25^{o}C, and RLU measurements taken after 2 minutes. Standard curves were interpolated for all four sensors.* ***A & C*** *n = 3, performed on the same day with the same reagents.* ***B & D*** *N = 3, performed on separate days, using fresh reagents. Data points were plotted as raw RLU data (A & B) or fold gain from 0 analyte blank measurements (C & D), error bars represent ±SEM. Limit of Detection (LoD) values indicated with dashed line. Interpolation of standard curves were completed using Prism 9 GraphPad software.*

Table 7. Sensitivity (LoD), accuracy (% recovery), and precision (% CV) *of TmAb NanoBiT assays, as determined from raw bioluminescence* ***(Figure 44 A&C****), or fold gain data (****Figure 43****,* ***Figure 44 B&D****), to define a quantifiable range.*

Sensor target	Feature	Intra-assay (Raw data)	Intra-assay (Fold gain)	Inter-assay (Raw data)	Inter-assay (Fold gain)
rituximab (L-R / S-R)	Sensitivity (LoD)	8 pM	8 pM	17 pM	4 pM
	Quantifiable range	8 pM – 17 nM	8 pM – 17 nM	17 pM – 269 pM	8 pM – 2 nM
	% Recovery	82 – 110%	82 – 110%	95– 109%	96 – 106%
	% CV	1 – 15%	0.5 – 18%	5 – 18%	5 – 24*%
trastuzumab (L-T / T-S)	Sensitivity (LoD)	17 pM	17 pM	269 pM	67 pM
	Quantifiable range	33 pM – 2 nM	33 pM – 2 nM	540 pM – 5 nM†	269 pM – 17 nM
	% Recovery	82 – 110%	82 – 110%	88 – 109%	88 – 110%
	% CV	1 – 10%	1 – 10%	53 – 54%	3-17%
ipilimumab (I-L / I-S)	Sensitivity (LoD)	8 pM	134 pM	33 pM	17 pM
	Quantifiable range	134 pM – 2 nM	134 pM – 2 nM	33 pM – 269 pM†	33 pM – 5 nM
	% Recovery	91 – 101%	93 – 110%	92 – 111%	86 – 111%
	% CV	1 – 10%	1 – 6%	15 – 61%	1– 20%
adalimumab (L-A / S-A)	Sensitivity (LoD)	8 pM	8 pM	67 pM	33 pM
	Quantifiable range	33 pM – 4 nM	33 pM – 8 nM	67 pM – 2 nM	67 pM – 5 nM
	% Recovery	92 – 105%	92 – 108%	88– 109%	81– 109%
	% CV	1 – 5%	1 – 9%	0.5 – 18%	1 – 19%

**%CV precision metrics > 20% only at the limit of quantification †Quantifiable range based on % recovery only*

3.5 Discussion

TDM is a valuable tool when using immunotherapies or immunosuppressive agents which can improve patient outcomes (73). TDM requires the measurement of drug concentrations in blood samples immediately before and immediately after each cyclical dosage to determine peak and trough concentrations (343). Knowledge of these values provides the possibility of immediate dose adjustment for an individual, as well as providing valuable data on the pharmacokinetic (PK) and pharmacodynamic (PD) profile of the drug in question. These parameters can inform clinical staff on how to maintain an effective circulating drug concentration. Currently, TDM is performed on rituximab, ipilimumab, adalimumab and trastuzumab in an ELISA format (33-35, 325, 343), but these require long wash and incubation steps leading to slow time-to-result thus limiting the effect of TDM.

The TmAb NanoBiT assays developed here measured TmAb drug levels accurately and precisely, down to reported trough concentrations for all four therapeutics with a time-to-result of under 10 minutes. Intra-assay variability for the sensors developed was low, with high sensitivity, accuracy and precision when detecting TmAb in 0.1% pooled human serum. When assessing inter-assay variability, the sensors against rituximab and adalimumab exhibited high sensitivity, accuracy, and precision (**Table 7**). Sensors against trastuzumab and ipilimumab showed high sensitivity and accuracy, the precision of these sensors was improved by analysing fold-gain data. Normalisation of the data against blank measurements to give fold-gain values recovered the %CV values of these sensors to provide a wider range of quantification. Substantial intra- and inter-assay variability is commonly seen in binding assays when using raw data due to a range of condition variations (344). Utilising blank or background signal to produce normalised ratio values works as a local control which limits confounding factors and specimen-to-specimen variability, giving more consistent results (345). The use of fold-gain data improved LoD and the upper limit of quantification (ULOQ) (**Table 7**).

Table 8. The reported limit of detection, dilution factor and timeframe to result of commercially available ELISA kits for the detection of rituximab, adalimumab, ipilimumab and trastuzumab in human serum*. Reported performance of LUMinescent AntiBody Sensor (LUMABS) for the detection of trastuzumab* (346)*.*

TmAb	Commercial ELISA	Biosensor	LoD	Dilution Factor	Time
rituximab	ab237640 (Abcam)		~ 31 pM	1000 x	~2.5 hrs
adalimumab	ab237641 (Abcam)		~ 68 pM	10 x	~2.5 hrs
trastuzumab	ab237645 (Abcam)		~ 75 pM	1000 x	~2.5 hrs
ipilimumab	ab237653 (Abcam)		~ 67 pM	300 x	~2.5 hrs
trastuzumab		LUMABS	~303 nM	N/A	~2.5 hrs

Bioluminescent reporters are appealing for PoC applications as they do not require external excitation and have been used in the development of homogenous assays for the detection of mAbs (346-348). One such example is the LUMinescent AntiBody Sensor (LUMABS) which has been adapted for quantification of trastuzumab (346) (**Table 8**). Similar to the assay reported here, LUMABS is a homogenous assay that does not require wash steps, however, requires 2.5 hours of incubation prior to signal output. The sensitivity of this system for trastuzumab detection is 5x lower than the reported sensitivity of the TmAb NanoBiT, however, due to the ratiometric nature of the LUMABS signal, undiluted serum samples can be used. Including the time taken to dilute serum, the TmAb NanoBiT sensor would still be 10x faster than LUMABS. Paper-based adaptions of LUMABS for mAb detection have decreased the time-to-result, however this has not yet been used for quantification of TmAbs (348). LUMABS

use antibody epitopes as recognition elements which are highly selective but require prior knowledge of epitope binding. The use of Affimer proteins, which can be selected through phage display, broadens the scope of targets the NanoBiT system can be adapted to. As an alternative to epitopes, *de novo* proteins have since been implemented into LUMABS (347).

The sensitivity of the TmAb NanoBiT biosensor would allow for substantial dilution of patient samples to keep analyte concentrations within the range of quantification. Trough concentrations of rituximab are reported between 8 – 400 nM (349), with circulating levels < 84 nM after the first cycle of treatment associated with poor treatment outcome for follicular lymphoma patients (343). With a 1000x dilution of serum samples, the minimal effective concentration (C_{min}) falls within the TmAb NanoBiT assay range of quantification. The current standard for serum rituximab measurements is an ELISA with a LoD of 3 ng/mL (≈31 pM) in commercial kits using a 1000x diluted serum sample (**Table 8**). The LoD (4 pM) and LLOQ (8 pM) of the sensors presented here are thus in the same range with the significant advantage of a shorter timeframe, with sample collection to result possible within 10 minutes if reagents are preprepared. Similarly, the quantifiable range for the ipilimumab and trastuzumab sensors cover the reported trough concentration range and C_{min} values for both drug therapies (35, 318), while the LoD and LLOQ are in the same range as commercially available ELISA kits (**Table 8**). The sensitivity of these biosensors also compares favourably to other split luciferase assays developed for monoclonal antibody detection (350, 351). Besides the improvement in time-to-result, homogenous assays as employed here do not require any wash steps and are thus ideally suited to be developed into bedside or PoC sensors.

During the maintenance period (between dosing), adalimumab concentrations < 50 nM in paediatric cases and < 35 nM in adult cases are associated with irritable bowel disease (IBD) and Crohn's disease remission (34, 352, 353). Currently the adalimumab sensor has a LLOQ of 67 pM and after serum dilution samples with adalimumab

concentrations < 50 nM would be just outside of the quantifiable range. During the optimisation stage of this work there was minimal difference in assay activity in up to 1% serum. To this end, higher serum concentrations could be trialled to obtained lower LLOQ for the adalimumab sensor. Assay optimisation was performed on the rituximab sensor L-R/S-R, so it is unsurprising that this was the best-performing sensor. Performance of the adalimumab sensor could possibly be further improved with individual optimisation.

Biosensor performance has so far been validated by spiking pooled human serum, further assessment using patient samples would provide better insight into the real-world applications. The 1:1000 dilution factor applied to spiked samples to maintain TmAb concentrations within the quantifiable range, would suggest that any matrix effects would be negligible. However, there are elements within patient samples that are not represented by pooled serum from healthy individuals. As already discussed in the previous chapter, tumour shedding in advanced HER2+ breast cancer produces circulating exosomes containing HER2 extracellular domain (ECD) which can bind to and reduce the pharmacological effect of trastuzumab (320). Biological treatments, such as immunotherapies, also carry the risk of developing anti-drug antibodies (ADAs). For patients treated with trastuzumab, ipilimumab and rituximab, the risk of ADA formation is low (354), however, the prevalence of ADAs in adalimumab treatment is much higher(355). HER2 ECD and ADAs typically interact with the variable regions of TmAb, with inhibitory effects. The remaining free (pharmacologically active) TmAb concentration is the target of TDM (322). It can be speculated, with recognition elements targeting the variable regions of TmAb, that the NanoBiT sensing system would not measure bound, inactive TmAb concentrations. Future testing of the TmAb NanoBiT sensors on samples taken from patients undergoing these treatments would help inform on the applicability as a PoC test.

3.6 Conclusion

In conclusion, a TmAb NanoBiT assays was developed by combining anti-idiotypic Affimer proteins and NanoBiT split luciferase technology to provide a platform for rapid quantification of four immunotherapies. Assay conditions such as incubation time, sensor component and substrate concentration were optimised to develop an assay with a possible time-to-result within 10 minutes. Low pM LoD values and quantifiable ranges that fall within the therapeutic ranges of ipilimumab, rituximab and trastuzumab were determined in 0.1% spiked human serum. The sensors for detection of these three TmAbs had comparable or improved performance metrics to the current ELISA standards. The possibility of a time-to-result within 10 minutes without any wash steps make the sensors presented here an appealing alternative to ELISA detection, with the prospect of implementing into a PoC device in the future.

The concentration-therapeutic efficacy relationship of therapeutic monoclonal antibodies means that serum drug concentrations outside of the therapeutic window can have negative impacts on patient health. TDM for immunotherapies is currently limited by centralised testing methods with long sample-collection to result timeframes. The TmAb NanoBiT assays, with a time-to-result within 10 minutes, could thus improve patient welfare by providing the opportunity for rapid, precise dose adjustments to improve treatment outcomes and prevent adverse reactions.

4 Chapter 4: Nanobodies as effective recognition elements within chimeric protein switch biosensors

4.1 Abstract

Nanobodies have gained recognition as versatile affinity reagents, showing promise in diverse applications, including diagnostics and therapeutics. Their small size, high affinity, and specificity make them comparable to Affimer proteins. This research explores the potential of V_HH and V_{NAR} nanobodies as recognition elements in chimeric protein switch biosensors for point-of-care applications. The study builds upon the introduction of two biosensor formats, BLA-BLIP and NanoBiT, which originally utilised Affimer proteins. The construction of these biosensors involves genetic fusion and recombinant protein expression, with a focus on bacterial expression systems. The limitations of bacterial expression systems for eukaryotic proteins with disulphide bonds, and strategies for achieving efficient protein yields are discussed. Notably, the number of disulphide bonds negatively correlated with expression as globular proteins outside of inclusion bodies in *E. coli.* The use of denaturation and dilution-mediated refolding led to successful extraction and purification of nanobody NanoBiT sensor constructs. The resulting proof-of-concept sensor displayed high sensitivity and specificity, with a low pM limit of detection and a broad quantifiable range. This work provides a foundation for the development of rapid, cost-effective, and clinically relevant nanobody NanoBiT biosensors, with the potential to transform protein detection in healthcare applications.

4.2 Introduction

In the experimental chapters prior, two chimeric protein switch biosensor formats were introduced – the one component modular allosteric enzyme switch sensor known as BLA-BLIP and the two-component proximity switch known as NanoBiT. Thus far, both sensor formats were developed with the implementation of Affimer proteins as the recognition elements.

When detecting pathogens, disease biomarkers or other proteins the use of immune derived binders offers the benefit of being selected through the naturally evolved process of the immune response. Scaffold-based binding proteins, such as Affimers, tend to rely exclusively on one region or binding loop, whereas, naturally derived antibody proteins create binding regions at the interface of multiple variable regions, arguably increasing the likelihood of the antibody having high affinity (356). This would suggest that an alternative, immune derived binding protein could be a better alternative to Affimer proteins as recognition elements within a point-of-care biosensor.

The development of chimeric protein switch biosensors is easier when using small, single domain recognition elements. Creating chimeric proteins with large and complex proteins such as antibodies is difficult due to the constraints of recombinant protein expression. Although there are options to conjugate proteins after purification (357), the benefits of genetic fusion can outweigh the benefits of using antibodies. The main disadvantage of conjugation techniques is low site specificity which can lead to structural variability (358, 359). The discovery of heavy-chain-only antibodies, the variable domains of which can be successfully isolated, has provided an alternative to classic antibodies. Single domain fragments of heavy-chain-only antibodies are collectively known as nanobodies (250, 360-362). Nanobodies were introduced in depth in section 1.4.1.3 explaining the desirable features that make them valuable tools for the development of point-of-care (PoC) diagnostic tests.

Until recently, nanobodies had not been widely used in protein switch biosensors, although their value as recognition elements has been recognised (177, 254, 363, 364). The published work so far on nanobody protein switch biosensors has exclusively used camelid nanobodies, known as V_HH nanobodies. As mentioned in section 1.4.1.3, a second class of single domain antibody derived from shark and skate species has been discovered, known as V_{NAR} nanobodies. V_{NAR} nanobodies differ structurally to V_HH nanobodies in that they have four variable regions compared to the three CDRs of V_HHs, instead of CDR2 in V_HHs, V_{NAR} nanobodies have two shorter variable regions

know as hypervariable (HV) 2 and HV4. Despite these differences they still possess the desirable characteristics of being single domain and having a high solubility, a good thermal stability, a refolding capacity, and high affinity binding (365, 366).

The feasibility of using V_HH and V_{NAR} nanobodies as recognition elements was investigated in this project. Nanobodies raised in nurse shark, alpaca, llama, and dromedary camel species were implemented into either the BLA-BLIP one-component protein switch sensor or the NanoBiT two-component protein switch sensor.

The chimeric protein switch sensors that have been introduced throughout this thesis have been constructed by genetically fusing the sensor domains at a molecular level and expressing them as recombinant proteins. Recombinant protein expression is most commonly carried out in bacterial expression systems, due to the relative simplicity of the system (367). However, the simplicity of *E. coli* can be its downfall as complex recombinant proteins can be detrimental to the growth of *E. coli* by imparting a metabolic burden on the host and in some instances having a toxic effect (368, 369). There are other limitations to bacterial expression. For example, when expressing recombinant proteins that contain disulphide bonds in bacteria, there is a necessity for an oxidising environment to facilitate the formation of disulphide bonds. The cytoplasm of bacteria, which is the main compartment where proteins are expressed, is highly reducing. Therefore, transport to the periplasm might be necessary to facilitate proper protein folding (370).

The periplasm of *E. coli* contains four proteins that work as catalysts for disulphide bond formation, these are known as disulphide bond protein A-D (DsbA-D) (370-372). DsbA and DsbB work together to form disulphide bonds by catalysing an oxidative reaction between two cysteine thiol groups with the simultaneous release of two electrons and two protons. This reaction can only occur between two cysteine residues that are consecutive within the primary amino acid sequence of the protein. However, to attain their native structure many proteins require disulphide bond formation between non-consecutive cysteine residues. This is where DsbC and DsbD work to perform

disulphide bond isomerisation, they work to catalyse the rearrangement of incorrectly oxidised disulphides so more stables bonds can be formed between alternative cysteine residues within the protein structure.

During the plasmid design phase of recombinant protein expression, a N-terminal signal sequence can be added to direct the protein to the periplasm. This is commonly known as a periplasmic leader sequence. However, there is a limited capacity to move proteins through the cytoplasmic membrane into the periplasm and this can easily become overloaded (373). Additionally, the periplasm makes up only around 8-16% of the total cell volume of *E. coli.* (374, 375). Without extensive optimisation of expression conditions, these factors are typically causative of low protein yields in periplasmic expression. To avoid these limitations, there have been recent advances in engineering bacterial strains for the formation of disulphide bonds within the cytoplasm. Multiple strains have been engineered which work to introduce oxidative proteins to the cytoplasm whilst knocking out reducing pathways. The most successful oxidative strain to date is the SHuffle *E. coli* B strain developed by New England Biolabs, but a range of engineered strains have been reviewed (376).

In eukaryotic cells the endoplasmic reticulum acts as an oxidising cellular compartment where disulphide bonds can be synthesised by sulfhydryl oxidase (377). Yeast are the simplest form of eukaryotic organisms and can be utilised as an expression system to produce proteins that cannot be produced in *E. coli*. *Pichia pastoris* is a methylotrophic yeast strain that has become popular due to its low costs and simple expression system relative to higher order eukaryotes. *P. pastoris* benefits from including an endoplasmic reticulum to facilitate proper folding of heterologous proteins and being equipped with a secretion pathway that can be used to export recombinant proteins into the culture media for easy isolation (378, 379). However, this system does also have its drawbacks. Unlike bacteria, yeast is not very transformation efficient. Yeast also grows around 2-3x slower than *E. coli* which can increase production costs and the level of expression can be variable (380). Another limitation of this expression

system is the limit of selectable marker genes and antibiotic resistance selection is uncommon and requires costly reagents. Protein expression in *P. pastoris* is inducible with methanol, however, at high concentrations methanol is toxic therefore a balance between adequate concentrations to induce expression whilst maintaining cell viability is needed (381, 382). Contamination of the expression media is also common and can lead to degradation of secreted proteins (383).

The aim of this work was the determine if V_HH and V_{NAR} nanobody recognition elements can be implemented into the one-component and two-component chimeric protein switch sensors established in the preceding chapters. An expression and purification protocol was developed and the performance of the sensors characterised as a proof-of-concept study for the future design of nanobody protein switch sensors to be used as point-of-care biosensors.

4.3 Methods

4.3.1 Sensor cloning

4.3.1.1 BLA-BLIP

All primers (Integrated DNA Technologies) used for cloning can be found in **Appendix A: Primer tables**. Synthetic DNA encoding the nanobodies were purchased from Genscript in pUC57 vectors. The insert DNA was PCR amplified with primers to insert appropriate restriction sites on the 3' and 5' end of each nanobody insert. Restriction cloning was used to introduce the nanobody insert DNA into the BLA-BLIP sensor construct vector (based on the expression vector pET28a), as described previously by Adamson *et al.* (170). All DNA was purified using the Illustra GFX PCR DNA and Gel Band Purification Kit (GE Healthcare). Subcloned vectors were transformed into competent *E. coli* XL-1 cells (Agilent Technologies) (genotype: recA1 endA1 gyrA96 thi-1 hsdR17 supE44 relA1 lac [F´ proAB laclq ZΔM15 Tn10 (Tetr)) or NEB-5α competent cells (NEB) (genotype: *fhuA2Δ(argF-lacZ)U169 phoA glnV44 Φ80 Δ(lacZ)M15 gyrA96 recA1 relA1 endA1 thi-1 hsdR17*). Charge Switch Pro Plasmid Miniprep Kit

(Invitrogen) was used for all plasmid DNA purification and successful sub-cloning was confirmed by gene sequencing of the full sensor constructs (GeneWiz) (sequences available **in Appendix C: DNA and Protein Sequences**).

For yeast expression, BLA-BLIP construct gene-sequences were introduced into pPICZα *Pichia pastoris* expression vector for secretory expression (380). First a Q5 site directed mutagenesis kit was used, according to the manufacturer's instructions (NEB), to introduce an EcoRI restriction site into the multiple cloning site of pPICZα. PCR amplification was used on the pET28a+ plasmid containing the PCT 2 BLA-BLIP sequence to introduce EcoRI and XbaI restriction sites to the 3' and 5' ends. Once PCT 2 was successfully subcloned into pPICZα, correct sequences were confirmed with sequencing (Genewiz) using 5' AOXI and 3' AOXI sequencing primers. The plasmids were then linearised to prepare for electroporation using a single site digest with the restriction enzyme SacI.

4.3.1.2 NanoBiT

The DNA and primers (Integrated DNA Technologies) used in this method are detailed in **Appendix C: DNA and Protein Sequences** and **Appendix A: Primer tables**, respectively. All sensor constructs were generated in a pET28a vector containing NheI, NotI, SpeI and SalI restriction sites between the NcoI and XhoI sites of the vector, with an in-frame 6xHis-tag sequence and stop-codon following XhoI. Sequential restriction enzyme cloning was used to insert DNA encoding LgBiT, SmBiT (101) or nanobody sequences between NheI/NotI and SpeI/SalI and a $(GSG)_7$ linker sequence between NotI and SpeI. The vector was digested with appropriate restriction enzymes (NEB), dephosphorylated with antarctic phosphatase (NEB), separated on an agarose gel, and then purified. All DNA was purified using the Illustra GFX PCR DNA and Gel Band Purification Kit (GE Healthcare). The insert DNA was PCR amplified with primers encoding appropriate restriction sites, then treated with DpnI (NEB) to remove parental vector DNA. Insert DNA encoding SmBiT101 and $(GSG)_7$ linker sequences were generated by PCR of overlapping primers encoding appropriate restriction sites.

Amplified insert DNA was purified, digested with appropriate restriction enzymes and then re-purified. The digested vector and insert were ligated with T4 DNA ligase (NEB) and transformed into *E. coli* XL-1 cells (Agilent Technologies) (genotype: recA1 endA1 gyrA96 thi-1 hsdR17 supE44 relA1 lac [F´ proAB lacIq ZΔM15 Tn10 (Tetr)) or NEB-5α competent cells (NEB) (genotype: *fhuA2Δ(argF-lacZ)U169 phoA glnV44 Φ80 Δ(lacZ)M15 gyrA96 recA1 relA1 endA1 thi-1 hsdR17*). Plasmid DNA was purified using the ChargeSwitch Pro Plasmid Miniprep Kit (Invitrogen) or Monarch® miniprep kit (NEB) and successful generation of constructs was confirmed by sequencing (Genewiz) with T7 / T7term primers.

4.3.2 Sensor expression and purification

4.3.2.1 BLA-BLIP

4.3.2.1.1 Bacterial

BLA-BLIP nanobody sensor expression used the protocol previously detailed and used in chapter 2 for TmAb_BLA-BLIP expression (170). Briefly, plasmids containing the sensor constructs were transformed into *E. coli* BL21 (DE3) competent cells (genotype: fhuA2 [lon] ompT gal (λ DE3) [dcm] ΔhsdS λ DE3 = λ sBamHIo ΔEcoRI-B int::(lacI::PlacUV5::T7 gene1) i21 Δnin5). 500 mL LB media (with 50 μg mL^{-1} kanamycin) was inoculated with a 10 mL starter culture and grown at 37°C, 220 rpm. At OD_{600} ~0.6, cultures were induced with 0.3 mM isopropylβ-D-thiogalactoside (IPTG) and grown overnight at 15°C, 150 rpm. Cells were harvested and the periplasmic protein extracted by osmotic shock. The cell pellet was resuspended in 15 ml TSE buffer (30 mM Tris, 20 % w/v sucrose, 1 mM EDTA, pH 8) and placed on a roller mixer at 4°C for 15 min. Cells were pelleted at ca. 17000 ×*g* for 20 min and the supernatant retained as periplasmic fraction 1 (P1). The pellet was resuspended in 15 ml of ice cold 5 mM $MgSO_4$ and placed on a roller mixer at 4°C for 20 min. Cells were pelleted at ca. 17000 ×*g* for 20 min and the supernatant retained as periplasmic fraction 2 (P2). Fractions P1 and P2 were combined, adjusted to 50 mM Tris, 150 mM NaCl, 20 mM imidazole, pH 7.4 by addition of small amounts of concentrated stock solution. The sensor construct was batch purified

with Super Ni-NTA resin (Generon) via the N-terminal 6xHis tag. The resin was washed thrice with 20 ml wash buffer (50 mM Tris, 150 mM NaCl, 20 mM imidazole, pH 7.4) and protein eluted with 4 X 500 µl elution buffer (50 mM Tris, 150 mM NaCl, 250 mM imidazole, pH 7.4). Eluates were pooled and further purified via the C-terminal Strep-II tag using the Strep-Tactin spin column kit (IBA). The double tag purified protein was buffer exchanged into storage solution (50 mM Tris, 150 mM NaCl, pH 7.4) using Zeba spin desalting columns (Thermofischer). Protein concentration was determined by BCA assay and purity checked via 12.5% SDS-PAGE. Aliquots were stored at -80°C. Adaptions to the expression protocol are detailed throughout the results section including smaller volume (50 mL) expression trials with differing expression conditions, cell strains and purification techniques.

4.3.2.1.2 Yeast

Wild type GS115 Pichia pastoris was grown up to an OD_{600} of between 1-1.3 to make electro competent cells. Cultures were pelleted at 1500 ×*g* for 5 minutes to remove the media and cell pellets re-suspended in sterile 500 mL dH_2O. Resuspended cultures were pelleted again at 1500 ×*g* and resuspended in 25 mL dH_2O, to wash any remaining salt from the growth media off the cells. After a final centrifugation, they were re-suspended in 1 mL 1 M sorbitol and stored on ice.

Linearised pPICZα plasmids containing BLA-BLIP sensor DNA were electroporated using a BioRad MicroPuler electroporator according to the manufacturer instructions for *Pichia pastoris*. 80 µL of electro competent cells were mixed with 5 µg of linearized DNA in 10 µL dH_2O on ice. Cells were added to a 0.2 cm cuvette and pulsed once at 2 kV. 1 mL of 1M sorbitol was added immediately after and the cells were transferred into a sterile falcon tube.

Cells were incubated at 30°C for 1 hour. After 1 hour, 1 mL of YPD media (1% yeast extract, 2% peptone, 2% dextrose) was added to the cells and incubated at 30°C, 150 rpm for an additional hour. 5 plates containing YPDA (1% yeast extract, 2% peptone,

2% dextrose, 2% agar), 1 M sorbitol and 100 µg/mL Zeocin, were created for each construct. Cells were spun down and resuspended in 1 mL YPD. 200 µL of each construct culture plated out (x5) and grown for 96 hours at 30°C.

~20 single colonies were picked and used to inoculated 200 µL of Buffered Glycerol-complex Medium (BMGY) (1% yeast extract, 2% peptone, 100 mM potassium phosphate, 1.4% yeast nitrogen base, $4x10^{-5}$% biotin, 1% glycerol) and grew for 24 hours 30°C, 220 rpm. Simultaneously, each colony was spread onto a fresh YPDA plate with 100 µg/mL zeocin for reselection to ensure the antibiotic resistance gene had been integrated. After 24-hour growth, the 200 µL expression cultures were spun down at 1500 x*g* for 5 minutes, media removed and resuspended in 200 µL Buffered Methanol-complex Medium (BMMY) (1% yeast extract, 2% peptone, 100 mM potassium phosphate, 1.4% yeast nitrogen base, 4x10-5% biotin, 0.5% methanol) to induce protein expression. After a further 24 hours at 30°C, 220 rpm cultures were span down and the supernatant gently removed. As the sensors were expressed in a secretory expression vector (pPICZα), recombinant protein should be found in the expression media.

The best expressing colonies were made up into high density glycerol stock (20% glycerol). For larger scale expression, 50 mL BMGY was inoculated with 20 µL glycerol stock and grown at 30°C, 220 rpm to an OD_{600} of 1. BMGY cultures were pelleted at 1500 x*g* and resuspended in 50 mL BMMY (1.5% methanol) to induce expression. Cultures were grown over a 72-hour period at 30°C, 220 rpm. Samples of supernatant were collected every 24 hours to analyse the optimal time-point for protein secretion.

4.3.2.2 NanoBiT

The pET28a vectors with sensor constructs were transformed into SHuffle® T7 competent cells (NEB) (genotype: *fhuA2 lacZ::T7 gene1 [lon] ompT gal sulA11 R(mcr-73::miniTn10*--Tet^S*)2 [dcm] R(zgb-210::Tn10*--Tet^S*) endA1 ?(mcrC-mrr)114::IS10*). A 1 mL starter culture was added to 50 mL LB media (with 50 µg mL^{-1} kanamycin) and grown

at 37°C, 220 rpm before induction at OD_{600} ca. 0.6 with 0.3 mM IPTG and grown overnight at 16°C, 180 rpm. Cells were harvested at 4000 ×*g* for 20 min, resuspended in 4 mL lysis buffer (pH 7.4, 50 mM Tris, 300 mM NaCl, 10 mM imidazole, 1X cOmplete EDTA-free protease inhibitor (Merck), 0.001% v/v benzonase nuclease (Merck)) and incubated on a roller mixer for 1 hour at 4°C. Cells were lysed by two methods; by sonication (UP50H, Hielscher or Fischebrand™ sonic dismembrator) for 2 min (5s on / 5s off) at 100% amplitude then pelleted at 17000 x*g* for 20 min. Alternatively, the cell suspension was passed twice through a cell disrupter (Constant Systems) at 30 kPsi and cell debris removed by centrifugation at 17000 x*g* for 20 min. The supernatant was added to 250 µL Super Co-NTA resin (Generon) that had been pre-equilibrated with wash buffer (pH 7.4, 50 mM Tris, 300 mM NaCl, 10 mM imidazole) and incubated on a roller mixer for 1 hour at 4°C. Using gravity flow columns, the resin was washed thrice with 5 mL wash buffer and protein eluted with 3 x 0.5 mL elution buffer (pH 7.4, 50 mM Tris, 300 mM NaCl, 300 mM imidazole). Pure fractions (as assessed via 15% SDS-PAGE) were buffer exchanged into storage buffer (50 mM Tris, 150 mM NaCl, pH 7.4) using Zeba spin desalting columns (ThermoFisher). Protein concentration was determined by BCA assay and aliquots stored at -80°C.

4.3.2.2.1 Solubilisation of NanoBiT constructs from inclusion bodies.

Purification of denatured insoluble protein inclusion bodies was carried out using two protocols, a urea denaturation protocol, and a Pierce™ Radio-Immunoprecipitation Assay (RIPA) buffer (25 mM Tris•HCl, 150 mM NaCl, 1% NP-40, 1% sodium deoxycholate, 0.1% SDS, pH 7.6) (Thermo Scientific) protocol.

The urea denaturation protocol involved first purifying the nanobody NanoBiT from the sonication supernatant as described above to recover any soluble protein that had been expressed. The remaining cellular debris (insoluble fraction) was then incubated with 8 M urea for 1 hour at 4°C while gently mixing. This fraction was centrifuged at 17000 x*g* for 20 min and the supernatant added to 250 µL Super Co-NTA resin (Generon) that had been pre-equilibrated with urea wash buffer (pH 7.4, 50 mM Tris,

300 mM NaCl, 10 mM imidazole, 8 M urea) and incubated on a roller mixer for 1 hour at 4°C. Using gravity flow columns, the resin was washed with wash buffer containing an incrementally lesser concentration of urea with 6 M, 4 M and 2 M. The resin was then washed thrice with wash buffer containing no urea and protein eluted with 3 x 0.5 mL elution buffer (pH 7.4, 50 mM Tris, 300 mM NaCl, 300 mM imidazole). Pure fractions (as assessed by SDS-PAGE) were buffer exchanged into storage buffer (50 mM Tris, 150 mM NaCl, pH 7.4) using Zeba spin desalting columns (ThermoFisher). Protein concentration was determined by BCA assay and aliquots stored at -80°C.

Purification utilising Pierce™ RIPA buffer for cell lysis first involved harvesting cells at 4000 x*g* and resuspending the cell pellet in 3 mL RIPA buffer (supplemented with 1X cOmplete EDTA-free protease inhibitor, 0.001% v/v benzonase nuclease) and incubating at 4°C for 30 minutes. The resuspended cells were sonicated at 100% Amplitude for 4 minutes (5s on/ 5s off), then pelleted at 17000 x*g* for 20 min. The supernatant was then incubated with 250 µL Super Co-NTA resin for 1 hour, while gently mixing at 4°C. Recovery of protein from Co-NTA resin via gravity flow was then carried out as described in section 4.3.2.2.

4.3.3 Expression Analysis

4.3.3.1 SDS-PAGE and Western blot

Sodium Dodecyl Sulfate–Polyacrylamide gel electrophoresis (SDS-PAGE) and Western blot were performed using the Miniprotean tetra cell (Bio-Rad). The sample buffer for reducing SDS-PAGE is 60 mM Tris•HCl pH 6.8, 1% w/v SDS, 5% v/v glycerol, 0.005% w/v bromophenol blue and 1% v/v 2-mercapto-ethanol (2-ME). Proteins separated by SDS-PAGE were either stained with Quick Coomassie stain (Protein Ark) or subjected to Western blot. For western blots, separated proteins were transferred onto nitrocellulose membranes via semi-dry blotting using the Bio-Rad Trans Blot Turbo system according to the manufacturer's instructions. Blots were incubated, at room temperature for 1 hour with blocking buffer (Tris Buffered Saline (TBS) (20 mM Tris and 150 mM NaCl, pH 7.4) with 3% bovine serum albumin (BSA)).

His-tagged protein was detected using HRP-conjugated anti-his tag mouse monoclonal antibody (R&D systems, 1:4000). Strep-tagged protein was detected using Streptactin-HRP (Bio-Rad, 1:5000), in blocking buffer. Antibody conjugates were incubated overnight at 4°C. Membranes were stained with 1-step™TMB-Blotting substrate solution (Thermo Fisher Scientific).

4.3.3.2 ELISA

A Nunc Maxisorb 96-well plate was first coated with 70 µL yeast culture supernatant and incubated overnight at room temperature. After washing thrice with PBST (PBS + 0.05% Tween-20), 100 µL casein blocking buffer (1:10 in PBST) was incubated in each well for 1 hour at 20°C, followed by washing thrice with PBST. Streptavidin HRP (Bio-Rad) (1 µg mL^{-1}) or anti-His tag HRP conjugate (1:4000) (R&D systems) in casein blocking buffer was then added to the wells and incubated at room temperature for 30 minutes. This step was followed by washing 6x with PBST and incubation with 50 µL of 1-step TMB for 15 minutes. 50 µL 2 M sulphuric acid was used to stop the reaction and the plate was then read at 450 nm using a plate reader (MultiSkan FC).

4.3.3.3 Nitrocefin Assay

For assays to detect enzyme activity in purification fractions, non-binding-surface 96-well plates (Corning) were used, with a final volume of 200 µl assay buffer (50 mM sodium phosphate, 100 mM NaCl and 1 mg mL^{-1} BSA, pH 7). 10 uL sensor containing elution fraction was incubated with 10 nM of target analyte for 15 minutes. Nitrocefin (Merck) was added at 50 µM and absorbance measured at 551 nm on a plate reader (MultiSkan FC, Thermo Scientific) after 10 minutes.

4.3.4 Sensor Characterisation

4.3.4.1 Targets

Lysozyme, from chicken egg white (Sigma) was used as the Hen Egg Lysozyme (HEL) target for all protein switch sensors targeting HEL. Human procalcitonin recombinant protein (Invitrogen) was used as the target for all sensors against procalcitonin (PCT).

Human C-reactive protein (CRP) (Millipore, Merck) was used as a negative control for sensor specificity.

4.3.4.2 NanoBiT assay

Assays were performed in PBSB (pH 7.4, PBS + 1 mg mL^{-1} BSA) dilution buffer. 10 µL LgBiT sensor (5x final conc.), 10 µL SmBiT sensor (5x final conc.) and 5 µL target analyte (10x final conc.) were added to a well of a white no-bind 384-well plate (Corning) and incubated for 30 mins, 25°C, shaking. Then 25 µL of 1:500 Nano-Glo was added to give a final dilution of 1:1000. Luminescence was read (500 ms integration) on a Tecan Spark plate reader. Any assay parameter changes are described in the results section. Unless otherwise specified in figure legends, these assays were performed with 30 min. incubation between nanobody NanoBiT sensor and analyte, followed by addition of 1:1000 NanoGlo and bioluminescence read after 2 min.

4.3.4.3 NanoBiT assay in serum

For experiments in 0.1 – 10% serum, assays were performed in PBSB (pH 7.4, PBS + 1 mg mL^{-1} BSA) dilution buffer. 10 µL 10 nM LgBiT + 10 nM SmBiT in PBSB (2 nM each final conc.) and 5 µL target analyte (10x final conc.) in PBSB were added to 10 µL human serum (Clinical Trials Laboratory Services) at 5x the final serum concentration (in PBSB) in a white no-bind 384-well plate (Corning) and incubated for 30 mins, 25°C, shaking in the Tecan Spark plate reader. Bioluminescence was initiated by addition of 25 µL of 1:500 Nano-Glo to give a final dilution of 1:1000. Luminescence was read (500 ms integration) on a Tecan Spark plate reader After 2 minutes unless specified otherwise.

4.3.4.4 NanoBiT assay with Furimazine derivatives

For experiments using furimazine derivatives, assays were performed as in section 4.3.4.2, except NanoGlo was replaced with 25 µL of varying concentrations of furimazine, luciferin 108 or luciferin 103 (kindly gifted by Yves L Janin, Alliance Sorbonne Université) (384, 385). Final concentrations of furimazine derivatives are

shown in the results section. Luminescence was read (500 ms integration) on a Tecan Spark plate reader 2 minutes after substrate addition, unless specified otherwise.

4.3.5 Data Analysis

All data analysis was performed as described in section 3.3.4.

4.4 Results

4.4.1 Hen Egg Lysozyme proof-of-concept nanobody BLA-BLIP

Nanobodies have ideal features to be used as recognition elements within a protein switch biosensor, specifically their small size (12-14 kDa) and high affinity binding properties (386-388). As a proof-of-concept study, the feasibility of introducing nanobodies into protein switch biosensors was explored using a nurse shark (*Ginglymostoma cirratum*) derived V_{NAR} (389) and dromedary camel (*Camelus dromedarius*) derived V_HH (361), both raised against hen egg lysozyme (HEL). HEL is commonly used as a proof-of-concept analyte and inferred as a model analyte. This is due to it being abundantly available with a well-characterised structure and vast knowledge of its activity and stability (390, 391).

4.4.1.1 Selection of nanobodies as recognition elements

The two nanobodies chosen as recognition elements for the development of anti-HEL protein switch biosensors were selected from literature and both have structural data available on their binding to HEL. The V_HH is known as D2L24 (361) and the V_{NAR} 5A7 (389) with K_D values of ~7.5 nM and ~22 nM respectively. Multiple anti-HEL V_HH clones have been characterised (361, 392), and among the published clones with available structural data, D2L24 was chosen due to its unique ability to bind to different epitopes of HEL than other V_HH proteins published, setting it apart from the others. This selection meant that we could use both 5A7 and D2L24 to bind to non-overlapping epitopes (**Figure 45**).

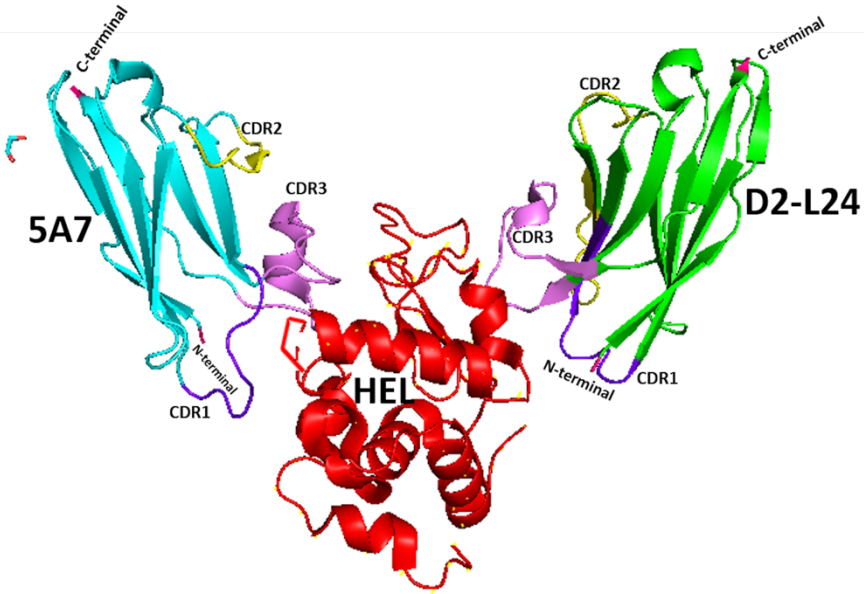

Figure 45. V_{NAR} 5A7 (blue) and V_HH D2L24 (green) bound to the non-overlapping epitopes of HEL. *Complementary determining regions (CDR) of each nanobody are labelled with CDR3 (pink) having the most contact residues with HEL for both nanobodies. The remaining contact residues are within CDR1 of both nanobodies. Structural data of each nanobody bound to HEL was obtained from the protein data bank (PDB) at https://www.rcsb.org/ (361, 393) (PDB accession code 1T6V &1ZVH). Overlapping of the structural information to create an image of how the two nanobodies could bind without interacting with one-another was processed using PyMol software.*

4.4.1.2 HEL nanobody BLA-BLIP sensor design

Implementing anti-HEL nanobodies into the one component modular allosteric enzyme switch sensor introduced in Chapter 2, BLA-BLIP, was the starting point for this work. As previously described, the BLA-BLIP biosensors include three separate linker regions, which connect the different domains of the sensor. From previous work, within this thesis and predating this thesis (170), it is known that the linker regions are integral to the performance of the BLA-BLIP sensors. Optimisation of the rigid linker 1 and linker 3 regions, has shown that 3 amino acid residues is the optimal length. However, the optimal length of the flexible linker 2 region is dependent on the analyte. The semi-flexible linker – $(GSG)_6A(EAAAK)_6A(GSG)_6A(EAAAK)_6A(GSG)_6$ – was previously used to bridge the distance between TmAb variable regions, however, a more flexible $(GSG)_7$ linker has been used for the detection of CRP (170). With structural data available, the distance between the termini of each HEL nanobody could be measured

to determine the linker length necessary to span the distance between the relative epitopes (**Figure 45**). Distances between 66.5 Å and 65.1 Å were measured between the nanobodies. The average length of an amino acid in an extended peptide chain is approximately 3.5 Å (394, 395). Therefore, the distance between the two anti-HEL nanobodies could theoretically be spanned with a $(GSG)_7$ linker within the BLA-BLIP sensor.

A pre-existing pET28a+ plasmid containing the BLA-BLIP construct, with a $(GSG)_7$ linker 2 and two Affimers raised against C-reactive protein (CRP), was used as the backbone to develop the anti-HEL nanobody BLA-BLIP constructs. Restriction sites flanking position A and position B were used to sub clone in the nanobodies 5A7 and D2L24 in both orientations to create the constructs HEL 1 and HEL 2 (**Figure 46**). HEL 1 and HEL 2 were the original nanobody BLA-BLIP constructs developed, all subsequent constructs were developed to aid the understanding of expression issues. HEL 3 and HEL 4 increased the linker 1 and linker 3 length. HEL 5 removed the presence of V_{NAR} recognition elements. HEL 6 and HEL 7 changed the length of linker 2.

Figure 46. Schematic diagrams of all HEL BLA-BLIP constructs created. *The template pET28a+ plasmid containing the enzyme and inhibitor and a $(GSG)_7$ linker 2 connecting recognition element position A and B was used to create 7 HEL constructs throughout this project. V_{NAR} are labelled with a shark symbol and V_HH are labelled with a camel symbol.*

4.4.1.3 HEL nanobody BLA-BLIP expression

A bacterial expression protocol from previous work with BLA-BLIP sensors, specifically those that utilised Affimer recognition elements as seen in Chapter 2, was used to express HEL 1 and HEL 2. This protocol involved expressing the BLA-BLIP construct with a periplasmic leader sequence in BL21 (DE3) *E. coli* cells, inducing expression with IPTG and extracting the protein via osmotic shock. A two-step purification protocol was then applied to the periplasmic fractions as described in section 4.3. Briefly, this included first purifying via the N-terminal 6xHis-tag and then further purifying the

eluates via the C-terminal strep-II tag. Analysis of purification fractions, including the periplasmic and unbound fractions, yielded no protein recovery after osmotic shock when expressing HEL 1. Visualisation of protein via SDS-PAGE of HEL 2 purification fractions showed recovery of protein at the correct molecular weight (~79 kDa) in elution fractions from his-tag purification (**Figure 47**). Further purification of the HEL 2 BLA-BLIP sensor using streptactin spin columns resulted in a complete loss of recovered protein. Attempts to increase the concentration of desthiobiotin – used to elute strep-II labelled protein from streptactin resin – was unsuccessful in recovering the HEL 2 BLA-BLIP protein.

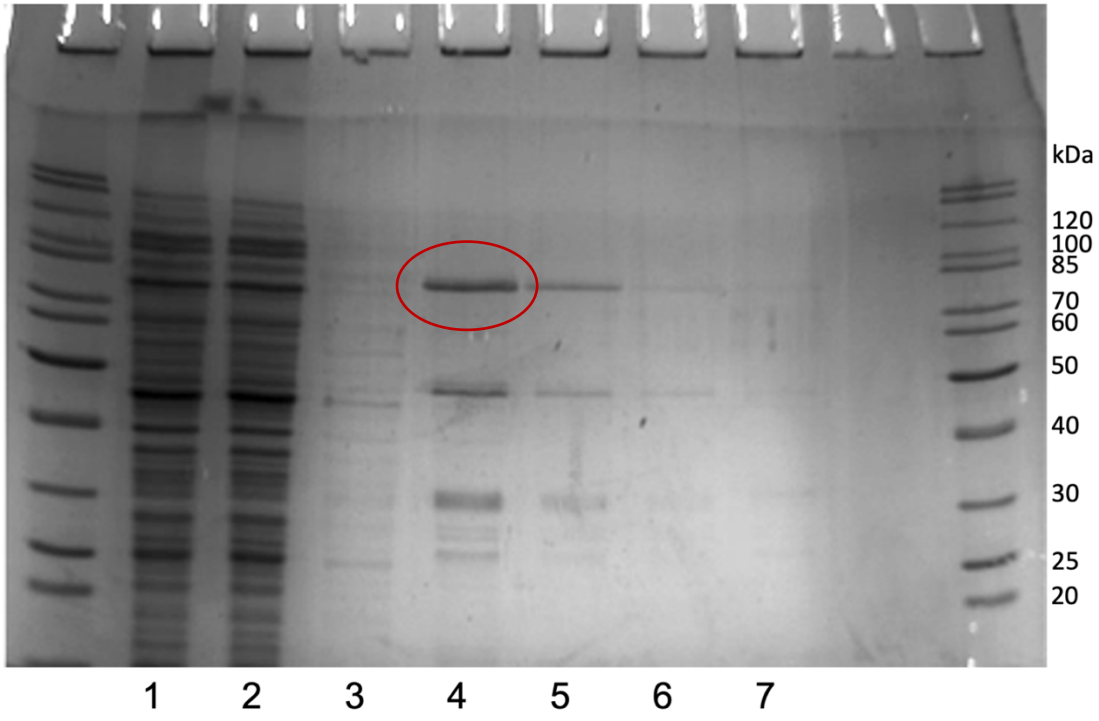

Figure 47. 12.5% SDS-PAGE analysis of HEL 2 protein recovery from Ni-NTA purification via N-terminal His-tag.1: the combined periplasmic fractions *collected from osmotic shock of the expressing BL21(DE3) cultures.* ***2****: the unbound fraction collected after P1/2 incubation with Ni-NTA resin.* ***3****: wash fraction.* ***4-7****: elutions 1-4. Pageruler unstained protein ladder used as a reference.*

Many avenues were explored to investigate the expression and purification issues encountered with HEL BLA-BLIP (**Table A 13** in **Appendix B: BLA-BLIP Expression Table**). First, adaptions to the construct were made by changing the linker lengths. By assessing the structure of the nanobodies in comparison to previously used Affimer

proteins which were successfully expressed within the BLA-BLIP construct, the proximity of the N-terminal to the CDR regions of the nanobodies was revealed (**Figure 48**). In HEL 1 and HEL 2 the N-terminal of the nanobody in position A is directly linked to the C-terminal of ß-lactamase inhibitor protein (BLIP). Lengthening of the linkers that anchor the nanobody to the enzyme-inhibitor complex (L1 and L3) was carried out to create two further constructs, HEL 3 and HEL 4 (**Figure 46**). These alterations did not result in successful expression of HEL 3, and HEL 4 protein recovered via his-tag purification was still lost during the second step of protein purification.

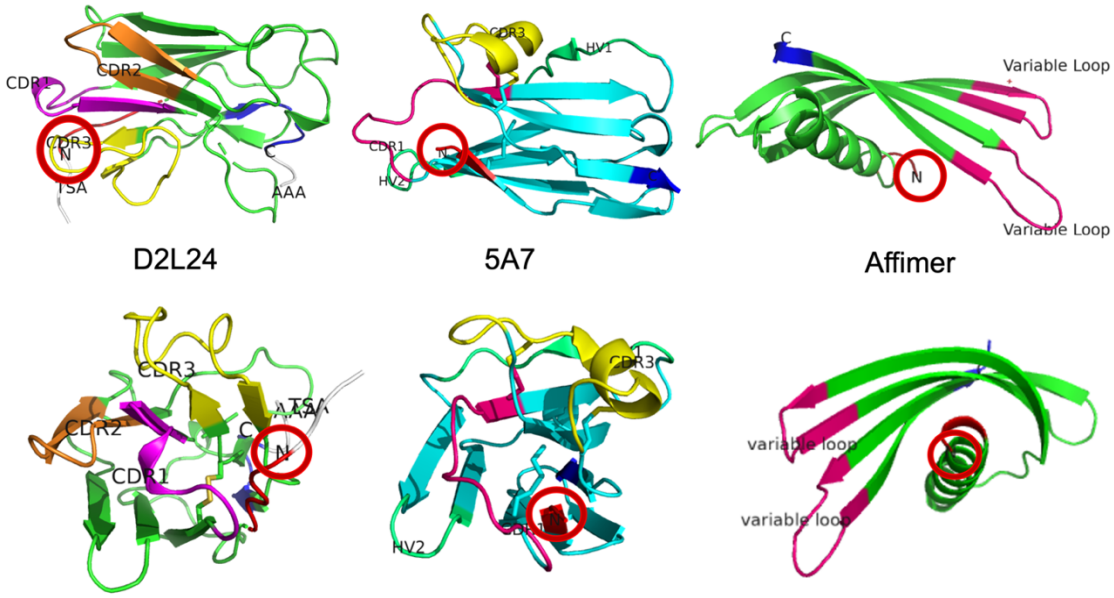

Figure 48. A comparison of N-terminal positions in relation to binding regions between anti-HEL nanobodies and Affimer proteins. *The C-terminal is labelled in blue, the N-terminal is red. For the D2L24 and 5A7 CDR1 is highlighted pink and CDR3 yellow. In D2L24 CDR2 is orange and HSV1 and HSV2 are labelled green in 5A7. The Affimer scaffold structure is seen in green and the variable binding loops are pink. The N-terminal of each protein is labelled with a red circle from front-on and side-on angles. Structural data was exported from PDB at https://www.rcsb.org/ (262, 361, 393) and adapted using PyMol software.*

Affimer proteins have the benefit of not containing any canonical disulphide bonds, which make them desirable for bacterial expression as an oxidising environment to facilitate the formation of disulphide bonds is not necessary. When using Affimers as recognition elements within the BLA-BLIP construct, the oxidising environment of the

periplasm is still necessary due to two canonical disulphide bonds in BLIP and one in BLA. However, introducing nanobodies into the biosensor introduces additional disulphide bonds – one in D2L24 and three in 5A7. We hypothesised that these additional disulphides could be contributing to the low expression of the nanobody BLA-BLIP sensors thus far.

At this point, a positive control was brought in for comparison. E37F is a nanobody BLA-BLIP construct that has successfully been expressed and purified. This construct has two alpaca (*Vicugna pacos*) derived V_HH nanobodies raised against *Clostridium difficile* Toxin B (396). E3 and 7F each contain one canonical disulphide bond and when cloned into the BLA-BLIP construct, could be fully purified via the N-terminal his tag and C-terminal strep tag (**Figure 49**).

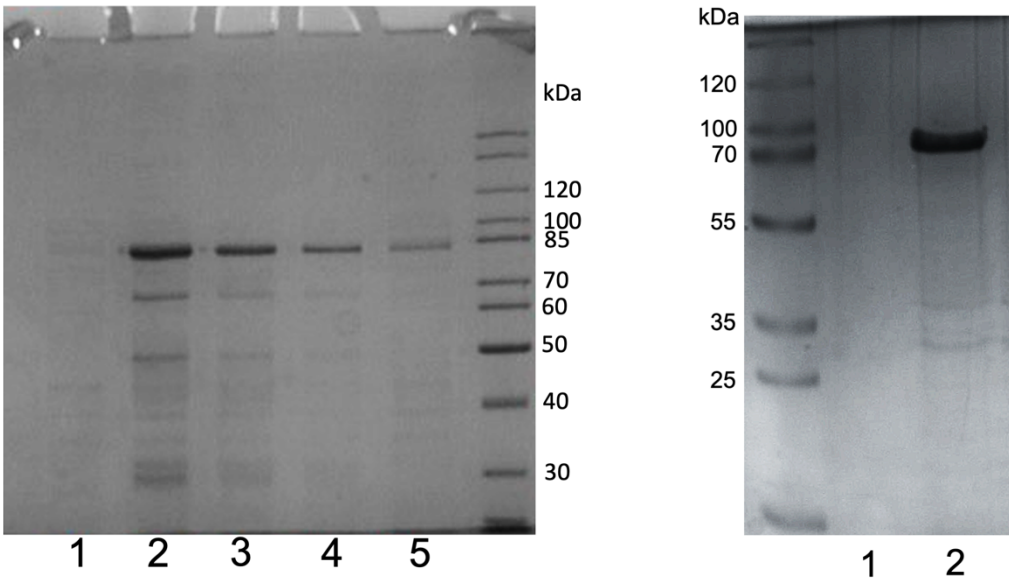

Figure 49. 12.5% SDS-PAGE visualisation of purified E37F Toxin B BLA-BLIP sensor. Left*: His tag purification fractions* ***1****: Pooled wash fractions,* ***2-5****: Elution fractions 1-4. Pageruler unstained protein ladder used as a reference.* ***Right****: Strep tag purification fractions.* ***1****: Pooled wash fractions,* ***2****: Elution fraction 1. Pageruler pre-stained ladder used as a reference.*

As no pure protein had been obtained so far (except E37F BLA-BLIP), BLA-BLIP activity assays were conducted on the elution fractions to assess whether any functional sensor protein was expressed (**Figure 50**). Elution fractions from E37F were used as a positive control and blank buffer as a negative control. Enzymatic activity

was seen in both elution fractions for E37F as expected, and activity was confirmed in the his-tag elution fraction of HEL 2 but lost in the strep elution. This confirms that active HEL 2 sensor protein was produced but there was an issue with the second step of purification. With no visible protein via SDS-PAGE analysis and no enzyme activity in purification fractions, work on HEL 1 was not taken further.

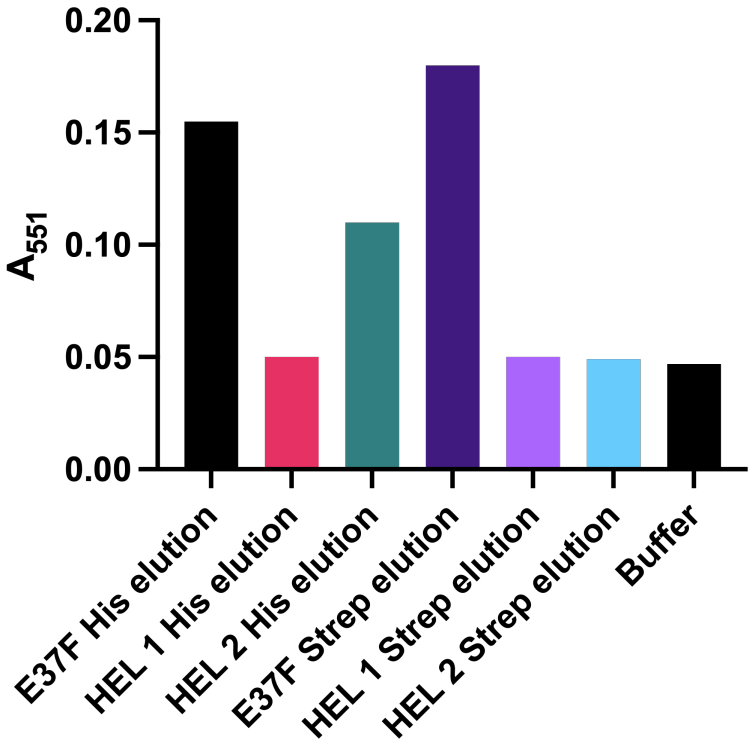

Figure 50. Enzymatic activity of HEL 2 elution fraction is lost during strep-tag purification step. *BLA-BLIP activity assays were conduction of his tag and strep tag elution fractions for E37F (positive control), HEL 1, HEL 2, and blank buffer (negative control) to determine whether functional enzyme was expressed. 10 uL sensor containing elution fraction was incubated with 10 nM of target analyte for 15 minutes before nitrocefin was added at 50 μM and absorbance measured at 551 nm on a plate reader after 10 minutes. Data is presented as raw A_{551} absorbance data where n=1.*

To further test the hypothesis that additional disulphide bonds were impacting the expression of the HEL BLA-BLIP sensors, a new construct HEL 5 was created (**Figure 46**). This construct removed 5A7 and replaced it with a second copy of D2L24, to assess whether the two additional disulphide bonds present in V_{NAR} 5A7 was the cause of the expression issues. HEL 5 had improved expression compared to HEL 2 but was not as strongly expressed as E37F. In addition to the difference in nanobodies, another factor that differentiates E37F from the HEL BLA-BLIP constructs was linker 2. E37F

utilised a $(GSG)_{20}$ linker to encompass the large size of toxin B (~270 kDa), whereas all HEL BLA-BLIP constructs thus far have a $(GSG)_7$ linker 2. To investigate whether the length of middle linker was impacting expression two more constructs HEL 6 and HEL 7 were developed with $(GSG)_{20}$ and $(GSG)_3$ linker 2 respectively (**Figure 46**). Increasing the length of linker 2 had no impact on expression compared to HEL 2 and decreasing the length of linker 2 inhibited expression of full-length sensor protein (**Table A 13**).

A helper plasmid known as pTUM4 was introduced to aid disulphide bond formation in the periplasm. pTUM4 promotes the overexpression of four bacterial proteins involved in disulphide bond formation in the periplasm: disulphide bond protein A (DsbA); disulphide bond protein C (DsbC); FkpA – a periplasmic peptidyl-prolyl cis/trans isomerase that supresses the formation of inclusion bodies – and SurA − a periplasmic peptidyl-prolyl isomerase required for the efficient folding of extra-cytoplasmic proteins (397). With the increased number of disulphide bonds present within the HEL BLA-BLIP constructs, it was hypothesised that co-expression with the helper plasmid pTUM4 could aid the correct folding of disulphide bonds and subsequently improve solubility of full-length sensor proteins within the periplasm. In the case of HEL 2 and HEL 5, co-expression with pTUM4 prevented expression of the recombinant protein in BL21 (DE3), this was thought to be due to the extra strain on the cells when relying on double antibiotic resistance selection. Changes in the expression protocol to maintain a constant growth temperature before and after induction were also tested, as a consistent 30°C temperature was recommended for co-expression with pTUM4. However, this did not yield success.

4.4.2 Procalcitonin BLA-BLIP sensors

The development and expression of a proof-of-concept HEL BLA-BLIP sensor was unsuccessful, when introducing a camelid-derived V_HH and a shark-derived V_{NAR} as recognition elements. However, with successful expression of the E37F toxin B BLA-BLIP with two alpaca-derived V_HH, the development of a procalcitonin (PCT) BLA-BLIP

was undertaken using two llama (*Lama glama*) derived V_HH proteins that had previously been used in a sandwich ELISA (398). As described for the development of HEL BLA-BLIP sensor constructs, two PCT BLA-BLIP sensors (PCT 1 and PCT 2) were created by subcloning PCT nanobodies – PCT2 and PCT3 – into position A and B (**Figure 51**).

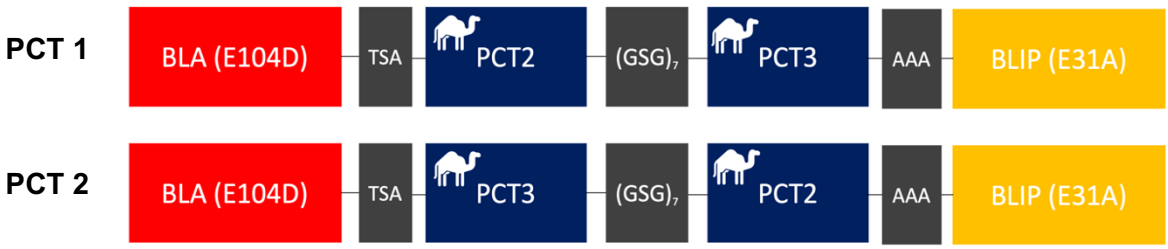

Figure 51. Schematic diagrams of PCT BLA-BLIP constructs. *Nanobodies PCT2 and PCT3 were subcloned into the pET28a+ BLA-BLIP template vector using the restriction sites flanking position A and B to produce two sensors (PCT 1 and PCT 2).*

Despite the use of two V_HH nanobodies as recognition elements, the PCT BLA-BLIP sensors behaved similarly to the HEL BLA-BLIP sensors when expressed in *E. coli* (**Table A 13**). No expression of full length PCT 1 protein was seen and PCT 2 could be purified via the his-tag but lost during strep-tag purification steps. For that reason, no bacterial expression optimisation was attempted for these constructs. Instead, an alternative expression system was explored. *Pichia pastoris* is a yeast species that is commonly used for secretory expression of recombinant proteins. Compared to bacterial growth, yeast expression has the major advantage of posttranslational modification in the oxidative environment of the endoplasmic reticulum, which allows for disulphide bond formation.

P. pastoris EasySelect™ expression protocol was used to express PCT 2 using a pPICZα expression plasmid (399). Approximately twenty *P. pastoris* colonies containing the PCT 2 BLA-BLIP gene were assessed through a small scale (200 µL) expression to determine the best expressing colonies. Direct ELISA analyses targeting

both the N-terminal his-tag and C-terminal strep-tag were used to select the best expressing colonies.

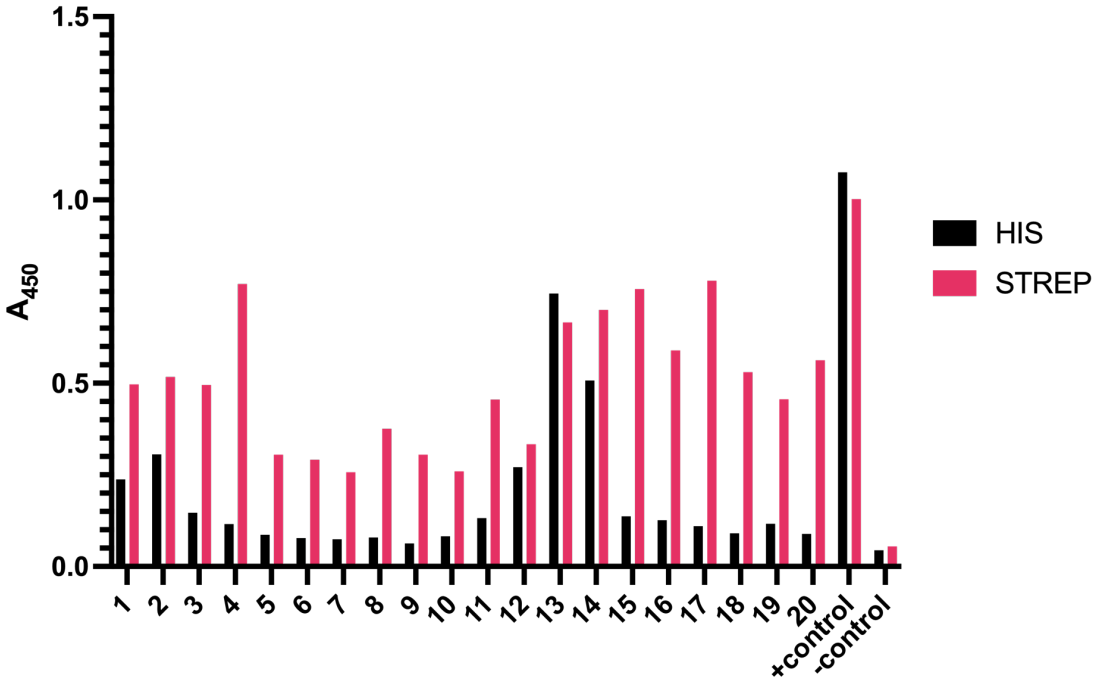

Figure 52. Direct ELISA screening of 20 PCT 2 BLA-BLIP colonies from* P. pastoris *transformation. *Supernatant from small scale expression of 20 yeast colonies were analysed via direct ELISA, with measurements of the signal produced when targeting the his-tag and the strep-tag on the N- and C-terminal of the sensors. Positive controls were previously purified BB_Trast from section chapter 2 which were known to have a strep-tag and his-tag present, negative controls were PBS buffer. Data is presented as raw absorbance data, n = 1.*

Out of twenty PCT 2 BLA-BLIP colonies, two colonies showed promising expression in the direct ELISA – colonies 13 and 14 (**Figure 52**). A 50 mL expression of colony 13 was undertaken, and the supernatant analysed every 24 hours over a 72-hour period to ascertain the optimal point of protein secretion. Western blot analysis of the supernatant showed no secretion of the PCT 2 BLA-BLIP sensor. Due to the extent of work necessary to optimise *P. pastoris* expression of BLA-BLIP constructs, it was concluded that nanobodies were, at this stage, not compatible as recognition elements within a one-component modular allosteric protein switch, in spite of earlier success with E37F BLA-BLIP targeting *C. diff* toxin B.

4.4.3 Nanobodies within a NanoBiT proximity switch sensor

Large, multi-domain proteins that require folding and post translational modifications can be difficult to propagate in bacterial expression systems (400, 401). The inclusion of nanobodies as recognition elements in the BLA-BLIP one component modular allosteric enzyme switch, introduced two eukaryotic proteins that require disulphide bond formation into a large multidomain protein structure (~80 kDa). After exploring a range of different avenues to improve the expression of the HEL or PCT nanobody BLA-BLIP sensor in *E. coli* and *P. pastoris* expression systems, it was speculated that the large size and complexity of the full sensor protein was not feasible.

In order to produce stable and active chimeric protein switch biosensors, that employ nanobodies as recognition elements, a different sensor format was explored. By creating a two-component proximity switch sensor, the size and complexity of the individual recombinant proteins could be limited to decrease the burden on the expression system. It was hypothesised that separate, smaller sensor components could be more easily expressed in *E. coli*.

4.4.3.1 HEL NanoBiT proximity switch design

The HEL V_HH and V_{NAR} nanobodies used for the development of the nanobody BLA-BLIP sensor in section 4.4.1 were used here for the development of HEL nanobody NanoBiT proximity switch sensors. The general concept and background of the NanoBiT proximity switch system was introduced in chapter 3. The NanoBiT system consists of an 18 kDa LgBiT and a short SmBiT peptide. Here HEL Nanobodies were genetically fused via the N- or C-terminal to the LgBiT and to two SmBiT sensor domains SmBiT101 (VTGYRLFEKES) or SmBiT114 (VTGYRLFEEIL) with differing affinities for the LgBiT – 2.5 μM and 190 μM respectively (**Figure 53**). Two separate SmBiT peptides were compared to optimise the sensor, which requires a balance between low level background complementation and a high level of analyte-induced reconstitution.

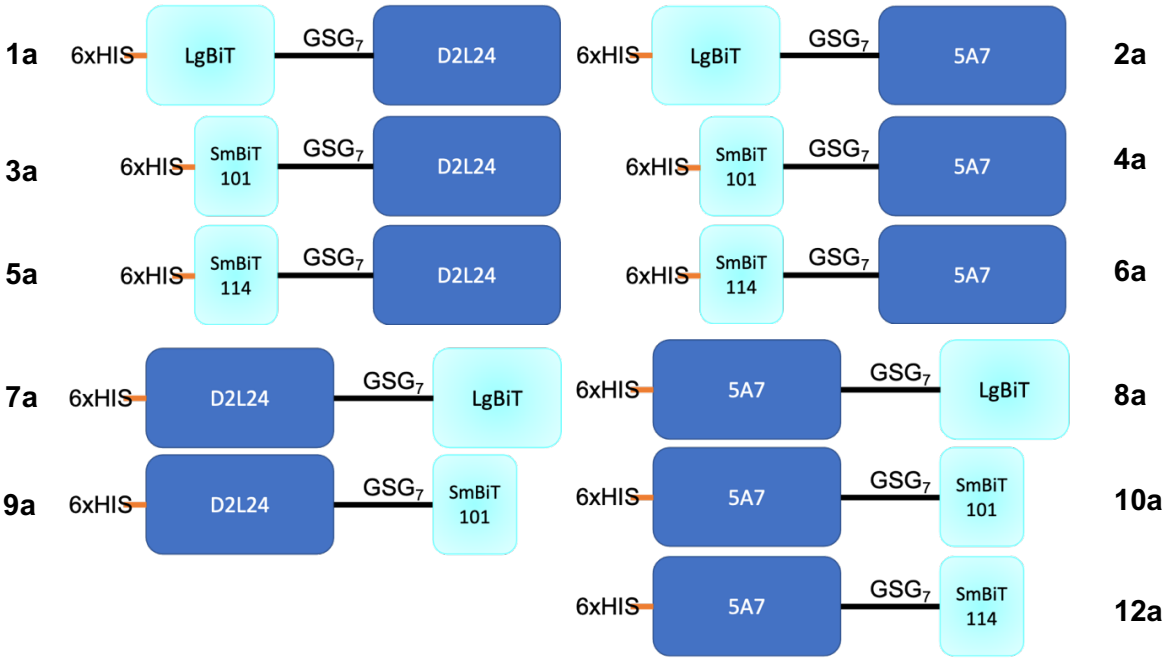

Figure 53. Schematic diagram of HEL nanobody NanoBiT sensor constructs. *Eleven constructs were cloned with either 5A7 (**odd numbers**) or D2L24 (**even numbers**) as the recognition element. Three reporter proteins were used: LgBiT and either SmBiT101 or SmBiT114. Reporter proteins were cloned onto the N-terminal (**1a-6a**) or the C-terminal (**7a-12a**) of the nanobody with a $(GSG)_7$ linker separating the reporter protein from the recognition element.*

4.4.3.2 HEL NanoBiT proximity switch expression

HEL nanobody NanoBiT constructs were expressed in *E. coli* SHuffle® T7 express competent cells, an *E. coli* B strain engineered to promote disulphide bond formation in the cytoplasm (245). Cell lysates were analysed on SDS-PAGE western blots to determine which construct showed the best levels of expression (**Figure 54**). LgBiT constructs with the NanoBiT fragment genetically fused to the C-terminal of the nanobody showed better levels of expression (constructs 7a and 8a) than when fused to the N-terminal. SmBiT101 nanobody constructs expressed better than SmBiT114 nanobody constructs. Due to insufficient expression, N-terminal LgBit constructs (1a and 2a) and SmBiT114 (5a, 6a and 12a) constructs were not taken forward for further experiments.

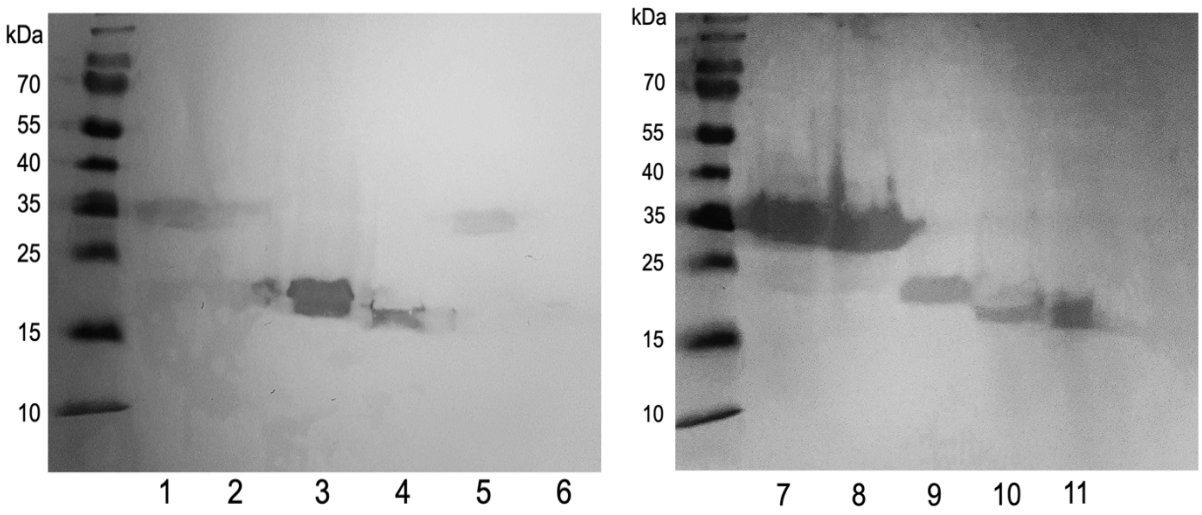

Figure 54. Western blot analysis of HEL nanobody NanoBiT cell lysates. *N-terminal his tag of constructs detected with HRP conjugated anti-his-tag monoclonal antibody. Labelling of constructs here refers labelling in* ***Figure 53****.* ***1****: 1a,* ***2****: 2a,* ***3****: 3a,* ***4****: 4a,* ***5****: 5a,* ***6****: 6a,* ***7****: 7a,* ***8****: 8a,* ***9****: 9a,* ***10****: 10a,* ***11****: 12a.*

HEL nanobody NanoBiT sensor proteins were then expressed and purified via metal affinity chromatography (**Figure 55**). Using sonication as the extraction method resulted in the recovery of full-length sensor protein for only one construct (7a). The lysis buffer used to aid extraction of the protein from cells would normally include lysozyme to aid cell wall degradation prior to sonication. As the nanobodies used in the HEL nanobody NanoBiT sensors are raised against lysozyme, it was not used in the lysis buffer.

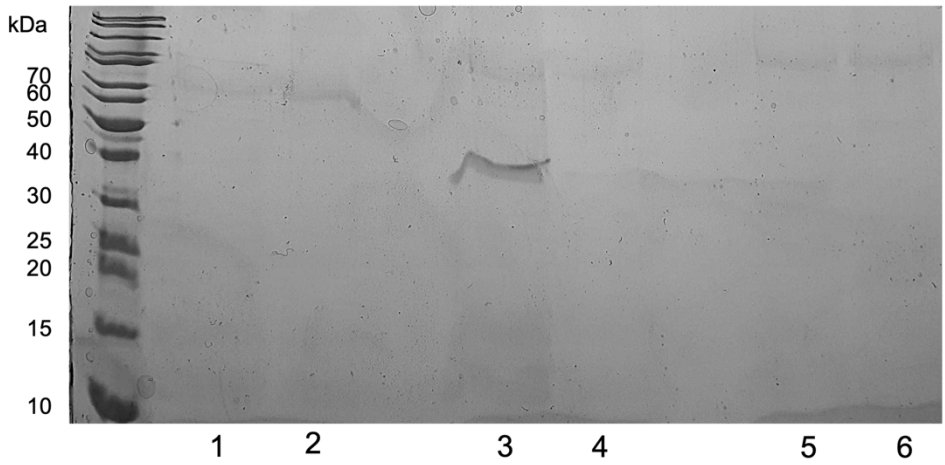

Figure 55. 15% SDS-PAGE analysis of purified HEL nanobody NanoBiT constructs. ***1****: 3a,* ***2****: 4a,* ***3****: 7a,* ***4****: 8a,* ***5****: 9a,* ***6****: 10a. Unstained protein standard, broad range (NEB) was used as a protein ladder.*

Using two of the HEL nanobody NanoBiT sensors, a comparison between sonication and cell disruption as an extraction technique was conducted. Slightly more soluble protein was purified after sonication than cell disruption. Insufficient amounts of soluble protein were extracted from cultures expressing 4a via either technique. Analysis of the insoluble fraction, that is the remaining cellular debris which has been incubated in reducing SDS-PAGE loading buffer, showed a high level of insoluble protein was expressed.

Thus, although some soluble HEL nanobody NanoBiT sensor protein had been expressed, it was clear that a large quantity of the expressed protein remains in inclusion bodies. Nanobodies have a unique characteristic in their ability to refold and retain their activity after thermal or chemical denaturation (215, 402). The decision was made to solubilise the inclusion bodies using 8 M urea and refold on Co-NTA resin by diluting out urea from the wash buffer and subsequently eluting from the Co-NTA resin. This protocol was used to purify protein from cultures expressing HEL nanobody NanoBiT sensor construct 7a and 4a to determine its feasibility. Each fraction recovered using the method detailed in section 4.3.2.2.1 was analysed on SDS-PAGE. This protocol was highly successful for recovering pure protein for construct 7a with a yield of ~22 mg L^{-1} (**Figure 56**), however, this was not the case for recovering pure protein for construct 4a with a low impure yield obtained.

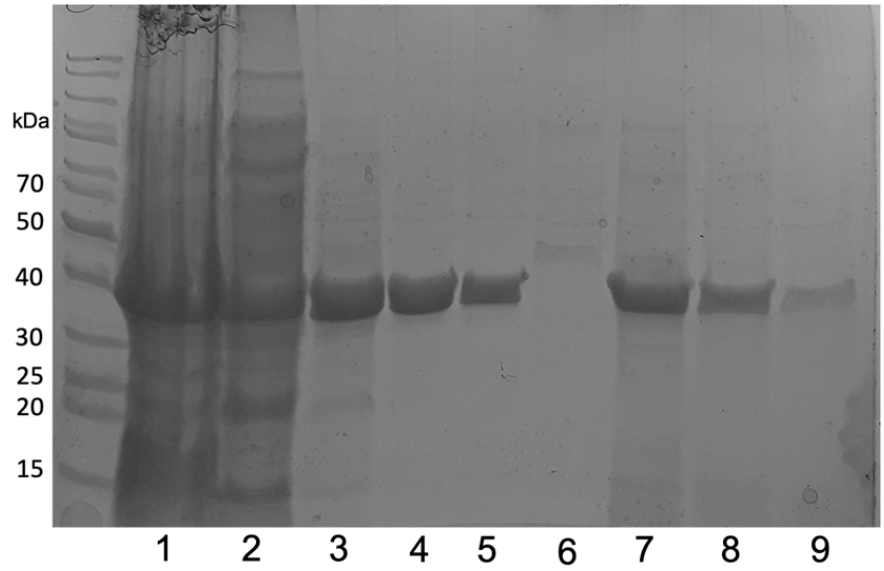

Figure 56. Purification fraction of HEL nanobody NanoBiT sensor construct 7a solubilised with 8M urea. ***1****: Cell debris incubated with 8 M urea,* ***2****: unbound fraction from incubation with 8 M urea,* ***3****: 6 M urea wash fraction,* ***4****: 4 M urea wash fraction,* ***5****: 2 M urea wash fraction,* ***6****: pooled 0 M urea wash fractions,* ***7****: elution fraction 1,* ***8****: elution fraction 2,* ***9****: elution fraction 3. Page ruler unstained protein ladder was used as the protein standard. 15% SDS-PAGE.*

Another method of solubilising protein is the use of detergents instead of denaturants such as urea and guanidine HCl. RIPA buffer is a commercially available lysis and extraction buffer containing ionic and non-ionic detergents (25 mM Tris•HCl, 150 mM NaCl, 1% NP-40, 1% sodium deoxycholate, 0.1% SDS, pH 7.6). HEL nanobody NanoBiT sensor construct 4a was first purified using the RIPA buffer protocol detailed in section 4.3.2.2.1, with successful recovery of pure, full length sensor protein this protocol was carried out on cultures containing constructs 8a, 3a and 10a (**Figure 57**). This protocol provided the following approximate yields: 3.42 mg L^{-1} of construct 3a, 1.5 mg L^{-1} of construct 4a, 7.6 mg L^{-1} of construct 8a and 5.2 mg L^{-1} of construct 10a.

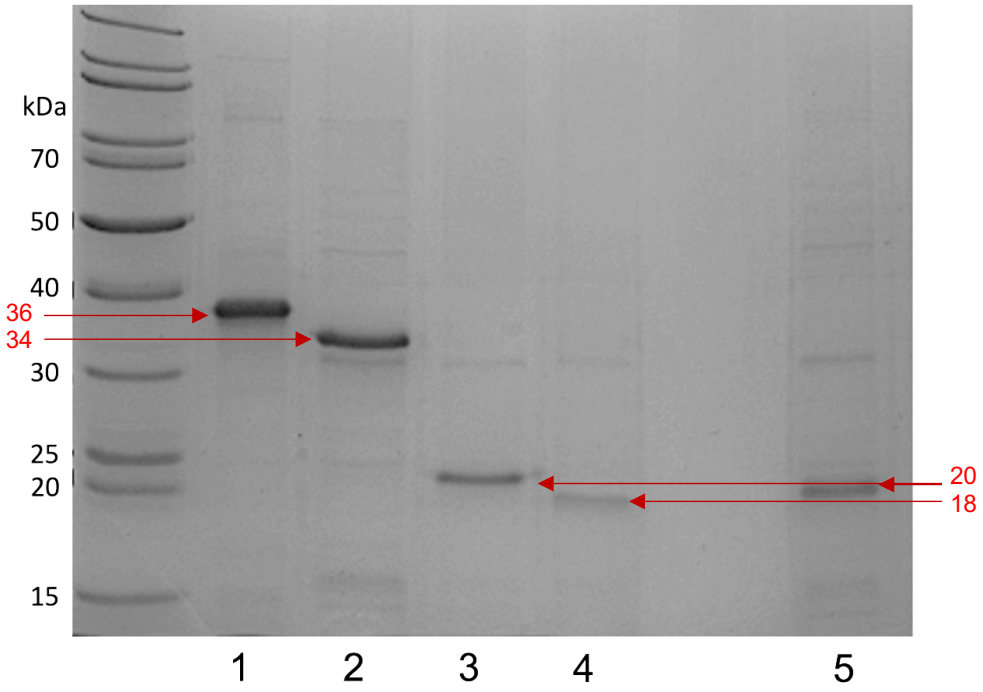

Figure 57. Purified HEL nanobody NanoBiT sensor proteins.1*: 7a purified via urea protocol,* ***2****: 8a purified via RIPA buffer protocol,* ***3****: 3a purified via RIPA buffer protocol,* ***4****: 4a purified via RIPA buffer protocol,* ***5****: 10a purified via RIPA buffer protocol. Page ruler unstained protein ladder used as the protein standard.15% SDS-PAGE.*

4.4.3.3 HEL NanoBiT proximity switch characterisation

The five purified constructs made up three LgBiT / SmBiT combinations as follows: 4a + 7a, 10a + 7a and 3a + 8a. The activity of each sensor combination, in response to increasing concentrations of HEL, was assessed in the NanoBiT assay (**Figure 58**). The 10a / 7a combination outperformed 4a / 7a with a significantly (p<0.05) greater RLU response at all HEL concentration points measured. The 3a / 8a combination produced no signal in response to HEL. All work from this point forward was conducted on the 10a / 7a sensor combination and is referred to as the HEL nanobody NanoBiT sensor in the text.

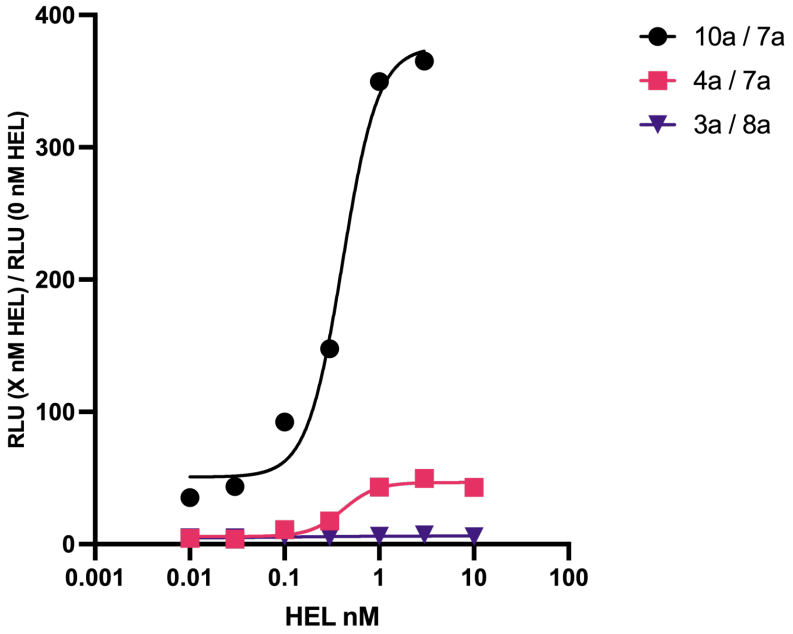

Figure 58. The best performing NanoBiT pair for HEL detection was the D2L24_GSG$_7$_LgBiT (7a) and 5A7_GSG$_7$_SmBiT101 (10a) combination. *Fold gain data for the three possible sensor combinations purified were plotted as n=1 and sigmoidal, 4 parameter logistic (4PL) fits were used.*

At 10 pM HEL concentrations, the activity gain of the HEL nanobody NanoBiT sensor (10a / 7a) was already at 50-fold, therefore lower concentrations of HEL were used to determine the sensor LoD. Changes to the concentration of sensor components were also made to ascertain whether a higher (4 nM) or lower (1 nM) sensor concentration provided a better range of quantification (**Figure 59**). The higher the concentration of the sensor, the higher the RLU measured, however, once normalised to the background to produce fold activity gain data, 2 nM of sensor provided the most sensitive response to HEL with the LoD calculated to be 1 pM.

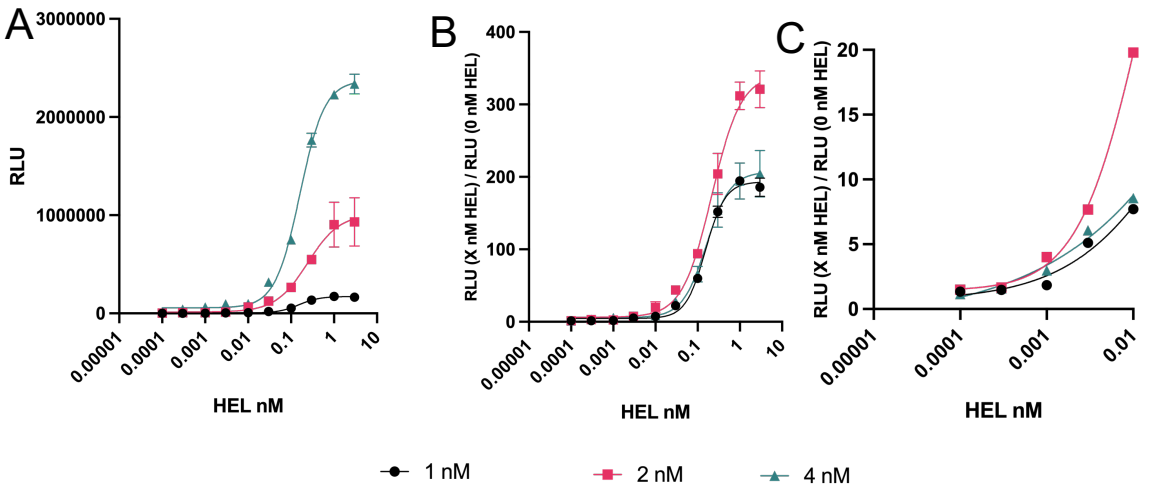

Figure 59. Higher concentrations of sensor components lower the sensitivity of the assay. *RLU (**A**) and Fold gain (**B**) data from NanoBiT assays performed on the selected optimal LgBiT / SmBiT101 pair for HEL with varying sensor concentrations (1 nM, 2 nM, 4 nM). Measurements taken 2 minutes after substrate incubation. (**C**) Zoomed in figure B to show activity between 0.1-10 pM and sensor LoD. Sigmoidal, 4 parameter logistic (4PL) fits were used. n = 2 for sensor concentrations 1 nM and 4 nM N = 3 for 2 nM sensor concentrations, data is plotted as the mean with ±SEM, where error bars are not visible, they are within the symbol.*

With the HEL nanobody NanoBiT sensor showing high sensitivity for HEL detection, the specificity of the sensor was evaluated (**Figure 60**). When incubated with 30 nM non-specific targets – PCT and C-reactive protein (CRP) – the HEL nanobody NanoBiT sensor showed no significant (p<0.05) change in response compared to blank buffer.

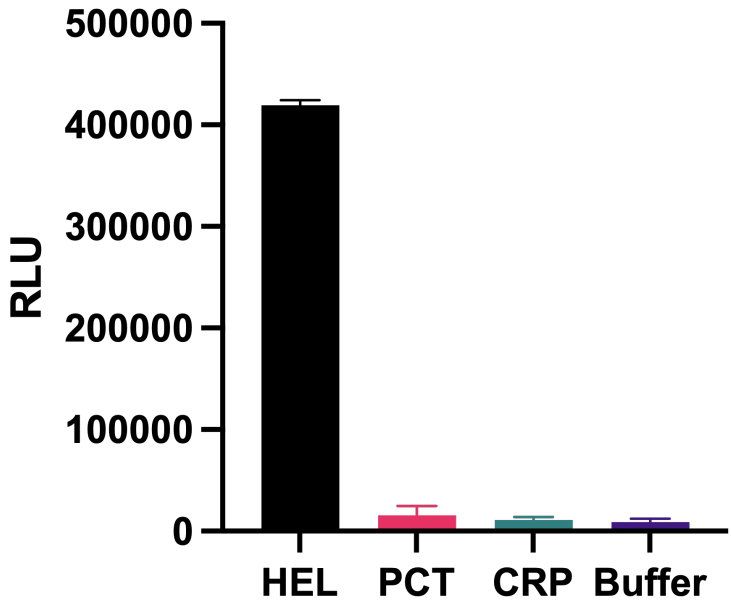

Figure 60. The HEL nanobody NanoBiT sensor is highly specific to HEL. *30 nM of HEL, PCT, CRP or PBSB was incubated with 2 nM of LgBiT/SmBiT101 sensor mixture for 30 minutes, and RLU response measured. Data is plotted as a mean of 3 repeats with error bars representing ±SEM.*

To determine the feasibility of using a nanobody NanoBiT sensor for the detection of clinically relevant biomarkers, the performance of the proof-of-concept HEL nanobody NanoBiT sensor was assessed in pooled human serum (**Figure 61**). The activity of the sensor in 0.1%, 1% and 10% serum were compared to the activity in buffer. At 3 nM HEL, no significant difference in signal was observed between 0%,0.1%, 1%, however, activity was significantly diminished in 10% serum. At 3 pM (around the LoD) there are significant differences between 0.1%, 1% and 10% compared to 0% (p<0.05 serum). Despite the differences in signal, the calculated LoD was similar in 0.1% and 1% serum compared to buffer. In buffer the LoD was calculated to be 1 pM, in both 0.1% and 1% serum the LoD was calculated to be 3 pM.

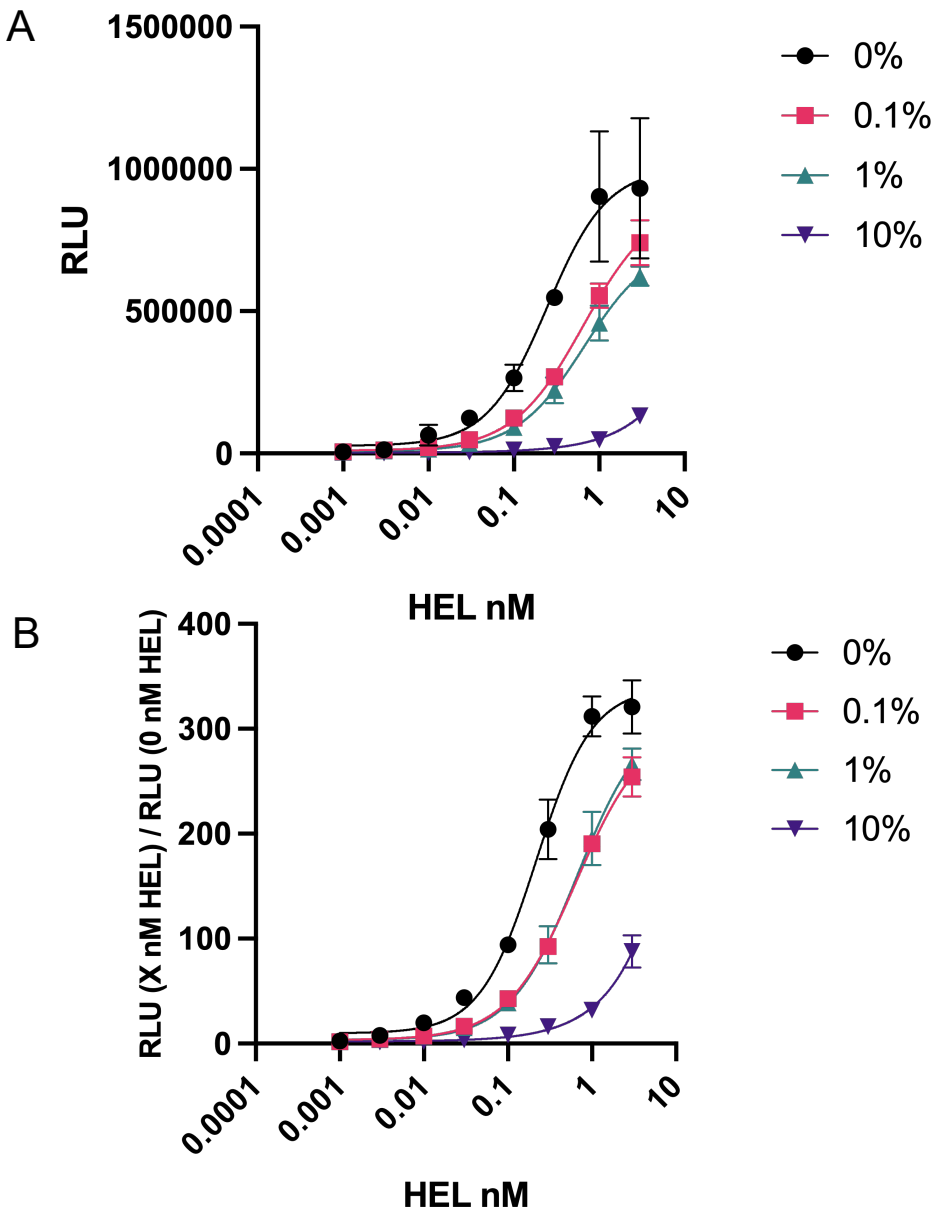

Figure 61. In 1% serum the HEL nanobody NanoBiT sensor can still detect concentration of HEL down to 3 pM. *The activity of the sensor was tested in 0.1-10% serum. Data is plotted as RLU (**A**) and fold gain (**B**) and sigmoidal, 4 parameter logistic (4PL) fits were used. 0%, 0.1% and 1% serum data points were plotted as a mean of three repeats, 10% serum data points were plotted as a mean of two repeats. Error bars represent ±SEM.*

Table 9. An interpolated standard curve for the HEL nanobody NanoBiT sensor provided quantifiable ranges based on accuracy and precision of the sensors in spiked 1% human serum. *Percentage recovery and percentage coefficient variance (%CV) values for HEL nanobody NanoBiT were used to determine the quantifiable range of the sensor based on recovery values between 80 – 120% and % CV < 25%. Calculations were made for raw RLU data and fold gain data.*

	RLU	Fold gain
Quantifiable Range	3 –100 pM	3 pM – 3 nM
% recovery	97– 100%	87 – 118%
% CV	9– 21%	5 – 23%

Data generated from experiments in 1% serum (n = 3) were used to create a standard curve and concentrations interpolated back to determine percentage recovery and percentage coefficient of variance (CV) to assess accuracy and precision respectively. Quantifiable ranges were subsequently calculated by percentage recovery between 80% and 120% and percentage CV < 25% (**Table 9**) (307).

4.4.3.4 Alternative NanoBiT substrate reagents

The luciferase NanoLuc uses coelenterazines as its substrate to produce photons. The development of the NanoLuc reporting system by Promega included the creation of the artificial coelenterazine analogue furimazine – commercially known as NanoGlo (340). The emission of light by NanoLuc reporter system is the result of NanoLuc catalysing the oxidative decarboxylation of the coelenterazine substrate which releases the product coelenteramide in an excited state which relaxes via the emission of photons (384, 385). These substrates are commonly known as luciferins. O-acetylated versions of luciferins, which act as a highly stable pro-luciferin that can be hydrolysed into their active form, have been discovered and named hikarazines. 150 analogues of these hikarazines have been developed as alternative substrates for the NanoLuc enzyme.

Two hikarazines and a non-commercial furimazine were synthesised by the group of Janin (384, 385) and their effect on the HEL nanobody NanoBiT sensor assessed (**Figure 62**). The novel substrates were first tested at a concentration of 13 μM, as suggested by the published methods (384, 385). At higher concentrations of HEL, the activity of the sensor was less stable with the novel substrates. Measurements of signal over time showed that the bioluminescent signal did not hit saturation over a 30-minute timeframe (**Figure 63**). This was attributed to the high concentration of substrate, so a lower concentration of 2 μM was used which resulted in a much faster plateau in signal (**Figure 64**).

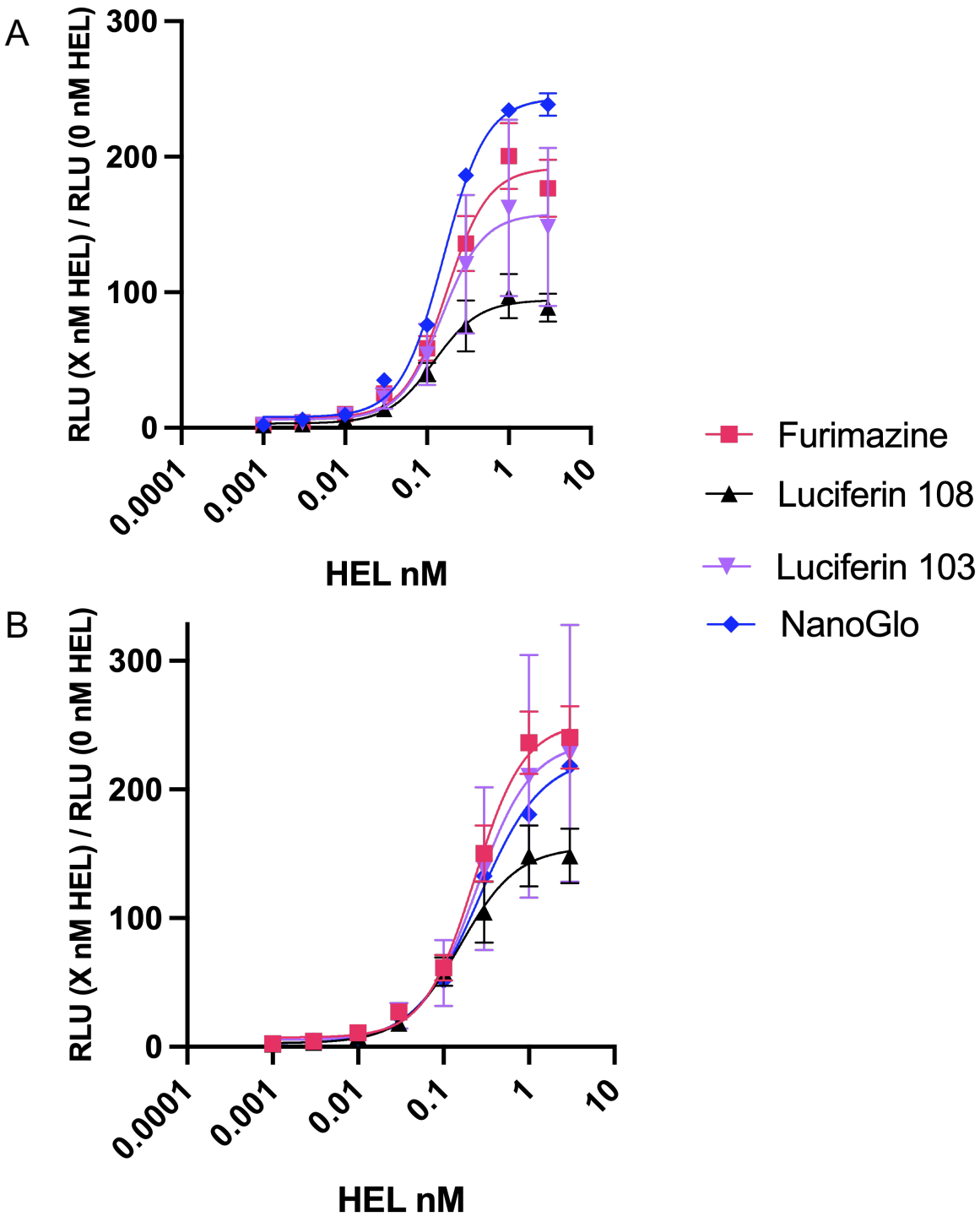

Figure 62. Novel furimazine derivatives increase bioluminescence emission. *2 minutes (**A**) after substrate incubation, NanoGlo produces the highest bioluminescent signal in response to the nanobody NanoBiT detecting HEL. 20 minutes (**B**) after substrate incubation the novel luciferin substrates have a higher RLU output. Data is presented as fold gain and plotted as a mean of three repeats, ± SEM.* 4 parameter logistic (4PL) fits were used.

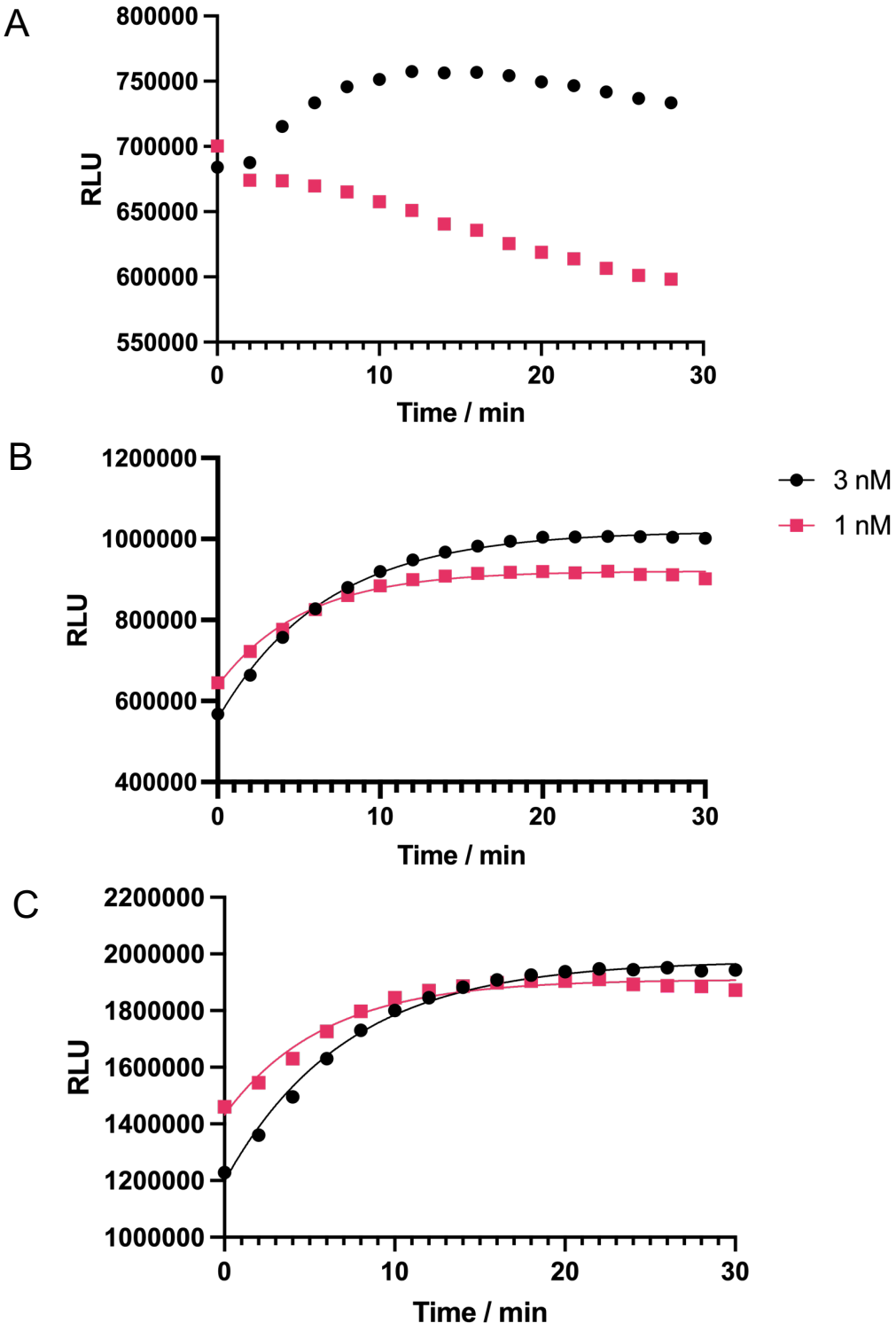

Figure 63. NanoGlo signal decays over 30 minutes whereas synthesised Furimazine and luciferin 103 signal increases. A *NanoGlo substrate at a final dilution of 1:1000 from commercial stock.* ***B*** *Luciferin 103 substrate at a final concentration of 13 µM.* ***C*** *Synthesised furimazine substrate at a final concentration of 13 µM. Changes in the sensor signal are shown when 2 nM sensor was incubated with 3 nM and 1 nM HEL.*

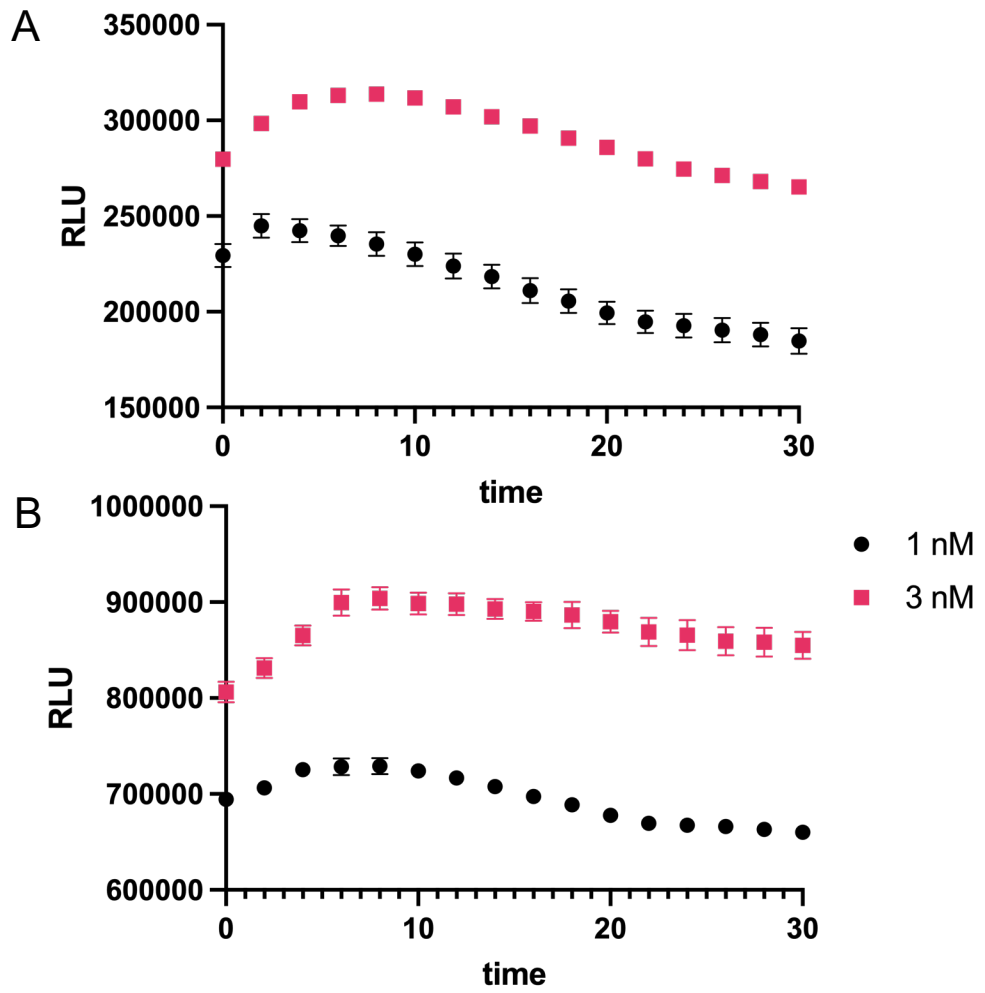

Figure 64. Lower substrate concentrations lower the overall signal but reduce the time to saturation. A *Luciferin 103 used as the NanoBiT substrate.* ***B*** *Synthesised furimazine used as the NanoBiT substrate. Final concentrations of substrate were 2 µM. Changes in the sensor signal are shown when 2 nM sensor was incubated with 3 nM and 1 nM HEL. Error bars represent ±SEM, where n=3.*

4.4.3.5 PCT nanobody NanoBiT sensor design

Two nanobodies raised again PCT were introduced in section 4.4.2 for the development of a one component modular allosteric enzyme switch to detect PCT. Overall, the introduction of nanobodies into the NanoBiT proximity switch in section 4.4.3 yielded more success in terms of expression and purification of functional sensor proteins than the expression attempts in section 4.4.1. On account of this, the decision was made to implement the PCT nanobodies PCT 2 and PCT 3 as recognition elements into the NanoBiT sensor construct (**Figure 65**).

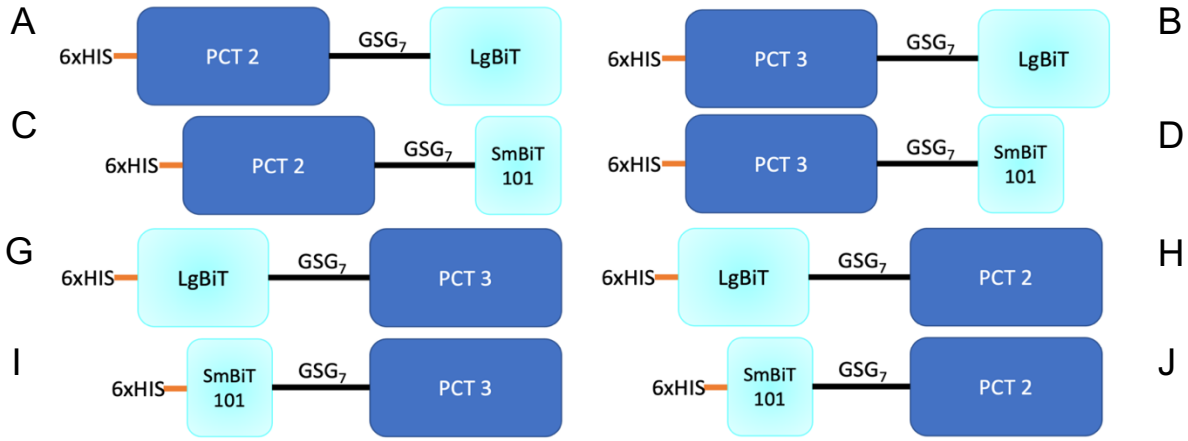

Figure 65. Schematic diagrams of eight PCT NanoBiT constructs cloned. *Two reporter proteins were used: LgBiT and SmBiT101. Reporter proteins were cloned onto the C-terminal (**A-F**) or the N-terminal (**G-L**) of each nanobody with a $(GSG)_7$ linker separating the reporter protein from the recognition element.*

4.4.3.6 PCT nanobody NanoBiT sensor production

The eight PCT NanoBiT sensors cloned were subsequently expressed in SHuffle T7 *E. coli* as described in section 4.3.2.2 and purified using the RIPA buffer protocol described in section 4.3.2.2.1. An increase in imidazole concentration to 30 mM was made to the wash buffer due to impurities in the elution fractions. Purified, desalted protein was analysed via SDS-PAGE (**Figure 66**) Construct I could not be purified and so was not taken forward for characterisation.

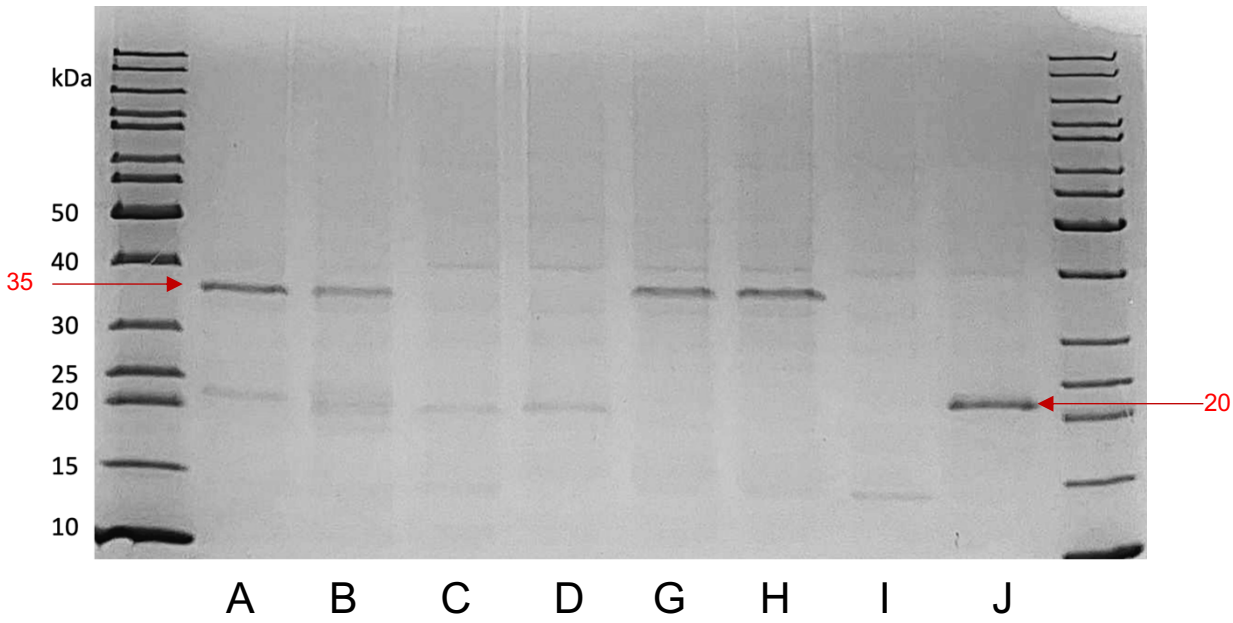

Figure 66. Eight PCT nanobody NanoBiT constructs were expressed and purified. *15& SDS-PAGE analysis. Lanes are in reference to the construct labelling in* ***Figure 65****.*

4.4.3.7 PCT nanobody NanoBiT sensor characterisation

All possible sensor combinations were trialled in the NanoBiT assay to assess their response to increasing concentrations of PCT (**Figure 67**). A hook effect was observed when concentrations of PCT exceeded the concentration of sensor components (2 nM). Half of the PCT sensor combinations showed promising preliminary results. This, combined with the performance of the proof-of-concept HEL nanobody NanoBiT, indicate that a clinically relevant PCT nanobody NanoBiT sensor could be developed with further optimisation.

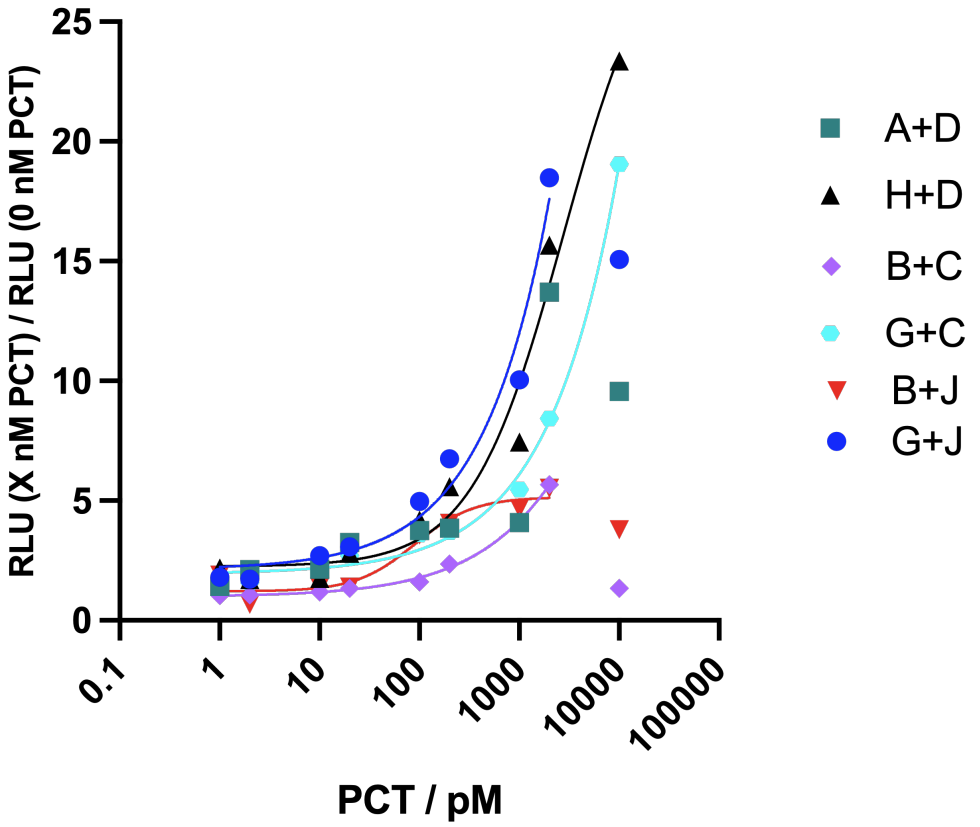

Figure 67. Initial screening of sensor activity in repose to increasing concentrations of PCT showed promising potential. *2 nM of sensor components were incubated with varying concentrations of PCT. Data points are plotted as n = 1, and sigmoidal 4PL fits were used.*

4.5 Discussion

Nanobodies have become popular affinity reagents across several fields of research, including in the design of therapeutics and diagnostics (403). Similarly to Affimer proteins, nanobodies benefit from having a small size, high affinity and selectivity to their targets. However, compared to Affimers, nanobodies have the advantage of being immune derived. Immune derived proteins are considered to have superior binding properties to scaffold-based proteins for a number of reasons. Immune-derived proteins have evolved through a natural selection process within an organism's immune system. This evolution results in highly specific binding capabilities that have been refined over time to recognise a vast array of foreign molecules. The diversity of the immune system improves the range of molecules that immune binders such as

nanobodies can be raised against compared to scaffold-based proteins such as Affimers.

It was hypothesised that the replacement of Affimer proteins with nanobodies as recognition elements within the one component modular allosteric enzyme switch – BLA-BLIP – would create a higher affinity sensor with a better scope for adaption to a range of target analytes. The expression and purification of these constructs was more difficult than originally anticipated and a number of avenues were explored to resolve these issues. Until recently, the utilisation of nanobodies in biosensors has been in ELISA formats or affixed to sensor surfaces where the binding of an analyte changes the signal potential (404-408). Where nanobodies had been expressed as genetic fusions with other proteins or large tags such as GFP, the nanobody probes were used as intracellular imaging probes where extraction and purification were not necessary (409). *E. coli* nanobody production in literature has largely focused on the production of nanobodies 'alone' in the periplasmic space. Alternatively, they have used mammalian or yeast expression systems (360, 410, 411).

Issues with the expression of soluble nanobody BLA-BLIP protein are hypothesised to be a consequence of misfolding of this multi domain protein. Studies on the folding of proteins largely focus on small domain proteins and there is little knowledge available on the folding of large multi domain proteins. However, it is accepted that the folding of each domain can affect neighbouring domains in a multi-domain protein (412, 413). Therefore, the effect of one misfolded protein within the multi-domain BLA-BLIP structure could have detrimental effects on the folding of other domains leading to aggregated, insoluble protein. Further to this, studies have shown that increasing the linker length in multi-domain proteins can permit folding where previously they were unable to, potentially due to steric hinderance between domains (414). Optimisation of the linkers to extend the available space for individual domain folding did not improve the expression of the nanobody BLA-BLIP sensor protein, and so other potential causes of misfolding were explored.

The number of disulphide bonds within a protein negatively correlates with solubility when expressed in *E. coli* (415). Comparisons of the sequence structures of nanobodies from comprehensive databases revealed that the number of canonical disulphide bonds in V_HHs correlated with the camelid species they are derived from (416). Generally, llama derived V_HHs have one disulphide bond, whereas dromedary and alpaca derived V_HHs can be fit into two subsets with either a single or double canonical disulphide bond. The double disulphide usually corresponds to a longer CDR3 region, with the second bond stabilising it. The E3 and 7F toxin B nanobodies are of the first subset of alpaca nanobodies with one canonical disulphide bond in each. The HEL D2L24 nanobody is of the first subset of dromedary nanobodies with one canonical disulphide bond. Both PCT nanobodies are llama derived with one canonical disulphide bond, however, they also both contain extra a non-canonical disulphide bond between CDR1 and CDR3. V_{NAR} nanobodies derived from sharks can similarly be classified into four isotypes depending on the number of disulphide bonds present (252). All four isotypes have one canonical disulphide bond, type I V_{NAR} have two additional disulphide bonds between CDR3 and the framework regions, type II have a non-canonical disulphide bond between CDR1 and CDR3, type III are the same as type II with a conserved tryptophan in CDR1 and type IV only have the one canonical disulphide bond. The HEL V_{NAR} used in this work – 5A7 – was a type I V_{NAR} with three disulphide bonds in total. When integrated into the BLA-BLIP sensor structure, the overall nanobody BLA-BLIP structures have numerous disulphide bonds (**Table 10**).

Table 10. Total number of disulphide bonds present in nanobody BLA-BLIP constructs.

BLA-BLIP CONSTRUCT	TOTAL NUMBER OF DISULPHIDE BONDS
E37F	5
HEL 2	7
PCT 2	7

Expression in *E. coli* of multi-domain proteins or those that contain disulphide bonds is known to be limited (417-419). More cysteines within a protein sequence can increase the likelihood of incorrect disulphide bond formation. Disulphide shuffling, also known as disulphide bond reshuffling, is a biochemical process involving the rearrangement of disulphide bonds within proteins (420). This can result in incorrect folding which can be toxic to the expression host, affect secretion from the cytoplasm due to a lack of solubility or could result in a structural change to the sensor that causes issues with functionality. My attempts at yeast expression were unsuccessful, however yeast has previously been used for expression of disulphide containing multi domain proteins (421). Despite this there are still limits to the size and complexity of multi-domain disulphide bond containing proteins being expressed in yeast, with limited secretion of soluble protein with higher numbers of domains and disulphide bonds (421, 422).

The extended length of the CDR3 in nanobodies is the dominating contributor to high affinity binding with the long loop of CDR3 commonly interacting with the antigen (423). Nanobodies with longer CDR3s have the added benefit of being able to interact with hard to reach, “hidden” epitopes that have previously been difficult to raise binders against (361, 362). The additional CDR3 length is usually concurrent with an additional stabilising disulphide bond. With expression and purification possible for the toxin B BLA-BLIP sensor E37F, but notable issues associated with all other nanobody BLA-BLIP sensors, I propose that the number of disulphide bonds within the structure is a critical factor involved in proper protein production in *E. coli.*

To circumvent the disulphide bond centred expression issues, whilst still being able to utilise a range of nanobodies with variable CDR3 lengths and associated disulphide bonds, an alternative sensor design had to be explored. Replacing the ß-lactamase and ß-lactamase inhibitor protein (BLA-BLIP) reporter system removed three disulphide bonds from the sensor construct to be expressed. The NanoBiT system, introduced in depth in chapter 3, uses the NanoLuc engineered luciferase as the reporter which is devoid of any disulphide bonds. Further to this, the two-component design of the

NanoBiT system requires individual sensor domains to be purified separately. This design involves expressing the two nanobody recognition elements independently, attached to either the LgBiT or the SmBiT fragments of the split luciferase reporter system. By utilising this sensor design, the number of disulphide bonds involved in the folding of each chimeric protein is limited to the number of native disulphide bonds within the nanobody itself. This provided a minimum of one and a maximum of three disulphide bonds when expressing the HEL nanobody NanoBiT sensor components containing D2L24 and 5A7 respectively.

Issues with soluble expression of the nanobody NanoBiT chimeric proteins were still apparent with SHuffle T7 *E. coli*. Where the D2L24 V_HH was the recognition element, fusion to the LgBiT helped stabilise and promote proper folding of the V_HH, however, the yield of soluble protein was still low. Fusion of an insoluble recombinant protein to a stable protein can improve the solubility and yield of the protein (424). Maltose-binding protein and small ubiquitin related modifier are commonly used fusion partners for this purpose (425). The LgBiT fusion did not provide stabilisation to the 5A7 V_{NAR}, nor did the SmBiT fusion to either nanobody. For this reason, an alternative method of recovering soluble protein was explored.

High-level expression of insoluble proteins in *E. coli* can accumulate as aggregates known as inclusion bodies (426). Solubilisation of inclusion bodies using a high concentration of chaotropic denaturants such as urea or guanidine hydrochloride results in loss of the secondary structure of the protein as well as solubilisation. The solubilised, denatured proteins can be refolded by slow removal of the denaturant by dialysis or dilution (427). The use of urea-facilitated denaturation and dilution-mediated refolding was successfully used to purify soluble and functional D2L24-LgBiT (7a) protein. The ability of nanobodies to refold after denaturation and retain their activity is well known (215, 402), however, the capacity for split luciferase fragments to retain their activity after being subject to such harsh conditions is a novel finding. Denaturation and refolding with this protocol did not result in pure protein for the 5A7-

SmBiT101 (4a) sensor protein. An alternative denaturation step was attempted using a mixture of ionic and non-ionic detergents (RIPA buffer) that are used for cell lysis and protein solubilisation whilst avoiding protein degradation or effecting biological activity. RIPA is generally used for lysis of mammalian cells (428, 429), however, here we used it for bacterial lysis. Chaotropic salts are strong denaturants that fully disrupt protein structure. Detergents, on the other hand, are milder denaturants that partially disrupt protein structure by solubilizing hydrophobic regions. It can be speculated that the milder denaturation aids with the subsequent refolding. Detergents are effective at solubilizing hydrophobic regions of proteins, which may make them more accessible for subsequent refolding steps, alternatively, partially denaturing the protein with a milder denaturant may retain some structural elements, which could facilitate the refolding process. Correct disulphide pairing of refolded antibody fragments has been observed using mild detergents compared to chaotropic salts for denaturation (430). Using either urea-facilitated denaturation or detergent-facilitated denaturation and dilution-mediated refolding successfully improved the yield of pure, folded protein extracted from the *E. coli* cytoplasm.

The activity of the nanobody NanoBiT sensor produced here showed high sensitivity and specificity to the target analyte with an LoD value calculated to be within the low pM range and a quantifiable range spanning three orders of magnitude. The sensor performance was observed in 1% serum, which, as a proof-of-concept study is encouraging for future work developing clinically relevant nanobody NanoBiT sensors. Promising initial results were seen with the development of nanobody NanoBiT sensors for the detection of PCT. PCT is a biomarker with high clinical relevance, it is currently used to aid in the diagnosis of sepsis and monitoring antibiotic treatment of sepsis. Effective monitoring of PCT levels can help discriminate between viral and bacterial infections as well as guiding antibiotic use (431). Improving the availability of PCT monitoring tools with the development of a point-of-care (PoC) test has the potential to improve sepsis survival rates by accelerating the delivery of treatment to patients.

Further to this, proper diagnosis of bacterial infections and antibiotic management are becoming increasingly crucial to mitigate antibiotic resistance (432, 433).

As discussed in chapter 3, the NanoBiT sensors developed in this project maintain the sensitivity and selectivity of current gold standards of protein detection with the added benefit of superior speed, with rapid protein detection attainable within a 30-minute time frame. The development of such biosensors could facilitate the production of rapid, PoC tests that could be used in healthcare settings without the need for trained personnel and large, expensive laboratory equipment. Handheld, portable luminometers are being developed for a range of luminescent based assays (434, 435) which provides the PoC platform necessary for the NanoBiT assay to be integrated into healthcare settings. The current commercial substrate accompanying the Promega NanoBiT system costs approximately £100 per µg, however there are research groups synthesising alternative reagents available at a considerably lower cost of approximately £26 per mg. In the context of substrate use with the nanobody NanoBiT sensor presented here, it currently costs £5 for enough NanoGlo substrate to run 200 tests, it would cost 0.13p for enough of the alternative substrate reagents to run the same number of tests. The alternative substrates assessed could effectively be used to measure the activity of the nanobody NanoBiT sensor in response to increasing concentrations of HEL. With further optimisation, the use of alternative luciferins as substrates will be a viable option for reducing running costs. This is promising for the future development of rapid, affordable PoC devices that employ nanobody NanoBiT sensors.

4.6 Conclusion

After extensive testing of expression conditions, it can be concluded that when using nanobodies that contain more than one disulphide bond as recognition elements, the number of disulphide bonds present in the one component modular allosteric enzyme switch sensor – BLA-BLIP – exceeds the limitations of *E. coli* as an expression system.

However, using an alternative chimeric protein switch sensor format – the NanoBiT system – reduced the complexity of the sensor components, and improved the expression of nanobodies as recognition elements. Challenges were still met when recovering soluble protein but the unique refolding properties of nanobodies allowed for the sensor components to be solubilised from inclusion bodies and purified by dilution-mediated refolding. It was discovered that the split luciferase fragments were also able to retain their enzymatic activity after denaturation and refolding. From this work an effective expression and purification method for nanobody NanoBiT fusion proteins was developed, and functional sensors characterised with the ability to detect target analyte down to low pM concentrations. With large repertoires of nanobodies available against an array of target analytes, the work presented here is encouraging for the future development of clinically relevant nanobody NanoBiT biosensors for rapid protein detection.

5 Conclusions and Future Directions

5.1 Aims

The aims and objectives of this PhD were: A) to compare the performance of two different chimeric protein switch biosensors as platforms for therapeutic drug monitoring (TDM) of therapeutic monoclonal antibodies (TmAbs); and B) to explore the possibility of developing a modular chimeric protein switch biosensor platform with nanobody recognition elements.

5.2 Chimeric protein switch biosensors for therapeutic drug monitoring.

Chimeric protein switch biosensors exploit structural changes within a protein complex to convert binding events into biochemical activity that can be measured (137, 301). Generally, chimeric protein switch biosensors can be classified as either one- or multi-component sensors. Two established chimeric protein switch biosensors were adapted to detect four TmAbs that would benefit from more efficient TDM. The one-component modular allosteric switch known as BLA-BLIP was first developed for the detection of monoclonal antibodies whilst utilising peptide epitopes specific to the antibody variable regions (169). Affimer proteins were introduced as recognition elements into the BLA-BLIP sensor to develop a more adaptable platform with interchangeable recognition elements for a number of targets (170). To determine that value of this biosensor as a TDM platform, the BLA-BLIP sensor was adapted to sense four TmAbs with the previously selected Affimer proteins (303).

Although the BLA-BLIP sensor was able to de adapted for the detection of trastuzumab and ipilimumab, the design was less modular than anticipated and detection of adalimumab and rituximab was unsuccessful. Due to this, an alternative chimeric protein switch biosensor was employed to create effective TDM platforms for TmAbs. The NanoBiT proximity switch has been used as a mechanism for *in vivo* imaging (436, 437), and more recently it has been developed into a method for analyte detection utilising a range of recognition elements, including Affimers (186, 197, 350). Therefore,

it was decided to develop NanoBiT sensors to evaluate how applicable these sensors can be at detecting clinically relevant targets. Using the same Affimer proteins for the detection of TmAbs introduced into the BLA-BLIP sensor, TmAb NanoBiT sensors were developed for TDM. These sensors showed superior activity to the BLA-BLIP sensors with higher increases in activity and broader quantifiable ranges, additionally the format was adaptable to all four TmAb. The superior fold gain at high (3 nM) concentrations of analyte seen for the NanoBiT sensor (~10 – 100-fold gain) compared to the BLA-BLIP sensor (~2 – 4-fold gain) means that discrepancies between two concentrations are easier to make, which would improve the accuracy of the measurements. The TmAb NanoBiT sensor protocol was optimised to a run time of approximately 5 minutes, which is advantageous over the BLA-BLIP sensor. In every aspect of performance, the NanoBiT sensor surpassed the BLA-BLIP sensor.

The creation of four TmAb NanoBiT sensors was successful with quantifiable ranges in spiked serum calculated to be within the clinically relevant concentration ranges for all four TmAbs targeted. The next step in this work is to validate the sensors with patient samples to establish how accurate they are in a clinical setting. Further to this, the development of a hand-held device that can be used as an interface for the NanoBiT sensor would be beneficial to the future design of point-of-care, therapeutic drug monitoring devices that can be applied bedside to improve the turnaround time of results. The creation of hand-held luminometers is an area of research that is gaining traction due to the extensive application of luminescent reporters in diagnostics and analytics (434, 435). These advances in the development of hardware are encouraging for the future implementation of these superior TDM methods into PoC settings.

5.3 Chimeric nanobody protein switch biosensors

Nanobodies are valuable molecular tools within research, therapeutic design, and diagnostic test development. Their high affinity binding properties, small size and stability make them ideal candidates for use as recognition elements within a chimeric protein switch biosensor. Nanobodies have been underused as recognition elements

within this biosensor format, although there are reported instances of their use within biosensor development, this has largely focused on their use as affinity reagents in classic immunoassay formats or as reagents within biosensor formats that utilise immobilisation techniques to transduce binding events into readable signals. Despite this, there was no literature on their use in chimeric protein switches. The work presented here now significantly advances the literature.

The expression of proteins that contain disulphide bonds in bacterial expression systems is known to be challenging due to restricted machinery available in a bacterial cell. Specifically, bacteria do not contain an endoplasmic reticulum which in higher order organisms is responsible for post-translational modifications such as disulphide bond formation. The periplasmic space of a bacterial cell is an oxidative environment that can facilitate disulphide bond formation; however, the capacity of the periplasm is limited due to its small size and finite availability of the necessary chaperones and other proteins necessary to catalyse the covalent reaction between two sulphur groups to form disulphide bonds (370, 375, 376, 438). This was evident in the attempts made here to express a large, multidomain protein that contained up to eight disulphide bonds.

The previously noted superiority of the NanoBiT sensor compared to the BLA-BLIP sensor, when using Affimer recognition elements, informed the decision to explore the possibility of using nanobodies as the recognition elements within this format. The failure to express nanobodies in the BLA-BLIP sensor was attributed to the excessive number of disulphide bonds necessary for the native structure of the multi-domain protein to properly fold. By using the two-component NanoBiT system, the number of disulphide bonds could be limited as each nanobody NanoBiT fragment would be expressed and purified separately. The refold ability of nanobodies was exploited to produce a denature and dilution-mediated refold purification protocol which was successfully implemented to produce five HEL nanobody NanoBiT sensors and seven PCT nanobody NanoBiT sensors. The best performing HEL nanobody NanoBiT sensor

combination was further characterised and showed low pM LoD values with a broad quantifiable range in up to 1% spiked human serum. Additionally high selectivity for the target analyte was observed. With a range of nanobodies against numerous targets characterised in the literature, the scope of potential nanobody NanoBiT sensors that could be developed in the future is great, with nanobodies continuously being selected against new targets.

To further this work, the initial development of a PCT sensor to aid the diagnosis and treatment of sepsis was introduced. Going forward, additional analysis of these sensors will be conducted, including optimisation of the sensor components and validation using patient serum samples with a confirmed sepsis diagnosis and healthy individuals. It is hypothesised that by also using a CRP Affimer NanoBiT sensor designed by a colleague, a multiplexed test can be developed utilising rapid, specific, and sensitive CRP and PCT detection. CRP and PCT are both markers of sepsis (439), and can also help differentiate between bacterial and viral infections (440). Sepsis is a medical emergency and early intervention is critical to patient survival. By introducing a biosensor like the nanobody NanoBiT, that can detect relevant protein biomarkers in a matter of minutes, the turnaround time for confirmatory tests could be dramatically shortened, improving the likelihood of early medical intervention occurring.

Another nanobody NanoBiT project currently in its initial stages is the development of a rapid PoC test for Ebola virus (EBV). Two V_{NAR} nanobodies and one V_HH nanobody against EBV nucleoprotein (NP) were selected from the literature (441, 442). Future work on this project aims to characterise potential EBV-NP nanobody NanoBiT sensors for the development of a rapid PoC test for EBV diagnosis. The gold standard for EBV diagnosis is RT-PCR which, as mentioned in the introduction to this thesis, is a lengthy and laborious process (443). With the limited treatment options available for EBV (444), the purpose of this sensor will be to improve the efficiency of isolating infected individual to prevent the spread of EBV, and aid in limiting the occurrence of EBV epidemics.

5.4 Outlooks

The work documented throughout this PhD thesis has described the value of developing rapid, point-of-care diagnostic tests as alternatives to current gold standards. After exploring two different sensor platforms it can be concluded that the use of a two-component luminescent proximity switch (NanoBiT) has multiple advantages over the use of a one-component enzyme switch (BLA-BLIP). Most prominently, the expression issues encountered with BLA-BLIP were overcome when switching to the NanoBiT system which opened the opportunity to use nanobodies as recognition elements. Further to this, the performance of the NanoBiT sensors surpassed the performance of the BLA-BLIP sensors when utilised as a therapeutic drug monitoring platform. Introducing nanobody recognition elements into the NanoBiT sensor platform, provided a proof-of-concept senor with excellent sensitivity and specificity. The scope for future development of nanobody NanoBiT sensors is large with nanobodies available against a broad range of analytes, and the possibility of further developing these sensors into a handheld device is fathomable in the near future. Overall, these sensors have the capacity to dramatically improve the speed, efficiency, and accuracy of diagnostics and contribute to better healthcare outcomes.

List of Abbreviations

Abbreviation	Definition
2-ME	2 mercapto-ethanol
4PL	Four parameter logistics
A&E	Accident and Emergency
ADA	Anti-drug antibodies
ADCC	Antibody dependent cell-mediated cytotoxicity
AFB_1	Aflatoxin B_1
AFF	Alternate Frame Folding
AIV	Avian influenza virus
BCA	Bicinchoninic acid
BLA-BLIP	ß-lactamase – ß-lactamase inhibitor protein
BMGY	Buffered glycerol complex media
BMMY	Buffered methanol complex media
BSA	Bovine serum albumin
CD20	cluster of differentiate 20
CDC	Complement dependent cytotoxicity
cDNA	Complementary deoxyribonucleic acid
CDR	Complementary determining regions
CGM	Continuous glucose monitoring
C_{max}	Maximum concnetration
Co-NTA	Cobalt-Nitrilotriacetic acid
COVID-19	Corona virus disease 2019
CRP	C-reactive protein
CTLA4	Cytotoxic T-lymphocyte antigen 4
CV	Coefficient of variation
DARPins	Designed ankyrin repeat proteins
DNA	Deoxyribonucleic acid
DsbA-D	Disulphide bond protein A-D
dsDNA	Double stranded deoxyribonucleic acid
dT	Deoxythymine
E. coli	*Escherichia coli*

EBV	Ebola Virus
ECD	Extracellular domain
EDC	1-Ethyl-3-(3-dimethylaminopropyl) carbodiimide
EIA	Enzyme immunoassay
ELISA	Enzyme linked immunoassay
F(ab')2	Fragment antigen binding heterodimer
Fab	Fragment antigen binding
FAST	Fluorescence-activating and absorption shifting tag
FDA	Food and Drug administration
FPIA	Fluorescence polarization immunoassay
FPLC	Fast protein liquid chromatography
GOx	Glucose oxidase
GP	General practitioner
H_2O_2	Hydrogen peroxide
HBR	4-hydroxybenzyidene rhodanine
HcAb	Heavy chain only antibody
hCG	human chorionic gonadotropin
HCV	Hepatitis C virus
HER2	Human epidermal growth factor receptor 2
HIV	Human immunodeficiency virus
HRP	Horseradish peroxidase
HV	Hypervariable
ICU	Intensive care unit
IgG	Immunoglobulin G
IgNAR	Immunoglobulin new antigen receptor
IPTG	isopropylβ-D-thiogalactoside
ISD	Immunosuppressive drugs
ISF	Interstitial fluid
K_D	Equilibrium dissociation constant
KDa	Kilodaltons
LB	Luria broth
LC-MS/MS	Liquid chromatography–tandem mass spectrometry
LFD	Lateral flow device
LLOQ	Lower limit of quantification
LnNP	Lanthanide-doped nanoparticles

LoD	Limit of detection
LOQ	Limit of quantification
LUMABS	LUMinescent AntiBody Sensor
mAb	Monoclonal antibody
MAPK	Mitogen-activated protein kinase
mw	Molecular weight
MWCO	Molecular weight cut off
NanoBiT	Nano Luciferase binary technology
NHS	N-Hydroxysuccinimide
Ni-NTA	Nickel-nitrilotriacetic acid
Ni-NTA	Nickel-Nitrilotriacetic acid
NP	Nucleoprotein
OF	Oral fluid
P. pastoris	*Pichia pastoris*
PBS	Phosphate buffered saline
PBST	Phosphate buffered saline + Tween-20
PCR	Polymerase chain reaction
PCT	Procalcitonin
PD	Pharmacodynamic
PK	Pharmacokinetic
PoC	Point-of-care
PoCT	Point-of-care test
PYP	Photoactive yellow protein
QD	Quantum dots
qPCR	Quantitative polymerase chain reaction
RAF	Rapidly accelerated fibrosarcoma
RAS	Rat sarcoma
RIPA	Radioimmunoprecipitation assay
RLU	Relative light units
RNA	Ribonucleic acid
RPM	Revolutions per minute
RT-PCR	Reverse transcriptase polymerase chain reaction
RT-qPCR	Reverse transcriptase quantitative polymerase chain reaction
SAR	Severe adverse reaction
SARS-CoV-2	Severe acute respiratory syndrome coronavirus 2

ScFv	Single chain variable fragment
SD	Standard deviation
SdAb	Single domain antibody
SDS-PAGE	Sodium dodecyl-sulphate polyacrylamide gel electrophoresis
SEM	Standard error mean
SMBG	Self-monitoring blood glucose
TBS	Tris buffered saline
TCEP	Tris(2-carboxyethyl) phosphine
TDM	Therapeutic drug monitoring
TmAb	Therapeutic monoclonal antibody
TMB	3,3′,5,5′-Tetramethylbenzidine
TNF-α	Tumour necrosis factor - alpha
ULOQ	Upper limit of quantification
V_HH	Variable heavy domain of heavy chain
V_{NAR}	Variable domain of new antigen receptor
vRNA	Viral ribonucleic acid
WB	Western blot
YPD	Yeast, peptone, dextrose
YPDA	Yeast, peptone, dextrose, agar

References

1. Rogers, K.R. Recent advances in biosensor techniques for environmental monitoring. *Anal Chim Acta.* 2006, **568**(1), 222-231.
2. Kumar, H. and Neelam. Enzyme-based electrochemical biosensors for food safety: a review. *Nanobiosens. dis. diagn.* 2016. 29-41.
3. Alhadrami, H.A. Biosensors: Classifications, medical applications, and future prospective. *Biotechnol. Appl. Biochem.* 2018, **65**(3), 497-508.
4. Zhang, P., Bao, Y., Draz, M.S., Lu, H., Liu, C. and Han, H. Rapid and quantitative detection of C-reactive protein based on quantum dots and immunofiltration assay. *Int J Nanomedicine.* 2015, **10**, 6161-6173.
5. Holdgate, G., Embrey, K., Milbradt, A. and Davies, G. Biophysical methods in early drug discovery. *Admet dmpk.* 2019, **7**(4), 222-241.
6. Jayasena, T., Poljak, A., Braidy, N., Zhong, L., Rowlands, B., Muenchhoff, J., Grant, R., Smythe, G., Teo, C., Raftery, M. and Sachdev, P. Application of Targeted Mass Spectrometry for the Quantification of Sirtuins in the Central Nervous System. *Sci. Rep.* 2016, **6**(1), 35391.
7. Van Gool, A., Corrales, F., Čolović, M., Krstić, D., Oliver-Martos, B., Martínez-Cáceres, E., Jakasa, I., Gajski, G., Brun, V., Kyriacou, K., Burzynska-Pedziwiatr, I., Wozniak, L.A., Nierkens, S., Pascual García, C., Katrlik, J., Bojic-Trbojevic, Z., Vacek, J., Llorente, A., Antohe, F., Suica, V., Suarez, G., t'Kindt, R., Martin, P., Penque, D., Martins, I.L., Bodoki, E., Iacob, B.-C., Celikbas, E., Timur, S., Allinson, J., Sutton, C., Luider, T., Wittfooth, S. and Sammar, M. Analytical techniques for multiplex analysis of protein biomarkers. *Expert Rev Proteomics.* 2020, **17**(4), 257-273.
8. Garibyan, L. and Avashia, N. Polymerase chain reaction. *J Invest Dermatol.* 2013, **133**(3), 1-4.
9. Mullis, K., Faloona, F., Scharf, S., Saiki, R., Horn, G. and Erlich, H. Specific enzymatic amplification of DNA in vitro: the polymerase chain reaction. *Cold Spring Harb Symp Quant Biol.* 1986, **51 Pt 1**, 263-273.
10. Niesters, H.G.M. Quantitation of Viral Load Using Real-Time Amplification Techniques. *Methods.* 2001, **25**(4), 419-429.
11. Adams, G. A beginner's guide to RT-PCR, qPCR and RT-qPCR. *The Biochemist.* 2020, **42**(3), 48-53.
12. Kralik, P. and Ricchi, M. A Basic Guide to Real Time PCR in Microbial Diagnostics: Definitions, Parameters, and Everything. *Front Microbiol.* 2017, **8**, 108.
13. Tahamtan, A. and Ardebili, A. Real-time RT-PCR in COVID-19 detection: issues affecting the results. *Expert Rev Mol Diagn.* 2020, **20**(5), 453-454.
14. Mahmood, T. and Yang, P.C. Western blot: technique, theory, and trouble shooting. *N Am J Med Sci.* 2012, **4**(9), 429-434.
15. Hirano, S. Western blot analysis. *Methods Mol Biol.* 2012, **926**, 87-97.
16. Cárdenas, A.M., Baughan, E. and Hodinka, R.L. Evaluation of the Bio-Rad Multispot HIV-1/HIV-2 Rapid Test as an alternative to Western blot for confirmation of HIV infection. *J Clin Virol.* 2013, **58 Suppl 1**, e97-e103.
17. Yeh, C.T., Han, C.M., Lo, S.Y., Ou, J.H., Fan, K.D., Sheen, I.S., Chu, C.M. and Liaw, Y.F. Early detection of anti-HCc antibody in acute hepatitis C virus (HCV) by western blot (immunoblot) using a recombinant HCV core protein fragment. *J Clin Microbiol.* 1994, **32**(9), 2235-2241.
18. Sanchez, E., Vannier, E., Wormser, G.P. and Hu, L.T. Diagnosis, Treatment, and Prevention of Lyme Disease, Human Granulocytic Anaplasmosis, and Babesiosis: A Review. *Jama.* 2016, **315**(16), 1767-1777.

19. Weinstein, A. Laboratory Testing for Lyme Disease: Time for a Change? *Clin Infect Dis.* 2008, **47**(2), 196-197.
20. Nandi, S., Maity, S., Bhunia, S.C. and Saha, M.K. Comparative assessment of commercial ELISA kits for detection of HIV in India. *BMC Res Notes.* 2014, **7**, 436.
21. Juarez, S.I., Nuñez, A.E., Aranda, M.M., Mojica, D., Kim, A.A. and Parekh, B. Field Evaluation of Four Rapid Tests for Diagnosis of HIV Infection in Panama. *J Clin Microbiol.* 2016, **54**(4), 1127-1129.
22. Parekh, B.S., Ou, C.Y., Fonjungo, P.N., Kalou, M.B., Rottinghaus, E., Puren, A., Alexander, H., Hurlston Cox, M. and Nkengasong, J.N. Diagnosis of Human Immunodeficiency Virus Infection. *Clin Microbiol Rev.* 2019, **32**(1), e00064-00018.
23. Branda, J.A. and Steere, A.C. Laboratory Diagnosis of Lyme Borreliosis. *Clin Microbiol Rev.* 2021, **34**(2).
24. Clarisse, T., Michèle, S., Olivier, T., Valérie, E., Vincent, L.M., Jacques-Antoine, H., Michel, G. and Florence, V. Detection and quantification of staphylococcal enterotoxin A in foods with specific and sensitive polyclonal antibodies. *Food Control.* 2013, **32**(1), 255-261.
25. Kuang, H., Wang, W., Xu, L., Ma, W., Liu, L., Wang, L. and Xu, C. Monoclonal antibody-based sandwich ELISA for the detection of staphylococcal enterotoxin A. *Int J Environ Res Public Health.* 2013, **10**(4), 1598-1608.
26. Josephy, P.D., Eling, T. and Mason, R.P. The horseradish peroxidase-catalyzed oxidation of 3,5,3',5'-tetramethylbenzidine. Free radical and charge-transfer complex intermediates. *J Biol Chem.* 1982, **257**(7), 3669-3675.
27. Jiang, X., Wu, M., Albo, J. and Rao, Q. Non-Specific Binding and Cross-Reaction of ELISA: A Case Study of Porcine Hemoglobin Detection. *Foods.* 2021, **10**(8).
28. Sakamoto, S., Putalun, W., Vimolmangkang, S., Phoolcharoen, W., Shoyama, Y., Tanaka, H. and Morimoto, S. Enzyme-linked immunosorbent assay for the quantitative/qualitative analysis of plant secondary metabolites. *J nat med.* 2018, **72**(1), 32-42.
29. Deshmukh, T.M., Dudhmal, M.T., Thorat, N.C., Sarje, P.D., Walimbe, A.M. and Lole, K.S. Application of a truncated ORF2 protein-based ELISA for diagnosis of hepatitis E in an endemic area. *Appl Microbiol Biotechnol.* 2022, **106**(24), 8259-8272.
30. Gornowicz-Porowska, J., Seraszek-Jaros, A., Bowszyc-Dmochowska, M., Bartkiewicz, P., Kaczmarek, E. and Dmochowski, M. Clinical evaluation of a multiparametric ELISA as a rapid tool for routinely diagnosing IgG-mediated autoimmune blistering dermatoses in ethnic Slavs. *J Clin Lab Anal.* 2018, **32**(4), e22336.
31. Zhang, W., Guo, X.X., Wang, X.F. and Wang, M.S. Cerebrospinal fluid IgG against TB-SA for diagnosis of tuberculous meningitis. *Eur Rev Med Pharmacol Sci.* 2016, **20**(3), 462-466.
32. Alexander, T.S. Human Immunodeficiency Virus Diagnostic Testing: 30 Years of Evolution. *Clin Vaccine Immunol.* 2016, **23**(4), 249.
33. Berinstein, N.L., Grillo-López, A.J., White, C.A., Bence-Bruckler, I., Maloney, D., Czuczman, M., Green, D., Rosenberg, J., McLaughlin, P. and Shen, D. Association of serum Rituximab (IDEC-C2B8) concentration and anti-tumor response in the treatment of recurrent low-grade or follicular non-Hodgkin's lymphoma. *Ann Oncol.* 1998, **9**(9), 995-1001.
34. Lucafò, M., Curci, D., Bramuzzo, M., Alvisi, P., Martelossi, S., Silvestri, T., Guastalla, V., Labriola, F., Stocco, G. and Decorti, G. Serum Adalimumab Levels After Induction Are Associated With Long-Term Remission in Children With Inflammatory Bowel Disease. *Front Pediatr.* 2021, **9**, 646671.
35. Quartino, A.L., Hillenbach, C., Li, J., Li, H., Wada, R.D., Visich, J., Li, C., Heinzmann, D., Jin, J.Y. and Lum, B.L. Population pharmacokinetic and exposure-response analysis for trastuzumab administered using a

subcutaneous "manual syringe" injection or intravenously in women with HER2-positive early breast cancer. *Cancer Chemother Pharmacol.* 2016, **77**(1), 77-88.

36. Gorovits, B., Baltrukonis, D.J., Bhattacharya, I., Birchler, M.A., Finco, D., Sikkema, D., Vincent, M.S., Lula, S., Marshall, L. and Hickling, T.P. Immunoassay methods used in clinical studies for the detection of anti-drug antibodies to adalimumab and infliximab. *Clin Exp Immunol.* 2018, **192**(3), 348-365.
37. Ahirwar, R., Bhattacharya, A. and Kumar, S. Unveiling the underpinnings of various non-conventional ELISA variants: a review article. *Expert Rev Mol Diagn.* 2022, **22**(7), 761-774.
38. Lee, L.J., Yang, S.T., Lai, S., Bai, Y., Huang, W.C. and Juang, Y.J. Microfluidic enzyme-linked immunosorbent assay technology. *Adv Clin Chem.* 2006, **42**, 255-295.
39. Nahar, P., Bora, U., Sharma, G.L. and Kannoujia, D.K. Microwave-mediated enzyme-linked immunosorbent assay procedure. *Anal Biochem.* 2012, **421**(2), 764-766.
40. Toh, S.Y., Citartan, M., Gopinath, S.C. and Tang, T.H. Aptamers as a replacement for antibodies in enzyme-linked immunosorbent assay. *Biosens Bioelectron.* 2015, **64**, 392-403.
41. Santiago, I. Trends and Innovations in Biosensors for COVID-19 Mass Testing. *Chembiochem.* 2020, **21**(20), 2880-2889.
42. Peeling, R.W., Wedderburn, C.J., Garcia, P.J., Boeras, D., Fongwen, N., Nkengasong, J., Sall, A., Tanuri, A. and Heymann, D.L. Serology testing in the COVID-19 pandemic response. *Lancet Infect Dis.* 2020, **20**(9), 245-249.
43. Drain, P.K., Hyle, E.P., Noubary, F., Freedberg, K.A., Wilson, D., Bishai, W.R., Rodriguez, W. and Bassett, I.V. Diagnostic point-of-care tests in resource-limited settings. *Lancet Infect Dis.* 2014, **14**(3), 239-249.
44. Gnoth, C. and Johnson, S. Strips of Hope: Accuracy of Home Pregnancy Tests and New Developments. *Geburtshilfe Frauenheilkd.* 2014, **74**(7), 661-669.
45. Butler, S.A., Khanlian, S.A. and Cole, L.A. Detection of early pregnancy forms of human chorionic gonadotropin by home pregnancy test devices. *Clin Chem.* 2001, **47**(12), 2131-2136.
46. Norman, R.J., Menabawey, M., Lowings, C., Buck, R.H. and Chard, T. Relationship between blood and urine concentrations of intact human chorionic gonadotropin and its free subunits in early pregnancy. *Obstet Gynecol.* 1987, **69**(4), 590-593.
47. Bastian, L.A., Nanda, K., Hasselblad, V. and Simel, D.L. Diagnostic efficiency of home pregnancy test kits. A meta-analysis. *Arch Fam Med.* 1998, **7**(5), 465-469.
48. Daviaud, J., Fournet, D., Ballongue, C., Guillem, G.P., Leblanc, A., Casellas, C. and Pau, B. Reliability and feasibility of pregnancy home-use tests: laboratory validation and diagnostic evaluation by 638 volunteers. *Clin Chem.* 1993, **39**(1), 53-59.
49. Peto, T., Affron, D., Afrough, B., Agasu, A., Ainsworth, M., Allanson, A., Allen, K., Allen, C., Archer, L., Ashbridge, N., Aurfan, I., Avery, M., Badenoch, E., Bagga, P., Balaji, R., Baldwin, E., Barraclough, S., Beane, C., Bell, J., Benford, T., Bird, S., Bishop, M., Bloss, A., Body, R., Boulton, R., Bown, A., Bratten, C., Bridgeman, C., Britton, D., Brooks, T., Broughton-Smith, M., Brown, P., Buck, B., Butcher, E., Byrne, W., Calderon, G., Campbell, S., Carr, O., Carter, P., Carter, D., Cathrall, M., Catton, M., Chadwick, J., Chapman, D., Chau, K.K., Chaudary, T., Chidavaenzi, S., Chilcott, S., Choi, B., Claasen, H., Clark, S., Clarke, R., Clarke, D., Clayton, R., Collins, K., Colston, R., Connolly, J., Cook, E., Corcoran, M., Corley, B., Costello, L., Coulson, C., Crook, A., Crook, D.W., D'Arcangelo, S., Darby, M.-A., Davis, J., de Koning, R., Derbyshire, P., Devall, P., Dolman, M., Draper, N., Driver, M., Dyas, S., Eaton, E., Edwards, J., Elderfield, R., Ellis, K., Ellis, G., Elwell, S., Evans, R., Evans, B., Evans, M., Evans, R., Eyre, D., Fahey, C., Fenech, V., Field, J., Field, A., Foord, T.,

Fowler, T., French, M., Fuchs, H., Gan, J., Gernon, J., Ghadiali, G., Ghuman, N., Gibbons, K., Gill, G., Gilmour, K., Goel, A., Gordon, S., Graham, T., Grassam-Rowe, A., Green, D., Gronert, A., Gumsley-Read, T., Hall, C., Hallis, B., Hammond, S., Hammond, P., Hanney, B., Hardy, V., Harker, G., Harris, A., Havinden-Williams, M., Hazell, E., Henry, J., Hicklin, K., Hollier, K., Holloway, B., Hoosdally, S.J., Hopkins, S., Hughes, L., Hurdowar, S., Hurford, S.-A., Jackman, J., Jackson, H., Johns, R., Johnston, S., Jones, J., Kanyowa, T., Keating-Fedders, K., Kempson, S., Khan, I., Khulusi, B., Knight, T., Krishna, A., Lahert, P., Lampshire, Z., Lasserson, D., Lee, K., Lee, L.Y.W., Legard, A., Leggio, C., Liu, J., Lockett, T., Logue, C., Lucas, V., Lumley, S.F., Maripuri, V., Markham, D., Marshall, E., Matthews, P.C., McKee, S., McKee, D.F., McLeod, N., McNulty, A., Mellor, F., Michel, R., Mighiu, A., Miller, J., Mirza, Z., Mistry, H., Mitchell, J., Moeser, M.E., Moore, S., Muthuswamy, A., Myers, D., Nanson, G., Newbury, M., Nicol, S., Nuttall, H., Nwanaforo, J.J., Oliver, L., Osbourne, W., Osbourne, J., Otter, A., Owen, J., Panchalingam, S., Papoulidis, D., Pavon, J.D., Peace, A., Pearson, K., Peck, L., Pegg, A., Pegler, S., Permain, H., Perumal, P., Peto, L., Peto, T.E.A., Pham, T., Pickford, H.L., Pinkerton, M., Platton, M., Price, A., Protheroe, E., Purnell, H., Rawden, L., Read, S., Reynard, C., Ridge, S., Ritter, T.G., Robinson, J., Robinson, P., Rodger, G., Rowe, C., Rowell, B., Rowlands, A., Sampson, S., Saunders, K., Sayers, R., Sears, J., Sedgewick, R., Seeney, L., Selassie, A., Shail, L., Shallcross, J., Sheppard, L., Sherkat, A., Siddiqui, S., Sienkiewicz, A., Sinha, L., Smith, J., Smith, E., Stanton, E., Starkey, T., Stawiarski, A., Sterry, A., Stevens, J., Stockbridge, M., Stoesser, N., Sukumaran, A., Sweed, A., Tatar, S., Thomas, H., Tibbins, C., Tiley, S., Timmins, J., Tomas-Smith, C., Topping, O., Turek, E., Neibler, T., Trigg-Hogarth, K., Truelove, E., Turnbull, C., Tyrrell, D., Vaughan, A., Vertannes, J., Vipond, R., Wagstaff, L., Waldron, J., Walker, P., Walker, A.S., Walters, M., Wang, J.Y., Watson, E., Webberley, K., Webster, K., Westland, G., Wickens, I., Willcocks, J., Willis, H., Wilson, S., Wilson, B., Woodhead, L., Wright, D., Xavier, B., Yelnoorkar, F., Zeidan, L. and Zinyama, R. COVID-19: Rapid antigen detection for SARS-CoV-2 by lateral flow assay: A national systematic evaluation of sensitivity and specificity for mass-testing. *EClinicalMedicine.* 2021, **36**, 100924.

50. García-Fiñana, M., Hughes, D.M., Cheyne, C.P., Burnside, G., Stockbridge, M., Fowler, T.A., Fowler, V.L., Wilcox, M.H., Semple, M.G. and Buchan, I. Performance of the Innova SARS-CoV-2 antigen rapid lateral flow test in the Liverpool asymptomatic testing pilot: population based cohort study. *Bmj.* 2021, **374**, n1637.
51. Truong, T.T., Dien Bard, J. and Butler-Wu, S.M. Rapid Antigen Assays for SARS-CoV-2: Promise and Peril. *Clin Lab Med.* 2022, **42**(2), 203-222.
52. Burbelo, P.D., Riedo, F.X., Morishima, C., Rawlings, S., Smith, D., Das, S., Strich, J.R., Chertow, D.S., Davey, R.T. and Cohen, J.I. Sensitivity in Detection of Antibodies to Nucleocapsid and Spike Proteins of Severe Acute Respiratory Syndrome Coronavirus 2 in Patients With Coronavirus Disease 2019. *J Infect Dis.* 2020, **222**(2), 206-213.
53. Ke, Z., Oton, J., Qu, K., Cortese, M., Zila, V., McKeane, L., Nakane, T., Zivanov, J., Neufeldt, C.J., Cerikan, B., Lu, J.M., Peukes, J., Xiong, X., Kräusslich, H.G., Scheres, S.H.W., Bartenschlager, R. and Briggs, J.A.G. Structures and distributions of SARS-CoV-2 spike proteins on intact virions. *Nature.* 2020, **588**(7838), 498-502.
54. Boehringer, H.R. and O'Farrell, B.J. Lateral Flow Assays in Infectious Disease Diagnosis. *Clin Chem.* 2021, **68**(1), 52-58.
55. Jegerlehner, S., Suter-Riniker, F., Jent, P., Bittel, P. and Nagler, M. Diagnostic accuracy of a SARS-CoV-2 rapid antigen test in real-life clinical settings. *Int J Infect Dis.* 2021, **109**, 118-122.
56. Debes, J.D., van Oord, G. and Boonstra, A. Validation of Whole Blood Rapid Diagnosis Test for Hepatitis B. *Ann Glob Health.* 2020, **86**(1), 53.

57. Vetter, B.N., Reipold, E.I., Ongarello, S., Fajardo, E., Tyshkovskiy, A., Ben, I. and Vasylyev, M. Prospective evaluation of hepatitis C virus antibody detection in whole blood collected on dried blood spots with the INNOTEST® HCV Ab IV enzyme immunoassay. *J Clin Virol.* 2021, **137**, 104783.
58. Faraoni, S., Rocchetti, A., Gotta, F., Ruggiero, T., Orofino, G., Bonora, S. and Ghisetti, V. Evaluation of a rapid antigen and antibody combination test in acute HIV infection. *J Clin Virol.* 2013, **57**(1), 84-87.
59. Maltha, J., Gillet, P. and Jacobs, J. Malaria rapid diagnostic tests in travel medicine. *Clin Microbiol Infect.* 2013, **19**(5), 408-415.
60. Ashida, S., Yamasaki, I., Kawada, C., Fukuhara, H., Fukata, S., Tamura, K., Karashima, T., Inoue, K. and Shuin, T. Evaluation of a rapid one-step PSA test for primary prostate cancer screening. *BMC Urology.* 2021, **21**(1), 135.
61. Ecke, T.H., Weiß, S., Stephan, C., Hallmann, S., Arndt, C., Barski, D., Otto, T. and Gerullis, H. UBC(®) Rapid Test-A Urinary Point-of-Care (POC) Assay for Diagnosis of Bladder Cancer with a focus on Non-Muscle Invasive High-Grade Tumors: Results of a Multicenter-Study. *Int J Mol Sci.* 2018, **19**(12), 3841.
62. Lim, W.Y., Thevarajah, T.M., Goh, B.T. and Khor, S.M. Paper microfluidic device for early diagnosis and prognosis of acute myocardial infarction via quantitative multiplex cardiac biomarker detection. *Biosens Bioelectron.* 2019, **128**, 176-185.
63. Didyuk, O., Econom, N., Guardia, A., Livingston, K. and Klueh, U. Continuous Glucose Monitoring Devices: Past, Present, and Future Focus on the History and Evolution of Technological Innovation. *J Diabetes Sci Technol.* 2021, **15**(3), 676-683.
64. Kharroubi, A.T. and Darwish, H.M. Diabetes mellitus: The epidemic of the century. *World J Diabetes.* 2015, **6**(6), 850-867.
65. Guilbault, G.G. and Lubrano, G.J. An enzyme electrode for the amperometric determination of glucose. *Anal Chim Acta.* 1973, **64**(3), 439-455.
66. Yoo, E.H. and Lee, S.Y. Glucose biosensors: an overview of use in clinical practice. *Sensors (Basel).* 2010, **10**(5), 4558-4576.
67. Saeedi, P., Petersohn, I., Salpea, P., Malanda, B., Karuranga, S., Unwin, N., Colagiuri, S., Guariguata, L., Motala, A.A., Ogurtsova, K., Shaw, J.E., Bright, D. and Williams, R. Global and regional diabetes prevalence estimates for 2019 and projections for 2030 and 2045: Results from the International Diabetes Federation Diabetes Atlas, 9(th) edition. *Diabetes Res Clin Pract.* 2019, **157**, 107843.
68. Mariani, H.S., Layden, B.T. and Aleppo, G. Continuous Glucose Monitoring: A Perspective on Its Past, Present, and Future Applications for Diabetes Management. *Clin Diabetes.* 2017, **35**(1), 60-65.
69. Samant, P.P., Niedzwiecki, M.M., Raviele, N., Tran, V., Mena-Lapaix, J., Walker, D.I., Felner, E.I., Jones, D.P., Miller, G.W. and Prausnitz, M.R. Sampling interstitial fluid from human skin using a microneedle patch. *Sci Transl Med.* 2020, **12**(571), eaaw0285.
70. Tran, B.Q., Miller, P.R., Taylor, R.M., Boyd, G., Mach, P.M., Rosenzweig, C.N., Baca, J.T., Polsky, R. and Glaros, T. Proteomic Characterization of Dermal Interstitial Fluid Extracted Using a Novel Microneedle-Assisted Technique. *J Proteome Res.* 2018, **17**(1), 479-485.
71. Tehrani, F., Teymourian, H., Wuerstle, B., Kavner, J., Patel, R., Furmidge, A., Aghavali, R., Hosseini-Toudeshki, H., Brown, C., Zhang, F., Mahato, K., Li, Z., Barfidokht, A., Yin, L., Warren, P., Huang, N., Patel, Z., Mercier, P.P. and Wang, J. An integrated wearable microneedle array for the continuous monitoring of multiple biomarkers in interstitial fluid. *Nat Biomed Eng.* 2022, **6**(11), 1214-1224.
72. Rocchitta, G., Spanu, A., Babudieri, S., Latte, G., Madeddu, G., Galleri, G., Nuvoli, S., Bagella, P., Demartis, M., Fiore, V., Manetti, R. and Serra, P. Analytical Problems in Exposing Amperometric Enzyme Biosensors to Biological Fluids. *Sensors.* 2016, **16**, 780.

73. Taddeo, A., Prim, D., Bojescu, E.-D., Segura, J.-M. and Pfeifer, M.E. Point-of-Care Therapeutic Drug Monitoring for Precision Dosing of Immunosuppressive Drugs. *J Appl Lab Med.* 2020, **5**(4), 738-761.
74. Crouch, D.J., Walsh, J.M., Flegel, R., Cangianelli, L., Baudys, J. and Atkins, R. An evaluation of selected oral fluid point-of-collection drug-testing devices. *J Anal Toxicol.* 2005, **29**(4), 244-248.
75. Desrosiers, N.A., Milman, G., Mendu, D.R., Lee, D., Barnes, A.J., Gorelick, D.A. and Huestis, M.A. Cannabinoids in oral fluid by on-site immunoassay and by GC-MS using two different oral fluid collection devices. *Anal Bioanal Chem.* 2014, **406**(17), 4117-4128.
76. Dobri, S.C.D., Moslehi, A.H. and Davies, T.C. Are oral fluid testing devices effective for the roadside detection of recent cannabis use? A systematic review. *Public Health.* 2019, **171**, 57-65.
77. Bhalla, N., Jolly, P., Formisano, N. and Estrela, P. Introduction to biosensors. *Essays Biochem.* 2016, **60**(1), 1-8.
78. Naresh, V. and Lee, N. A Review on Biosensors and Recent Development of Nanostructured Materials-Enabled Biosensors. *Sensors (Basel).* 2021, **21**(4), 1109.
79. Naresh, V. and Lee, N. A Review on Biosensors and Recent Development of Nanostructured Materials-Enabled Biosensors. *Sensors.* 2021, **21**(4), 1109.
80. Nguyen, H.H., Lee, S.H., Lee, U.J., Fermin, C.D. and Kim, M. Immobilized Enzymes in Biosensor Applications. *Materials.* 2019, **12**(1), 121.
81. Ozdemir, M.S., Marczak, M., Bohets, H., Bonroy, K., Roymans, D., Stuyver, L., Vanhoutte, K., Pawlak, M. and Bakker, E. A Label-Free Potentiometric Sensor Principle for the Detection of Antibody–Antigen Interactions. *Anal Chem.* 2013, **85**(9), 4770-4776.
82. Karachaliou, C.-E., Koukouvinos, G., Goustouridis, D., Raptis, I., Kakabakos, S., Livaniou, E. and Petrou, P. Recent Developments in the Field of Optical Immunosensors Focusing on a Label-Free, White Light Reflectance Spectroscopy-Based Immunosensing Platform. *Sensors.* 2022, **22**(14), 5114.
83. Tallapragada, S.D., Layek, K., Mukherjee, R., Mistry, K.K. and Ghosh, M. Development of screen-printed electrode based immunosensor for the detection of HER2 antigen in human serum samples. *Bioelectrochemistry.* 2017, **118**, 25-30.
84. Homola, J. Surface Plasmon Resonance Sensors for Detection of Chemical and Biological Species. *Chem Rev.* 2008, **108**(2), 462-493.
85. Jena, S.C., Shrivastava, S., Saxena, S., Kumar, N., Maiti, S.K., Mishra, B.P. and Singh, R.K. Surface plasmon resonance immunosensor for label-free detection of BIRC5 biomarker in spontaneously occurring canine mammary tumours. *Sci. Rep.* 2019, **9**(1), 13485.
86. Luppa, P.B., Sokoll, L.J. and Chan, D.W. Immunosensors--principles and applications to clinical chemistry. *Clin Chim Acta.* 2001, **314**(1-2), 1-26.
87. Rapp, B.E., Gruhl, F.J. and Länge, K. Biosensors with label-free detection designed for diagnostic applications. *Anal Bioanal Chem.* 2010, **398**(6), 2403-2412.
88. El-Sherif, D.M., Abouzid, M., Gaballah, M.S., Ahmed, A.A., Adeel, M. and Sheta, S.M. New approach in SARS-CoV-2 surveillance using biosensor technology: a review. *Environ Sci Pollut Res.* 2022, **29**(2), 1677-1695.
89. Tang, J., Tang, D., Li, Q., Su, B., Qiu, B. and Chen, G. Sensitive electrochemical immunoassay of carcinoembryonic antigen with signal dual-amplification using glucose oxidase and an artificial catalase. *Anal Chim Acta.* 2011, **697**(1-2), 16-22.
90. Wang, H., Li, X., Mao, K., Li, Y., Du, B., Zhang, Y. and Wei, Q. Electrochemical immunosensor for α-fetoprotein detection using ferroferric oxide and horseradish peroxidase as signal amplification labels. *Anal Biochem.* 2014, **465**, 121-126.

91. Mollarasouli, F., Kurbanoglu, S. and Ozkan, S.A. The Role of Electrochemical Immunosensors in Clinical Analysis. *Biosensors* 2019, **9**(3), 86.
92. Vira, S., Mekhedov, E., Humphrey, G. and Blank, P.S. Fluorescent-labeled antibodies: Balancing functionality and degree of labeling. *Anal Biochem.* 2010, **402**(2), 146-150.
93. Blake, R.D. and Delcourt, S.G. Thermal stability of DNA. *Nucleic Acids Res.* 1998, **26**(14), 3323-3332.
94. Saccà, B. and Niemeyer, C.M. Functionalization of DNA nanostructures with proteins. *Chem Soc Rev.* 2011, **40**(12), 5910-5921.
95. Rodriguez, M.C., Kawde, A.N. and Wang, J. Aptamer biosensor for label-free impedance spectroscopy detection of proteins based on recognition-induced switching of the surface charge. *Chem Commun (Camb).* 2005.(34), 4267-4269.
96. Tang, J., Yu, T., Guo, L., Xie, J., Shao, N. and He, Z. In vitro selection of DNA aptamer against abrin toxin and aptamer-based abrin direct detection. *Biosens Bioelectron.* 2007, **22**(11), 2456-2463.
97. Xiao, Y., Lubin, A.A., Heeger, A.J. and Plaxco, K.W. Label-free electronic detection of thrombin in blood serum by using an aptamer-based sensor. *Angew Chem Int Ed Engl.* 2005, **44**(34), 5456-5459.
98. Long, F., Zhu, A., Shi, H., Wang, H. and Liu, J. Rapid on-site/in-situ detection of heavy metal ions in environmental water using a structure-switching DNA optical biosensor. *Sci. Rep.* 2013, **3**(1), 2308.
99. McGhee, C.E., Loh, K.Y. and Lu, Y. DNAzyme sensors for detection of metal ions in the environment and imaging them in living cells. *Curr Opin Biotechnol.* 2017, **45**, 191-201.
100. Prante, M., Segal, E., Scheper, T., Bahnemann, J. and Walter, J. Aptasensors for Point-of-Care Detection of Small Molecules. *Biosensors.* 2020, **10**(9), 108.
101. Wang, M., Tang, Y., Chen, Y., Cao, Y. and Chen, G. Catalytic hairpin assembly-programmed formation of clickable nucleic acids for electrochemical detection of liver cancer related short gene. *Anal Chim Acta.* 2019, **1045**, 77-84.
102. Xu, Y., Xiang, W., Wang, Q., Cheng, N., Zhang, L., Huang, K. and Xu, W. A smart sealed nucleic acid biosensor based on endogenous reference gene detection to screen and identify mammals on site. *Sci Rep.* 2017, **7**, 43453.
103. Zambry, N.S., Awang, M.S., Beh, K.K., Hamzah, H.H., Bustami, Y., Obande, G.A., Khalid, M.F., Ozsoz, M., Manaf, A.A. and Aziah, I. A label-free electrochemical DNA biosensor used a printed circuit board gold electrode (PCBGE) to detect SARS-CoV-2 without amplification. *Lab Chip.* 2023, **23**(6), 1622-1636.
104. Luo, Y., Yu, H., Alkhamis, O., Liu, Y., Lou, X., Yu, B. and Xiao, Y. Label-Free, Visual Detection of Small Molecules Using Highly Target-Responsive Multimodule Split Aptamer Constructs. *Anal Chem.* 2019, **91**(11), 7199-7207.
105. Ivanov, A.P., Instuli, E., McGilvery, C.M., Baldwin, G., McComb, D.W., Albrecht, T. and Edel, J.B. DNA Tunneling Detector Embedded in a Nanopore. *Nano Lett.* 2011, **11**(1), 279-285.
106. Japrung, D., Dogan, J., Freedman, K.J., Nadzeyka, A., Bauerdick, S., Albrecht, T., Kim, M.J., Jemth, P. and Edel, J.B. Single-Molecule Studies of Intrinsically Disordered Proteins Using Solid-State Nanopores. *Anal Chem.* 2013, **85**(4), 2449-2456.
107. Wang, S., Zhou, Z., Ma, N., Yang, S., Li, K., Teng, C., Ke, Y. and Tian, Y. DNA Origami-Enabled Biosensors. *Sensors* 2020, **20**(23), 6899.
108. Hua, Y., Ma, J., Li, D. and Wang, R. DNA-Based Biosensors for the Biochemical Analysis: A Review. *Biosensors* 2022, **12**(3), 183.
109. Zhou, W., Saran, R. and Liu, J. Metal Sensing by DNA. *Chem Rev.* 2017, **117**(12), 8272-8325.
110. Fu, T., Ren, S., Gong, L., Meng, H., Cui, L., Kong, R.-M., Zhang, X.-B. and Tan, W. A label-free DNAzyme fluorescence biosensor for amplified detection of

Pb2+-based on cleavage-induced G-quadruplex formation. *Talanta.* 2016, **147**, 302-306.
111. Yun, W., Cai, D., Jiang, J., Zhao, P., Huang, Y. and Sang, G. Enzyme-free and label-free ultra-sensitive colorimetric detection of Pb2+ using molecular beacon and DNAzyme based amplification strategy. *Biosens Bioelectron.* 2016, **80**, 187-193.
112. Zhang, J., Tang, Y., Teng, L., Lu, M. and Tang, D. Low-cost and highly efficient DNA biosensor for heavy metal ion using specific DNAzyme-modified microplate and portable glucometer-based detection mode. *Biosens Bioelectron.* 2015, **68**, 232-238.
113. Zuo, P., Yin, B.-C. and Ye, B.-C. DNAzyme-based microarray for highly sensitive determination of metal ions. *Biosens Bioelectron.* 2009, **25**(4), 935-939.
114. Dehghani, S., Nosrati, R., Yousefi, M., Nezami, A., Soltani, F., Taghdisi, S.M., Abnous, K., Alibolandi, M. and Ramezani, M. Aptamer-based biosensors and nanosensors for the detection of vascular endothelial growth factor (VEGF): A review. *Biosens Bioelectron.* 2018, **110**, 23-37.
115. Ghorbani, F., Abbaszadeh, H., Dolatabadi, J.E.N., Aghebati-Maleki, L. and Yousefi, M. Application of various optical and electrochemical aptasensors for detection of human prostate specific antigen: A review. *Biosens Bioelectron.* 2019, **142**, 111484.
116. Mao, K., Zhang, H., Wang, Z., Cao, H., Zhang, K., Li, X. and Yang, Z. Nanomaterial-based aptamer sensors for arsenic detection. *Biosens Bioelectron.* 2020, **148**, 111785.
117. Mehlhorn, A., Rahimi, P. and Joseph, Y. Aptamer-Based Biosensors for Antibiotic Detection: A Review. *Biosensors.* 2018, **8**(2), 54.
118. Robin, P., Barnabei, L., Marocco, S., Pagnoncelli, J., Nicolis, D., Tarantelli, C., Tavilla, A.C., Robortella, R., Cascione, L., Mayoraz, L., Journot, C.M.A., Mensi, M., Bertoni, F., Stefanini, I. and Gerber-Lemaire, S. A DNA biosensors-based microfluidic platform for attomolar real-time detection of unamplified SARS-CoV-2 virus. *Biosens Bioelectron.* 2023, **13**, 100302.
119. Williamson, P., Piskunen, P., Ijäs, H., Butterworth, A., Linko, V. and Corrigan, D.K. Signal Amplification in Electrochemical DNA Biosensors Using Target-Capturing DNA Origami Tiles. *ACS Sens.* 2023, **8**(4), 1471-1480.
120. Brennan, L.M., Widder, M.W., McAleer, M.K., Mayo, M.W., Greis, A.P. and van der Schalie, W.H. Preparation and testing of impedance-based fluidic biochips with RTgill-W1 cells for rapid evaluation of drinking water samples for toxicity. *J Vis Exp.* 2016.(109), e53555.
121. Galarion, L.H., Mitchell, J.K., Randall, C.P. and O'Neill, A.J. An extensively validated whole-cell biosensor for specific, sensitive and high-throughput detection of antibacterial inhibitors targeting cell-wall biosynthesis. *J Antimicrob Chemother.* 2023, **78**(3), 646-655.
122. Kylilis, N., Riangrungroj, P., Lai, H.-E., Salema, V., Fernández, L.Á., Stan, G.-B.V., Freemont, P.S. and Polizzi, K.M. Whole-Cell Biosensor with Tunable Limit of Detection Enables Low-Cost Agglutination Assays for Medical Diagnostic Applications. *ACS Sens.* 2019, **4**(2), 370-378.
123. Liu, F., Nordin, A., Li, F. and Voiculescu, I. A lab-on-chip cell-based biosensor for label-free sensing of water toxicants. *Lab Chip.* 2014, **14**(7), 1270-1280.
124. Miettinen, K., Leelahakorn, N., Almeida, A., Zhao, Y., Hansen, L.R., Nikolajsen, I.E., Andersen, J.B., Givskov, M., Staerk, D., Bak, S. and Kampranis, S.C. A GPCR-based yeast biosensor for biomedical, biotechnological, and point-of-use cannabinoid determination. *Nat Commun.* 2022, **13**(1), 3664.
125. Sun, J.-Z., Peter Kingori, G., Si, R.-W., Zhai, D.-D., Liao, Z.-H., Sun, D.-Z., Zheng, T. and Yong, Y.-C. Microbial fuel cell-based biosensors for environmental monitoring: a review. *Water Sci Technol.* 2015, **71**(6), 801-809.
126. Gheorghiu, M. A short review on cell-based biosensing: challenges and breakthroughs in biomedical analysis. *J Biomed Res.* 2020, **35**(4), 255-263.

127. Gupta, N., Renugopalakrishnan, V., Liepmann, D., Paulmurugan, R. and Malhotra, B.D. Cell-based biosensors: Recent trends, challenges and future perspectives. *Biosens Bioelectron.* 2019, **141**, 111435.
128. Polat, E.O., Cetin, M.M., Tabak, A.F., Bilget Güven, E., Uysal, B.Ö., Arsan, T., Kabbani, A., Hamed, H. and Gül, S.B. Transducer Technologies for Biosensors and Their Wearable Applications. *Biosensors.* 2022, **12**(6), 385.
129. Narita, F., Wang, Z., Kurita, H., Li, Z., Shi, Y., Jia, Y. and Soutis, C. A Review of Piezoelectric and Magnetostrictive Biosensor Materials for Detection of COVID-19 and Other Viruses. *Adv Mater.* 2021, **33**(1), 2005448.
130. Vasuki, S., Varsha, V., Mithra, R., Dharshni, S., Abinaya, R., Dharshini, N. and Sivarajasekar, N. Thermal Biosensors and Their Applications. *Am Int J Res Sci Technol Eng Math.* 2019. 292-264.
131. Yakovleva, M., Bhand, S. and Danielsson, B. The enzyme thermistor—A realistic biosensor concept. A critical review. *Anal Chim Acta.* 2013, **766**, 1-12.
132. Madhurantakam, S., Muthukumar, S. and Prasad, S. Emerging Electrochemical Biosensing Trends for Rapid Diagnosis of COVID-19 Biomarkers as Point-of-Care Platforms: A Critical Review. *ACS Omega.* 2022, **7**(15), 12467-12473.
133. Singh, A., Sharma, A., Ahmed, A., Sundramoorthy, A.K., Furukawa, H., Arya, S. and Khosla, A. Recent Advances in Electrochemical Biosensors: Applications, Challenges, and Future Scope. *Biosensors.* 2021, **11**(9), 336.
134. Sumitha, M.S. and Xavier, T.S. Recent advances in electrochemical biosensors – A brief review. *Hybrid Advances.* 2023, **2**, 100023.
135. Nikkhah, M., Karami, S., Khatami, S.H., Taheri-Anganeh, M., Savardashtaki, A., Mahmoodzadeh, A., Shabaninejad, Z., Vakili, O., Mousavi, P., Ghanizadeh Gerayeli, F., Behrouj, H., Ghasemi, H. and Movahedpour, A. Review of electrochemical and optical biosensors for testosterone measurement. *Biotechnol. Appl. Biochem.* 2023, **70**(1), 318-329.
136. Chen, Y.T., Lee, Y.C., Lai, Y.H., Lim, J.C., Huang, N.T., Lin, C.T. and Huang, J.J. Review of Integrated Optical Biosensors for Point-Of-Care Applications. *Biosensors* 2020, **10**(12), 209.
137. Adamson, H. and Jeuken, L.J.C. Engineering Protein Switches for Rapid Diagnostic Tests. *ACS Sens.* 2020, **5**(10), 3001-3012.
138. Fernandes, G.M., Silva, W.R., Barreto, D.N., Lamarca, R.S., Lima Gomes, P.C.F., Flávio da S Petruci, J. and Batista, A.D. Novel approaches for colorimetric measurements in analytical chemistry – A review. *Anal Chim Acta.* 2020, **1135**, 187-203.
139. Zhao, L., Wu, Z., Liu, G., Lu, H., Gao, Y., Liu, F., Wang, C., Cui, J. and Lu, G. High-activity Mo, S co-doped carbon quantum dot nanozyme-based cascade colorimetric biosensor for sensitive detection of cholesterol. *J Mater Chem B.* 2019, **7**(44), 7042-7051.
140. Zhao, V.X.T., Wong, T.I., Zheng, X.T., Tan, Y.N. and Zhou, X. Colorimetric biosensors for point-of-care virus detections. *Mater Sci Energy Technol.* 2020, **3**, 237-249.
141. Askaravi, M., Rezatofighi, S.E., Rastegarzadeh, S. and Seifi Abad Shapouri, M.R. Development of a new method based on unmodified gold nanoparticles and peptide nucleic acids for detecting bovine viral diarrhea virus-RNA. *AMB Express.* 2017, **7**(1), 137.
142. Saleh, M. and El-Matbouli, M. Rapid detection of Cyprinid herpesvirus-3 (CyHV-3) using a gold nanoparticle-based hybridization assay. *J Virol Methods.* 2015, **217**, 50-54.
143. Shawky, S.M., Bald, D. and Azzazy, H.M.E. Direct detection of unamplified hepatitis C virus RNA using unmodified gold nanoparticles. *Clin Biochem.* 2010, **43**(13), 1163-1168.
144. Liu, Y., Zhang, L., Wei, W., Zhao, H., Zhou, Z., Zhang, Y. and Liu, S. Colorimetric detection of influenza A virus using antibody-functionalized gold nanoparticles. *Analyst.* 2015, **140**(12), 3989-3995.

145. Dixon, A.S., Schwinn, M.K., Hall, M.P., Zimmerman, K., Otto, P., Lubben, T.H., Butler, B.L., Binkowski, B.F., Machleidt, T., Kirkland, T.A., Wood, M.G., Eggers, C.T., Encell, L.P. and Wood, K.V. NanoLuc Complementation Reporter Optimized for Accurate Measurement of Protein Interactions in Cells. *ACS Chem Biol.* 2016, **11**(2), 400-408.
146. Vlasenko, L.V. and Nechitailo, K.S. Bacterial luminescent biosensors in the system for assessing the mechanisms of antibacterial activity of carbon-based nanomaterials. *IOP Conference Series: Earth and Environmental Science.* 2022, **979**(1), 012056.
147. Dacres, H., Wang, J., Dumancic, M.M. and Trowell, S.C. Experimental determination of the Förster distance for two commonly used bioluminescent resonance energy transfer pairs. *Anal Chem.* 2010, **82**(1), 432-435.
148. De, A. The new era of bioluminescence resonance energy transfer technology. *Curr Pharm Biotechnol.* 2011, **12**(4), 558-568.
149. Sun, S., Yang, X., Wang, Y. and Shen, X. In Vivo Analysis of Protein-Protein Interactions with Bioluminescence Resonance Energy Transfer (BRET): Progress and Prospects. *Int J Mol Sci.* 2016, **17**(10), 1704.
150. Song, F., Tang, P.S., Durst, H., Cramb, D.T. and Chan, W.C. Nonblinking plasmonic quantum dot assemblies for multiplex biological detection. *Angew Chem Int Ed Engl.* 2012, **51**(35), 8773-8777.
151. Wu, Y., Chakrabortty, S., Gropeanu, R.A., Wilhelmi, J., Xu, Y., Er, K.S., Kuan, S.L., Koynov, K., Chan, Y. and Weil, T. pH-responsive quantum dots via an albumin polymer surface coating. *J Am Chem Soc.* 2010, **132**(14), 5012-5014.
152. Kumar, M., Zhang, D., Broyles, D. and Deo, S.K. A rapid, sensitive, and selective bioluminescence resonance energy transfer (BRET)-based nucleic acid sensing system. *Biosens Bioelectron.* 2011, **30**(1), 133-139.
153. Arts, R., den Hartog, I., Zijlema, S.E., Thijssen, V., van der Beelen, S.H.E. and Merkx, M. Detection of Antibodies in Blood Plasma Using Bioluminescent Sensor Proteins and a Smartphone. *Anal Chem.* 2016, **88**(8), 4525-4532.
154. Xue, L., Yu, Q., Griss, R., Schena, A. and Johnsson, K. Bioluminescent Antibodies for Point-of-Care Diagnostics. *Angew Chem Int Ed Engl.* 2017, **56**(25), 7112-7116.
155. Syahir, A., Usui, K., Tomizaki, K.-y., Kajikawa, K. and Mihara, H. Label and Label-Free Detection Techniques for Protein Microarrays. *Microarrays.* 2015, **4**(2), 228-244.
156. Stojanovic, M.N., de Prada, P. and Landry, D.W. Fluorescent Sensors Based on Aptamer Self-Assembly. *Journal of the American Chemical Society.* 2000, **122**(46), 11547-11548.
157. Arroyo-Currás, N., Somerson, J., Vieira, P.A., Ploense, K.L., Kippin, T.E. and Plaxco, K.W. Real-time measurement of small molecules directly in awake, ambulatory animals. *Proc Natl Acad Sci U S A.* 2017, **114**(4), 645-650.
158. Algar, W.R., Hildebrandt, N., Vogel, S.S. and Medintz, I.L. FRET as a biomolecular research tool — understanding its potential while avoiding pitfalls. *Nature Methods.* 2019, **16**(9), 815-829.
159. Wu, Y. and Jiang, T. Developments in FRET- and BRET-Based Biosensors. *Micromachines.* 2022, **13**(10), 1789.
160. Verma, A.K., Noumani, A., Yadav, A.K. and Solanki, P.R. FRET Based Biosensor: Principle Applications Recent Advances and Challenges. *Diagnostics.* 2023, **13**(8), 1375.
161. Aydin, M., Aydin, E.B. and Sezgintürk, M.K. Advances in immunosensor technology. *Adv Clin Chem.* 2021, **102**, 1-62.
162. Stein, V. and Alexandrov, K. Synthetic protein switches: design principles and applications. *Trends Biotechnol.* 2015, **33**(2), 101-110.
163. Armbruster, D.A. and Pry, T. Limit of blank, limit of detection and limit of quantitation. *Clin Biochem Rev.* 2008, **29 Suppl 1**(Suppl 1), S49-52.

164. Tullman, J., Nicholes, N., Dumont, M.R., Ribeiro, L.F. and Ostermeier, M. Enzymatic protein switches built from paralogous input domains. *Biotechnol Bioeng.* 2016, **113**(4), 852-858.
165. Guo, Z., Johnston, W.A., Stein, V., Kalimuthu, P., Perez-Alcala, S., Bernhardt, P.V. and Alexandrov, K. Engineering PQQ-glucose dehydrogenase into an allosteric electrochemical Ca(2+) sensor. *Chem Commun (Camb).* 2016, **52**(3), 485-488.
166. Guntas, G., Mansell, T.J., Kim, J.R. and Ostermeier, M. Directed evolution of protein switches and their application to the creation of ligand-binding proteins. *Proc Natl Acad Sci U S A.* 2005, **102**(32), 11224-11229.
167. Crasson, O., Rhazi, N., Jacquin, O., Freichels, A., Jérôme, C., Ruth, N., Galleni, M., Filée, P. and Vandevenne, M. Enzymatic functionalization of a nanobody using protein insertion technology. *Protein Eng Des Sel.* 2015, **28**(10), 451-460.
168. Nicholes, N., Date, A., Beaujean, P., Hauk, P., Kanwar, M. and Ostermeier, M. Modular protein switches derived from antibody mimetic proteins. *Protein Eng Des Sel.* 2016, **29**(2), 77-85.
169. Banala, S., Aper, S.J., Schalk, W. and Merkx, M. Switchable reporter enzymes based on mutually exclusive domain interactions allow antibody detection directly in solution. *ACS Chem Biol.* 2013, **8**(10), 2127-2132.
170. Adamson, H., Ajayi, M., Campbell, E., Brachi, E., Tiede, C., Tang, A., Adams, L., Ford, R., Davidson, A., Johnson, M., McPherson, M., Tomlinson, D. and Jeuken, L. Affimer-Enzyme-Inhibitor Switch Sensor for Rapid Wash-free Assays of Multimeric Proteins. *ACS Sens.* 2019, **4**, 3014-3022.
171. Janssen, B.M.G., Engelen, W. and Merkx, M. DNA-Directed Control of Enzyme–Inhibitor Complex Formation: A Modular Approach to Reversibly Switch Enzyme Activity. *ACS Synth Biol.* 2015, **4**(5), 547-553.
172. Drikic, M., Olsen, S. and De Buck, J. Detecting total immunoglobulins in diverse animal species with a novel split enzymatic assay. *BMC Vet Res.* 2019, **15**(1), 374.
173. Ni, Y., Rosier, B.J.H.M., van Aalen, E.A., Hanckmann, E.T.L., Biewenga, L., Pistikou, A.-M.M., Timmermans, B., Vu, C., Roos, S., Arts, R., Li, W., de Greef, T.F.A., van Borren, M.M.G.J., van Kuppeveld, F.J.M., Bosch, B.-J. and Merkx, M. A plug-and-play platform of ratiometric bioluminescent sensors for homogeneous immunoassays. *Nat Commun.* 2021, **12**(1), 4586.
174. Guo, Z., Murphy, L., Stein, V., Johnston, W.A., Alcala-Perez, S. and Alexandrov, K. Engineered PQQ-Glucose Dehydrogenase as a Universal Biosensor Platform. *J Am Chem Soc.* 2016, **138**(32), 10108-10111.
175. Fleming, A. Penicillin. *Nobel Lectures.* 1945. 83 - 93.
176. Su, J., Beh, C., Ohmuro-Matsuyama, Y., Kitaguchi, T., Hoon, S. and Ueda, H. Creation of stable and strictly regulated enzyme switch for signal-on immunodetection of various small antigens. *J Biosci Bioeng.* 2019, **128**(6), 677-682.
177. Su, J., Dong, J., Kitaguchi, T., Ohmuro-Matsuyama, Y. and Ueda, H. Noncompetitive homogeneous immunodetection of small molecules based on beta-glucuronidase complementation. *Analyst.* 2018, **143**(9), 2096-2101.
178. Dixon, A.S., Baumgartner, B.K., Krippner, S. and Shawn, O. Bioluminescence activated by antibody-enzyme fragment complementation following target engagement. In: *Front Bioeng Biotechnol Conference Abstract: 10th World Biomaterials Congress.*, *01/01*, *Montréal, Canada*. 2016, p.1.
179. Dixon, A.S., Kim, S.J., Baumgartner, B.K., Krippner, S. and Owen, S.C. A Tri-part Protein Complementation System Using Antibody-Small Peptide Fusions Enables Homogeneous Immunoassays. *Sci Rep.* 2017, **7**(1), 8186.
180. Ng, K.K., Reinert, Z.E., Corver, J., Resurreccion, D., Hensbergen, P.J. and Prescher, J.A. A Bioluminescent Sensor for Rapid Detection of PPEP-1, a Clostridioides difficile Biomarker. *Sensors (Basel).* 2021, **21**(22), 7485.
181. Hashimoto, J., Watanabe, T., Seki, T., Karasawa, S., Izumikawa, M., Seki, T., Iemura, S., Natsume, T., Nomura, N., Goshima, N., Miyawaki, A., Takagi, M.

and Shin-Ya, K. Novel in vitro protein fragment complementation assay applicable to high-throughput screening in a 1536-well format. *J Biomol Screen.* 2009, **14**(8), 970-979.

182. Rossi, F., Charlton, C.A. and Blau, H.M. Monitoring protein-protein interactions in intact eukaryotic cells by beta-galactosidase complementation. *Proc Natl Acad Sci U S A.* 1997, **94**(16), 8405-8410.
183. Richards, F.M. On the enzymatic activity of subtilisin-modified ribonuclease. *Proc Natl Acad Sci U S A.* 1958, **44**(2), 162-166.
184. Ullmann, A., Jacob, F. and Monod, J. Characterization by in vitro complementation of a peptide corresponding to an operator-proximal segment of the beta-galactosidase structural gene of Escherichia coli. *J Mol Biol.* 1967, **24**(2), 339-343.
185. Johnsson, N. and Varshavsky, A. Split ubiquitin as a sensor of protein interactions in vivo. *Proc Natl Acad Sci U S A.* 1994, **91**(22), 10340-10344.
186. Kim, S.J., Dixon, A.S., Adamovich, P.C., Robinson, P.D. and Owen, S.C. Homogeneous Immunoassay Using a Tri-Part Split-Luciferase for Rapid Quantification of Anti-TNF Therapeutic Antibodies. *ACS Sens.* 2021, **6**(5), 1807-1814.
187. Kim, S.J., Dixon, A.S. and Owen, S.C. Split-enzyme immunoassay to monitor EGFR-HER2 heterodimerization on cell surfaces. *Acta Biomater.* 2021, **135**, 225-233.
188. Weissleder, R. and Ntziachristos, V. Shedding light onto live molecular targets. *Nat Med.* 2003, **9**(1), 123-128.
189. Paulmurugan, R. and Gambhir, S.S. Monitoring Protein−Protein Interactions Using Split Synthetic Renilla Luciferase Protein-Fragment-Assisted Complementation. *Anal Chem.* 2003, **75**(7), 1584-1589.
190. Remy, I. and Michnick, S.W. A highly sensitive protein-protein interaction assay based on Gaussia luciferase. *Nat Methods.* 2006, **3**(12), 977-979.
191. Paulmurugan, R., Umezawa, Y. and Gambhir, S. Noninvasive imaging of protein–protein interactions in living subjects by using reporter protein complementation and reconstitution strategies. *Proc Natl Acad Sci U S A.* 2002, **99**(24), 15608-15613.
192. Ohmuro-Matsuyama, Y. and Ueda, H. Homogeneous Noncompetitive Luminescent Immunodetection of Small Molecules by Ternary Protein Fragment Complementation. *Anal Chem.* 2018, **90**(5), 3001-3004.
193. Stains, C.I., Furman, J.L., Porter, J.R., Rajagopal, S., Li, Y., Wyatt, R.T. and Ghosh, I. A General Approach for Receptor and Antibody-Targeted Detection of Native Proteins Utilizing Split-Luciferase Reassembly. *ACS Chem Biol.* 2010, **5**(10), 943-952.
194. Verhoef, L.G., Mattioli, M., Ricci, F., Li, Y.C. and Wade, M. Multiplex detection of protein-protein interactions using a next generation luciferase reporter. *Biochim Biophys Acta.* 2016, **1863**(2), 284-292.
195. Adamson, H., Ajayi, M.O., Gilroy, K.E., McPherson, M.J., Tomlinson, D.C. and Jeuken, L.J.C. Rapid Quantification of C. difficile Glutamate Dehydrogenase and Toxin B (TcdB) with a NanoBiT Split-Luciferase Assay. *Anal Chem.* 2022, **94**(23), 8156-8163.
196. McArthur, N., Cruz-Teran, C., Thatavarty, A., Reeves, G.T. and Rao, B.M. Experimental and Analytical Framework for “Mix-and-Read” Assays Based on Split Luciferase. *ACS Omega.* 2022, **7**(28), 24551-24560.
197. Cooley, R., Kara, N., Hui, N.S., Tart, J., Roustan, C., George, R., Hancock, D.C., Binkowski, B.F., Wood, K.V., Ismail, M. and Downward, J. Development of a cell-free split-luciferase biochemical assay as a tool for screening for inhibitors of challenging protein-protein interaction targets. *Wellcome Open Res.* 2020, **5**, 20.
198. Edwardraja, S., Guo, Z., Whitfield, J., Lantadilla, I.R., Johnston, W.A., Walden, P., Vickers, C.E. and Alexandrov, K. Caged Activators of Artificial Allosteric Protein Biosensors. *ACS Synth Biol.* 2020, **9**(6), 1306-1314.

199. Kerppola, T.K. Bimolecular Fluorescence Complementation (BiFC) Analysis as a Probe of Protein Interactions in Living Cells. *Annu Rev Biophys.* 2008, **37**(1), 465-487.
200. Magliery, T.J., Wilson, C.G.M., Pan, W., Mishler, D., Ghosh, I., Hamilton, A.D. and Regan, L. Detecting Protein−Protein Interactions with a Green Fluorescent Protein Fragment Reassembly Trap: Scope and Mechanism. *J Am Chem Soc.* 2005, **127**(1), 146-157.
201. Ghosh, I., Hamilton, A.D. and Regan, L. Antiparallel leucine zipper-directed protein reassembly: application to the green fluorescent protein. *J Am Chem Soc.* 2000, **122**(23), 5658-5659.
202. Plamont, M.-A., Billon-Denis, E., Maurin, S., Gauron, C., Pimenta, F.M., Specht, C.G., Shi, J., Quérard, J., Pan, B., Rossignol, J., Moncoq, K., Morellet, N., Volovitch, M., Lescop, E., Chen, Y., Triller, A., Vriz, S., Saux, T.L., Jullien, L. and Gautier, A. Small fluorescence-activating and absorption-shifting tag for tunable protein imaging in vivo. *Proc Natl Acad Sci U S A.* 2016, **113**(3), 497-502.
203. Tebo, A.G. and Gautier, A. A split fluorescent reporter with rapid and reversible complementation. *Nat Commun.* 2019, **10**(1), 2822.
204. Xu, W., Xiong, Y., Lai, W., Xu, Y., Li, C. and Xie, M. A homogeneous immunosensor for AFB1 detection based on FRET between different-sized quantum dots. *Biosens Bioelectron.* 2014, **56**, 144-150.
205. Akter, S. and Lamminmäki, U. A 15-min non-competitive homogeneous assay for microcystin and nodularin based on time-resolved Förster resonance energy transfer (TR-FRET). *Anal Bioanal Chem.* 2021, **413**(24), 6159-6170.
206. Morales, M.A. and Halpern, J.M. Guide to Selecting a Biorecognition Element for Biosensors. *Bioconjug Chem.* 2018, **29**(10), 3231-3239.
207. Olaleye, O., Govorukhina, N., van de Merbel, N.C. and Bischoff, R. Non-Antibody-Based Binders for the Enrichment of Proteins for Analysis by Mass Spectrometry. *Biomolecules.* 2021, **11**(12), 1791.
208. Liew, O.W., Ling, S.S.M., Lilyanna, S., Zhou, Y., Wang, P., Chong, J.P.C., Ng, Y.X., Lim, A.E.S., Leong, E.R.Y., Lin, Q., Lim, T.K., Lin, Q., Ng, E.M.W., Ng, T.W. and Richards, A.M. Epitope-directed monoclonal antibody production using a mixed antigen cocktail facilitates antibody characterization and validation. *Commun Biol.* 2021, **4**(1), 441.
209. Nilsson, P., Paavilainen, L., Larsson, K., Odling, J., Sundberg, M., Andersson, A.C., Kampf, C., Persson, A., Al-Khalili Szigyarto, C., Ottosson, J., Björling, E., Hober, S., Wernérus, H., Wester, K., Pontén, F. and Uhlen, M. Towards a human proteome atlas: high-throughput generation of mono-specific antibodies for tissue profiling. *Proteomics.* 2005, **5**(17), 4327-4337.
210. Crivianu-Gaita, V., Romaschin, A. and Thompson, M. High efficiency reduction capability for the formation of Fab′ antibody fragments from F(ab)2 units. *Biochem Biophys Rep.* 2015, **2**, 23-28.
211. Kayser, V., Chennamsetty, N., Voynov, V., Forrer, K., Helk, B. and Trout, B.L. Glycosylation influences on the aggregation propensity of therapeutic monoclonal antibodies. *Biotechnol J.* 2011, **6**(1), 38-44.
212. Sun, H., Wu, G.M., Chen, Y., Tian, Y., Yue, Y.H. and Zhang, G.L. Expression, production, and renaturation of a functional single-chain variable antibody fragment (scFv) against human ICAM-1. *Braz J Med Biol Res.* 2014, **47**(7), 540–547.
213. Yuasa, N., Koyama, T. and Fujita-Yamaguchi, Y. Purification and refolding of anti-T-antigen single chain antibodies (scFvs) expressed in Escherichia coli as inclusion bodies. *Biosci Trends.* 2014, **8**(1), 24-31.
214. Rouet, R., Lowe, D., Dudgeon, K., Roome, B., Schofield, P., Langley, D., Andrews, J., Whitfeld, P., Jermutus, L. and Christ, D. Expression of high-affinity human antibody fragments in bacteria. *Nat Protoc.* 2012, **7**(2), 364-373.

215. Xu, L., Song, X. and Jia, L. A camelid nanobody against EGFR was easily obtained through refolding of inclusion body expressed in Escherichia coli. *Biotechnol Appl Biochem.* 2017, **64**(6), 895-901.
216. Yamagata, M. and Sanes, J.R. Reporter-nanobody fusions (RANbodies) as versatile, small, sensitive immunohistochemical reagents. *Proc Natl Acad Sci U S A.* 2018, **115**(9), 2126-2131.
217. Von Behring, E. Uber das Zustandekommen der Diphtherie-Immunitat und der Tetanus-Immunitat bei Thieren. *Deut. Med. Wochenschr.* 1890, **16**, 1113-1114.
218. Olopoenia, L.A. and King, A.L. Widal agglutination test - 100 years later: still plagued by controversy. *Postgrad Med J.* 2000, **76**(892), 80-84.
219. KÖHler, G. and Milstein, C. Continuous cultures of fused cells secreting antibody of predefined specificity. *Nature.* 1975, **256**(5517), 495-497.
220. Saeed, A.F.U.H., Wang, R., Ling, S. and Wang, S. Antibody Engineering for Pursuing a Healthier Future. *Front Microbiol.* 2017, **8**, 495.
221. Parray, H.A., Shukla, S., Samal, S., Shrivastava, T., Ahmed, S., Sharma, C. and Kumar, R. Hybridoma technology a versatile method for isolation of monoclonal antibodies, its applicability across species, limitations, advancement and future perspectives. *Int Immunopharmacol.* 2020, **85**, 106639.
222. Sharma, S., Byrne, H. and O'Kennedy, R.J. Antibodies and antibody-derived analytical biosensors. *Essays Biochem.* 2016, **60**(1), 9-18.
223. Conroy, P.J., Hearty, S., Leonard, P. and O'Kennedy, R.J. Antibody production, design and use for biosensor-based applications. *Semin Cell Dev Biol.* 2009, **20**(1), 10-26.
224. Schroeder, H.W., Jr. and Cavacini, L. Structure and function of immunoglobulins. *J Allergy Clin Immunol.* 2010, **125**(2 Suppl 2), S41-52.
225. McCullough, K.C. and Summerfield, A. Basic Concepts of Immune Response and Defense Development. *ILAR J.* 2005, **46**(3), 230-240.
226. Zeng, X., Shen, Z. and Mernaugh, R. Recombinant antibodies and their use in biosensors. *Anal Bioanal Chem.* 2012, **402**, 3027-3038.
227. Byrne, B., Stack, E., Gilmartin, N. and O'Kennedy, R. Antibody-Based Sensors: Principles, Problems and Potential for Detection of Pathogens and Associated Toxins. *Sensors.* 2009, **9**, 4407-4445.
228. Iqbal, S.S., Mayo, M.W., Bruno, J.G., Bronk, B.V., Batt, C.A. and Chambers, J.P. A review of molecular recognition technologies for detection of biological threat agents. *Biosens Bioelectron.* 2000, **15**, 549-578.
229. Al Qaraghuli, M.M., Palliyil, S., Broadbent, G., Cullen, D.C., Charlton, K.A. and Porter, A.J. Defining the complementarities between antibodies and haptens to refine our understanding and aid the prediction of a successful binding interaction. *BMC Biotechnology.* 2015, **15**, 99.
230. Tiede, C., Tang, A.A., Deacon, S.E., Mandal, U., Nettleship, J.E., Owen, R.L., George, S.E., Harrison, D.J., Owens, R.J., Tomlinson, D.C. and McPherson, M.J. Adhiron: a stable and versatile peptide display scaffold for molecular recognition applications. *Protein Eng Des Sel.* 2014, **27**(5), 145-155.
231. Weller, M.G. Quality Issues of Research Antibodies. *Anal Chem Insights.* 2016, **11**, 21-27.
232. Bordeaux, J., Welsh, A., Agarwal, S., Killiam, E., Baquero, M., Hanna, J., Anagnostou, V. and Rimm, D. Antibody validation. *BioTechniques.* 2010, **48**(3), 197-209.
233. Lamoyi, E. Preparation of F(ab')2 fragments from mouse IgG of various subclasses. *Methods Enzymol.* 1986, **121**, 652-663.
234. Porter, R.R. The hydrolysis of rabbit y-globulin and antibodies with crystalline papain. *Biochem J.* 1959, **73**(1), 119-126.
235. Liu, C.G., Zhu, M.C. and Chen, Z.N. Preparation and purification of F(ab')(2) fragment from anti hepatoma mouse IgG(1) mAb. *World J Gastroenterol.* 1999, **5**(6), 522-524.

236. Rouet, R., Dudgeon, K., Christie, M., Langley, D. and Christ, D. Fully Human VH Single Domains That Rival the Stability and Cleft Recognition of Camelid Antibodies. *J Biol Chem.* 2015, **290**(19), 11905-11917.
237. Li, K., Zettlitz, K.A., Lipianskaya, J., Zhou, Y., Marks, J.D., Mallick, P., Reiter, R.E. and Wu, A.M. A fully human scFv phage display library for rapid antibody fragment reformatting. *Protein Eng Des Sel.* 2015, **28**(10), 307-316.
238. Watkins, N.A., Du, L.M., Scott, J.P., Ouwehand, W.H. and Hillery, C.A. Single-chain antibody fragments derived from a human synthetic phage-display library bind thrombospondin and inhibit sickle cell adhesion. *Blood.* 2003, **102**(2), 718-724.
239. Huang, G., Zhong, Z., Miersch, S., Sidhu, S.S., Hou, S.C. and Wu, D. Construction of Synthetic Phage Displayed Fab Library with Tailored Diversity. *J Vis Exp.* 2018, **1**(135), 1–16.
240. Omar, N. and Lim, T.S. Construction of Naive and Immune Human Fab Phage-Display Library. *Methods Mol Biol.* 2018, **1701**, 25-44.
241. Woycechowsky, K.J. and Raines, R.T. Native disulfide bond formation in proteins. *Curr opin chem biol.* 2000, **4**(5), 533-539.
242. Gaciarz, A., Veijola, J., Uchida, Y., Saaranen, M.J., Wang, C., Hörkkö, S. and Ruddock, L.W. Systematic screening of soluble expression ofantibody fragments in the cytoplasm of E. coli. *Microb Cell Fact.* 2016, **15**(1), 22.
243. Marisch, K., Bayer, K., Cserjan-Puschmann, M., Luchner, M. and Striedner, G. Evaluation of three industrial Escherichia coli strains in fed-batch cultivations during high-level SOD protein production. *Microb Cell Fact.* 2013, **12**(1), 58.
244. Goldenberg, M.M. Trastuzumab, a recombinant DNA-derived humanized monoclonal antibody, a novel agent for the treatment of metastatic breast cancer. *Clin Ther.* 1999, **21**(2), 309-318.
245. Lobstein, J., Emrich, C.A., Jeans, C., Faulkner, M., Riggs, P. and Berkmen, M. SHuffle, a novel Escherichia coli protein expression strain capable of correctly folding disulfide bonded proteins in its cytoplasm. *Microb Cell Fact.* 2012, **11**, 56.
246. Charles A Janeway, J., Paul Travers, Mark Walport, and Mark J Shlomchik. Immunobiology: The Immune System in Health and Disease. . In: *The Immune System in Health and Disease.* . 5th Edition ed. New York: Garland Science 2001.
247. Al Qaraghuli, M.M., Kubiak-Ossowska, K., Ferro, V.A. and Mulheran, P.A. Structural Analysis of Anti-Hapten Antibodies to Identify Long-Range Structural Movements Induced by Hapten Binding. *Front Mol Biosci.* 2021, **8**, 633526.
248. Kang, D., Ahn, H.J., Lee, J., Kim, S.K., Pyun, J., Song, C.-S., Kim, S.J. and Lee, J. An NIR dual-emitting/absorbing inorganic compact pair: A self-calibrating LRET system for homogeneous virus detection. *Biosens Bioelectron.* 2021, **190**, 113369.
249. Hamers-Casterman, C., Atarhouch, T., Muyldermans, S., Robinson, G., Hammers, C., Songa, E.B., Bendahman, N. and Hammers, R. Naturally occurring antibodies devoid of light chains. *Nature.* 1993, **363**(6428), 446-448.
250. Arbabi-Ghahroudi, M. Camelid Single-Domain Antibodies: Historical Perspective and Future Outlook. *Front Immunol.* 2017, **8**, 1589.
251. Greenberg, A.S., Avila, D., Hughes, M., Hughes, A., McKinney, E.C. and Flajnik, M.F. A new antigen receptor gene family that undergoes rearrangement and extensive somatic diversification in sharks. *Nature.* 1995, **374**(6518), 168-173.
252. Cheong, W.S., Leow, Y., Majeed, A. and Leow, H. Diagnostic and therapeutic potential of shark variable new antigen receptor (VNAR) single domain antibody. *Int J Biol Macromol.* 2020, **147**, 369-375.
253. Muyldermans, S. A guide to: generation and design of nanobodies. *The FEBS Journal.* 2021, **288**(7), 2084-2102.
254. Sonneson, G.J. and Horn, J.R. Hapten-Induced Dimerization of a Single-Domain VHH Camelid Antibody. *Biochemistry.* 2009, **48**(29), 6693-6695.

255. Yu, X., Yang, Y.-P., Dikici, E., Deo, S.K. and Daunert, S. Beyond Antibodies as Binding Partners: The Role of Antibody Mimetics in Bioanalysis. *Annu rev anal chem.* 2017, **10**(1), 293-320.
256. Peltomaa, R., Benito-Peña, E., Barderas, R. and Moreno-Bondi, M.C. Phage Display in the Quest for New Selective Recognition Elements for Biosensors. *ACS Omega.* 2019, **4**(7), 11569-11580.
257. Galán, A., Comor, L., Horvatić, A., Kuleš, J., Guillemin, N., Mrljak, V. and Bhide, M. Library-based display technologies: where do we stand? *Mol BioSyst.* 2016, **12**(8), 2342-2358.
258. Ullman, C.G., Frigotto, L. and Cooley, R.N. In vitro methods for peptide display and their applications. *Brief Funct Genomics.* 2011, **10**(3), 125-134.
259. Löfblom, J., Frejd, F.Y. and Ståhl, S. Non-immunoglobulin based protein scaffolds. *Curr Opin Biotechnol.* 2011, **22**(6), 843-848.
260. Tang, A.A.-S., Tiede, C., Hughes, D.J., McPherson, M.J. and Tomlinson, D.C. Isolation of isoform-specific binding proteins (Affimers) by phage display using negative selection. *Sci Signal.* 2017, **10**(505), eaan0868.
261. Tang, A.A.S., Tiede, C., McPherson, M.J. and Tomlinson, D.C. Isolation of Artificial Binding Proteins (Affimer Reagents) for Use in Molecular and Cellular Biology. In: Poterszman, A. ed. *Multiprotein Complexes: Methods and Protocols*. New York, NY: Springer US, 2021, pp.105-121.
262. Tiede, C., Bedford, R., Heseltine, S.J., Smith, G., Wijetunga, I., Ross, R., AlQallaf, D., Roberts, A.P.E., Balls, A., Curd, A., Hughes, R.E., Martin, H., Needham, S.R., Zanetti-Domingues, L.C., Sadigh, Y., Peacock, T.P., Tang, A.A., Gibson, N., Kyle, H., Platt, G.W., Ingram, N., Taylor, T., Coletta, L.P., Manfield, I., Knowles, M., Bell, S., Esteves, F., Maqbool, A., Prasad, R.K., Drinkhill, M., Bon, R.S., Patel, V., Goodchild, S.A., Martin-Fernandez, M., Owens, R.J., Nettleship, J.E., Webb, M.E., Harrison, M., Lippiat, J.D., Ponnambalam, S., Peckham, M., Smith, A., Ferrigno, P.K., Johnson, M., McPherson, M.J. and Tomlinson, D.C. Affimer proteins are versatile and renewable affinity reagents. *eLife.* 2017, **6**, e24903.
263. Binz, H.K., Stumpp, M.T., Forrer, P., Amstutz, P. and Plückthun, A. Designing repeat proteins: well-expressed, soluble and stable proteins from combinatorial libraries of consensus ankyrin repeat proteins. *J Mol Biol.* 2003, **332**(2), 489-503.
264. Münch, R.C., Mühlebach, M.D., Schaser, T., Kneissl, S., Jost, C., Plückthun, A., Cichutek, K. and Buchholz, C.J. DARPins: An Efficient Targeting Domain for Lentiviral Vectors. *Mol Ther.* 2011, **19**(4), 686-693.
265. Koide, A., Bailey, C.W., Huang, X. and Koide, S. The fibronectin type III domain as a scaffold for novel binding proteins11Edited by J. Wells. *J Mol Biol.* 1998, **284**(4), 1141-1151.
266. Batori, V., Koide, A. and Koide, S. Exploring the potential of the monobody scaffold: effects of loop elongation on the stability of a fibronectin type III domain. *Protein Eng.* 2002, **15**(12), 1015-1020.
267. Stumpp, M.T., Binz, H.K. and Amstutz, P. DARPins: A new generation of protein therapeutics. *Drug Discov Today.* 2008, **13**(15), 695-701.
268. Carrasco-López, C., Zhao, E.M., Gil, A.A., Alam, N., Toettcher, J.E. and Avalos, J.L. Development of light-responsive protein binding in the monobody non-immunoglobulin scaffold. *Nat Commun.* 2020, **11**(1), 4045.
269. Hantschel, O., Biancalana, M. and Koide, S. Monobodies as enabling tools for structural and mechanistic biology. *Curr Opin Struct Biol.* 2020, **60**, 167-174.
270. Kondo, T., Matsuoka, K., Umemoto, S., Fujino, T., Hayashi, G., Iwatani, Y. and Murakami, H. Monobodies with potent neutralizing activity against SARS-CoV-2 Delta and other variants of concern. *Life Sci Alliance.* 2022, **5**(6), e202101322.
271. Park, S.-H., Park, S., Kim, D.-Y., Pyo, A., Kimura, R.H., Sathirachinda, A., Choy, H.E., Min, J.-J., Gambhir, S.S. and Hong, Y. Isolation and Characterization of a Monobody with a Fibronectin Domain III Scaffold That Specifically Binds EphA2. *PLOS ONE.* 2015, **10**(7), e0132976.

272. Sullivan, M.A., Wentworth, T., Kobie, J.J. and Sanz, I. Anti-idiotypic monobodies for immune response profiling. *Methods.* 2012, **58**(1), 62-68.
273. Sekhon, H., Ha, J.-H., Presti, M.F., Procopio, S.B., Mirsky, P.O., John, A.M. and Loh, S.N. Adaptable, Turn-On Monobody (ATOM) Fluorescent Biosensors for Multiplexed Detection in Cells. *bioRxiv.* 2023. 534597.
274. Ha, J.-H. and Loh, S.N. Construction of Allosteric Protein Switches by Alternate Frame Folding and Intermolecular Fragment Exchange. In: Stein, V. ed. *Synthetic Protein Switches: Methods and Protocols*. New York, NY: Springer New York, 2017, pp.27-29.
275. Presti, M.F., Ha, J.-H. and Loh, S.N. An adaptable, monobody-based biosensor scaffold with FRET output. *bioRxiv.* 2022. 505460.
276. Lehmann, M., Loch, C., Middendorf, A., Studer, D., Lassen, S.F., Pasamontes, L., van Loon, A.P.G.M. and Wyss, M. The consensus concept for thermostability engineering of proteins: further proof of concept. *Protein Eng Des Sel.* 2002, **15**(5), 403-411.
277. Martin, H.L., Bedford, R., Heseltine, S.J., Tang, A.A., Haza, K.Z., Rao, A., McPherson, M.J. and Tomlinson, D.C. Non-immunoglobulin scaffold proteins: Precision tools for studying protein-protein interactions in cancer. *New Biotechnol.* 2018, **45**, 28-35.
278. Koutsoumpeli, E., Tiede, C., Murray, J., Tang, A., Bon, R.S., Tomlinson, D.C. and Johnson, S. Antibody Mimetics for the Detection of Small Organic Compounds Using a Quartz Crystal Microbalance. *Anal Chem.* 2017, **89**(5), 3051-3058.
279. Sharma, R., Deacon, S.E., Nowak, D., George, S.E., Szymonik, M.P., Tang, A.A.S., Tomlinson, D.C., Davies, A.G., McPherson, M.J. and Wälti, C. Label-free electrochemical impedance biosensor to detect human interleukin-8 in serum with sub-pg/ml sensitivity. *Biosens Bioelectron.* 2016, **80**, 607-613.
280. Xie, C., Tiede, C., Zhang, X., Wang, C., Li, Z., Xu, X., McPherson, M.J., Tomlinson, D.C. and Xu, W. Development of an Affimer-antibody combined immunological diagnosis kit for glypican-3. *Sci Rep.* 2017, **7**(1), 9608.
281. Chevaliez, S., Poiteau, L., Rosa, I., Soulier, A., Roudot-Thoraval, F., Laperche, S., Hézode, C. and Pawlotsky, J.M. Prospective assessment of rapid diagnostic tests for the detection of antibodies to hepatitis C virus, a tool for improving access to care. *Clin Microbiol Infect.* 2016, **22**(5), 451-459.
282. Hamilton, R.G. and Franklin Adkinson, N., Jr. *In vitro* assays for the diagnosis of IgE-mediated disorders. *J Allergy Clin Immunol.* 2004, **114**(2), 213-225.
283. Zhang, B., Kumar, R.B., Dai, H. and Feldman, B.J. A plasmonic chip for biomarker discovery and diagnosis of type 1 diabetes. *Nat Med.* 2014, **20**(8), 948-953.
284. Luque-Uría, Á., Peltomaa, R., Nevanen, T.K., Arola, H.O., Iljin, K., Benito-Peña, E. and Moreno-Bondi, M.C. Recombinant Peptide Mimetic NanoLuc Tracer for Sensitive Immunodetection of Mycophenolic Acid. *Anal Chem.* 2021, **93**(29), 10358-10364.
285. Jossen, J. and Dubinsky, M. Therapeutic drug monitoring in inflammatory bowel disease. *Curr Opin Pediatr.* 2016, **28**(5), 620-625.
286. Konkle, B.A. Direct Oral Anticoagulants: Monitoring Anticoagulant Effect. *Hematol Oncol Clin North Am.* 2016, **30**(5), 995-1006.
287. Paci, A., Veal, G., Bardin, C., Levêque, D., Widmer, N., Beijnen, J., Astier, A. and Chatelut, E. Review of therapeutic drug monitoring of anticancer drugs part 1 – Cytotoxics. *Eur J Cancer.* 2014, **50**(12), 2010-2019.
288. Du, F.H., Mills, E.A. and Mao-Draayer, Y. Next-generation anti-CD20 monoclonal antibodies in autoimmune disease treatment. *Auto Immun Highlights.* 2017, **8**(1), 12.
289. Hansel, T.T., Kropshofer, H., Singer, T., Mitchell, J.A. and George, A.J. The safety and side effects of monoclonal antibodies. *Nat Rev Drug Discov.* 2010, **9**(4), 325-338.

290. Scott, A.M., Allison, J.P. and Wolchok, J.D. Monoclonal antibodies in cancer therapy. *Cancer Immun.* 2012, **12**, 14.
291. Hunt, J.S., Chen, H.L., Hu, X.L., Chen, T.Y. and Morrison, D.C. Tumor necrosis factor-alpha gene expression in the tissues of normal mice. *Cytokine.* 1992, **4**(5), 340-346.
292. Press, M.F., Cordon-Cardo, C. and Slamon, D.J. Expression of the HER-2/neu proto-oncogene in normal human adult and fetal tissues. *Oncogene.* 1990, **5**(7), 953-962.
293. Oude Munnink, T., Henstra, M., Segerink, L., Movig, K. and Brummelhuis-Visser, P. Therapeutic drug monitoring of monoclonal antibodies in inflammatory and malignant disease: Translating TNF-α experience to oncology. *Clin Pharmacol Ther.* 2016, **99**(4), 419-431.
294. Feng, Y., Roy, A., Masson, E., Chen, T.-T., Humphrey, R. and Weber, J.S. Exposure–Response Relationships of the Efficacy and Safety of Ipilimumab in Patients with Advanced Melanoma. *Clin Cancer Res.* 2013, **19**(14), 3977-3986.
295. Smith, M.R. Rituximab (monoclonal anti-CD20 antibody): mechanisms of action and resistance. *Oncogene.* 2003, **22**(47), 7359-7368.
296. Zhao, S., Chadwick, L., Mysler, E. and Moots, R.J. Review of Biosimilar Trials and Data on Adalimumab in Rheumatoid Arthritis. *Curr Rheumatol Rep.* 2018, **20**(10), 57.
297. Schmitz, E.M., van de Kerkhof, D., Hamann, D., van Dongen, J.L., Kuijper, P.H., Brunsveld, L., Scharnhorst, V. and Broeren, M.A. Therapeutic drug monitoring of infliximab: performance evaluation of three commercial ELISA kits. *Clin Chem Lab Med.* 2016, **54**(7), 1211-1219.
298. Steijns, L.S., Bouw, J. and van der Weide, J. Evaluation of fluorescence polarization assays for measuring valproic acid, phenytoin, carbamazepine and phenobarbital in serum. *Ther Drug Monit.* 2002, **24**(3), 432-435.
299. El Amrani, M., van den Broek, M.P.H., Göbel, C. and van Maarseveen, E.M. Quantification of active infliximab in human serum with liquid chromatography–tandem mass spectrometry using a tumor necrosis factor alpha -based pre-analytical sample purification and a stable isotopic labeled infliximab bio-similar as internal standard: A target-based, sensitive and cost-effective method. *J Chromatogr A.* 2016, **1454**, 42-48.
300. Chatelut, E., Hendrikx, J.J.M.A., Martin, J., Ciccolini, J. and Moes, D.J.A.R. Unraveling the complexity of therapeutic drug monitoring for monoclonal antibody therapies to individualize dose in oncology. *Pharmacol Res Perspect.* 2021, **9**(2), e00757.
301. Guo, Z., Johnston, W.A., Whitfield, J., Walden, P., Cui, Z., Wijker, E., Edwardraja, S., Retamal Lantadilla, I., Ely, F., Vickers, C., Ungerer, J.P.J. and Alexandrov, K. Generalizable Protein Biosensors Based on Synthetic Switch Modules. *J Am Chem Soc.* 2019, **141**(20), 8128-8135.
302. Vallée-Bélisle, A. and Plaxco, K.W. Structure-switching biosensors: inspired by Nature. *Curr Opin Struct Biol.* 2010, **20**(4), 518-526.
303. Adamson, H., Nicholl, A., Tiede, C., Tang, A.A., Davidson, A., Curd, H., Wignall, A., Ford, R., Nuttall, J., McPherson, M.J., Johnson, M. and Tomlinson, D.C. Affimers as anti-idiotypic affinity reagents for pharmacokinetic analysis of biotherapeutics. *BioTechniques.* 2019, **67**(6), 261-269.
304. Shapiro, A.B., Walkup, G.K. and Keating, T.A. Correction for interference by test samples in high-throughput assays. *J Biomol Screen.* 2009, **14**(8), 1008-1016.
305. Shamsuddin, S.H., Jayne, D.G., Tomlinson, D.C., McPherson, M.J. and Millner, P.A. Selection and characterisation of Affimers specific for CEA recognition. *Sci Rep.* 2021, **11**(1), 744.
306. Smith, P.K., Krohn, R.I., Hermanson, G.T., Mallia, A.K., Gartner, F.H., Provenzano, M.D., Fujimoto, E.K., Goeke, N.M., Olson, B.J. and Klenk, D.C. Measurement of protein using bicinchoninic acid. *Anal Biochem.* 1985, **150**(1), 76-85.

307. Administration, F.a.D. and (CDER), C.f.D.E.a.R. *Bioanalytical Method Validation Guidance for Industry.* Maryland: FDA, 2018.
308. Janeway CA Jr, T.P., Walport M and Mark J Shlomchik. Immunobiology. In: *The Immune System in Health and Disease.* . 5th ed. New York: Garland Science, 2001.
309. Townsend, C.L., Laffy, J.M.J., Wu, Y.-C.B., Silva O'Hare, J., Martin, V., Kipling, D., Fraternali, F. and Dunn-Walters, D.K. Significant Differences in Physicochemical Properties of Human Immunoglobulin Kappa and Lambda CDR3 Regions. *Front Immunol.* 2016, **7**, 388.
310. Jani, M., Isaacs, J.D., Morgan, A.W., Wilson, A.G., Plant, D., Hyrich, K.L., Chinoy, H. and Barton, A. Detection of anti-drug antibodies using a bridging ELISA compared with radioimmunoassay in adalimumab-treated rheumatoid arthritis patients with random drug levels. *Rheumatology (Oxford, England).* 2016, **55**(11), 2050-2055.
311. Callaghan, C.H. Irreversible Effects of Serum Proteins on Beta-Lactam Antibiotics. *Antimicrob Agents Chemother.* 1978, **13**(4), 628.
312. Dalhoff, A. and Brunner, H. Mode of interaction between immunoglobulin G and mezlocillin against beta-lactamase producing bacteria. *Arzneimittelforschung.* 1983, **33**(12), 1666-1671.
313. Dimeski, G. Interference testing. *Clin Biochem Rev.* 2008, **29 Suppl 1**(Suppl 1), S43-S48.
314. Zhang, Z., Zhang, X., Fung, K.Y. and Ng, K.M. Product Design: Enzymatic Biosensors for Body Fluid Analysis. *Ind Eng Chem Res.* 2019, **58**(31), 14284-14294.
315. Lipson, E.J. and Drake, C.G. Ipilimumab: An Anti-CTLA-4 Antibody for Metastatic Melanoma. *Clin Cancer Res.* 2011, **17**(22), 6958-6962.
316. Hamilton, R.G. 74 - Laboratory Tests for Allergic and Immunodeficiency Diseases. In: Adkinson, N.F. et al. eds. *Middleton's Allergy* 8ed. London: W.B. Saunders, 2014, pp.1187-1204.
317. Iria, I., Soares, R.R.G., Brás, E.J.S., Chu, V., Gonçalves, J. and Conde, J.P. Accurate and rapid microfluidic ELISA to monitor Infliximab titers in patients with inflammatory bowel diseases. *Analyst.* 2022, **147**(3), 480-488.
318. Koguchi, Y., Iwamoto, N., Shimada, T., Chang, S.-C., Cha, J., Piening, B., Curti, B., Urba, W. and Redmond, W. 760 Trough levels of ipilimumab in serum as a potential predictive biomarker of clinical outcomes for patients with advanced melanoma after treatment with ipilimumab. *J ImmunoTher Cancer.* 2020, **8**(3), A455.
319. Leyland-Jones, B., Colomer, R., Trudeau, M.E., Wardley, A., Latreille, J., Cameron, D., Cubedo, R., Al-Sakaff, N., Feyereislova, A., Catalani, O., Fukushima, Y., Brewster, M. and Cortés, J. Intensive loading dose of trastuzumab achieves higher-than-steady-state serum concentrations and is well tolerated. *J Clin Oncol.* 2010, **28**(6), 960-966.
320. Ciravolo, V., Huber, V., Ghedini, G.C., Venturelli, E., Bianchi, F., Campiglio, M., Morelli, D., Villa, A., Mina, P.D., Menard, S., Filipazzi, P., Rivoltini, L., Tagliabue, E. and Pupa, S.M. Potential role of HER2-overexpressing exosomes in countering trastuzumab-based therapy. *J Cell Physiol.* 2012, **227**(2), 658-667.
321. Damen, C.W., Derissen, E.J., Schellens, J.H., Rosing, H. and Beijnen, J.H. The bioanalysis of the monoclonal antibody trastuzumab by high-performance liquid chromatography with fluorescence detection after immuno-affinity purification from human serum. *J Pharm Biomed Anal.* 2009, **50**(5), 861-866.
322. Wright, J.D., Boudinot, F.D. and Ujhelyi, M.R. Measurement and analysis of unbound drug concentrations. *Clin Pharmacokinet.* 1996, **30**(6), 445-462.
323. Hsieh, P.-H., Kacew, A.J., Dreyer, M., Serritella, A.V., Knoebel, R.W., Strohbehn, G.W. and Ratain, M.J. Alternative trastuzumab dosing strategies in HER2-positive early breast cancer are associated with patient out-of-pocket savings. *npj Breast Cancer.* 2022, **8**(1), 32.

324. Levêque, D., Gigou, L. and Bergerat, J.P. Clinical pharmacology of trastuzumab. *Curr Clin Pharmacol.* 2008, **3**(1), 51-55.
325. Feng, Y., Masson, E., Dai, D., Parker, S.M., Berman, D. and Roy, A. Model-based clinical pharmacology profiling of ipilimumab in patients with advanced melanoma. *Br j clin pharmacol.* 2014, **78**(1), 106-117.
326. Cobleigh, M.A., Vogel, C.L., Tripathy, D., Robert, N.J., Scholl, S., Fehrenbacher, L., Wolter, J.M., Paton, V., Shak, S., Lieberman, G. and Slamon, D.J. Multinational Study of the Efficacy and Safety of Humanized Anti-HER2 Monoclonal Antibody in Women Who Have HER2-Overexpressing Metastatic Breast Cancer That Has Progressed After Chemotherapy for Metastatic Disease. *J Clin Oncol.* 1999, **17**(9), 2639-2639.
327. Pegram, M.D., Lipton, A., Hayes, D.F., Weber, B.L., Baselga, J.M., Tripathy, D., Baly, D., Baughman, S.A., Twaddell, T., Glaspy, J.A. and Slamon, D.J. Phase II study of receptor-enhanced chemosensitivity using recombinant humanized anti-p185HER2/neu monoclonal antibody plus cisplatin in patients with HER2/neu-overexpressing metastatic breast cancer refractory to chemotherapy treatment. *J Clin Oncol.* 1998, **16**(8), 2659-2671.
328. Golynskiy, M.V., Rurup, W.F. and Merkx, M. Antibody detection by using a FRET-based protein conformational switch. *Chembiochem.* 2010, **11**(16), 2264-2267.
329. Porchetta, A., Ippodrino, R., Marini, B., Caruso, A., Caccuri, F. and Ricci, F. Programmable Nucleic Acid Nanoswitches for the Rapid, Single-Step Detection of Antibodies in Bodily Fluids. *J Am Chem Soc.* 2018, **140**(3), 947-953.
330. Olaleye, O., Graf, C., Spanov, B., Govorukhina, N., Groves, M.R., van de Merbel, N.C. and Bischoff, R. Determination of Binding Sites on Trastuzumab and Pertuzumab to Selective Affimers Using Hydrogen–Deuterium Exchange Mass Spectrometry. *J Am Chem Soc Mass Spec.* 2023, **34**(4), 775-783.
331. Welch, N.G., Scoble, J.A., Muir, B.W. and Pigram, P.J. Orientation and characterization of immobilized antibodies for improved immunoassays (Review). *Biointerphases.* 2017, **12**(2), 02D301.
332. Wolbink, G.J., Voskuyl, A.E., Lems, W.F., de Groot, E., Nurmohamed, M.T., Tak, P.P., Dijkmans, B.A.C. and Aarden, L. Relationship between serum trough infliximab levels, pretreatment C reactive protein levels, and clinical response to infliximab treatment in patients with rheumatoid arthritis. *Ann Rheum Dis.* 2005, **64**(5), 704-707.
333. El Amrani, M., Bosman, S.M., Egas, A.C., Hack, C.E., Huitema, A.D.R. and van Maarseveen, E.M. Simultaneous Quantification of Free Adalimumab and Infliximab in Human Plasma Using a Target-Based Sample Purification and Liquid Chromatography-Tandem Mass Spectrometry. *Ther Drug Monit.* 2019, **41**(5), 640-647.
334. Yokozeki, T., Ueda, H., Arai, R., Mahoney, W. and Nagamune, T. A Homogeneous Noncompetitive Immunoassay for the Detection of Small Haptens. *Anal Chem.* 2002, **74**(11), 2500-2504.
335. Golay, J., Semenzato, G., Rambaldi, A., Foà, R., Gaidano, G., Gamba, E., Pane, F., Pinto, A., Specchia, G., Zaja, F. and Regazzi, M. Lessons for the clinic from rituximab pharmacokinetics and pharmacodynamics. *MAbs.* 2013, **5**(6), 826-837.
336. Igarashi, T., Kobayashi, Y., Ogura, M., Kinoshita, T., Ohtsu, T., Sasaki, Y., Morishima, Y., Murate, T., Kasai, M., Uike, N., Taniwaki, M., Kano, Y., Ohnishi, K., Matsuno, Y., Nakamura, S., Mori, S., Ohashi, Y. and Tobinai, K. Factors affecting toxicity, response and progression-free survival in relapsed patients with indolent B-cell lymphoma and mantle cell lymphoma treated with rituximab: a Japanese phase II study. *Ann Oncol.* 2002, **13**(6), 928-943.
337. Tobinai, K., Igarashi, T., Itoh, K., Kobayashi, Y., Taniwaki, M., Ogura, M., Kinoshita, T., Hotta, T., Aikawa, K., Tsushita, K., Hiraoka, A., Matsuno, Y., Nakamura, S., Mori, S. and Ohashi, Y. Japanese multicenter phase II and

pharmacokinetic study of rituximab in relapsed or refractory patients with aggressive B-cell lymphoma. *Ann Oncol.* 2004, **15**(5), 821-830.

338. Gibson, D.J., Ward, M.G., Rentsch, C., Friedman, A.B., Taylor, K.M., Sparrow, M.P. and Gibson, P.R. Review article: determination of the therapeutic range for therapeutic drug monitoring of adalimumab and infliximab in patients with inflammatory bowel disease. *Aliment Pharmacol Ther.* 2020, **51**(6), 612-628.
339. England, C.G., Ehlerding, E.B. and Cai, W. NanoLuc: A Small Luciferase Is Brightening Up the Field of Bioluminescence. *Bioconjug Chem.* 2016, **27**(5), 1175-1187.
340. Hall, M.P., Unch, J., Binkowski, B.F., Valley, M.P., Butler, B.L., Wood, M.G., Otto, P., Zimmerman, K., Vidugiris, G., Machleidt, T., Robers, M.B., Benink, H.A., Eggers, C.T., Slater, M.R., Meisenheimer, P.L., Klaubert, D.H., Fan, F., Encell, L.P. and Wood, K.V. Engineered Luciferase Reporter from a Deep Sea Shrimp Utilizing a Novel Imidazopyrazinone Substrate. *ACS Chem Biol.* 2012, **7**(11), 1848-1857.
341. Luker, K.E., Smith, M.C., Luker, G.D., Gammon, S.T., Piwnica-Worms, H. and Piwnica-Worms, D. Kinetics of regulated protein-protein interactions revealed with firefly luciferase complementation imaging in cells and living animals. *Proc Natl Acad Sci U S A.* 2004, **101**(33), 12288-12293.
342. Jäger, U., Fridrik, M., Zeitlinger, M., Heintel, D., Hopfinger, G., Burgstaller, S., Mannhalter, C., Oberaigner, W., Porpaczy, E., Skrabs, C., Einberger, C., Drach, J., Raderer, M., Gaiger, A., Putman, M. and Greil, R. Rituximab serum concentrations during immuno-chemotherapy of follicular lymphoma correlate with patient gender, bone marrow infiltration and clinical response. *Haematologica.* 2012, **97**(9), 1431-1438.
343. Liu, S., Huang, H., Chen, R.-x., Wang, Z., Guan, Y.-p., Peng, C., Fang, X.-j., Chen, Z.-j., Guan, S.-x., Zhu, X., Ren, Q.-g., Yao, Y.-y., Huang, H.-b., Huang, M., Wang, X.-d. and Lin, T.-y. Low initial trough concentration of rituximab is associated with unsatisfactory response of first-line R-CHOP treatment in patients with follicular lymphoma with grade 1/2. *Acta Pharmacol Sin.* 2021, **42**(4), 641-647.
344. Ramanakumar, A.V., Thomann, P., Candeias, J.M., Ferreira, S., Villa, L.L. and Franco, E.L. Use of the normalized absorbance ratio as an internal standardization approach to minimize measurement error in enzyme-linked immunosorbent assays for diagnosis of human papillomavirus infection. *J Clin Microbiol.* 2010, **48**(3), 791-796.
345. Ramachandran, S., Singhal, M., McKenzie, K.G., Osborn, J.L., Arjyal, A., Dongol, S., Baker, S.G., Basnyat, B., Farrar, J., Dolecek, C., Domingo, G.J., Yager, P. and Lutz, B. A Rapid, Multiplexed, High-Throughput Flow-Through Membrane Immunoassay: A Convenient Alternative to ELISA. *Diagnostics.* 2013, **3**(2), 244-260.
346. van Rosmalen, M., Ni, Y., Vervoort, D.F.M., Arts, R., Ludwig, S.K.J. and Merkx, M. Dual-Color Bioluminescent Sensor Proteins for Therapeutic Drug Monitoring of Antitumor Antibodies. *Anal Chem.* 2018, **90**(5), 3592-3599.
347. Yang, C., Sesterhenn, F., Bonet, J., van Aalen, E.A., Scheller, L., Abriata, L.A., Cramer, J.T., Wen, X., Rosset, S., Georgeon, S., Jardetzky, T., Krey, T., Fussenegger, M., Merkx, M. and Correia, B.E. Bottom-up de novo design of functional proteins with complex structural features. *Nat Chem Biol.* 2021, **17**(4), 492-500.
348. Tenda, K., van Gerven, B., Arts, R., Hiruta, Y., Merkx, M. and Citterio, D. Paper-Based Antibody Detection Devices Using Bioluminescent BRET-Switching Sensor Proteins. *Angew Chem Int Ed Engl.* 2018, **57**(47), 15369-15373.
349. Liu, S., Wang, Z., Chen, R., Wang, X., Fang, X., Chen, Z., Guan, S., Liu, T., Lin, T., Huang, M. and Huang, H. Rituximab Concentration Varies in Patients With Different Lymphoma Subtypes and Correlates With Clinical Outcome. *Front Pharmacol.* 2022, **13**, 788824.

350. Yao, Z., Drecun, L., Aboualizadeh, F., Kim, S.J., Li, Z., Wood, H., Valcourt, E.J., Manguiat, K., Plenderleith, S., Yip, L., Li, X., Zhong, Z., Yue, F.Y., Closas, T., Snider, J., Tomic, J., Drews, S.J., Drebot, M.A., McGeer, A., Ostrowski, M., Mubareka, S., Rini, J.M., Owen, S. and Stagljar, I. A homogeneous split-luciferase assay for rapid and sensitive detection of anti-SARS CoV-2 antibodies. *Nat Commun.* 2021, **12**(1), 1806.
351. Elledge, S.K., Zhou, X.X., Byrnes, J.R., Martinko, A.J., Lui, I., Pance, K., Lim, S.A., Glasgow, J.E., Glasgow, A.A., Turcios, K., Iyer, N.S., Torres, L., Peluso, M.J., Henrich, T.J., Wang, T.T., Tato, C.M., Leung, K.K., Greenhouse, B. and Wells, J.A. Engineering luminescent biosensors for point-of-care SARS-CoV-2 antibody detection. *Nat Biotechnol.* 2021, **39**(8), 928-935.
352. Mazor, Y., Almog, R., Kopylov, U., Ben Hur, D., Blatt, A., Dahan, A., Waterman, M., Ben-Horin, S. and Chowers, Y. Adalimumab drug and antibody levels as predictors of clinical and laboratory response in patients with Crohn's disease. *Aliment Pharmacol Ther.* 2014, **40**(6), 620-628.
353. Roblin, X., Marotte, H., Rinaudo, M., Del Tedesco, E., Moreau, A., Phelip, J.M., Genin, C., Peyrin-Biroulet, L. and Paul, S. Association between pharmacokinetics of adalimumab and mucosal healing in patients with inflammatory bowel diseases. *Clin Gastroenterol Hepatol.* 2014, **12**(1), 80-84.
354. van Brummelen, E.M., Ros, W., Wolbink, G., Beijnen, J.H. and Schellens, J.H. Antidrug Antibody Formation in Oncology: Clinical Relevance and Challenges. *Oncologist.* 2016, **21**(10), 1260-1268.
355. Menting, S.P., van Lümig, P.P., de Vries, A.C., van den Reek, J.M., van der Kleij, D., de Jong, E.M., Spuls, P.I. and Lecluse, L.L. Extent and consequences of antibody formation against adalimumab in patients with psoriasis: one-year follow-up. *JAMA Dermatol.* 2014, **150**(2), 130-136.
356. Burkovitz, A. and Ofran, Y. Understanding differences between synthetic and natural antibodies can help improve antibody engineering. *MAbs.* 2016, **8**(2), 278-287.
357. Wouters, S.F.A., Vugs, W.J.P., Arts, R., de Leeuw, N.M., Teeuwen, R.W.H. and Merkx, M. Bioluminescent Antibodies through Photoconjugation of Protein G–Luciferase Fusion Proteins. *Bioconjug Chem.* 2020, **31**(3), 656-662.
358. Lu, L., Duong, V.T., Shalash, A.O., Skwarczynski, M. and Toth, I. Chemical Conjugation Strategies for the Development of Protein-Based Subunit Nanovaccines. *Vaccines (Basel).* 2021, **9**(6), 563.
359. Tsuchikama, K. and An, Z. Antibody-drug conjugates: recent advances in conjugation and linker chemistries. *Protein Cell.* 2018, **9**(1), 33-46.
360. Baghban, R., Gargari, S.L.M., Rajabibazl, M., Nazarian, S. and Bakherad, H. Camelid-derived heavy-chain nanobody against Clostridium botulinum neurotoxin E in Pichia pastoris. *Biotechnol. Appl. Biochem.* 2016, **63**(2), 200-205.
361. De Genst, E., Silence, K., Decanniere, K., Conrath, K., Loris, R., Kinne, J., Muyldermans, S. and Wyns, L. Molecular basis for the preferential cleft recognition by dromedary heavy-chain antibodies. *Proc Natl Acad Sci U S A.* 2006, **103**(12), 4586-4591.
362. Zavrtanik, U., Lukan, J., Loris, R., Lah, J. and Hadži, S. Structural Basis of Epitope Recognition by Heavy-Chain Camelid Antibodies. *J Mol Biol.* 2018, **430**(21), 4369-4386.
363. He, Q., McCoy, M.R., Yang, H., Lin, M., Cui, X., Zhao, S., Morisseau, C., Li, D. and Hammock, B.D. Mix-and-Read Nanobody-Based Sandwich Homogeneous Split-Luciferase Assay for the Rapid Detection of Human Soluble Epoxide Hydrolase. *Anal Chem.* 2023, **95**(14), 6038-6045.
364. Xie, X., He, Z., Qu, C., Sun, Z., Cao, H. and Liu, X. Nanobody/NanoBiT system-mediated bioluminescence immunosensor for one-step homogeneous detection of trace ochratoxin A in food. *J Hazard Mater.* 2022, **437**, 129435.
365. Holliger, P. and Hudson, P.J. Engineered antibody fragments and the rise of single domains. *Nat Biotechnol.* 2005, **23**(9), 1126-1136.

366. Wesolowski, J., Alzogaray, V., Reyelt, J., Unger, M., Juarez, K., Urrutia, M., Cauerhff, A., Danquah, W., Rissiek, B., Scheuplein, F., Schwarz, N., Adriouch, S., Boyer, O., Seman, M., Licea, A., Serreze, D.V., Goldbaum, F.A., Haag, F. and Koch-Nolte, F. Single domain antibodies: promising experimental and therapeutic tools in infection and immunity. *Med Microbiol Immunol.* 2009, **198**(3), 157-174.
367. Rosano, G.L. and Ceccarelli, E.A. Recombinant protein expression in Escherichia coli: advances and challenges. *Front Microbiol.* 2014, **5**, 172.
368. Bentley, W.E., Mirjalili, N., Andersen, D.C., Davis, R.H. and Kompala, D.S. Plasmid-encoded protein: The principal factor in the “metabolic burden” associated with recombinant bacteria. *Biotechnol Bioeng.* 1990, **35**(7), 668-681.
369. Dumon-Seignovert, L., Cariot, G. and Vuillard, L. The toxicity of recombinant proteins in Escherichia coli: a comparison of overexpression in BL21(DE3), C41(DE3), and C43(DE3). *Protein Expr Purif.* 2004, **37**(1), 203-206.
370. Denoncin, K. and Collet, J.F. Disulfide bond formation in the bacterial periplasm: major achievements and challenges ahead. *Antioxid Redox Signal.* 2013, **19**(1), 63-71.
371. Bardwell, J.C., Lee, J.O., Jander, G., Martin, N., Belin, D. and Beckwith, J. A pathway for disulfide bond formation in vivo. *Proc Natl Acad Sci U S A.* 1993, **90**(3), 1038-1042.
372. Rietsch, A., Bessette, P., Georgiou, G. and Beckwith, J. Reduction of the periplasmic disulfide bond isomerase, DsbC, occurs by passage of electrons from cytoplasmic thioredoxin. *J Bacteriol.* 1997, **179**(21), 6602-6608.
373. Schlegel, S., Rujas, E., Ytterberg, A.J., Zubarev, R.A., Luirink, J. and de Gier, J.-W. Optimizing heterologous protein production in the periplasm of E. coli by regulating gene expression levels. *Microb Cell Fact.* 2013, **12**(1), 24.
374. Gąciarz, A., Khatri, N.K., Velez-Suberbie, M.L., Saaranen, M.J., Uchida, Y., Keshavarz-Moore, E. and Ruddock, L.W. Efficient soluble expression of disulfide bonded proteins in the cytoplasm of Escherichia coli in fed-batch fermentations on chemically defined minimal media. *Microb Cell Fact.* 2017, **16**(1), 108.
375. Graham, L.L., Beveridge, T.J. and Nanninga, N. Periplasmic space and the concept of the periplasm. *Trends Biochem Sci.* 1991, **16**, 328-329.
376. Berkmen, M. Production of disulfide-bonded proteins in Escherichia coli. *Protein Expr Purif.* 2012, **82**(1), 240-251.
377. Mamathambika, B.S. and Bardwell, J.C. Disulfide-Linked Protein Folding Pathways. *Annu Rev Cell Dev Biol.* 2008, **24**(1), 211-235.
378. Ahmad, M., Hirz, M., Pichler, H. and Schwab, H. Protein expression in Pichia pastoris: recent achievements and perspectives for heterologous protein production. *Appl Microbiol Biotechnol.* 2014, **98**(12), 5301-5317.
379. Yang, S., Kuang, Y., Li, H., Liu, Y., Hui, X., Li, P., Jiang, Z., Zhou, Y., Wang, Y., Xu, A., Li, S., Liu, P. and Wu, D. Enhanced production of recombinant secretory proteins in Pichia pastoris by optimizing Kex2 P1' site. *PLOS ONE.* 2013, **8**(9), e75347.
380. Karbalaei, M., Rezaee, S.A. and Farsiani, H. Pichia pastoris: A highly successful expression system for optimal synthesis of heterologous proteins. *J Cell Physiol.* 2020, **235**(9), 5867-5881.
381. Santoso, A., Herawati, N. and Rubiana, Y. Effect of methanol induction and incubation time on expression of human erythropoietin in methylotropic yeast Pichia pastoris. *Makara J Technol.* 2012, **16**(1), 29-34.
382. Wang, Z., Wang, Y., Zhang, D., Li, J., Hua, Z., Du, G. and Chen, J. Enhancement of cell viability and alkaline polygalacturonate lyase production by sorbitol co-feeding with methanol in Pichia pastoris fermentation. *Biores technol.* 2010, **101**(4), 1318-1323.
383. Priest, F.G. and Campbell, I. *Brewing microbiology.* Springer, 1996.
384. Coutant, E.P., Goyard, S., Hervin, V., Gagnot, G., Baatallah, R., Jacob, Y., Rose, T. and Janin, Y.L. Gram-scale synthesis of luciferins derived from

coelenterazine and original insights into their bioluminescence properties. *Org Biomolr Chem.* 2019, **17**(15), 3709-3713.

385. Coutant, E.P. and Janin, Y.L. Synthetic Routes to Coelenterazine and Other Imidazo[1,2-a]pyrazin-3-one Luciferins: Essential Tools for Bioluminescence-Based Investigations. *Chemistry.* 2015, **21**(48), 17158-17171.
386. Esparza, T.J., Martin, N.P., Anderson, G.P., Goldman, E.R. and Brody, D.L. High affinity nanobodies block SARS-CoV-2 spike receptor binding domain interaction with human angiotensin converting enzyme. *Sci Rep.* 2020, **10**(1), 22370.
387. Srinivasan, L., Alzogaray, V., Selvakumar, D., Nathan, S., Yoder, J.B., Wright, K.M., Klinke, S., Nwafor, J.N., Labanda, M.S., Goldbaum, F.A., Schön, A., Freire, E., Tomaselli, G.F., Amzel, L.M., Ben-Johny, M. and Gabelli, S.B. Development of high-affinity nanobodies specific for NaV1.4 and NaV1.5 voltage-gated sodium channel isoforms. *J Biol Chem.* 2022, **298**(4), 101763.
388. Yao, H., Cai, H., Li, T., Zhou, B., Qin, W., Lavillette, D. and Li, D. A high-affinity RBD-targeting nanobody improves fusion partner's potency against SARS-CoV-2. *PLoS Pathog.* 2021, **17**(3), e1009328.
389. Dooley, H., Flajnik, M.F. and Porter, A.J. Selection and characterization of naturally occurring single-domain (IgNAR) antibody fragments from immunized sharks by phage display. *Mol Immunol.* 2003, **40**(1), 25-33.
390. Banciu, R.M., Numan, N. and Vasilescu, A. Optical biosensing of lysozyme. *J Mol Struct.* 2022, **1250**, 131639.
391. Blake, C.C.F., Koenig, D.F., Mair, G.A., North, A.C.T., Phillips, D.C. and Sarma, V.R. Structure of Hen Egg-White Lysozyme: A Three-dimensional Fourier Synthesis at 2 Å Resolution. *Nature.* 1965, **206**(4986), 757-761.
392. Saerens, D., Pellis, M., Loris, R., Pardon, E., Dumoulin, M., Matagne, A., Wyns, L., Muyldermans, S. and Conrath, K. Identification of a universal VHH framework to graft non-canonical antigen-binding loops of camel single-domain antibodies. *J Mol Biol.* 2005, **352**(3), 597-607.
393. Stanfield, R.L., Dooley, H., Flajnik, M.F. and Wilson, I.A. Crystal Structure of a Shark Single-Domain Antibody V Region in Complex with Lysozyme. *Science.* 2004, **305**(5691), 1770-1773.
394. Dietz, H. and Rief, M. Protein structure by mechanical triangulation. *Proc Natl Acad Sci U S A.* 2006, **103**(5), 1244-1247.
395. Yang, G., Cecconi, C., Baase, W.A., Vetter, I.R., Breyer, W.A., Haack, J.A., Matthews, B.W., Dahlquist, F.W. and Bustamante, C. Solid-state synthesis and mechanical unfolding of polymers of T4 lysozyme. *Proc Natl Acad Sci U S A.* 2000, **97**(1), 139-144.
396. Chen, P., Lam, K.H., Liu, Z., Mindlin, F.A., Chen, B., Gutierrez, C.B., Huang, L., Zhang, Y., Hamza, T., Feng, H., Matsui, T., Bowen, M.E., Perry, K. and Jin, R. Structure of the full-length Clostridium difficile toxin B. *Nat Struct Mol Biol.* 2019, **26**(8), 712-719.
397. Schlapschy, M., Grimm, S. and Skerra, A. A system for concomitant overexpression off our periplasmic folding catalysts to improve secretory protein production in Escherichia coli. *Protein Eng Des Sel.* 2006, **19**, 385-390.
398. Yan, J., Wang, P., Zhu, M., Guanghui, L., Romão, E., Xiong, S. and Wan, Y. Characterization and applications of Nanobodies against human procalcitonin selected from a novel naïve Nanobody phage display library. *J nanobiotechnology.* 2015, **13**, 33.
399. Kaczmarek, M.B., Struszczyk-Swita, K., Xiao, M., Szczęsna-Antczak, M., Antczak, T., Gierszewska, M., Steinbüchel, A. and Daroch, M. Polycistronic Expression System for Pichia pastoris Composed of Chitino- and Chitosanolytic Enzymes. *Front Bioeng Biotechnol.* 2021, **9**, 710922.
400. Jana, S. and Deb, J.K. Strategies for efficient production of heterologous proteins in Escherichia coli. *Appl Microbiol Biotechnol.* 2005, **67**(3), 289-298.

401. Khow, O. and Suntrarachun, S. Strategies for production of active eukaryotic proteins in bacterial expression system. *Asian Pac J Trop Biomed.* 2012, **2**(2), 159-162.
402. Kunz, P., Zinner, K., Mücke, N., Bartoschik, T., Muyldermans, S. and Hoheisel, J.D. The structural basis of nanobody unfolding reversibility and thermoresistance. *Sci. Rep.* 2018, **8**(1), 7934.
403. Jin, B.K., Odongo, S., Radwanska, M. and Magez, S. Nanobodies: A Review of Generation, Diagnostics and Therapeutics. *Int J Mol Sci.* 2023, **24**(6), 5994.
404. Gelkop, S., Sobarzo, A., Brangel, P., Vincke, C., Romão, E., Fedida-Metula, S., Strom, N., Ataliba, I., Mwiine, F.N., Ochwo, S., Velazquez-Salinas, L., McKendry, R.A., Muyldermans, S., Lutwama, J.J., Rieder, E., Yavelsky, V. and Lobel, L. The Development and Validation of a Novel Nanobody-Based Competitive ELISA for the Detection of Foot and Mouth Disease 3ABC Antibodies in Cattle. *Front Vet Sci.* 2018, **5**, 250.
405. Gu, K., Song, Z., Zhou, C., Ma, P., Li, C., Lu, Q., Liao, Z., Huang, Z., Tang, Y., Li, H., Zhao, Y., Yan, W., Lei, C. and Wang, H. Development of nanobody-horseradish peroxidase-based sandwich ELISA to detect Salmonella Enteritidis in milk and in vivo colonization in chicken. *J nanobiotechnology.* 2022, **20**(1), 167.
406. Katz, H.E. Antigen sensing via nanobody-coated transistors. *Nat Biomed Eng.* 2021, **5**(7), 639-640.
407. Liu, X., Tang, Z., Duan, Z., He, Z., Shu, M., Wang, X., Gee, S.J., Hammock, B.D. and Xu, Y. Nanobody-based enzyme immunoassay for ochratoxin A in cereal with high resistance to matrix interference. *Talanta.* 2017, **164**, 154-158.
408. Zhang, W.T., Liu, T.T., Wu, M., Chen, X.C., Han, L., Shi, Z.Z., Li, Y.Y., Li, X.Y., Xu, H.X., Gong, L.K., Xu, P.H. and Geng, Y. Development of a nanobody-based immunoassay for the sensitive detection of fibrinogen-like protein 1. *Acta Pharmacol Sin.* 2021, **42**(11), 1921-1929.
409. Keller, L., Bery, N., Tardy, C., Ligat, L., Favre, G., Rabbitts, T.H. and Olichon, A. Selection and Characterization of a Nanobody Biosensor of GTP-Bound RHO Activities. *Antibodies (Basel).* 2019, **8**(1), 8.
410. Chen, Q., Zhou, Y., Yu, J., Liu, W., Li, F., Xian, M., Nian, R., Song, H. and Feng, D. An efficient constitutive expression system for Anti-CEACAM5 nanobody production in the yeast Pichia pastoris. *Protein Expr Purif.* 2019, **155**, 43-47.
411. Lyu, M., Shi, X., Liu, X., Liu, Y., Zhu, X., Liao, L., Zhao, H., Sun, N., Wang, S., Chen, L., Fan, L., Xu, Q., Zhu, Q., Gao, K., Chen, H., Zhu, Y., Li, Z., Guo, W., Zheng, Y., Gu, Y., Liu, L., Wang, M. and Liu, Y. Generation and Screening of Antigen-Specific Nanobodies from Mammalian Cells Expressing the BCR Repertoire Library Using Droplet-Based Microfluidics. *Anal Chem.* 2022, **94**(22), 7970-7980.
412. Batey, S., Nickson, A.A. and Clarke, J. Studying the folding of multidomain proteins. *Hfsp j.* 2008, **2**(6), 365-377.
413. Han, J.H., Batey, S., Nickson, A.A., Teichmann, S.A. and Clarke, J. The folding and evolution of multidomain proteins. *Nat Rev Mol Cell Biol.* 2007, **8**(4), 319-330.
414. Tian, P. and Best, R.B. Structural Determinants of Misfolding in Multidomain Proteins. *PLOS Comput Biol.* 2016, **12**(5), e1004933.
415. Francis, D.M. and Page, R. Strategies to optimize protein expression in E. coli. *Curr Protoc Protein Sci.* 2010, **5**(1), 1-29.
416. Barakat, S., Berksöz, M., Zahedimaram, P., Piepoli, S. and Erman, B. Nanobodies as molecular imaging probes. *Free Radic Biol Med.* 2022, **182**, 260-275.
417. Oberg, K., Chrunyk, B.A., Wetzel, R. and Fink, A.L. Nativelike secondary structure in interleukin-1 beta inclusion bodies by attenuated total reflectance FTIR. *Biochemistry.* 1994, **33**(9), 2628-2634.

418. Ritz, D. and Beckwith, J. Roles of thiol-redox pathways in bacteria. *Annu Rev Microbiol.* 2001, **55**, 21-48.
419. Vincentelli, R., Bignon, C., Gruez, A., Canaan, S., Sulzenbacher, G., Tegoni, M., Campanacci, V. and Cambillau, C. Medium-scale structural genomics: strategies for protein expression and crystallization. *Acc Chem Res.* 2003, **36**(3), 165-172.
420. Coghlan, J., Benet, A., Kumaran, P., Ford, M., Veale, L., Skilton, S.J., Saveliev, S. and Schwendeman, A.A. Streamlining the Characterization of Disulfide Bond Shuffling and Protein Degradation in IgG1 Biopharmaceuticals Under Native and Stressed Conditions. *Front Bioeng Biotechnol.* 2022, **10**, 862456.
421. Liu, Z., Tyo, K.E., Martínez, J.L., Petranovic, D. and Nielsen, J. Different expression systems for production of recombinant proteins in Saccharomyces cerevisiae. *Biotechnol Bioeng.* 2012, **109**(5), 1259-1268.
422. Robinson, A.S., Hines, V. and Wittrup, K.D. Protein disulfide isomerase overexpression increases secretion of foreign proteins in Saccharomyces cerevisiae. *Biotechnology (N Y).* 1994, **12**(4), 381-384.
423. Valdés-Tresanco, M.S., Molina-Zapata, A., Pose, A.G. and Moreno, E. Structural Insights into the Design of Synthetic Nanobody Libraries. *Molecules.* 2022, **27**(7), 2198.
424. Malik, A. Protein fusion tags for efficient expression and purification of recombinant proteins in the periplasmic space of E. coli. *3 Biotech.* 2016, **6**(1), 44.
425. Costa, S., Almeida, A., Castro, A. and Domingues, L. Fusion tags for protein solubility, purification and immunogenicity in Escherichia coli: the novel Fh8 system. *Front Microbiol.* 2014, **5**, 63.
426. Kane, J.F. and Hartley, D.L. Formation of recombinant protein inclusion bodies in Escherichia coli. *Trends in Biotechnology.* 1988, **6**(5), 95-101.
427. Singh, S.M. and Panda, A.K. Solubilization and refolding of bacterial inclusion body proteins. *J Biosci Bioeng.* 2005, **99**(4), 303-310.
428. Carling, P.J., Mortiboys, H., Green, C., Mihaylov, S., Sandor, C., Schwartzentruber, A., Taylor, R., Wei, W., Hastings, C., Wong, S., Lo, C., Evetts, S., Clemmens, H., Wyles, M., Willcox, S., Payne, T., Hughes, R., Ferraiuolo, L., Webber, C., Hide, W., Wade-Martins, R., Talbot, K., Hu, M.T. and Bandmann, O. Deep phenotyping of peripheral tissue facilitates mechanistic disease stratification in sporadic Parkinson's disease. *Prog Neurobiol.* 2020, **187**, 101772.
429. Koo, M.J., Rooney, K.T., Choi, M.E., Ryter, S.W., Choi, A.M. and Moon, J.S. Impaired oxidative phosphorylation regulates necroptosis in human lung epithelial cells. *Biochem Biophys Res Commun.* 2015, **464**(3), 875-880.
430. Kurucz, I., Titus, J.A., Jost, C.R. and Segal, D.M. Correct disulfide pairing and efficient refolding of detergent-solubilized single-chain Fv proteins from bacterial inclusion bodies. *Mol Immunol.* 1995, **32**(17-18), 1443-1452.
431. Gregoriano, C., Heilmann, E., Molitor, A. and Schuetz, P. Role of procalcitonin use in the management of sepsis. *J Thorac Dis.* 2020, **12**(Suppl 1), S5-s15.
432. Luxton, T.N., King, N., Wälti, C., Jeuken, L.J.C. and Sandoe, J.A.T. A Systematic Review of the Effect of Therapeutic Drug Monitoring on Patient Health Outcomes during Treatment with Carbapenems. *Antibiotics.* 2022, **11**(10), 1311.
433. Kaprou, G.D., Bergšpica, I., Alexa, E.A., Alvarez-Ordóñez, A. and Prieto, M. Rapid Methods for Antimicrobial Resistance Diagnostics. *Antibiotics* 2021, **10**(2), 209.
434. Lei, J., Shi, L., Liu, W., Li, B. and Jin, Y. Portable and sensitive detection of cancer cells via a handheld luminometer. *Analyst.* 2022, **147**(14), 3219-3224.
435. Lebel, P., Elledge, S., Wiener, D.M., Jeyakumar, I., Phelps, M., Jacobsen, A., Huynh, E., Charlton, C., Puccinelli, R., Mondal, P., Saha, S., Tato, C.M. and Gómez-Sjöberg, R. A handheld luminometer with sub-attomole limit of detection for distributed applications in global health. *medRxiv.* 2023. 23290120.

436. Gaspar, N., Zambito, G., Dautzenberg, I.J.C., Cramer, S.J., Hoeben, R.C., Lowik, C., Walker, J.R., Kirkland, T.A., Smith, T.P., van Weerden, W.M., de Vrij, J. and Mezzanotte, L. NanoBiT System and Hydrofurimazine for Optimized Detection of Viral Infection in Mice-A Novel in Vivo Imaging Platform. *Int J Mol Sci.* 2020, **21**(16), 5863.
437. Su, Y., Walker, J.R., Park, Y., Smith, T.P., Liu, L.X., Hall, M.P., Labanieh, L., Hurst, R., Wang, D.C., Encell, L.P., Kim, N., Zhang, F., Kay, M.A., Casey, K.M., Majzner, R.G., Cochran, J.R., Mackall, C.L., Kirkland, T.A. and Lin, M.Z. Novel NanoLuc substrates enable bright two-population bioluminescence imaging in animals. *Nat Methods.* 2020, **17**(8), 852-860.
438. Dalbey, R.E. and Kuhn, A. Protein Traffic in Gram-negative bacteria – how exported and secreted proteins find their way. *FEMS Microbiol Rev.* 2012, **36**(6), 1023-1045.
439. Cui, N., Zhang, H., Chen, Z. and Yu, Z. Prognostic significance of PCT and CRP evaluation for adult ICU patients with sepsis and septic shock: retrospective analysis of 59 cases. *J Int Med Res.* 2019, **47**(4), 1573-1579.
440. Simon, L., Gauvin, F., Amre, D.K., Saint-Louis, P. and Lacroix, J. Serum Procalcitonin and C-Reactive Protein Levels as Markers of Bacterial Infection: A Systematic Review and Meta-analysis. *Clin Infect Dis.* 2004, **39**(2), 206-217.
441. Anderson, G., Teichler, D., Zabetakis, D., Shriver-Lake, L., Liu, J., Lonsdale, S., Goodchild, S. and Goldman, E. Importance of Hypervariable Region 2 for Stability and Affinity of a Shark Single-Domain Antibody Specific for Ebola Virus Nucleoprotein. *PLOS ONE.* 2016, **11**, e0160534.
442. Sherwood, L.J. and Hayhurst, A. Ebolavirus nucleoprotein C-termini potently attract single domain antibodies enabling monoclonal affinity reagent sandwich assay (MARSA) formulation. *PLOS ONE.* 2013, **8**(4), e61232.
443. Bettini, A., Lapa, D. and Garbuglia, A.R. Diagnostics of Ebola virus. *Front Public Health.* 2023, **11**, 1123024.
444. Krishnasamy, L. and Saikumar, C. Updates on Treatment of Ebola Virus Disease. *Malays J Med Sci.* 2015, **22**(6), 54-57.

Appendix A: Primer tables

Table A 1. Primers used to introduce Linker 1 (L1) to Affimer DNA.

Primer	Sequence
Aff-SpeI	AACGACTAGTAACTCCCTGGAAATCGAAGAACTG
Aff-SalI	TAATGTCGACTACTGGTTTGAACTCCTGCAGTTCTTTG
Aff-SpeI-ASS	AACGACTAGTGCAGCTTCAAGTAACTCCCTGGAAATCGAAGAACTG

Table A 2. Primers used to introduce Linker 3 (L3) to Affimer DNA.

Primer	Sequence
Aff-NheI	ATGGCTAGCAACTCCCTGGAAATCGAAG
Aff-NotI	TAATGCGGCCGCTACTGGTTTGAACTCCTGCAGTTCTTTG
Aff-NotI-ASS	ATTAGCGGCCGCACTTGAAGCTACTGGTTTGAACTCCTGCAGTTCTTTG

Table A 3. Primers used to introduce longer Linker 2 (L2) to Affimer DNA.

Primer	Sequence
Aff-SpeI	AACGACTAGTAACTCCCTGGAAATCGAAGAACTG
Aff-SalI-$(GSG)_4$	TAATGTCGACGCCAGACCCGCCAGAACCACCTGACCCA CCGGAGCCTACTGGTTTGAACTCCTGCAGTTCTTTG
Aff-NheI-$(GSG)_4$	ATGAGCTAGCGGCTCCGGGGGTCAGGTGGTTCTGGCGG GTCTGGCAACTCCCTGGAAATCGAAGAACTG
Aff-NotI	TAATGCGGCCGCTACTGGTTTGAACTCCTGCAGTTCTTTG

Table A 4. Primers used to introduce Cystein residues to Affimer DNA.

Primer	Sequence
Aff-NheI	ATGGCTAGCAACTCCCTGGAAATCGAAG
Aff-NotI	TAATGCGGCCGCTACTGGTTTGAACTCCTGCAGTTCTTTG

Table A 5. Primers used for Affimer amplification in NanoBiT subcloning.

Primer	Sequence
NheI-Aff-f	ATGCGCTAGCAACTCCCTGGAAATCGAAGAACTG
NotI-Aff-r	TAATGCGGCCGCTACTGGTTTGAACTCCTGCAGTTCTTTG
SpeI-Aff-f	AACGACTAGTGCAAACTCCCTGGAAATCGAAGAACTG
SalI-Aff-r	TAATGTCGACTACTGGTTTGAACTCCTGCAGTTCTTTG

Table A 6. Primers used for LgBiT amplification.

Primer	Sequence
LgBiT-NheI-f	TAATGCTAGCGTTTTTACCCTGGAAGATTTCG
LgBiT-NotI-r	TTATGCGGCCGCGCTATTAATGGTCACACGAAAC
LgBiT-SpeI-f	TAAAACTAGTGTTTTTACCCTGGAAGATTTCG
LgBiT-SalI-r	TAATGTCGACGCTATTAATGGTCACACGAAAC

Table A 7. Primers used to generate SmBiT (101).

Primer	Sequence
SmBiT101-NheI-f	TAATGCTAGCGTAACAGGATATAGGCTATTTGAAAAAGAGAGC
SmBiT101-NotI-r	TTATGCGGCCGCGCTCTCTTTTTCAAATAGCCTATATCCTGTTAC
SmBiT101-SpeI-f	TAAAACTAGTGTAACAGGATATAGGCTATTTGAAAAAGAGAGC
SmBiT101-SalI-r	TAATGTCGACGCTCTCTTTTTCAAATAGCCTATATCCTGTTAC

Table A 8. Primers used to generate GSG_7 linker in NanoBiT constructs.

Primer	Sequence
NotI-GSG_7-f	TTATGCGGCCGCTGGGTCCGGCGGTTCAGGCGGCTCTGGTGGCTCCGGTGGGTCAGGT
SpeI-GSG_7-r	TAAAACTAGTGCCAGACCCGCCAGAACCACCTGACCCACCGGAGCCACCAGAGCC

Table A 9. Primers used to introduce restriction sites onto anti-HEL nanobodies.

Primer	Sequence
5A7-NheI	ATATGCTAGCGCGCGCGTGGATCAG
5A7-NotI	TAATGCGGCCGCGTTCACGGTCACCGC
5A7-SpeI	TAATACTAGTGCGCGCGTGGATCAG
5A7-SalI	AATTGTCGACGTTCACGGTCACCGC
D2L24-NheI	ATAAGCTAGCGATGTGCAGCTGGTGGA
D2L24-NotI	TAATGCGGCCGCGCTGCTCACGGTCACCT
D2L24-SpeI	AAATGAATTCGATGTGCAGCTGGTGGA
D2L24-SalI	TATAGCGGCCGCGCTGCTCACGGTCACCT
5A7-NotI-ASSAAASAAA	AATAGCGGCCGCAGACGCAGCAGCAGAAGAAGCGTTCACGGTCACCGCG
5A7-SpeI-TSAASSAAAS	AATAACTAGTGCGGCTTCTTCTGCTGCTGCGTCTGCGCGCGTGGATCAGACCC
D2L24-NotI-ASSAAASAAA	AATAGCGGCCGCAGACGCAGCAGCAGAAGAAGCGCTGCTCACGGTCACC
D2L24-SpeI-TSAASSAAAS	AATAACTAGTGCAGCTTCGTCCGCTGCCGCGTCTGATGTGCAGCTGGTGG

Table A 10. Primers for introducing restriction sites to PCT nanobodies.

Primer	Sequence
PCT2-NheI	ATAAGCTAGCCAGGTGCAGCTTCAAGAGAG
PCT2-NotI	TAATGCGGCCGCGCTCGACACGGTAACTTGTG
PCT2-SpeI	ATAAACTAGTCAGGTGCAGCTTCAAGAGAG
PCT2-SalI	TTAAGTCGACGCTCGACACGGTAACTTGTG
PCT3-NheI	ATTAGCTAGCCAGGTACAGTTGCAAGAGTCTGG
PCT3-NotI	TTAAGCGGCCGCGCTCGACACCGTGACTTGCGTA
PCT3-SpeI	AATAACTAGTCAGGTACAGTTGCAAGAGTCTGG
PCT3-SalI	TTAAGTCGACGCTCGACACCGTGACTTGCGTA

Table A 11. Primers for cloning PCT 2 BLA-BLIP into pPICZα expression plasmid for yeast expression. *Q5 site directed mutagenesis for introduction of* EcoR*I restriction site into pPICZα expression plasmid and primers to PCR amplify PCT2 BLA-BLIP out of pET28a plasmid.*

Primer	Sequence
Q5 EcoRI FWD	GGCTGAAGCTGAATTCTGTAAGTGTGGTC
Q5 EcoRI REV	TCTCTTTTCTCGAGAGATAC
BB_FWD_EcoRI	AATTGAATTCATGGCTTCTGTTTTCGCTGCTCAC
BB_REV_XbaI	ATATTCTAGATTTTTCGAACTGCGGGTG

Table A 12. Sequencing primers.

Primer	Sequence
T7	TAATACGACTCACTATAGGG
T7-term	GCTAGTTATTGCTCAGCGG
5’ AOXI	GACTGGTTCCAATTGACAAGC
3’ AOXI	GCAAATGGCATTCTGACATCC

Appendix B: BLA-BLIP Expression Table

Table A 13. All expression attempts for nanobody BLA-BLIP constructs. *This includes the use of different cell lines; outlines the change of construct composition; notes the effects of helper plasmids; different growth and induction temperatures used in the expression protocol; and the used of differing nanobodies by changing the target analyte. The success of expression was visualised western blots and successful protein recovery from purification methods was depicted by correct sized bands on SDS-PAGE.*

Target analyte	Name	Construct	Cell Line	Helper plasmid	Expression protocol	Expression via western blot	His tag purification	Strep tag purification	Notes
Hen Egg Lysozyme (HEL)	HEL 1	BB_5A7-D2L24	BL21 (DE3)	N/A	1*	N/A	NO	NO	Scale up to 500 mL improved yield from His tag purification but did not solve loss of protein through strep tag purification
HEL	HEL 2	BB_D2L24-5A7	BL21 (DE3)	N/A	1	N/A	YES	NO	
HEL	HEL 2	BB_D2L24-5A7	BL21 (DE3)	pTUM4	1	NO	N/A	N/A	N/A = No purification experiments took place due to poor expression levels seen
HEL	HEL 2	BB_D2L24-5A7	BL21	NO	1	NO	N/A	N/A	
HEL	HEL 2	BB_D2L24-5A7	BL21	pTUM4	1	NO	N/A	N/A	
HEL	HEL 2	BB_D2L24-5A7	DH5α	NO	1	NO	N/A	N/A	
HEL	HEL 2	BB_D2L24-5A7	DH5α	pTUM4	1	NO	N/A	N/A	
HEL	HEL 2	BB_D2L24-5A7	XL1-BLUE	NO	1	NO	N/A	N/A	
HEL	HEL 2	BB_D2L24-5A7	XL1-BLUE	pTUM4	1	NO	N/A	N/A	
HEL	HEL 2	BB_D2L24-5A7	DH5α	NO	2†	POOR	N/A	N/A	
HEL	HEL 2	BB_D2L24-5A7	DH5α	pTUM4	2	POOR	N/A	N/A	
HEL	HEL 2	BB_D2L24-5A7	XL1-BLUE	NO	2	NO	N/A	N/A	

HEL	HEL 2	BB_D2L24-5A7	XL1-BLUE	pTUM4	2	NO	N/A	N/A	
HEL	HEL 3	BB_5A7-D2L24	BL21 (DE3)	N/A	1	NO	N/A	N/A	L1 = TSAASSAAAS L3 = ASSAAASAA
HEL	HEL 4	BB_D2L24-5A7	BL21 (DE3)	N/A	1	POOR	NO	NO	L1 = TSAASSAAAS L3 = ASSAAASAA
HEL	HEL 5	BB_D2L24-D2L24	BL21 (DE3)	N/A	1	YES	YES	NO	N/A = No purification experiments took place due to poor expression levels seen
HEL	HEL 5	BB_D2L24-D2L24	BL21 (DE3)	pTUM4	1	NO	N/A	N/A	
HEL	HEL 5	BB_D2L24-D2L24	BL21	NO	1	NO	N/A	N/A	
HEL	HEL 5	BB_D2L24-D2L24	BL21	pTUM4	1	POOR	N/A	N/A	
HEL	HEL 5	BB_D2L24-D2L24	DH5α	NO	1	NO	N/A	N/A	
HEL	HEL 5	BB_D2L24-D2L24	DH5α	pTUM4	1	NO	N/A	N/A	
HEL	HEL 5	BB_D2L24-D2L24	XL1-BLUE	NO	1	NO	N/A	N/A	
HEL	HEL 5	BB_D2L24-D2L24	XL1-BLUE	pTUM4	1	NO	N/A	N/A	
HEL	HEL 5	BB_D2L24-D2L24	DH5α	NO	2	POOR	N/A	N/A	
HEL	HEL 5	BB_D2L24-D2L24	DH5α	pTUM4	2	POOR	N/A	N/A	
HEL	HEL 5	BB_D2L24-D2L24	XL1-BLUE	NO	2	NO	N/A	N/A	
HEL	HEL 5	BB_D2L24-D2L24	XL1-BLUE	pTUM4	2	NO	N/A	N/A	
HEL	HEL 6	BB_D2L24-5A7	BL21 (DE3)	N/A	1	POOR	N/A	N/A	L2 = $(GSG)_{20}$
HEL	HEL 7	BB_D2L24-5A7	BL21 (DE3)	N/A	1	NO	N/A	N/A	L2 = $(GSG)_3$

Procalcitonin (PCT)	PCT 1	BB_PCT2-PCT3	BL21 (DE3)	N/A	1	NO	NO	NO	
PCT	PCT 2	BB_PCT3-PCT2	BL21 (DE3)	N/A	1	YES	YES	NO	
Toxin B	E37F	BB_E3-7F	BL21 (DE3)	N/A	1	YES	YES	YES	Positive control
Toxin B	E37F	BB_E3-7F	BL21 (DE3)	pTUM4	1	YES	N/A	N/A	No purification experiments took place due to poor expression levels seen
Toxin B	E37F	BB_E3-7F	BL21	NO	1	POOR	N/A	N/A	
Toxin B	E37F	BB_E3-7F	BL21	pTUM4	1	POOR	N/A	N/A	
Toxin B	E37F	BB_E3-7F	DH5α	NO	1	NO	N/A	N/A	
Toxin B	E37F	BB_E3-7F	DH5α	pTUM4	1	NO	N/A	N/A	
Toxin B	E37F	BB_E3-7F	XL1-BLUE	NO	1	NO	N/A	N/A	
Toxin B	E37F	BB_E3-7F	XL1-BLUE	pTUM4	1	NO	N/A	N/A	
Toxin B	E37F	BB_E3-7F	DH5α	NO	2	POOR	N/A	N/A	
Toxin B	E37F	BB_E3-7F	DH5α	pTUM4	2	POOR	N/A	N/A	
Toxin B	E37F	BB_E3-7F	XL1-BLUE	NO	2	NO	N/A	N/A	
Toxin B	E37F	BB_E3-7F	XL1-BLUE	pTUM4	2	NO	N/A	N/A	

* Expression protocol 1: 2YT media (50 µg/mL kanamycin). 37°C 220 rpm. Induced at OD600 = 0.6 with 0.3 mM IPTG. 16°C 180 rpm O/N.

† Expression protocol 2: 2YT media (50 µg/mL kanamycin). 30°C 220 rpm. Induced at OD600 = 0.6 with 0.3 mM IPTG. 30°C 220 rpm O/N.

Appendix C: DNA and Protein Sequences

Within the BLA-BLIP and NanoBiT sensor sequence the Affimer variable region sequences are denoted as XXX. The sequences and plasmids will be shared with any academic who does not have a commercial interest, under an MTA.

BB_TRAST/BB_IPI/BB_RIT/BB_ADA:

Red – leader sequence

Blue – His-tag

Green – thrombin cleavage site

Yellow highlight – TEM1-β-lactamase(E104D)

Light grey highlight – linker 1 (L1)

Pink – Anti-idiotype Affimer

Green highlight – semi-flexible linker 2 (L2)

Dark grey highlight – linker 3 (L3)

Cyan highlight – β-lactamase inhibitor protein(E31A)

Orange – Strep-tag

DNA:

ATGGCTTCTATCCAGCACTTCCGTGTTGCTCTGATCCCGTTCTTCGCTGCTTTCTGCCTGCCGG
TTTTCGCTGCTCACCACCACCACCACCACCACCACCTGGTTCCGCGTGGTTCTCACCCGGAAAC
CCTGGTTAAAGTTAAAGACGCTGAAGACCAGCTGGGTGCTCGTGTTGGTTACATCGAACTGGAC
CTGAACTCTGGTAAAATCCTGGAATCTTTCCGTCCGGAGGAGAGGTTCCCGATGATGTCTACCT
TCAAAGTTCTGCTGTGCGGTGCTGTTCTGTCTCGTGTTGACGCTGGTCAGGAACAGCTGGGTCG
TCGTATCCACTACTCTCAGAACGACCTGGTTGACTACTCTCCGGTTACCGAAAAACACCTGACC
GACGGTATGACCGTTCGTGAACTGTGCTCTGCTGCTATCACCATGTCTGACAACACCGCTGCTA
ACCTGCTGCTGACCACCATCGGTGGTCCGAAAGAACTCACTGCGTTCCTGCACAACATGGGTGA
CCACGTTACCCGTCTGGACCGTTGGGAACCGGAACTGAACGAAGCTATCCCGAACGACGAACGT
GACACCACCATGCCGGCTGCTATGGCTACCACCCTGCGTAAACTGCTGACCGGTGAACTGCTGA
CCCTGGCTTCTCGTCAGCAGCTGATCGACTGGATGGAAGCTGACAAAGTTGCTGGTCCGCTGCT
GCGTTCTGCTCTGCCGGCTGGTTGGTTCATCGCTGACAAATCTGGTGCTGGTGAACGTGGTTCT
CGTGGTATCATCGCTGCTCTGGGTCCGGACGGTAAACCGTCTCGTATCGTTGTTATCTACACCA
CCGGTTCTCAGGCTACTATGGACGAACGTAACCGTCAGATCGCTGAAATCGGTGCTTCTCTGAT
CAAACACTGGACTAGTGCAAACTCCCTGGAAATCGAAGAACTGGCTCGTTTCGCTGTTGACGAA
CACAACAAAAAAGAAAACGCTCTGCTGGAATTCGTTCGTGTTGTTAAAGCGAAAGAACAGXXXX
XXXXXXXXXXXXXXXXXXXXACCATGTACTACCTGACCCTGGAAGCTAAAGACGGTGGTAAAAA
GAAACTGTACGAAGCGAAAGTTTGGGTTAAGXXXXXXXXXXXXXXXXXXXXXXXXXXAACTTC
AAAGAACTGCAGGAGTTCAAACCAGTAGTCGACGGTGGTTCTGGTGGTTCTGGTGGTTCTGGTG
GTTCTGGTGGTTCTGGTGGTTCTGGTGCTGAAGCTGCTGCTAAAGAAGCTGCTGCTAAAGAAGC
TGCTGCTAAAGAAGCTGCTGCTAAAGAAGCTGCTGCTAAAGAAGCTGCTGCTAAAGCTGGTTCT
GGTGGTTCTGGTGGTTCTGGTGGTTCTGGTGGTTCTGGTGGTTCTGGTGCTGAAGCTGCTGCTA
AAGAAGCTGCTGCTAAAGAAGCTGCTGCTAAAGAAGCTGCTGCTAAAGAAGCTGCTGCTAAAGA
AGCTGCTGCTAAAGCTGGTTCTGGTGGTTCTGGTGGTTCTGGTGGTTCTGGTGGTTCTGGTGGT
TCTGGTGGTGCTAGCAACTCCCTGGAAATCGAAGAACTGGCTCGTTTCGCTGTTGACGAACACA

ACAAAAAAGAAAACGCTCTGCTGGAATTCGTTCGTGTTGTTAAAGCGAAAGAACAGXXXXXXXX
XXXXXXXXXXXXXXXXACCATGTACTACCTGACCCTGGAAGCTAAAGACGGTGGTAAAAAGAAA
CTGTACGAAGCGAAAGTTTGGGTTAAGXXXXXXXXXXXXXXXXXXXXXXXXXXXXAACTTCAAAG
AACTGCAGGAGTTCAAACCAGTAGCGGCCGCTGCTGGTGTTATGACCGGTGCTAAATTCACCCA
GATCCAGTTCGGTATGACCCGTCAGCAGGTTCTGGACATCGCTGGTGCTGAAAACTGCGCTACT
GGCGGTAGCTTCGGTGACTCTATACACTGCCGTGGTCACGCTGCTGGTGACTACTACGCTTACG
CTACCTTCGGTTTCACCTCTGCTGCTGCTGACGCTAAAGTTGACTCTAAATCTCAGGAAAAACT
GCTGGCTCCGTCTGCTCCGACCCTGACCCTGGCTAAATTCAACCAGGTTACCGTTGGTATGACC
CGTGCTCAGGTTCTGGCTACCGTTGGTCAGGGTTCTTGCACCACCTGGTCTGAATACTACCCGG
CTTACCCGTCTACCGCTGGTGTTACCCTGTCTCTGTCTTGCTTCGACGTTGACGGTTACTCTTC
TACCGGTTTCTACCGTGGTTCTGCTCACCTGTGGTTCACCGACGGTGTTCTGCAGGGTAAACGT
CAGTGGGACCTGGTTGGTGGTCTCGGTGGTTGGTCTCACCCGCAGTTCGAAAAA

Protein:

MASIQHFRVALIPFFAAFCLPVFAAHHHHHHHHLVPRGSHPETLVKVKDAEDQLGARVGYIELD
LNSGKILESFRPEERFPMMSTFKVLLCGAVLSRVDAGQEQLGRRIHYSQNDLVDYSPVTEKHLT
DGMTVRELCSAAITMSDNTAANLLLTTIGGPKELTAFLHNMGDHVTRLDRWEPELNEAIPNDER
DTTMPAAMATTLRKLLTGELLTLASRQQLIDWMEADKVAGPLLRSALPAGWFIADKSGAGERGS
RGIIAALGPDGKPSRIVVIYTTGSQATMDERNRQIAEIGASLIKHWTSANSLEIEELARFAVDE
HNKKENALLEFVRVVKAKEQXXXXXXXXTMYYLTLEAKDGGKKKLYEAKVWVKXXXXXXXXXNF
KELQEFKPVVDGGSGGSGGSGGSGGSGGSGAEAAAKEAAAKEAAAKEAAAKEAAAKEAAAKAGS
GGSGGSGGSGGSGGSGAEAAAKEAAAKEAAAKEAAAKEAAAKEAAAKAGSGGSGGSGGSGGSGG
SGGASNSLEIEELARFAVDEHNKKENALLEFVRVVKAKEQXXXXXXXXTMYYLTLEAKDGGKKK
LYEAKVWVKXXXXXXXXXNFKELQEFKPVAAAAGVMTGAKFTQIQFGMTRQQVLDIAGAENCAT
GGSFGDSIHCRGHAAGDYYAYATFGFTSAAADAKVDSKSQEKLLAPSAPTLTLAKFNQVTVGMT
RAQVLATVGQGSCTTWSEYYPAYPSTAGVTLSLSCFDVDGYSSTGFYRGSAHLWFTDGVLQGKR
QWDLVGGLGGWSHPQFEK

NanoBiT Affimer constructs:

Blue – Anti-idiotype Affimer

Red – LargeBiT

Purple – SmallBiT101

Green – Polypeptide linker

Orange – His-tag

LgBit-GSG$_7$-AffX

Protein

MAASVFTLEDFVGDWEQTAAYNLDQVLDQGGVSSLLQNLAVSVTPIQRIVRSGENALKIDIHVI
IPYEGLSADQMAQIEEVFKVVYPVDDHHFKVILPYGTLVIDGVTPNMLNYFGRPYEGIAVFDGK
KITVTGTLWNGNKIIDERLITPDGSMLFRVTINSAAAGSGGSGGSGGSGGSGGSGGSGTSANSL
EIEELARFAVDEHNKKENALLEFVRVVKAKEQXXXXXXXXTMYYLTLEAKDGGKKKLYEAKVW
VKXXXXXXXXXNFKELQEFKPVVDLEHHHHHH

DNA

ATGGCGGCTAGCGTTTTTACCCTGGAAGATTTCGTGGGCGACTGGGAACAGACCGCGGCGTACA
ACCTGGACCAAGTGCTGGATCAAGGTGGCGTGAGCAGCCTGCTGCAGAACCTGGCGGTGAGCGT
TACCCCGATCCAACGTATTGTTCGTAGCGGCGAGAACGCGCTGAAGATCGACATTCACGTGATC
ATTCCGTACGAAGGCCTGAGCGCGGATCAGATGGCGCAAATCGAGGAAGTGTTCAAGGTGGTTT
ACCCGGTTGACGATCACCACTTTAAAGTGATCCTGCCGTATGGTACCCTGGTGATTGACGGCGT
TACCCCGAACATGCTGAACTACTTCGGTCGTCCGTATGAGGGCATCGCGGTTTTTGATGGTAAG
AAAATTACCGTGACCGGTACCCTGTGGAACGGCAACAAAATTATTGATGAGCGCCTGATTACCC
CGGACGGCAGCATGCTGTTTCGTGTGACCATTAATAGCGCGGCCGCTGGGTCCGGCGGTTCAGG
CGGCTCTGGTGGCTCCGGTGGGTCAGGTGGTTCTGGCGGGTCTGGCACTAGTGCAAACTCCCTG
GAAATCGAAGAACTGGCTCGTTTCGCTGTTGACGAACACAACAAAAAAGAAAACGCTCTGCTGG
AATTCGTTCGTGTTGTTAAAGCGAAAGAACAGXXXXXXXXXXXXXXXXXXXXXXXXXXACCAT
GTACTACCTGACCCTGGAAGCTAAAGACGGTGGTAAAAAGAAACTGTACGAAGCGAAAGTTTGG
GTTAAAXXXXXXXXXXXXXXXXXXXXXXXXAACTTCAAAGAACTGCAGGAGTTCAAACCAGTAG
TCGACCTCGAGCACCACCACCACCACCAC

AffX-GSG$_7$-LgBit

Protein

MAASNSLEIEELARFAVDEHNKKENALLEFVRVVKAKEQXXXXXXXXXTMYYLTLEAKDGGKKK
LYEAKVWVKXXXXXXXXXNFKELQEFKPVAAAGSGGSGGSGGSGGSGGSGGSGTSVFTLEDFVG
DWEQTAAYNLDQVLEQGGVSSLLQNLAVSVTPIQRIVRSGENALKIDIHVIIPYEGLSADQMAQ
IEEVFKVVYPVDDHHFKVILPYGTLVIDGVTPNMLNYFGRPYEGIAVFDGKKITVTGTLWNGNK
IIDERLITPDGSMLFRVTINSVDLEHHHHHH

DNA

ATGGCGGCTAGCAACTCCCTGGAAATCGAAGAACTGGCTCGTTTCGCTGTTGACGAACACAACA
AAAAAGAAAACGCTCTGCTGGAATTCGTTCGTGTTGTTAAAGCGAAAGAACAGXXXXXXXXXXX
XXXXXXXXXXXXXXXXXACCATGTACTACCTGACCCTGGAAGCTAAAGACGGTGGTAAAAAGAAA
CTGTACGAAGCGAAAGTTTGGGTTAAAXXXXXXXXXXXXXXXXXXXXXXXXAACTTCAAAGAAC
TGCAGGAGTTCAAACCAGTAGCGGCCGCTGGGTCCGGCGGTTCAGGCGGCTCTGGTGGCTCCGG
TGGGTCAGGTGGTTCTGGCGGGTCTGGCACTAGTGTTTTTACCCTGGAAGATTTCGTGGGCGAC
TGGGAACAGACCGCGGCGTACAACCTGGACCAAGTGCTGGAACAAGGTGGCGTGAGCAGCCTGC
TGCAGAACCTGGCGGTGAGCGTTACCCCGATCCAACGTATTGTTCGTAGCGGCGAGAACGCGCT
GAAGATCGACATTCACGTGATCATTCCGTACGAAGGCCTGAGCGCGGATCAGATGGCGCAAATC
GAGGAAGTGTTCAAGGTGGTTTACCCGGTTGACGATCACCACTTTAAAGTGATCCTGCCGTATG
GTACCCTGGTGATTGACGGCGTTACCCCGAACATGCTGAACTACTTCGGTCGTCCGTATGAGGG
CATCGCGGTTTTTGATGGTAAGAAAATTACCGTGACCGGTACCCTGTGGAACGGCAACAAAATT
ATTGATGAGCGCCTGATTACCCCGGACGGCAGCATGCTGTTTCGTGTGACCATTAATAGCGTCG
ACCTCGAGCACCACCACCACCACCAT

SmBit101-GSG$_7$-AffX

Protein

MAASVTGYRLFEKESAAAGSGGSGGSGGSGGSGGSGGSGTSANSLEIEELARFAVDEHNKKENA
LLEFVRVVKAKEQXXXXXXXXXTMYYLTLEAKDGGKKKLYEAKVWVKXXXXXXXXXNFKELQEF
KPVVDLEHHHHHH

DNA

ATGGCGGCTAGCGTAACAGGATATAGGCTATTTGAAAAAGAGAGCGCGGCCGCTGGGTCCGGCG
GTTCAGGCGGCTCTGGTGGCTCCGGTGGGTCAGGTGGTTCTGGCGGGTCTGGCACTAGTGCAAA
CTCCCTGGAAATCGAAGAACTGGCTCGTTTCGCTGTTGACGAACACAACAAAAAAGAAAACGCT
CTGCTGGAATTCGTTCGTGTTGTTAAAGCGAAAGAACAGXXXXXXXXXXXXXXXXXXXXXXXX
XXACCATGTACTACCTGACCCTGGAAGCTAAAGACGGTGGTAAAAAGAAACTGTACGAAGCGAA
AGTTTGGGTTAAAXXXXXXXXXXXXXXXXXXXXXXXXAACTTCAAAGAACTGCAGGAGTTCAAA
CCAGTAGTCGACCTCGAGCACCACCACCACCACCAC

AffX-GSG$_7$-SmBit101

Protein

MAASNSLEIEELARFAVDEHNKKENALLEFVRVVKAKEQXXXXXXXXXTMYYLTLEAKDGGKKK
LYEAKVWVKXXXXXXXXXNFKELQEFKPVAAAGSGGSGGSGGSGGSGGSGGSGTSVTGYRLFEK
ESVDLEHHHHHH

DNA

ATGGCGGCTAGCAACTCCCTGGAAATCGAAGAACTGGCTCGTTTCGCTGTTGACGAACACAACA
AAAAAGAAAACGCTCTGCTGGAATTCGTTCGTGTTGTTAAAGCGAAAGAACAGXXXXXXXXXXX
XXXXXXXXXXXXXXXXXACCATGTACTACCTGACCCTGGAAGCTAAAGACGGTGGTAAAAAGAAA
CTGTACGAAGCGAAAGTTTGGGTTAAAXXXXXXXXXXXXXXXXXXXXXXXXAACTTCAAAGAAC
TGCAGGAGTTCAAACCAGTAGCGGCCGCTGGGTCCGGCGGTTCAGGCGGCTCTGGTGGCTCCGG
TGGGTCAGGTGGTTCTGGCGGGTCTGGCACTAGTGTAACAGGATATAGGCTATTTGAAAAAGAG
AGCGTCGACCTCGAGCACCACCACCACCACCAC

HEL/PCT/Toxin B BLA-BLIP:

Red – leader sequence

Blue – His-tag

Green – thrombin cleavage site

Yellow highlight – TEM1-β-lactamase(E104D)

Light grey highlight – linker 1 (L1)

Pink – Nanobodies

Green highlight – semi-flexible linker 2 (L2)

Dark grey highlight – linker 3 (L3)

Cyan highlight – β-lactamase inhibitor protein(E31A)

Orange – Strep-tag

HEL 1:

DNA

ATGGCTTCTATCCAGCACTTCCGTGTTGCTCTGATCCCGTTCTTCGCTGCTTTCTGCCTGCCGG
TTTTCGCTGCTCACCACCACCACCACCACCACCACCTGGTTCCGCGTGGTTCTCACCCGGAAAC
CCTGGTTAAAGTTAAAGACGCTGAAGACCAGCTGGGTGCTCGTGTTGGTTACATCGAACTGGAC
CTGAACTCTGGTAAAATCCTGGAATCTTTCCGTCCGGAGGAGAGGTTCCCGATGATGTCTACCT
TCAAAGTTCTGCTGTGCGGTGCTGTTCTGTCTCGTGTTGACGCTGGTCAGGAACAGCTGGGTCG
TCGTATCCACTACTCTCAGAACGACCTGGTTGACTACTCTCCGGTTACCGAAAAACACCTGACC
GACGGTATGACCGTTCGTGAACTGTGCTCTGCTGCTATCACCATGTCTGACAACACCGCTGCTA
ACCTGCTGCTGACCACCATCGGTGGTCCGAAAGAACTCACTGCGTTCCTGCACAACATGGGTGA
CCACGTTACCCGTCTGGACCGTTGGGAACCGGAACTGAACGAAGCTATCCCGAACGACGAACGT
GACACCACCATGCCGGCTGCTATGGCTACCACCCTGCGTAAACTGCTGACCGGTGAACTGCTGA
CCCTGGCTTCTCGTCAGCAGCTGATCGACTGGATGGAAGCTGACAAAGTTGCTGGTCCGCTGCT
GCGTTCTGCTCTGCCGGCTGGTTGGTTCATCGCTGACAAATCTGGTGCTGGTGAACGTGGTTCT
CGTGGTATCATCGCTGCTCTGGGTCCGGACGGTAAACCGTCTCGTATCGTTGTTATCTACACCA
CCGGTTCTCAGGCTACTATGGACGAACGTAACCGTCAGATCGCTGAAATCGGTGCTTCTCTGAT
CAAACACTGGACTAGTGCGCGCGTGGATCAGACCCCGCGCAGCGTGACCAAAGAAACCGGCGAA
AGCCTGACCATTAACTGCGTGCTGCGCGATGCGAGCTATGCGCTGGGCAGCACCTGCTGGTATC
GCAAAAAAAGCGGCGAAGGCAACGAAGAAAGCATTAGCAAAGGCGGGCGCTATGTGGAAACCGT
GAACAGCGGCAGCAAAAGCTTTAGCCTGCGCATTAACGATCTGACCGTGGAAGATGGCGGCACC
TATCGCTGCGGCCTGGGCGTGGCGGGCGGCTATTGCGATTATGCGCTGTGCAGCAGCCGCTATG
CGGAATGCGGCGATGGCACCGCGGTGACCGTGAACGTCGACGGGTCCGGCGGTTCAGGCGGCTC
TGGTGGCTCCGGTGGGTCAGGTGGTTCTGGCGGGTCTGGCGCTAGCGATGTGCAGCTGGTGGAA
AGCGGCGGCGGCAGCGTGCAGGCGGGCGGCAGCCTGCGCCTGAGCTGCGCGGCGAGCGGCTATA
TTGCGAGCATTAACTATCTGGGCTGGTTTCGCCAGGCGCCGGGCAAAGAACGCGAAGGCGTGGC
GGCGGTGAGCCCGGCGGGCGGCACCCCGTATTATGCGGATAGCGTGAAAGGCCGCTTTACCGTG
AGCCTGGATAACGCGGAAAACACCGTGTATCTGCAGATGAACAGCCTGAAACCGGAAGATACCG
CGCTGTATTATTGCGCGGCGGCGCGCCAGGGCTGGTATATTCCGCTGAACAGCTATGGCTATAA
CTATTGGGCGCAGGGCACCCAGGTGACCGTGAGCAGCGCGGCCGCTGCTGGTGTTATGACCGGT
GCTAAATTCACCCAGATCCAGTTCGGTATGACCCGTCAGCAGGTTCTGGACATCGCTGGTGCTG
AAAACTGCGCTACTGGCGGTAGCTTCGGTGACTCTATACACTGCCGTGGTCACGCTGCTGGTGA
CTACTACGCTTACGCTACCTTCGGTTTCACCTCTGCTGCTGCTGACGCTAAAGTTGACTCTAAA
TCTCAGGAAAAACTGCTGGCTCCGTCTGCTCCGACCCTGACCCTGGCTAAATTCAACCAGGTTA
CCGTTGGTATGACCCGTGCTCAGGTTCTGGCTACCGTTGGTCAGGGTTCTTGCACCACCTGGTC
TGAATACTACCCGGCTTACCCGTCTACCGCTGGTGTTACCCTGTCTCTGTCTTGCTTCGACGTT
GACGGTTACTCTTCTACCGGTTTCTACCGTGGTTCTGCTCACCTGTGGTTCACCGACGGTGTTC
TGCAGGGTAAACGTCAGTGGGACCTGGTTGGTGGTCTCGGTGGTTGGTCTCACCCGCAGTTCGA
AAAA

Protein

MASIQHFRVALIPFFAAFCLPVFAAHHHHHHHHHLVPRGSHPETLVKVKDAEDQLGARVGYIELD
LNSGKILESFRPEERFPMMSTFKVLLCGAVLSRVDAGQEQLGRRIHYSQNDLVDYSPVTEKHLT
DGMTVRELCSAAITMSDNTAANLLLTTIGGPKELTAFLHNMGDHVTRLDRWEPELNEAIPNDER
DTTMPAAMATTLRKLLTGELLTLASRQQLIDWMEADKVAGPLLRSALPAGWFIADKSGAGERGS
RGIIAALGPDGKPSRIVVIYTTGSQATMDERNRQIAEIGASLIKHWTSARVDQTPRSVTKETGE
SLTINCVLRDASYALGSTCWYRKKSGEGNEESISKGGRYVETVNSGSKSFSLRINDLTVEDGGT
YRCGLGVAGGYCDYALCSSRYAECGDGTAVTVNVDGSGGSGGSGGSGGSGGSGGSGASDVQLVE
SGGGSVQAGGSLRLSCAASGYIASINYLGWFRQAPGKEREGVAAVSPAGGTPYYADSVKGRFTV
SLDNAENTVYLQMNSLKPEDTALYYCAAARQGWYIPLNSYGYNYWAQGTQVTVSSAAAAGVMTG
AKFTQIQFGMTRQQVLDIAGAENCATGGSFGDSIHCRGHAAGDYYAYATFGFTSAAADAKVDSK
SQEKLLAPSAPTLTLAKFNQVTVGMTRAQVLATVGQGSCTTWSEYYPAYPSTAGVTLSLSCFDV
DGYSSTGFYRGSAHLWFTDGVLQGKRQWDLVGGLGGWSHPQFEK

HEL 2:

DNA

ATGGCTTCTATCCAGCACTTCCGTGTTGCTCTGATCCCGTTCTTCGCTGCTTTCTGCCTGCCGG
TTTTCGCTGCTCACCACCACCACCACCACCACCACCTGGTTCCGCGTGGTTCTCACCCGGAAAC
CCTGGTTAAAGTTAAAGACGCTGAAGACCAGCTGGGTGCTCGTGTTGGTTACATCGAACTGGAC
CTGAACTCTGGTAAAATCCTGGAATCTTTCCGTCCGGAGGAGAGGTTCCCGATGATGTCTACCT
TCAAAGTTCTGCTGTGCGGTGCTGTTCTGTCTCGTGTTGACGCTGGTCAGGAACAGCTGGGTCG
TCGTATCCACTACTCTCAGAACGACCTGGTTGACTACTCTCCGGTTACCGAAAAACACCTGACC
GACGGTATGACCGTTCGTGAACTGTGCTCTGCTGCTATCACCATGTCTGACAACACCGCTGCTA
ACCTGCTGCTGACCACCATCGGTGGTCCGAAAGAACTCACTGCGTTCCTGCACAACATGGGTGA
CCACGTTACCCGTCTGGACCGTTGGGAACCGGAACTGAACGAAGCTATCCCGAACGACGAACGT
GACACCACCATGCCGGCTGCTATGGCTACCACCCTGCGTAAACTGCTGACCGGTGAACTGCTGA
CCCTGGCTTCTCGTCAGCAGCTGATCGACTGGATGGAAGCTGACAAAGTTGCTGGTCCGCTGCT
GCGTTCTGCTCTGCCGGCTGGTTGGTTCATCGCTGACAAATCTGGTGCTGGTGAACGTGGTTCT
CGTGGTATCATCGCTGCTCTGGGTCCGGACGGTAAACCGTCTCGTATCGTTGTTATCTACACCA
CCGGTTCTCAGGCTACTATGGACGAACGTAACCGTCAGATCGCTGAAATCGGTGCTTCTCTGAT
CAAACACTGGACTAGTATGTGCAGCTGGTGGAAAGCGGCGGCGGCAGCGTGCAGGCGGGCGGCA
GCCTGCGCCTGAGCTGCGCGGCGAGCGGCTATATTGCGAGCATTAACTATCTGGGCTGGTTTCG
CCAGGCGCCGGGCAAAGAACGCGAAGGCGTGGCGGCGGTGAGCCCGGCGGGCGGCACCCCGTAT
TATGCGGATAGCGTGAAAGGCCGCTTTACCGTGAGCCTGGATAACGCGGAAAACACCGTGTATC
TGCAGATGAACAGCCTGAAACCGGAAGATACCGCGCTGTATTATTGCGCGGCGGCGCGCCAGGG
CTGGTATATTCCGCTGAACAGCTATGGCTATAACTATTGGGCGCAGGGCACCCAGGTGACCGTG
AGCAGCGTCGACGGGTCCGGCGGTTCAGGCGGCTCTGGTGGCTCCGGTGGGTCAGGTGGTTCTG
GCGGGTCTGGCGCTAGCGCGCGCGTGGATCAGACCCCGCGCAGCGTGACCAAAGAAACCGGCGA
AAGCCTGACCATTAACTGCGTGCTGCGCGATGCGAGCTATGCGCTGGGCAGCACCTGCTGGTAT
CGCAAAAAAAGCGGCGAAGGCAACGAAGAAAGCATTAGCAAAGGCGGGCGCTATGTGGAAACCG
TGAACAGCGGCAGCAAAAGCTTTAGCCTGCGCATTAACGATCTGACCGTGGAAGATGGCGGCAC
CTATCGCTGCGGCCTGGGCGTGGCGGGCGGCTATTGCGATTATGCGCTGTGCAGCAGCCGCTAT
GCGGAATGCGGCGATGGCACCGCGGTGACCGTGAACGCGGCCGCTGCTGGTGTTATGACCGGTG
CTAAATTCACCCAGATCCAGTTCGGTATGACCCGTCAGCAGGTTCTGGACATCGCTGGTGCTGA
AAACTGCGCTACTGGCGGTAGCTTCGGTGACTCTATACACTGCCGTGGTCACGCTGCTGGTGAC
TACTACGCTTACGCTACCTTCGGTTTCACCTCTGCTGCTGCTGACGCTAAAGTTGACTCTAAAT
CTCAGGAAAAACTGCTGGCTCCGTCTGCTCCGACCCTGACCCTGGCTAAATTCAACCAGGTTAC
CGTTGGTATGACCCGTGCTCAGGTTCTGGCTACCGTTGGTCAGGGTTCTTGCACCACCTGGTCT
GAATACTACCCGGCTTACCCGTCTACCGCTGGTGTTACCCTGTCTCTGTCTTGCTTCGACGTTG
ACGGTTACTCTTCTACCGGTTTCTACCGTGGTTCTGCTCACCTGTGGTTCACCGACGGTGTTCT
GCAGGGTAAACGTCAGTGGGACCTGGTTGGTGGTCTCGGTGGTTGGTCTCACCCGCAGTTCGAA
AAA

Protein

MASIQHFRVALIPFFAAFCLPVFAAHHHHHHHHHLVPRGSHPETLVKVKDAEDQLGARVGYIELD
LNSGKILESFRPEERFPMMSTFKVLLCGAVLSRVDAGQEQLGRRIHYSQNDLVDYSPVTEKHLT
DGMTVRELCSAAITMSDNTAANLLLTTIGGPKELTAFLHNMGDHVTRLDRWEPELNEAIPNDER
DTTMPAAMATTLRKLLTGELLTLASRQQLIDWMEADKVAGPLLRSALPAGWFIADKSGAGERGS
RGIIAALGPDGKPSRIVVIYTTGSQATMDERNRQIAEIGASLIKHWTSDVQLVESGGGSVQAGG
SLRLSCAASGYIASINYLGWFRQAPGKEREGVAAVSPAGGTPYYADSVKGRFTVSLDNAENTVY
LQMNSLKPEDTALYYCAAARQGWYIPLNSYGYNYWAQGTQVTVSSVDGSGGSGGSGGSGGSGGS
GGSGASARVDQTPRSVTKETGESLTINCVLRDASYALGSTCWYRKKSGEGNEESISKGGRYVET
VNSGSKSFSLRINDLTVEDGGTYRCGLGVAGGYCDYALCSSRYAECGDGTAVTVNAAAAGVMTG
AKFTQIQFGMTRQQVLDIAGAENCATGGSFGDSIHCRGHAAGDYYAYATFGFTSAAADAKVDSK
SQEKLLAPSAPTLTLAKFNQVTVGMTRAQVLATVGQGSCTTWSEYYPAYPSTAGVTLSLSCFDV
DGYSSTGFYRGSAHLWFTDGVLQGKRQWDLVGGLGGWSHPQFEK

HEL 3:

DNA

ATGGCTTCTATCCAGCACTTCCGTGTTGCTCTGATCCCGTTCTTCGCTGCTTTCTGCCTGCCGG
TTTTCGCTGCTCACCACCACCACCACCACCACCACCTGGTTCCGCGTGGTTCTCACCCGGAAAC
CCTGGTTAAAGTTAAAGACGCTGAAGACCAGCTGGGTGCTCGTGTTGGTTACATCGAACTGGAC
CTGAACTCTGGTAAAATCCTGGAATCTTTCCGTCCGGAGGAGAGGTTCCCGATGATGTCTACCT
TCAAAGTTCTGCTGTGCGGTGCTGTTCTGTCTCGTGTTGACGCTGGTCAGGAACAGCTGGGTCG
TCGTATCCACTACTCTCAGAACGACCTGGTTGACTACTCTCCGGTTACCGAAAAACACCTGACC
GACGGTATGACCGTTCGTGAACTGTGCTCTGCTGCTATCACCATGTCTGACAACACCGCTGCTA
ACCTGCTGCTGACCACCATCGGTGGTCCGAAAGAACTCACTGCGTTCCTGCACAACATGGGTGA
CCACGTTACCCGTCTGGACCGTTGGGAACCGGAACTGAACGAAGCTATCCCGAACGACGAACGT
GACACCACCATGCCGGCTGCTATGGCTACCACCCTGCGTAAACTGCTGACCGGTGAACTGCTGA
CCCTGGCTTCTCGTCAGCAGCTGATCGACTGGATGGAAGCTGACAAAGTTGCTGGTCCGCTGCT
GCGTTCTGCTCTGCCGGCTGGTTGGTTCATCGCTGACAAATCTGGTGCTGGTGAACGTGGTTCT
CGTGGTATCATCGCTGCTCTGGGTCCGGACGGTAAACCGTCTCGTATCGTTGTTATCTACACCA
CCGGTTCTCAGGCTACTATGGACGAACGTAACCGTCAGATCGCTGAAATCGGTGCTTCTCTGAT
CAAACACTGGACTAGTGCAGCTTCGTCCGCTGCCGCGTCTGCGCGCGTGGATCAGACCCCGCGC
AGCGTGACCAAAGAAACCGGCGAAAGCCTGACCATTAACTGCGTGCTGCGCGATGCGAGCTATG
CGCTGGGCAGCACCTGCTGGTATCGCAAAAAAAGCGGCGAAGGCAACGAAGAAAGCATTAGCAA
AGGCGGGCGCTATGTGGAAACCGTGAACAGCGGCAGCAAAAGCTTTAGCCTGCGCATTAACGAT
CTGACCGTGGAAGATGGCGGCACCTATCGCTGCGGCCTGGGCGTGGCGGGCGGCTATTGCGATT
ATGCGCTGTGCAGCAGCCGCTATGCGGAATGCGGCGATGGCACCGCGGTGACCGTGAACGTCGA
CGGGTCCGGCGGTTCAGGCGGCTCTGGTGGCTCCGGTGGGTCAGGTGGTTCTGGCGGGTCTGGC
GCTAGCGATGTGCAGCTGGTGGAAAGCGGCGGCGGCAGCGTGCAGGCGGGCGGCAGCCTGCGCC
TGAGCTGCGCGGCGAGCGGCTATATTGCGAGCATTAACTATCTGGGCTGGTTTCGCCAGGCGCC
GGGCAAAGAACGCGAAGGCGTGGCGGCGGTGAGCCCGGCGGGCGGCACCCCGTATTATGCGGAT
AGCGTGAAAGGCCGCTTTACCGTGAGCCTGGATAACGCGGAAAACACCGTGTATCTGCAGATGA
ACAGCCTGAAACCGGAAGATACCGCGCTGTATTATTGCGCGGCGGCGCGCCAGGGCTGGTATAT
TCCGCTGAACAGCTATGGCTATAACTATTGGGCGCAGGGCACCCAGGTGACCGTGAGCAGCCGA
AGAAGACGACGACGCAGACGCGGCCGCTGCTGGTGTTATGACCGGTGCTAAATTCACCCAGATC
CAGTTCGGTATGACCCGTCAGCAGGTTCTGGACATCGCTGGTGCTGAAAACTGCGCTACTGGCG
GTAGCTTCGGTGACTCTATACACTGCCGTGGTCACGCTGCTGGTGACTACTACGCTTACGCTAC
CTTCGGTTTCACCTCTGCTGCTGCTGACGCTAAAGTTGACTCTAAATCTCAGGAAAAACTGCTG
GCTCCGTCTGCTCCGACCCTGACCCTGGCTAAATTCAACCAGGTTACCGTTGGTATGACCCGTG
CTCAGGTTCTGGCTACCGTTGGTCAGGGTTCTTGCACCACCTGGTCTGAATACTACCCGGCTTA
CCCGTCTACCGCTGGTGTTACCCTGTCTCTGTCTTGCTTCGACGTTGACGGTTACTCTTCTACC
GGTTTCTACCGTGGTTCTGCTCACCTGTGGTTCACCGACGGTGTTCTGCAGGGTAAACGTCAGT
GGGACCTGGTTGGTGGTCTCGGTGGTTGGTCTCACCCGCAGTTCGAAAAA

Protein

MASIQHFRVALIPFFAAFCLPVFAAHHHHHHHHHLVPRGSHPETLVKVKDAEDQLGARVGYIELD
LNSGKILESFRPEERFPMMSTFKVLLCGAVLSRVDAGQEQLGRRIHYSQNDLVDYSPVTEKHLT
DGMTVRELCSAAITMSDNTAANLLLTTIGGPKELTAFLHNMGDHVTRLDRWEPELNEAIPNDER
DTTMPAAMATTLRKLLTGELLTLASRQQLIDWMEADKVAGPLLRSALPAGWFIADKSGAGERGS
RGIIAALGPDGKPSRIVVIYTTGSQATMDERNRQIAEIGASLIKHWTSAASSAAASARVDQTPR
SVTKETGESLTINCVLRDASYALGSTCWYRKKSGEGNEESISKGGRYVETVNSGSKSFSLRIND
LTVEDGGTYRCGLGVAGGYCDYALCSSRYAECGDGTAVTVNVDGSGGSGGSGGSGGSGGSGG
ASDVQLVESGGGSVQAGGSLRLSCAASGYIASINYLGWFRQAPGKEREGVAAVSPAGGTPYYAD
SVKGRFTVSLDNAENTVYLQMNSLKPEDTALYYCAAARQGWYIPLNSYGYNYWAQGTQVTVSSA
SSAAASAAAAGVMTGAKFTQIQFGMTRQQVLDIAGAENCATGGSFGDSIHCRGHAAGDYYAYAT

FGFTSAAADAKVDSKSQEKLLAPSAPTLTLAKFNQVTVGMTRAQVLATVGQGSCTTWSEYYPAY
PSTAGVTLSLSCFDVDGYSSTGFYRGSAHLWFTDGVLQGKRQWDLVGGLGGWSHPQFEK

HEL 4:

DNA

ATGGCTTCTATCCAGCACTTCCGTGTTGCTCTGATCCCGTTCTTCGCTGCTTTCTGCCTGCCGG
TTTTCGCTGCTCACCACCACCACCACCACCACCACCTGGTTCCGCGTGGTTCTCACCCGGAAAC
CCTGGTTAAAGTTAAAGACGCTGAAGACCAGCTGGGTGCTCGTGTTGGTTACATCGAACTGGAC
CTGAACTCTGGTAAAATCCTGGAATCTTTCCGTCCGGAGGAGAGGTTCCCGATGATGTCTACCT
TCAAAGTTCTGCTGTGCGGTGCTGTTCTGTCTCGTGTTGACGCTGGTCAGGAACAGCTGGGTCG
TCGTATCCACTACTCTCAGAACGACCTGGTTGACTACTCTCCGGTTACCGAAAAACACCTGACC
GACGGTATGACCGTTCGTGAACTGTGCTCTGCTGCTATCACCATGTCTGACAACACCGCTGCTA
ACCTGCTGCTGACCACCATCGGTGGTCCGAAAGAACTCACTGCGTTCCTGCACAACATGGGTGA
CCACGTTACCCGTCTGGACCGTTGGGAACCGGAACTGAACGAAGCTATCCCGAACGACGAACGT
GACACCACCATGCCGGCTGCTATGGCTACCACCCTGCGTAAACTGCTGACCGGTGAACTGCTGA
CCCTGGCTTCTCGTCAGCAGCTGATCGACTGGATGGAAGCTGACAAAGTTGCTGGTCCGCTGCT
GCGTTCTGCTCTGCCGGCTGGTTGGTTCATCGCTGACAAATCTGGTGCTGGTGAACGTGGTTCT
CGTGGTATCATCGCTGCTCTGGGTCCGGACGGTAAACCGTCTCGTATCGTTGTTATCTACACCA
CCGGTTCTCAGGCTACTATGGACGAACGTAACCGTCAGATCGCTGAAATCGGTGCTTCTCTGAT
CAAACACTGGACTAGTGCAGCTTCGTCCGCTGCCGCGTCTATGTGCAGCTGGTGGAAAGCGGCG
GCGGCAGCGTGCAGGCGGGCGGCAGCCTGCGCCTGAGCTGCGCGGCGAGCGGCTATATTGCGAG
CATTAACTATCTGGGCTGGTTTCGCCAGGCGCCGGGCAAAGAACGCGAAGGCGTGGCGGCGGTG
AGCCCGGCGGGCGGCACCCCGTATTATGCGGATAGCGTGAAAGGCCGCTTTACCGTGAGCCTGG
ATAACGCGGAAAACACCGTGTATCTGCAGATGAACAGCCTGAAACCGGAAGATACCGCGCTGTA
TTATTGCGCGGCGGCGCGCCAGGGCTGGTATATTCCGCTGAACAGCTATGGCTATAACTATTGG
GCGCAGGGCACCCAGGTGACCGTGAGCAGCGTCGACGGGTCCGGCGGTTCAGGCGGCTCTGGTG
GCTCCGGTGGGTCAGGTGGTTCTGGCGGGTCTGGCGCTAGCGCGCGTGGATCAGACCCCGCG
CAGCGTGACCAAAGAAACCGGCGAAAGCCTGACCATTAACTGCGTGCTGCGCGATGCGAGCTAT
GCGCTGGGCAGCACCTGCTGGTATCGCAAAAAAAGCGGCGAAGGCAACGAAGAAAGCATTAGCA
AAGGCGGGCGCTATGTGGAAACCGTGAACAGCGGCAGCAAAAGCTTTAGCCTGCGCATTAACGA
TCTGACCGTGGAAGATGGCGGCACCTATCGCTGCGGCCTGGGCGTGGCGGGCGGCTATTGCGAT
TATGCGCTGTGCAGCAGCCGCTATGCGGAATGCGGCGATGGCACCGCGGTGACCGTGAACCGAA
GAAGACGACGACGCAGACGCGGCCGCTGCTGGTGTTATGACCGGTGCTAAATTCACCCAGATCC
AGTTCGGTATGACCCGTCAGCAGGTTCTGGACATCGCTGGTGCTGAAAACTGCGCTACTGGCGG
TAGCTTCGGTGACTCTATACACTGCCGTGGTCACGCTGCTGGTGACTACTACGCTTACGCTACC
TTCGGTTTCACCTCTGCTGCTGCTGACGCTAAAGTTGACTCTAAATCTCAGGAAAAACTGCTGG
CTCCGTCTGCTCCGACCCTGACCCTGGCTAAATTCAACCAGGTTACCGTTGGTATGACCCGTGC
TCAGGTTCTGGCTACCGTTGGTCAGGGTTCTTGCACCACCTGGTCTGAATACTACCCGGCTTAC
CCGTCTACCGCTGGTGTTACCCTGTCTCTGTCTTGCTTCGACGTTGACGGTTACTCTTCTACCG
GTTTCTACCGTGGTTCTGCTCACCTGTGGTTCACCGACGGTGTTCTGCAGGGTAAACGTCAGTG
GGACCTGGTTGGTGGTCTCGGTGGTTGGTCTCACCCGCAGTTCGAAAAA

Protein

MASIQHFRVALIPFFAAFCLPVFAAHHHHHHHHHLVPRGSHPETLVKVKDAEDQLGARVGYIELD
LNSGKILESFRPEERFPMMSTFKVLLCGAVLSRVDAGQEQLGRRIHYSQNDLVDYSPVTEKHLT
DGMTVRELCSAAITMSDNTAANLLLTTIGGPKELTAFLHNMGDHVTRLDRWEPELNEAIPNDER
DTTMPAAMATTLRKLLTGELLTLASRQQLIDWMEADKVAGPLLRSALPAGWFIADKSGAGERGS
RGIIAALGPDGKPSRIVVIYTTGSQATMDERNRQIAEIGASLIKHWTSAASSAAASDVQLVESG
GGSVQAGGSLRLSCAASGYIASINYLGWFRQAPGKEREGVAAVSPAGGTPYYADSVKGRFTVSL
DNAENTVYLQMNSLKPEDTALYYCAAARQGWYIPLNSYGYNYWAQGTQVTVSSVDGSGGSGGSG
GSGGSGGSGGSGASARVDQTPRSVTKETGESLTINCVLRDASYALGSTCWYRKKSGEGNEESIS
KGGRYVETVNSGSKSFSLRINDLTVEDGGTYRCGLGVAGGYCDYALCSSRYAECGDGTAVTVNA

SSAAASAAAAGVMTGAKFTQIQFGMTRQQVLDIAGAENCATGGSFGDSIHCRGHAAGDYYAYAT
FGFTSAAADAKVDSKSQEKLLAPSAPTLTLAKFNQVTVGMTRAQVLATVGQGSCTTWSEYYPAY
PSTAGVTLSLSCFDVDGYSSTGFYRGSAHLWFTDGVLQGKRQWDLVGGLGGWSHPQFEK

HEL 5:

DNA

ATGGCTTCTATCCAGCACTTCCGTGTTGCTCTGATCCCGTTCTTCGCTGCTTTCTGCCTGCCGG
TTTTCGCTGCTCACCACCACCACCACCACCACCACCTGGTTCCGCGTGGTTCTCACCCGGAAAC
CCTGGTTAAAGTTAAAGACGCTGAAGACCAGCTGGGTGCTCGTGTTGGTTACATCGAACTGGAC
CTGAACTCTGGTAAAATCCTGGAATCTTTCCGTCCGGAGGAGAGGTTCCCGATGATGTCTACCT
TCAAAGTTCTGCTGTGCGGTGCTGTTCTGTCTCGTGTTGACGCTGGTCAGGAACAGCTGGGTCG
TCGTATCCACTACTCTCAGAACGACCTGGTTGACTACTCTCCGGTTACCGAAAAACACCTGACC
GACGGTATGACCGTTCGTGAACTGTGCTCTGCTGCTATCACCATGTCTGACAACACCGCTGCTA
ACCTGCTGCTGACCACCATCGGTGGTCCGAAAGAACTCACTGCGTTCCTGCACAACATGGGTGA
CCACGTTACCCGTCTGGACCGTTGGGAACCGGAACTGAACGAAGCTATCCCGAACGACGAACGT
GACACCACCATGCCGGCTGCTATGGCTACCACCCTGCGTAAACTGCTGACCGGTGAACTGCTGA
CCCTGGCTTCTCGTCAGCAGCTGATCGACTGGATGGAAGCTGACAAAGTTGCTGGTCCGCTGCT
GCGTTCTGCTCTGCCGGCTGGTTGGTTCATCGCTGACAAATCTGGTGCTGGTGAACGTGGTTCT
CGTGGTATCATCGCTGCTCTGGGTCCGGACGGTAAACCGTCTCGTATCGTTGTTATCTACACCA
CCGGTTCTCAGGCTACTATGGACGAACGTAACCGTCAGATCGCTGAAATCGGTGCTTCTCTGAT
CAAACACTGGACTAGTATGTGCAGCTGGTGGAAAGCGGCGGCGGCAGCGTGCAGGCGGGCGGCA
GCCTGCGCCTGAGCTGCGCGGCGAGCGGCTATATTGCGAGCATTAACTATCTGGGCTGGTTTCG
CCAGGCGCCGGGCAAAGAACGCGAAGGCGTGGCGGCGGTGAGCCCGGCGGGCGGCACCCCGTAT
TATGCGGATAGCGTGAAAGGCCGCTTTACCGTGAGCCTGGATAACGCGGAAAACACCGTGTATC
TGCAGATGAACAGCCTGAAACCGGAAGATACCGCGCTGTATTATTGCGCGGCGGCGCGCCAGGG
CTGGTATATTCCGCTGAACAGCTATGGCTATAACTATTGGGCGCAGGGCACCCAGGTGACCGTG
AGCAGCGTCGACGGGTCCGGCGGTTCAGGCGGCTCTGGTGGCTCCGGTGGGTCAGGTGGTTCTG
GCGGGTCTGGCGCTAGCATGTGCAGCTGGTGGAAAGCGGCGGCGGCAGCGTGCAGGCGGGCGGC
AGCCTGCGCCTGAGCTGCGCGGCGAGCGGCTATATTGCGAGCATTAACTATCTGGGCTGGTTTC
GCCAGGCGCCGGGCAAAGAACGCGAAGGCGTGGCGGCGGTGAGCCCGGCGGGCGGCACCCCGTA
TTATGCGGATAGCGTGAAAGGCCGCTTTACCGTGAGCCTGGATAACGCGGAAAACACCGTGTAT
CTGCAGATGAACAGCCTGAAACCGGAAGATACCGCGCTGTATTATTGCGCGGCGGCGCGCCAGG
GCTGGTATATTCCGCTGAACAGCTATGGCTATAACTATTGGGCGCAGGGCACCCAGGTGACCGT
GAGCAGCGCGGCCGCTGCTGGTGTTATGACCGGTGCTAAATTCACCCAGATCCAGTTCGGTATG
ACCCGTCAGCAGGTTCTGGACATCGCTGGTGCTGAAAACTGCGCTACTGGCGGTAGCTTCGGTG
ACTCTATACACTGCCGTGGTCACGCTGCTGGTGACTACTACGCTTACGCTACCTTCGGTTTCAC
CTCTGCTGCTGCTGACGCTAAAGTTGACTCTAAATCTCAGGAAAAACTGCTGGCTCCGTCTGCT
CCGACCCTGACCCTGGCTAAATTCAACCAGGTTACCGTTGGTATGACCCGTGCTCAGGTTCTGG
CTACCGTTGGTCAGGGTTCTTGCACCACCTGGTCTGAATACTACCCGGCTTACCCGTCTACCGC
TGGTGTTACCCTGTCTCTGTCTTGCTTCGACGTTGACGGTTACTCTTCTACCGGTTTCTACCGT
GGTTCTGCTCACCTGTGGTTCACCGACGGTGTTCTGCAGGGTAAACGTCAGTGGGACCTGGTTG
GTGGTCTCGGTGGTTGGTCTCACCCGCAGTTCGAAAAA

Protein

MASIQHFRVALIPFFAAFCLPVFAAHHHHHHHHLVPRGSHPETLVKVKDAEDQLGARVGYIELD
LNSGKILESFRPEERFPMMSTFKVLLCGAVLSRVDAGQEQLGRRIHYSQNDLVDYSPVTEKHLT
DGMTVRELCSAAITMSDNTAANLLLTTIGGPKELTAFLHNMGDHVTRLDRWEPELNEAIPNDER
DTTMPAAMATTLRKLLTGELLTLASRQQLIDWMEADKVAGPLLRSALPAGWFIADKSGAGERGS
RGIIAALGPDGKPSRIVVIYTTGSQATMDERNRQIAEIGASLIKHWTSDVQLVESGGGSVQAGG
SLRLSCAASGYIASINYLGWFRQAPGKEREGVAAVSPAGGTPYYADSVKGRFTVSLDNAENTVY
LQMNSLKPEDTALYYCAAARQGWYIPLNSYGYNYWAQGTQVTVSSVDGSGGSGGSGGSGGSGGS
GGSGASDVQLVESGGGSVQAGGSLRLSCAASGYIASINYLGWFRQAPGKEREGVAAVSPAGGTP

YYADSVKGRFTVSLDNAENTVYLQMNSLKPEDTALYYCAAARQGWYIPLNSYGYNYWAQGTQVT
VSSAAAAGVMTGAKFTQIQFGMTRQQVLDIAGAENCATGGSFGDSIHCRGHAAGDYYAYATFGF
TSAAADAKVDSKSQEKLLAPSAPTLTLAKFNQVTVGMTRAQVLATVGQGSCTTWSEYYPAYPST
AGVTLSLSCFDVDGYSSTGFYRGSAHLWFTDGVLQGKRQWDLVGGLGGWSHPQFEK

HEL 6:

DNA

ATGGCTTCTATCCAGCACTTCCGTGTTGCTCTGATCCCGTTCTTCGCTGCTTTCTGCCTGCCGG
TTTTCGCTGCTCACCACCACCACCACCACCACCACCTGGTTCCGCGTGGTTCTCACCCGGAAAC
CCTGGTTAAAGTTAAAGACGCTGAAGACCAGCTGGGTGCTCGTGTTGGTTACATCGAACTGGAC
CTGAACTCTGGTAAAATCCTGGAATCTTTCCGTCCGGAGGAGAGGTTCCCGATGATGTCTACCT
TCAAAGTTCTGCTGTGCGGTGCTGTTCTGTCTCGTGTTGACGCTGGTCAGGAACAGCTGGGTCG
TCGTATCCACTACTCTCAGAACGACCTGGTTGACTACTCTCCGGTTACCGAAAAACACCTGACC
GACGGTATGACCGTTCGTGAACTGTGCTCTGCTGCTATCACCATGTCTGACAACACCGCTGCTA
ACCTGCTGCTGACCACCATCGGTGGTCCGAAAGAACTCACTGCGTTCCTGCACAACATGGGTGA
CCACGTTACCCGTCTGGACCGTTGGGAACCGGAACTGAACGAAGCTATCCCGAACGACGAACGT
GACACCACCATGCCGGCTGCTATGGCTACCACCCTGCGTAAACTGCTGACCGGTGAACTGCTGA
CCCTGGCTTCTCGTCAGCAGCTGATCGACTGGATGGAAGCTGACAAAGTTGCTGGTCCGCTGCT
GCGTTCTGCTCTGCCGGCTGGTTGGTTCATCGCTGACAAATCTGGTGCTGGTGAACGTGGTTCT
CGTGGTATCATCGCTGCTCTGGGTCCGGACGGTAAACCGTCTCGTATCGTTGTTATCTACACCA
CCGGTTCTCAGGCTACTATGGACGAACGTAACCGTCAGATCGCTGAAATCGGTGCTTCTCTGAT
CAAACACTGGACTAGTATGTGCAGCTGGTGGAAAGCGGCGGCGGCAGCGTGCAGGCGGGCGGCA
GCCTGCGCCTGAGCTGCGCGGCGAGCGGCTATATTGCGAGCATTAACTATCTGGGCTGGTTTCG
CCAGGCGCCGGGCAAAGAACGCGAAGGCGTGGCGGCGGTGAGCCCGGCGGGCGGCACCCCGTAT
TATGCGGATAGCGTGAAAGGCCGCTTTACCGTGAGCCTGGATAACGCGGAAAACACCGTGTATC
TGCAGATGAACAGCCTGAAACCGGAAGATACCGCGCTGTATTATTGCGCGGCGGCGCGCCAGGG
CTGGTATATTCCGCTGAACAGCTATGGCTATAACTATTGGGCGCAGGGCACCCAGGTGACCGTG
AGCAGCGTCGACGGGTCCGGCGGTTCAGGCGGCTCTGGTGGCTCCGGTGGGTCAGGTGGTTCTG
GCGGGTCTGGCGGGTCCGGCGGTTCAGGCGGCTCTGGTGGCTCCGGTGGGTCAGGTGGTTCTGG
CGGGTCTGGCGGGTCCGGCGGTTCAGGCGGCTCTGGTGGCTCCGGTGGGTCAGGTGGTTCTGGC
GCTAGCGCGCGCGTGGATCAGACCCCGCGCAGCGTGACCAAAGAAACCGGCGAAAGCCTGACCA
TTAACTGCGTGCTGCGCGATGCGAGCTATGCGCTGGGCAGCACCTGCTGGTATCGCAAAAAAAG
CGGCGAAGGCAACGAAGAAAGCATTAGCAAAGGCGGGCGCTATGTGGAAACCGTGAACAGCGGC
AGCAAAAGCTTTAGCCTGCGCATTAACGATCTGACCGTGGAAGATGGCGGCACCTATCGCTGCG
GCCTGGGCGTGGCGGGCGGCTATTGCGATTATGCGCTGTGCAGCAGCCGCTATGCGGAATGCGG
CGATGGCACCGCGGTGACCGTGAACGCGGCCGCTGCTGGTGTTATGACCGGTGCTAAATTCACC
CAGATCCAGTTCGGTATGACCCGTCAGCAGGTTCTGGACATCGCTGGTGCTGAAAACTGCGCTA
CTGGCGGTAGCTTCGGTGACTCTATACACTGCCGTGGTCACGCTGCTGGTGACTACTACGCTTA
CGCTACCTTCGGTTTCACCTCTGCTGCTGCTGACGCTAAAGTTGACTCTAAATCTCAGGAAAAA
CTGCTGGCTCCGTCTGCTCCGACCCTGACCCTGGCTAAATTCAACCAGGTTACCGTTGGTATGA
CCCGTGCTCAGGTTCTGGCTACCGTTGGTCAGGGTTCTTGCACCACCTGGTCTGAATACTACCC
GGCTTACCCGTCTACCGCTGGTGTTACCCTGTCTCTGTCTTGCTTCGACGTTGACGGTTACTCT
TCTACCGGTTTCTACCGTGGTTCTGCTCACCTGTGGTTCACCGACGGTGTTCTGCAGGGTAAAC
GTCAGTGGGACCTGGTTGGTGGTCTCGGTGGTTGGTCTCACCCGCAGTTCGAAAAA

Protein

MASIQHFRVALIPFFAAFCLPVFAAHHHHHHHHHLVPRGSHPETLVKVKDAEDQLGARVGYIELD
LNSGKILESFRPEERFPMMSTFKVLLCGAVLSRVDAGQEQLGRRIHYSQNDLVDYSPVTEKHLT
DGMTVRELCSAAITMSDNTAANLLLTTIGGPKELTAFLHNMGDHVTRLDRWEPELNEAIPNDER
DTTMPAAMATTLRKLLTGELLTLASRQQLIDWMEADKVAGPLLRSALPAGWFIADKSGAGERGS
RGIIAALGPDGKPSRIVVIYTTGSQATMDERNRQIAEIGASLIKHWTSDVQLVESGGGSVQAGG
SLRLSCAASGYIASINYLGWFRQAPGKEREGVAAVSPAGGTPYYADSVKGRFTVSLDNAENTVY

LQMNSLKPEDTALYYCAAARQGWYIPLNSYGYNYWAQGTQVTVSSVDGSGGSGGSGGSGGSGGS
GGSGGSGGSGGSGGSGGSGGSGGSGGSGGSGGSGGSGGSGGSGASARVDQTPRSVTKETGESLT
INCVLRDASYALGSTCWYRKKSGEGNEESISKGGRYVETVNSGSKSFSLRINDLTVEDGGTYRC
GLGVAGGYCDYALCSSRYAECGDGTAVTVNAAAAGVMTGAKFTQIQFGMTRQQVLDIAGAENCA
TGGSFGDSIHCRGHAAGDYYAYATFGFTSAAADAKVDSKSQEKLLAPSAPTLTLAKFNQVTVGM
TRAQVLATVGQGSCTTWSEYYPAYPSTAGVTLSLSCFDVDGYSSTGFYRGSAHLWFTDGVLQGK
RQWDLVGGLGGWSHPQFEK

HEL 7:

DNA

ATGGCTTCTATCCAGCACTTCCGTGTTGCTCTGATCCCGTTCTTCGCTGCTTTCTGCCTGCCGG
TTTTCGCTGCTCACCACCACCACCACCACCACCACCTGGTTCCGCGTGGTTCTCACCCGGAAAC
CCTGGTTAAAGTTAAAGACGCTGAAGACCAGCTGGGTGCTCGTGTTGGTTACATCGAACTGGAC
CTGAACTCTGGTAAAATCCTGGAATCTTTCCGTCCGGAGGAGAGGTTCCCGATGATGTCTACCT
TCAAAGTTCTGCTGTGCGGTGCTGTTCTGTCTCGTGTTGACGCTGGTCAGGAACAGCTGGGTCG
TCGTATCCACTACTCTCAGAACGACCTGGTTGACTACTCTCCGGTTACCGAAAAACACCTGACC
GACGGTATGACCGTTCGTGAACTGTGCTCTGCTGCTATCACCATGTCTGACAACACCGCTGCTA
ACCTGCTGCTGACCACCATCGGTGGTCCGAAAGAACTCACTGCGTTCCTGCACAACATGGGTGA
CCACGTTACCCGTCTGGACCGTTGGGAACCGGAACTGAACGAAGCTATCCCGAACGACGAACGT
GACACCACCATGCCGGCTGCTATGGCTACCACCCTGCGTAAACTGCTGACCGGTGAACTGCTGA
CCCTGGCTTCTCGTCAGCAGCTGATCGACTGGATGGAAGCTGACAAAGTTGCTGGTCCGCTGCT
GCGTTCTGCTCTGCCGGCTGGTTGGTTCATCGCTGACAAATCTGGTGCTGGTGAACGTGGTTCT
CGTGGTATCATCGCTGCTCTGGGTCCGGACGGTAAACCGTCTCGTATCGTTGTTATCTACACCA
CCGGTTCTCAGGCTACTATGGACGAACGTAACCGTCAGATCGCTGAAATCGGTGCTTCTCTGAT
CAAACACTGGACTAGTATGTGCAGCTGGTGGAAAGCGGCGGCGGCAGCGTGCAGGCGGGCGGCA
GCCTGCGCCTGAGCTGCGCGGCGAGCGGCTATATTGCGAGCATTAACTATCTGGGCTGGTTTCG
CCAGGCGCCGGGCAAAGAACGCGAAGGCGTGGCGGCGGTGAGCCCGGCGGGCGGCACCCCGTAT
TATGCGGATAGCGTGAAAGGCCGCTTTACCGTGAGCCTGGATAACGCGGAAAACACCGTGTATC
TGCAGATGAACAGCCTGAAACCGGAAGATACCGCGCTGTATTATTGCGCGGCGGCGCGCCAGGG
CTGGTATATTCCGCTGAACAGCTATGGCTATAACTATTGGGCGCAGGGCACCCAGGTGACCGTG
AGCAGCGTCGACGGGTCCGGCGGTTCAGGCGGCTCTGGTGCTAGCGCGCGCGTGGATCAGACCC
CGCGCAGCGTGACCAAAGAAACCGGCGAAAGCCTGACCATTAACTGCGTGCTGCGCGATGCGAG
CTATGCGCTGGGCAGCACCTGCTGGTATCGCAAAAAAAGCGGCGAAGGCAACGAAGAAAGCATT
AGCAAAGGCGGGCGCTATGTGGAAACCGTGAACAGCGGCAGCAAAAGCTTTAGCCTGCGCATTA
ACGATCTGACCGTGGAAGATGGCGGCACCTATCGCTGCGGCCTGGGCGTGGCGGGCGGCTATTG
CGATTATGCGCTGTGCAGCAGCCGCTATGCGGAATGCGGCGATGGCACCGCGGTGACCGTGAAC
GCGGCCGCTGCTGGTGTTATGACCGGTGCTAAATTCACCCAGATCCAGTTCGGTATGACCCGTC
AGCAGGTTCTGGACATCGCTGGTGCTGAAAACTGCGCTACTGGCGGTAGCTTCGGTGACTCTAT
ACACTGCCGTGGTCACGCTGCTGGTGACTACTACGCTTACGCTACCTTCGGTTTCACCTCTGCT
GCTGCTGACGCTAAAGTTGACTCTAAATCTCAGGAAAAACTGCTGGCTCCGTCTGCTCCGACCC
TGACCCTGGCTAAATTCAACCAGGTTACCGTTGGTATGACCCGTGCTCAGGTTCTGGCTACCGT
TGGTCAGGGTTCTTGCACCACCTGGTCTGAATACTACCCGGCTTACCCGTCTACCGCTGGTGTT
ACCCTGTCTCTGTCTTGCTTCGACGTTGACGGTTACTCTTCTACCGGTTTCTACCGTGGTTCTG
CTCACCTGTGGTTCACCGACGGTGTTCTGCAGGGTAAACGTCAGTGGGACCTGGTTGGTGGTCT
CGGTGGTTGGTCTCACCCGCAGTTCGAAAAA

Protein

MASIQHFRVALIPFFAAFCLPVFAAHHHHHHHHHLVPRGSHPETLVKVKDAEDQLGARVGYIELD
LNSGKILESFRPEERFPMMSTFKVLLCGAVLSRVDAGQEQLGRRIHYSQNDLVDYSPVTEKHLT
DGMTVRELCSAAITMSDNTAANLLLTTIGGPKELTAFLHNMGDHVTRLDRWEPELNEAIPNDER
DTTMPAAMATTLRKLLTGELLTLASRQQLIDWMEADKVAGPLLRSALPAGWFIADKSGAGERGS
RGIIAALGPDGKPSRIVVIYTTGSQATMDERNRQIAEIGASLIKHWTSDVQLVESGGGSVQAGG

SLRLSCAASGYIASINYLGWFRQAPGKEREGVAAVSPAGGTPYYADSVKGRFTVSLDNAENTVY
LQMNSLKPEDTALYYCAAARQGWYIPLNSYGYNYWAQGTQVTVSSVDGSGGSGGSGASARVDQT
PRSVTKETGESLTINCVLRDASYALGSTCWYRKKSGEGNEESISKGGRYVETVNSGSKSFSLRI
NDLTVEDGGTYRCGLGVAGGYCDYALCSSRYAECGDGTAVTVNAAAAGVMTGAKFTQIQFGMTR
QQVLDIAGAENCATGGSFGDSIHCRGHAAGDYYAYATFGFTSAAADAKVDSKSQEKLLAPSAPT
LTLAKFNQVTVGMTRAQVLATVGQGSCTTWSEYYPAYPSTAGVTLSLSCFDVDGYSSTGFYRGS
AHLWFTDGVLQGKRQWDLVGGLGGWSHPQFEK

PCT 1:

DNA

ATGGCTTCTATCCAGCACTTCCGTGTTGCTCTGATCCCGTTCTTCGCTGCTTTCTGCCTGCCGG
TTTTCGCTGCTCACCACCACCACCACCACCACCACCTGGTTCCGCGTGGTTCTCACCCGGAAAC
CCTGGTTAAAGTTAAAGACGCTGAAGACCAGCTGGGTGCTCGTGTTGGTTACATCGAACTGGAC
CTGAACTCTGGTAAAATCCTGGAATCTTTCCGTCCGGAGGAGAGGTTCCCGATGATGTCTACCT
TCAAAGTTCTGCTGTGCGGTGCTGTTCTGTCTCGTGTTGACGCTGGTCAGGAACAGCTGGGTCG
TCGTATCCACTACTCTCAGAACGACCTGGTTGACTACTCTCCGGTTACCGAAAAACACCTGACC
GACGGTATGACCGTTCGTGAACTGTGCTCTGCTGCTATCACCATGTCTGACAACACCGCTGCTA
ACCTGCTGCTGACCACCATCGGTGGTCCGAAAGAACTCACTGCGTTCCTGCACAACATGGGTGA
CCACGTTACCCGTCTGGACCGTTGGGAACCGGAACTGAACGAAGCTATCCCGAACGACGAACGT
GACACCACCATGCCGGCTGCTATGGCTACCACCCTGCGTAAACTGCTGACCGGTGAACTGCTGA
CCCTGGCTTCTCGTCAGCAGCTGATCGACTGGATGGAAGCTGACAAAGTTGCTGGTCCGCTGCT
GCGTTCTGCTCTGCCGGCTGGTTGGTTCATCGCTGACAAATCTGGTGCTGGTGAACGTGGTTCT
CGTGGTATCATCGCTGCTCTGGGTCCGGACGGTAAACCGTCTCGTATCGTTGTTATCTACACCA
CCGGTTCTCAGGCTACTATGGACGAACGTAACCGTCAGATCGCTGAAATCGGTGCTTCTCTGAT
CAAACACTGGACTAGTCAGGTGCAGCTTCAAGAGAGCGGGGGAGGTTCCGTTCAGGCCGGTGGA
TCCCTTCGCCTTTCGTGTGCGGCATCGACATCCAGTAATGTGAATGTATGTATGGGTTGGTTTC
GTCAAGCACCAGGAAAAGAACGTGAGGGCGTGGCTGTAATTGCTCGCGACTCCGAGACCAACTA
CGCTGCATCAGTGAAGGGACGCTTCACTATCTCTCAAGATAACGCAAAAAACACTTTGTACTTA
CAACTTAATTCCTTGAAACCAGAGGACACTGCAATGTACTACTGTGCCGCAGGACCCTGTGCGA
ATATTCGCGGCTCGTGGTCTAACTCACGCTTATTGCGCTATAATTTCTGGGGGCAAGGAACACA
AGTTACCGTGTCGAGCGTCGACGGGTCCGGCGGTTCAGGCGGCTCTGGTGGCTCCGGTGGGTCA
GGTGGTTCTGGCGGGTCTGGCGCTAGCCAGGTACAGTTGCAAGAGTCTGGGGGAGGTTCGGTTC
AAGTTCAAGTTGGCGGCAGTTTACGCCTTTCCTGTGCTGCTTCAGGTTATACATATAGCAGCGC
GTGTATGGGATGGTTTCGTCAAGCACCGGGTAAGGAGCGTGAATGGGTGGGGAGCATTGTGTCC
GATTCCGACGATCGCACGAACTATGCTGATGCCGTTAAAGGGCGCTTCACTATCACACAAGACA
ATGCAAAAAACACCGTATATTTACAAATGAACAGCCTGAAACCCGAGGATACCGCCATGTATTA
TTGTGCGGCCCGTCCAGGGAACTGCTTTATTGCCACCAAAACCCGTCGTTATGATTACTGGGGG
CAGGGTACGCAAGTCACGGTGTCGAGCGCGGCCGCTGCTGGTGTTATGACCGGTGCTAAATTCA
CCCAGATCCAGTTCGGTATGACCCGTCAGCAGGTTCTGGACATCGCTGGTGCTGAAAACTGCGC
TACTGGCGGTAGCTTCGGTGACTCTATACACTGCCGTGGTCACGCTGCTGGTGACTACTACGCT
TACGCTACCTTCGGTTTCACCTCTGCTGCTGCTGACGCTAAAGTTGACTCTAAATCTCAGGAAA
AACTGCTGGCTCCGTCTGCTCCGACCCTGACCCTGGCTAAATTCAACCAGGTTACCGTTGGTAT
GACCCGTGCTCAGGTTCTGGCTACCGTTGGTCAGGGTTCTTGCACCACCTGGTCTGAATACTAC
CCGGCTTACCCGTCTACCGCTGGTGTTACCCTGTCTCTGTCTTGCTTCGACGTTGACGGTTACT
CTTCTACCGGTTTCTACCGTGGTTCTGCTCACCTGTGGTTCACCGACGGTGTTCTGCAGGGTAA
ACGTCAGTGGGACCTGGTTGGTGGTCTCGGTGGTTGGTCTCACCCGCAGTTCGAAAAA

Protein

MASIQHFRVALIPFFAAFCLPVFAAHHHHHHHHLVPRGSHPETLVKVKDAEDQLGARVGYIELD
LNSGKILESFRPEERFPMMSTFKVLLCGAVLSRVDAGQEQLGRRIHYSQNDLVDYSPVTEKHLT

DGMTVRELCSAAITMSDNTAANLLLTTIGGPKELTAFLHNMGDHVTRLDRWEPELNEAIPNDER
DTTMPAAMATTLRKLLTGELLTLASRQQLIDWMEADKVAGPLLRSALPAGWFIADKSGAGERGS
RGIIAALGPDGKPSRIVVIYTTGSQATMDERNRQIAEIGASLIKHWTSQVQLQESGGGSVQAGG
SLRLSCAASTSSNVNVCMGWFRQAPGKEREGVAVIARDSETNYAASVKGRFTISQDNAKNTLYL
QLNSLKPEDTAMYYCAAGPCANIRGSWSNSRLLRYNFWGQGTQVTVSSVDGSGGSGGSGGSGGS
GGSGGSGASQVQLQESGGGSVQVQVGGSLRLSCAASGYTYSSACMGWFRQAPGKEREWVGSIVS
DSDDRTNYADAVKGRFTITQDNAKNTVYLQMNSLKPEDTAMYYCAARPGNCFIATKTRRYDYWG
QGTQVTVSSAAAAGVMTGAKFTQIQFGMTRQQVLDIAGAENCATGGSFGDSIHCRGHAAGDYYA
YATFGFTSAAADAKVDSKSQEKLLAPSAPTLTLAKFNQVTVGMTRAQVLATVGQGSCTTWSEYY
PAYPSTAGVTLSLSCFDVDGYSSTGFYRGSAHLWFTDGVLQGKRQWDLVGGLGGWSHPQFEK

PCT 2:

DNA

ATGGCTTCTATCCAGCACTTCCGTGTTGCTCTGATCCCGTTCTTCGCTGCTTTCTGCCTGCCGG
TTTTCGCTGCTCACCACCACCACCACCACCACCACCTGGTTCCGCGTGGTTCTCACCCGGAAAC
CCTGGTTAAAGTTAAAGACGCTGAAGACCAGCTGGGTGCTCGTGTTGGTTACATCGAACTGGAC
CTGAACTCTGGTAAAATCCTGGAATCTTTCCGTCCGGAGGAGAGGTTCCCGATGATGTCTACCT
TCAAAGTTCTGCTGTGCGGTGCTGTTCTGTCTCGTGTTGACGCTGGTCAGGAACAGCTGGGTCG
TCGTATCCACTACTCTCAGAACGACCTGGTTGACTACTCTCCGGTTACCGAAAAACACCTGACC
GACGGTATGACCGTTCGTGAACTGTGCTCTGCTGCTATCACCATGTCTGACAACACCGCTGCTA
ACCTGCTGCTGACCACCATCGGTGGTCCGAAAGAACTCACTGCGTTCCTGCACAACATGGGTGA
CCACGTTACCCGTCTGGACCGTTGGGAACCGGAACTGAACGAAGCTATCCCGAACGACGAACGT
GACACCACCATGCCGGCTGCTATGGCTACCACCCTGCGTAAACTGCTGACCGGTGAACTGCTGA
CCCTGGCTTCTCGTCAGCAGCTGATCGACTGGATGGAAGCTGACAAAGTTGCTGGTCCGCTGCT
GCGTTCTGCTCTGCCGGCTGGTTGGTTCATCGCTGACAAATCTGGTGCTGGTGAACGTGGTTCT
CGTGGTATCATCGCTGCTCTGGGTCCGGACGGTAAACCGTCTCGTATCGTTGTTATCTACACCA
CCGGTTCTCAGGCTACTATGGACGAACGTAACCGTCAGATCGCTGAAATCGGTGCTTCTCTGAT
CAAACACTGGACTAGTCCAGGTACAGTTGCAAGAGTCTGGGGGAGGTTCGGTTCAAGTTCAAGT
TGGCGGCAGTTTACGCCTTTCCTGTGCTGCTTCAGGTTATACATATAGCAGCGCGTGTATGGGA
TGGTTTCGTCAAGCACCGGGTAAGGAGCGTGAATGGGTGGGGAGCATTGTGTCCGATTCCGACG
ATCGCACGAACTATGCTGATGCCGTTAAAGGGCGCTTCACTATCACACAAGACAATGCAAAAAA
CACCGTATATTTACAAATGAACAGCCTGAAACCCGAGGATACCGCCATGTATTATTGTGCGGCC
CGTCCAGGGAACTGCTTTATTGCCACCAAAACCCGTCGTTATGATTACTGGGGGCAGGGTACGC
AAGTCACGGTGTCGAGCGTCGACGGGTCCGGCGGTTCAGGCGGCTCTGGTGGCTCCGGTGGGTC
AGGTGGTTCTGGCGGGTCTGGCGCTAGCCAGGTGCAGCTTCAAGAGAGCGGGGGAGGTTCCGTT
CAGGCCGGTGGATCCCTTCGCCTTTCGTGTGCGGCATCGACATCCAGTAATGTGAATGTATGTA
TGGGTTGGTTTCGTCAAGCACCAGGAAAAGAACGTGAGGGCGTGGCTGTAATTGCTCGCGACTC
CGAGACCAACTACGCTGCATCAGTGAAGGGACGCTTCACTATCTCTCAAGATAACGCAAAAAAC
ACTTTGTACTTACAACTTAATTCCTTGAAACCAGAGGACACTGCAATGTACTACTGTGCCGCAG
GACCCTGTGCGAATATTCGCGGCTCGTGGTCTAACTCACGCTTATTGCGCTATAATTTCTGGGG
GCAAGGAACACAAGTTACCGTGTCGAGCGCGGCCGCTGCTGGTGTTATGACCGGTGCTAAATTC
ACCCAGATCCAGTTCGGTATGACCCGTCAGCAGGTTCTGGACATCGCTGGTGCTGAAAACTGCG
CTACTGGCGGTAGCTTCGGTGACTCTATACACTGCCGTGGTCACGCTGCTGGTGACTACTACGC
TTACGCTACCTTCGGTTTCACCTCTGCTGCTGCTGACGCTAAAGTTGACTCTAAATCTCAGGAA
AAACTGCTGGCTCCGTCTGCTCCGACCCTGACCCTGGCTAAATTCAACCAGGTTACCGTTGGTA
TGACCCGTGCTCAGGTTCTGGCTACCGTTGGTCAGGGTTCTTGCACCACCTGGTCTGAATACTA
CCCGGCTTACCCGTCTACCGCTGGTGTTACCCTGTCTCTGTCTTGCTTCGACGTTGACGGTTAC
TCTTCTACCGGTTTCTACCGTGGTTCTGCTCACCTGTGGTTCACCGACGGTGTTCTGCAGGGTA
AACGTCAGTGGGACCTGGTTGGTGGTCTCGGTGGTTGGTCTCACCCGCAGTTCGAAAAA

Protein

MASIQHFRVALIPFFAAFCLPVFAAHHHHHHHHLVPRGSHPETLVKVKDAEDQLGARVGYIELD
LNSGKILESFRPEERFPMMSTFKVLLCGAVLSRVDAGQEQLGRRIHYSQNDLVDYSPVTEKHLT
DGMTVRELCSAAITMSDNTAANLLLTTIGGPKELTAFLHNMGDHVTRLDRWEPELNEAIPNDER
DTTMPAAMATTLRKLLTGELLTLASRQQLIDWMEADKVAGPLLRSALPAGWFIADKSGAGERGS
RGIIAALGPDGKPSRIVVIYTTGSQATMDERNRQIAEIGASLIKHWTSQVQLQESGGGSVQVQV
GGSLRLSCAASGYTYSSACMGWFRQAPGKEREWVGSIVSDSDDRTNYADAVKGRFTITQDNAKN
TVYLQMNSLKPEDTAMYYCAARPGNCFIATKTRRYDYWGQGTQVTVSSVDGSGGSGGSGGSGGS
GGSGGSGASQVQLQESGGGSVQAGGSLRLSCAASTSSNVNVCMGWFRQAPGKEREGVAVIARDS
ETNYAASVKGRFTISQDNAKNTLYLQLNSLKPEDTAMYYCAAGPCANIRGSWSNSRLLRYNFWG
QGTQVTVSSAAAAGVMTGAKFTQIQFGMTRQQVLDIAGAENCATGGSFGDSIHCRGHAAGDYYA
YATFGFTSAAADAKVDSKSQEKLLAPSAPTLTLAKFNQVTVGMTRAQVLATVGQGSCTTWSEYY
PAYPSTAGVTLSLSCFDVDGYSSTGFYRGSAHLWFTDGVLQGKRQWDLVGGLGGWSHPQFEK

E37F:

DNA

ATGGCTTCTATCCAGCACTTCCGTGTTGCTCTGATCCCGTTCTTCGCTGCTTTCTGCCTGCCGG
TTTTCGCTGCTCACCACCACCACCACCACCACCACCTGGTTCCGCGTGGTTCTCACCCGGAAAC
CCTGGTTAAAGTTAAAGACGCTGAAGACCAGCTGGGTGCTCGTGTTGGTTACATCGAACTGGAC
CTGAACTCTGGTAAAATCCTGGAATCTTTCCGTCCGGAGGAGAGGTTCCCGATGATGTCTACCT
TCAAAGTTCTGCTGTGCGGTGCTGTTCTGTCTCGTGTTGACGCTGGTCAGGAACAGCTGGGTCG
TCGTATCCACTACTCTCAGAACGACCTGGTTGACTACTCTCCGGTTACCGAAAAACACCTGACC
GACGGTATGACCGTTCGTGAACTGTGCTCTGCTGCTATCACCATGTCTGACAACACCGCTGCTA
ACCTGCTGCTGACCACCATCGGTGGTCCGAAAGAACTCACTGCGTTCCTGCACAACATGGGTGA
CCACGTTACCCGTCTGGACCGTTGGGAACCGGAACTGAACGAAGCTATCCCGAACGACGAACGT
GACACCACCATGCCGGCTGCTATGGCTACCACCCTGCGTAAACTGCTGACCGGTGAACTGCTGA
CCCTGGCTTCTCGTCAGCAGCTGATCGACTGGATGGAAGCTGACAAAGTTGCTGGTCCGCTGCT
GCGTTCTGCTCTGCCGGCTGGTTGGTTCATCGCTGACAAATCTGGTGCTGGTGAACGTGGTTCT
CGTGGTATCATCGCTGCTCTGGGTCCGGACGGTAAACCGTCTCGTATCGTTGTTATCTACACCA
CCGGTTCTCAGGCTACTATGGACGAACGTAACCGTCAGATCGCTGAAATCGGTGCTTCTCTGAT
CAAACACTGGACTAGTCAGGTGCAACTGGTTGAAAGCGGTGGCGGTCTGGTGCAAACCGGCGGT
AGCCTGCGTCTGAGCTGCGCGAGCAGCGGTAGCATTGCGGGTTTCGAAACCGTGACCTGGAGCC
GTCAGGCGCCGGGCAAGAGCCTGCAATGGGTTGCGAGCATGACCAAAACCAACAACGAAATTTA
CAGCGACAGCGTTAAGGGTCGTTTCATCATTAGCCGTGATAACGCGAAAAACACCGTGTACCTG
CAGATGAACAGCCTGAAGCCGGAGGACACCGGCGTTTATTTTTGCAAAGGTCCGGAACTGCGTG
GCCAGGGTATTCAGGTGACCGTTAGCAGCGTCGACGGGTCCGGCGGTTCAGGCGGCTCTGGTGG
CTCCGGTGGGTCAGGTGGTTCTGGCGGGTCTGGCGGGTCCGGCGGTTCAGGCGGCTCTGGTGGC
TCCGGTGGGTCAGGTGGTTCTGGCGGGTCTGGCGGGTCCGGCGGTTCAGGCGGCTCTGGTGGCT
CCGGTGGGTCAGGTGGTTCTGGCGCTAGCCAGGTGCAACTGGTTGAGAGCGGTGGCGGTCTGGT
GGAAGCGGGCGGTAGCCTGCGTCTGAGCTGCGTGGTTACCGGCAGCAGCTTTAGCACCAGCACG
ATGGCGTGGTACCGTCAGCCGCCGGGCAAGCAACGTGAATGGGTGGCGAGCTTCACCAGCGGCG
GTGCGATCAAGTACACCGACAGCGTTAAAGGTCGTTTTACCATGAGCCGTGATAACGCGAAGAA
AATGACCTATCTGCAGATGGAGAACCTGAAACCGGAAGACACCGCGGTGTACTATTGCGCGCTG
CATAACGCGGTTAGCGGTAGCAGCTGGGGTCGTGGTACCCAAGTGACCGTTAGCAGCGCGGCCG
CTGCTGGTGTTATGACCGGTGCTAAATTCACCCAGATCCAGTTCGGTATGACCCGTCAGCAGGT
TCTGGACATCGCTGGTGCTGAAAACTGCGCTACTGGCGGTAGCTTCGGTGACTCTATACACTGC
CGTGGTCACGCTGCTGGTGACTACTACGCTTACGCTACCTTCGGTTTCACCTCTGCTGCTGCTG
ACGCTAAAGTTGACTCTAAATCTCAGGAAAAACTGCTGGCTCCGTCTGCTCCGACCCTGACCCT
GGCTAAATTCAACCAGGTTACCGTTGGTATGACCCGTGCTCAGGTTCTGGCTACCGTTGGTCAG
GGTTCTTGCACCACCTGGTCTGAATACTACCCGGCTTACCCGTCTACCGCTGGTGTTACCCTGT
CTCTGTCTTGCTTCGACGTTGACGGTTACTCTTCTACCGGTTTCTACCGTGGTTCTGCTCACCT
GTGGTTCACCGACGGTGTTCTGCAGGGTAAACGTCAGTGGGACCTGGTTGGTGGTCTCGGTGGT
TGGTCTCACCCGCAGTTCGAAAAA

Protein

MASIQHFRVALIPFFAAFCLPVFAAHHHHHHHHLVPRGSHPETLVKVKDAEDQLGARVGYIELD
LNSGKILESFRPEERFPMMSTFKVLLCGAVLSRVDAGQEQLGRRIHYSQNDLVDYSPVTEKHLT
DGMTVRELCSAAITMSDNTAANLLLTTIGGPKELTAFLHNMGDHVTRLDRWEPELNEAIPNDER
DTTMPAAMATTLRKLLTGELLTLASRQQLIDWMEADKVAGPLLRSALPAGWFIADKSGAGERGS
RGIIAALGPDGKPSRIVVIYTTGSQATMDERNRQIAEIGASLIKHWTSQVQLVESGGGLVQTGG
SLRLSCASSGSIAGFETVTWSRQAPGKSLQWVASMTKTNNEIYSDSVKGRFIISRDNAKNTVYL
QMNSLKPEDTGVYFCKGPELRGQGIQVTVSSVDGSGGSGGSGGSGGSGGSGGSGGSGGSGG
SGGSGGSGGSGGSGGSGGSGGSGGSGGSGGSGASQVQLVESGGGLVEAGGSLRLSCVVTGSSFSTST
MAWYRQPPGKQREWVASFTSGGAIKYTDSVKGRFTMSRDNAKKMTYLQMENLKPEDTAVYYCAL
HNAVSGSSWGRGTQVTVSSAAAAGVMTGAKFTQIQFGMTRQQVLDIAGAENCATGGSFGDSIHC
RGHAAGDYYAYATFGFTSAAADAKVDSKSQEKLLAPSAPTLTLAKFNQVTVGMTRAQVLATVGQ
GSCTTWSEYYPAYPSTAGVTLSLSCFDVDGYSSTGFYRGSAHLWFTDGVLQGKRQWDLVGGLGG
WSHPQFEK

Nanobody NanoBiT constructs:

Blue – Nanobody

Red – LargeBiT

Purple – SmallBiT101

Green – Polypeptide linker

Orange – His-tag

LgBit-GSG$_7$-5A7

Protein

MAASVFTLEDFVGDWEQTAAYNLDQVLDQGGVSSLLQNLAVSVTPIQRIVRSGENALKIDIHVI
IPYEGLSADQMAQIEEVFKVVYPVDDHHFKVILPYGTLVIDGVTPNMLNYFGRPYEGIAVFDGK
KITVTGTLWNGNKIIDERLITPDGSMLFRVTINSAAAGSGGSGGSGGSGGSGGSGGSGTSAARV
DQTPRSVTKETGESLTINCVLRDASYALGSTCWYRKKSGEGNEESISKGGRYVETVNSGSKSFS
LRINDLTVEDGGTYRCGLGVAGGYCDYALCSSRYAECGDGTAVTVNVDLEHHHHHH

DNA

ATGGCGGCTAGCGTTTTTACCCTGGAAGATTTCGTGGGCGACTGGGAACAGACCGCGGCGTACA
ACCTGGACCAAGTGCTGGATCAAGGTGGCGTGAGCAGCCTGCTGCAGAACCTGGCGGTGAGCGT
TACCCCGATCCAACGTATTGTTCGTAGCGGCGAGAACGCGCTGAAGATCGACATTCACGTGATC
ATTCCGTACGAAGGCCTGAGCGCGGATCAGATGGCGCAAATCGAGGAAGTGTTCAAGGTGGTTT
ACCCGGTTGACGATCACCACTTTAAAGTGATCCTGCCGTATGGTACCCTGGTGATTGACGGCGT
TACCCCGAACATGCTGAACTACTTCGGTCGTCCGTATGAGGGCATCGCGGTTTTTGATGGTAAG
AAAATTACCGTGACCGGTACCCTGTGGAACGGCAACAAAATTATTGATGAGCGCCTGATTACCC
CGGACGGCAGCATGCTGTTTCGTGTGACCATTAATAGCGCGGCCGCTGGGTCCGGCGGTTCAGG
CGGCTCTGGTGGCTCCGGTGGGTCAGGTGGTTCTGGCGGGTCTGGCACTAGTGCAGCGCGCGTG
GATCAGACCCCGCGCAGCGTGACCAAAGAAACCGGCGAAAGCCTGACCATTAACTGCGTGCTGC
GCGATGCGAGCTATGCGCTGGGCAGCACCTGCTGGTATCGCAAAAAAAGCGGCGAAGGCAACGA
AGAAAGCATTAGCAAAGGCGGGCGCTATGTGGAAACCGTGAACAGCGGCAGCAAAAGCTTTAGC
CTGCGCATTAACGATCTGACCGTGGAAGATGGCGGCACCTATCGCTGCGGCCTGGGCGTGGCGG

GCGGCTATTGCGATTATGCGCTGTGCAGCAGCCGCTATGCGGAATGCGGCGATGGCACCGCGGT
GACCGTGAACGTCGACCTCGAGCACCACCACCACCACCAC

LgBit-GSG$_7$-D2L24

Protein

MAASVFTLEDFVGDWEQTAAYNLDQVLDQGGVSSLLQNLAVSVTPIQRIVRSGENALKIDIHVI
IPYEGLSADQMAQIEEVFKVVYPVDDHHFKVILPYGTLVIDGVTPNMLNYFGRPYEGIAVFDGK
KITVTGTLWNGNKIIDERLITPDGSMLFRVTINSAAAGSGGSGGSGGSGGSGGSGGSGTSADVQ
LVESGGGSVQAGGSLRLSCAASGYIASINYLGWFRQAPGKEREGVAAVSPAGGTPYYADSVKGR
FTVSLDNAENTVYLQMNSLKPEDTALYYCAAARQGWYIPLNSYGYNYWAQGTQVTVSSVDLEHH
HHHH

DNA

ATGGCGGCTAGCGTTTTTACCCTGGAAGATTTCGTGGGCGACTGGGAACAGACCGCGGCGTACA
ACCTGGACCAAGTGCTGGATCAAGGTGGCGTGAGCAGCCTGCTGCAGAACCTGGCGGTGAGCGT
TACCCCGATCCAACGTATTGTTCGTAGCGGCGAGAACGCGCTGAAGATCGACATTCACGTGATC
ATTCCGTACGAAGGCCTGAGCGCGGATCAGATGGCGCAAATCGAGGAAGTGTTCAAGGTGGTTT
ACCCGGTTGACGATCACCACTTTAAAGTGATCCTGCCGTATGGTACCCTGGTGATTGACGGCGT
TACCCCGAACATGCTGAACTACTTCGGTCGTCCGTATGAGGGCATCGCGGTTTTTGATGGTAAG
AAAATTACCGTGACCGGTACCCTGTGGAACGGCAACAAAATTATTGATGAGCGCCTGATTACCC
CGGACGGCAGCATGCTGTTTCGTGTGACCATTAATAGCGCGGCCGCTGGGTCCGGCGGTTCAGG
CGGCTCTGGTGGCTCCGGTGGGTCAGGTGGTTCTGGCGGGTCTGGCACTAGTGCAATGTGCAGC
TGGTGGAAAGCGGCGGCGGCAGCGTGCAGGCGGGCGGCAGCCTGCGCCTGAGCTGCGCGGCGAG
CGGCTATATTGCGAGCATTAACTATCTGGGCTGGTTTCGCCAGGCGCCGGGCAAAGAACGCGAA
GGCGTGGCGGCGGTGAGCCCGGCGGGCGGCACCCCGTATTATGCGGATAGCGTGAAAGGCCGCT
TTACCGTGAGCCTGGATAACGCGGAAAACACCGTGTATCTGCAGATGAACAGCCTGAAACCGGA
AGATACCGCGCTGTATTATTGCGCGGCGGCGCGCCAGGGCTGGTATATTCCGCTGAACAGCTAT
GGCTATAACTATTGGGCGCAGGGCACCCAGGTGACCGTGAGCAGCGTCGACCTCGAGCACCACC
ACCACCACCAC

5A7-GSG$_7$-LgBit

Protein

MAASARVDQTPRSVTKETGESLTINCVLRDASYALGSTCWYRKKSGEGNEESISKGGRYVETVN
SGSKSFSLRINDLTVEDGGTYRCGLGVAGGYCDYALCSSRYAECGDGTAVTVNAAAGSGGSGGS
GGSGGSGGSGGSGTSVFTLEDFVGDWEQTAAYNLDQVLEQGGVSSLLQNLAVSVTPIQRIVRSG
ENALKIDIHVIIPYEGLSADQMAQIEEVFKVVYPVDDHHFKVILPYGTLVIDGVTPNMLNYFGR
PYEGIAVFDGKKITVTGTLWNGNKIIDERLITPDGSMLFRVTINSVDLEHHHHHH

DNA

ATGGCGGCTAGCGCGCGCGTGGATCAGACCCCGCGCAGCGTGACCAAAGAAACCGGCGAAAGCC
TGACCATTAACTGCGTGCTGCGCGATGCGAGCTATGCGCTGGGCAGCACCTGCTGGTATCGCAA
AAAAAGCGGCGAAGGCAACGAAGAAAGCATTAGCAAAGGCGGGCGCTATGTGGAAACCGTGAAC
AGCGGCAGCAAAAGCTTTAGCCTGCGCATTAACGATCTGACCGTGGAAGATGGCGGCACCTATC

GCTGCGGCCTGGGCGTGGCGGGCGGCTATTGCGATTATGCGCTGTGCAGCAGCCGCTATGCGGA
ATGCGGCGATGGCACCGCGGTGACCGTGAACGCGGCCGCTGGGTCCGGCGGTTCAGGCGGCTCT
GGTGGCTCCGGTGGGTCAGGTGGTTCTGGCGGGTCTGGCACTAGTGTTTTTACCCTGGAAGATT
TCGTGGGCGACTGGGAACAGACCGCGGCGTACAACCTGGACCAAGTGCTGGAACAAGGTGGCGT
GAGCAGCCTGCTGCAGAACCTGGCGGTGAGCGTTACCCCGATCCAACGTATTGTTCGTAGCGGC
GAGAACGCGCTGAAGATCGACATTCACGTGATCATTCCGTACGAAGGCCTGAGCGCGGATCAGA
TGGCGCAAATCGAGGAAGTGTTCAAGGTGGTTTACCCGGTTGACGATCACCACTTTAAAGTGAT
CCTGCCGTATGGTACCCTGGTGATTGACGGCGTTACCCCGAACATGCTGAACTACTTCGGTCGT
CCGTATGAGGGCATCGCGGTTTTTGATGGTAAGAAAATTACCGTGACCGGTACCCTGTGGAACG
GCAACAAAATTATTGATGAGCGCCTGATTACCCCGGACGGCAGCATGCTGTTTCGTGTGACCAT
TAATAGCGTCGACCTCGAGCACCACCACCACCACCAT

D2L24-GSG$_7$-LgBit

Protein

MAASDVQLVESGGGSVQAGGSLRLSCAASGYIASINYLGWFRQAPGKEREGVAAVSPAGGTPYY
ADSVKGRFTVSLDNAENTVYLQMNSLKPEDTALYYCAAARQGWYIPLNSYGYNYWAQGTQVTVS
SAAAGSGGSGGSGGSGGSGGSGGSGTSVFTLEDFVGDWEQTAAYNLDQVLEQGGVSSLLQNLAV
SVTPIQRIVRSGENALKIDIHVIIPYEGLSADQMAQIEEVFKVVYPVDDHHFKVILPYGTLVID
GVTPNMLNYFGRPYEGIAVFDGKKITVTGTLWNGNKIIDERLITPDGSMLFRVTINSVDLEHHH
HHH

DNA

ATGGCGGCTAGCATGTGCAGCTGGTGGAAAGCGGCGGCGGCAGCGTGCAGGCGGGCGGCAGCCT
GCGCCTGAGCTGCGCGGCGAGCGGCTATATTGCGAGCATTAACTATCTGGGCTGGTTTCGCCAG
GCGCCGGGCAAAGAACGCGAAGGCGTGGCGGCGGTGAGCCCGGCGGGCGGCACCCCGTATTATG
CGGATAGCGTGAAAGGCCGCTTTACCGTGAGCCTGGATAACGCGGAAAACACCGTGTATCTGCA
GATGAACAGCCTGAAACCGGAAGATACCGCGCTGTATTATTGCGCGGCGGCGCGCCAGGGCTGG
TATATTCCGCTGAACAGCTATGGCTATAACTATTGGGCGCAGGGCACCCAGGTGACCGTGAGCA
GCGCGGCCGCTGGGTCCGGCGGTTCAGGCGGCTCTGGTGGCTCCGGTGGGTCAGGTGGTTCTGG
CGGGTCTGGCACTAGTGTTTTTACCCTGGAAGATTTCGTGGGCGACTGGGAACAGACCGCGGCG
TACAACCTGGACCAAGTGCTGGAACAAGGTGGCGTGAGCAGCCTGCTGCAGAACCTGGCGGTGA
GCGTTACCCCGATCCAACGTATTGTTCGTAGCGGCGAGAACGCGCTGAAGATCGACATTCACGT
GATCATTCCGTACGAAGGCCTGAGCGCGGATCAGATGGCGCAAATCGAGGAAGTGTTCAAGGTG
GTTTACCCGGTTGACGATCACCACTTTAAAGTGATCCTGCCGTATGGTACCCTGGTGATTGACG
GCGTTACCCCGAACATGCTGAACTACTTCGGTCGTCCGTATGAGGGCATCGCGGTTTTTGATGG
TAAGAAAATTACCGTGACCGGTACCCTGTGGAACGGCAACAAAATTATTGATGAGCGCCTGATT
ACCCCGGACGGCAGCATGCTGTTTCGTGTGACCATTAATAGCGTCGACCTCGAGCACCACCACC
ACCACCAT

SmBit101-GSG$_7$-5A7

Protein

MAASVTGYRLFEKESAAAGSGGSGGSGGSGGSGGSGGSGTSAARVDQTPRSVTKETGESLTINC
VLRDASYALGSTCWYRKKSGEGNEESISKGGRYVETVNSGSKSFSLRINDLTVEDGGTYRCGLG
VAGGYCDYALCSSRYAECGDGTAVTVNVDLEHHHHHH

DNA

ATGGCGGCTAGCGTAACAGGATATAGGCTATTTGAAAAAGAGAGCGCGGCCGCTGGGTCCGGCG
GTTCAGGCGGCTCTGGTGGCTCCGGTGGGTCAGGTGGTTCTGGCGGGTCTGGCACTAGTGCAGC
GCGCGTGGATCAGACCCCGCGCAGCGTGACCAAAGAAACCGGCGAAAGCCTGACCATTAACTGC
GTGCTGCGCGATGCGAGCTATGCGCTGGGCAGCACCTGCTGGTATCGCAAAAAAAGCGGCGAAG
GCAACGAAGAAAGCATTAGCAAAGGCGGGCGCTATGTGGAAACCGTGAACAGCGGCAGCAAAAG
CTTTAGCCTGCGCATTAACGATCTGACCGTGGAAGATGGCGGCACCTATCGCTGCGGCCTGGGC
GTGGCGGGCGGCTATTGCGATTATGCGCTGTGCAGCAGCCGCTATGCGGAATGCGGCGATGGCA
CCGCGGTGACCGTGAACGTCGACCTCGAGCACCACCACCACCACCAC

SmBit101-GSG$_7$-D2L24

Protein

MAASVTGYRLFEKESAAAGSGGSGGSGGSGGSGGSGGSGTSADVQLVESGGGSVQAGGSLRLSC
AASGYIASINYLGWFRQAPGKEREGVAAVSPAGGTPYYADSVKGRFTVSLDNAENTVYLQMNSL
KPEDTALYYCAAARQGWYIPLNSYGYNYWAQGTQVTVSSVDLEHHHHHH

DNA

ATGGCGGCTAGCGTAACAGGATATAGGCTATTTGAAAAAGAGAGCGCGGCCGCTGGGTCCGGCG
GTTCAGGCGGCTCTGGTGGCTCCGGTGGGTCAGGTGGTTCTGGCGGGTCTGGCACTAGTGCAAT
GTGCAGCTGGTGGAAAGCGGCGGCGGCAGCGTGCAGGCGGGCGGCAGCCTGCGCCTGAGCTGCG
CGGCGAGCGGCTATATTGCGAGCATTAACTATCTGGGCTGGTTTCGCCAGGCGCCGGGCAAAGA
ACGCGAAGGCGTGGCGGCGGTGAGCCCGGCGGGCGGCACCCCGTATTATGCGGATAGCGTGAAA
GGCCGCTTTACCGTGAGCCTGGATAACGCGGAAAACACCGTGTATCTGCAGATGAACAGCCTGA
AACCGGAAGATACCGCGCTGTATTATTGCGCGGCGGCGCGCCAGGGCTGGTATATTCCGCTGAA
CAGCTATGGCTATAACTATTGGGCGCAGGGCACCCAGGTGACCGTGAGCAGCGTCGACCTCGAG
CACCACCACCACCACCAC

5A7-GSG$_7$-SmBit101

Protein

MAASARVDQTPRSVTKETGESLTINCVLRDASYALGSTCWYRKKSGEGNEESISKGGRYVETVN
SGSKSFSLRINDLTVEDGGTYRCGLGVAGGYCDYALCSSRYAECGDGTAVTVNAAAGSGGSGGS
GGSGGSGGSGGSGTSVTGYRLFEKESVDLEHHHHHH

DNA

ATGGCGGCTAGCGCGCGCGTGGATCAGACCCCGCGCAGCGTGACCAAAGAAACCGGCGAAAGCC
TGACCATTAACTGCGTGCTGCGCGATGCGAGCTATGCGCTGGGCAGCACCTGCTGGTATCGCAA
AAAAAGCGGCGAAGGCAACGAAGAAAGCATTAGCAAAGGCGGGCGCTATGTGGAAACCGTGAAC
AGCGGCAGCAAAAGCTTTAGCCTGCGCATTAACGATCTGACCGTGGAAGATGGCGGCACCTATC
GCTGCGGCCTGGGCGTGGCGGGCGGCTATTGCGATTATGCGCTGTGCAGCAGCCGCTATGCGGA
ATGCGGCGATGGCACCGCGGTGACCGTGAACGCGGCCGCTGGGTCCGGCGGTTCAGGCGGCTCT
GGTGGCTCCGGTGGGTCAGGTGGTTCTGGCGGGTCTGGCACTAGTGTAACAGGATATAGGCTAT
TTGAAAAAGAGAGCGTCGACCTCGAGCACCACCACCACCACCAC

D2L24-GSG$_7$-SmBit101

Protein

MAASDVQLVESGGGSVQAGGSLRLSCAASGYIASINYLGWFRQAPGKEREGVAAVSPAGGTPYY
ADSVKGRFTVSLDNAENTVYLQMNSLKPEDTALYYCAAARQGWYIPLNSYGYNYWAQGTQVTVS
SAAAGSGGSGGSGGSGGSGGSGGSGTSVTGYRLFEKESVDLEHHHHHH

DNA

ATGGCGGCTAGCATGTGCAGCTGGTGGAAAGCGGCGGCGGCAGCGTGCAGGCGGGCGGCAGCCT
GCGCCTGAGCTGCGCGGCGAGCGGCTATATTGCGAGCATTAACTATCTGGGCTGGTTTCGCCAG
GCGCCGGGCAAAGAACGCGAAGGCGTGGCGGCGGTGAGCCCGGCGGGCGGCACCCCGTATTATG
CGGATAGCGTGAAAGGCCGCTTTACCGTGAGCCTGGATAACGCGGAAAACACCGTGTATCTGCA
GATGAACAGCCTGAAACCGGAAGATACCGCGCTGTATTATTGCGCGGCGGCGCGCCAGGGCTGG
TATATTCCGCTGAACAGCTATGGCTATAACTATTGGGCGCAGGGCACCCAGGTGACCGTGAGCA
GCGCGGCCGCTGGGTCCGGCGGTTCAGGCGGCTCTGGTGGCTCCGGTGGGTCAGGTGGTTCTGG
CGGGTCTGGCACTAGTGTAACAGGATATAGGCTATTTGAAAAAGAGAGCGTCGACCTCGAGCAC
CACCACCACCACCAC

SmBit114-GSG$_7$-5A7

Protein

MAASVTGYRLFEEILAAAGSGGSGGSGGSGGSGGSGGSGTSAARVDQTPRSVTKETGESLTINC
VLRDASYALGSTCWYRKKSGEGNEESISKGGRYVETVNSGSKSFSLRINDLTVEDGGTYRCGLG
VAGGYCDYALCSSRYAECGDGTAVTVNVDLEHHHHHH

DNA

ATGGCGGCTAGCGTAACAGGATATAGGCTATTTGAGGAAATACTGGCGGCCGCTGGGTCCGGCG
GTTCAGGCGGCTCTGGTGGCTCCGGTGGGTCAGGTGGTTCTGGCGGGTCTGGCACTAGTGCAGC
GCGCGTGGATCAGACCCCGCGCAGCGTGACCAAAGAAACCGGCGAAAGCCTGACCATTAACTGC
GTGCTGCGCGATGCGAGCTATGCGCTGGGCAGCACCTGCTGGTATCGCAAAAAAAGCGGCGAAG
GCAACGAAGAAAGCATTAGCAAAGGCGGGCGCTATGTGGAAACCGTGAACAGCGGCAGCAAAAG
CTTTAGCCTGCGCATTAACGATCTGACCGTGGAAGATGGCGGCACCTATCGCTGCGGCCTGGGC
GTGGCGGGCGGCTATTGCGATTATGCGCTGTGCAGCAGCCGCTATGCGGAATGCGGCGATGGCA
CCGCGGTGACCGTGAACGTCGACCTCGAGCACCACCACCACCACCAC

SmBit114-GSG$_7$-D2L24

Protein

MAASVTGYRLFEEILAAAGSGGSGGSGGSGGSGGSGGSGTSADVQLVESGGGSVQAGGSLRLSC
AASGYIASINYLGWFRQAPGKEREGVAAVSPAGGTPYYADSVKGRFTVSLDNAENTVYLQMNSL
KPEDTALYYCAAARQGWYIPLNSYGYNYWAQGTQVTVSSVDLEHHHHHH

DNA

ATGGCGGCTAGCGTAACAGGATATAGGCTATTTGAGGAAATACTGGCGGCCGCTGGGTCCGGCG
GTTCAGGCGGCTCTGGTGGCTCCGGTGGGTCAGGTGGTTCTGGCGGGTCTGGCACTAGTGCAAT
GTGCAGCTGGTGGAAAGCGGCGGCGGCAGCGTGCAGGCGGGCGGCAGCCTGCGCCTGAGCTGCG
CGGCGAGCGGCTATATTGCGAGCATTAACTATCTGGGCTGGTTTCGCCAGGCGCCGGGCAAAGA
ACGCGAAGGCGTGGCGGCGGTGAGCCCGGCGGGCGGCACCCCGTATTATGCGGATAGCGTGAAA
GGCCGCTTTACCGTGAGCCTGGATAACGCGGAAAACACCGTGTATCTGCAGATGAACAGCCTGA

AACCGGAAGATACCGCGCTGTATTATTGCGCGGCGGCGCGCCAGGGCTGGTATATTCCGCTGAA
CAGCTATGGCTATAACTATTGGGCGCAGGGCACCCAGGTGACCGTGAGCAGCGTCGACCTCGAG
CACCACCACCACCACCAC

5A7-GSG$_7$-SmBit114

Protein

MAASARVDQTPRSVTKETGESLTINCVLRDASYALGSTCWYRKKSGEGNEESISKGGRYVETVN
SGSKSFSLRINDLTVEDGGTYRCGLGVAGGYCDYALCSSRYAECGDGTAVTVNAAAGSGGSGGS
GGSGGSGGSGGSGTSVTGYRLFEEILVDLEHHHHHH

DNA

ATGGCGGCTAGCGCGCGCGTGGATCAGACCCCGCGCAGCGTGACCAAAGAAACCGGCGAAAGCC
TGACCATTAACTGCGTGCTGCGCGATGCGAGCTATGCGCTGGGCAGCACCTGCTGGTATCGCAA
AAAAAGCGGCGAAGGCAACGAAGAAAGCATTAGCAAAGGCGGGCGCTATGTGGAAACCGTGAAC
AGCGGCAGCAAAAGCTTTAGCCTGCGCATTAACGATCTGACCGTGGAAGATGGCGGCACCTATC
GCTGCGGCCTGGGCGTGGCGGGCGGCTATTGCGATTATGCGCTGTGCAGCAGCCGCTATGCGGA
ATGCGGCGATGGCACCGCGGTGACCGTGAACGCGGCCGCTGGGTCCGGCGGTTCAGGCGGCTCT
GGTGGCTCCGGTGGGTCAGGTGGTTCTGGCGGGTCTGGCACTAGTGTAACAGGATATAGGCTAT
TTGAGGAAATACTGGTCGACCTCGAGCACCACCACCACCACCAC

D2L24-GSG$_7$-SmBit114

Protein

MAASDVQLVESGGGSVQAGGSLRLSCAASGYIASINYLGWFRQAPGKEREGVAAVSPAGGTPYY
ADSVKGRFTVSLDNAENTVYLQMNSLKPEDTALYYCAAARQGWYIPLNSYGYNYWAQGTQVTVS
SAAAGSGGSGGSGGSGGSGGSGGSGTSVTGYRLFEEILVDLEHHHHHH

DNA

ATGGCGGCTAGCATGTGCAGCTGGTGGAAAGCGGCGGCGGCAGCGTGCAGGCGGGCGGCAGCCT
GCGCCTGAGCTGCGCGGCGAGCGGCTATATTGCGAGCATTAACTATCTGGGCTGGTTTCGCCAG
GCGCCGGGCAAAGAACGCGAAGGCGTGGCGGCGGTGAGCCCGGCGGGCGGCACCCCGTATTATG
CGGATAGCGTGAAAGGCCGCTTTACCGTGAGCCTGGATAACGCGGAAAACACCGTGTATCTGCA
GATGAACAGCCTGAAACCGGAAGATACCGCGCTGTATTATTGCGCGGCGGCGCGCCAGGGCTGG
TATATTCCGCTGAACAGCTATGGCTATAACTATTGGGCGCAGGGCACCCAGGTGACCGTGAGCA
GCGCGGCCGCTGGGTCCGGCGGTTCAGGCGGCTCTGGTGGCTCCGGTGGGTCAGGTGGTTCTGG
CGGGTCTGGCACTAGTGTAACAGGATATAGGCTATTTGAGGAAATACTGGTCGACCTCGAGCAC
CACCACCACCACCAC

LgBit-GSG$_7$-PCT2

Protein

MAASVFTLEDFVGDWEQTAAYNLDQVLDQGGVSSLLQNLAVSVTPIQRIVRSGENALKIDIHVI
IPYEGLSADQMAQIEEVFKVVYPVDDHHFKVILPYGTLVIDGVTPNMLNYFGRPYEGIAVFDGK
KITVTGTLWNGNKIIDERLITPDGSMLFRVTINSAAAGSGGSGGSGGSGGSGGSGGSGTSAQVQ
LVESGGGLVEAGGSLRLSCVVTGSSFSTSTMAWYRQPPGKQREWVASFTSGGAIKYTDSVKGRF
TMSRDNAKKMTYLQMENLKPEDTAVYYCALHNAVSGSSWGRGTQVTVSSVDLEHHHHHH

DNA

ATGGCGGCTAGCGTTTTTACCCTGGAAGATTTCGTGGGCGACTGGGAACAGACCGCGGCGTACA
ACCTGGACCAAGTGCTGGATCAAGGTGGCGTGAGCAGCCTGCTGCAGAACCTGGCGGTGAGCGT
TACCCCGATCCAACGTATTGTTCGTAGCGGCGAGAACGCGCTGAAGATCGACATTCACGTGATC
ATTCCGTACGAAGGCCTGAGCGCGGATCAGATGGCGCAAATCGAGGAAGTGTTCAAGGTGGTTT
ACCCGGTTGACGATCACCACTTTAAAGTGATCCTGCCGTATGGTACCCTGGTGATTGACGGCGT
TACCCCGAACATGCTGAACTACTTCGGTCGTCCGTATGAGGGCATCGCGGTTTTTGATGGTAAG
AAAATTACCGTGACCGGTACCCTGTGGAACGGCAACAAAATTATTGATGAGCGCCTGATTACCC
CGGACGGCAGCATGCTGTTTCGTGTGACCATTAATAGCGCGGCCGCTGGGTCCGGCGGTTCAGG
CGGCTCTGGTGGCTCCGGTGGGTCAGGTGGTTCTGGCGGGTCTGGCACTAGTGCACAGGTGCAA
CTGGTTGAGAGCGGTGGCGGTCTGGTGGAAGCGGGCGGTAGCCTGCGTCTGAGCTGCGTGGTTA
CCGGCAGCAGCTTTAGCACCAGCACGATGGCGTGGTACCGTCAGCCGCCGGGCAAGCAACGTGA
ATGGGTGGCGAGCTTCACCAGCGGCGGTGCGATCAAGTACACCGACAGCGTTAAAGGTCGTTTT
ACCATGAGCCGTGATAACGCGAAGAAAATGACCTATCTGCAGATGGAGAACCTGAAACCGGAAG
ACACCGCGGTGTACTATTGCGCGCTGCATAACGCGGTTAGCGGTAGCAGCTGGGGTCGTGGTAC
CCAAGTGACCGTTAGCAGCGTCGACCTCGAGCACCACCACCACCACCAC

LgBit-GSG$_7$-PCT3

Protein

MAASVFTLEDFVGDWEQTAAYNLDQVLDQGGVSSLLQNLAVSVTPIQRIVRSGENALKIDIHVI
IPYEGLSADQMAQIEEVFKVVYPVDDHHFKVILPYGTLVIDGVTPNMLNYFGRPYEGIAVFDGK
KITVTGTLWNGNKIIDERLITPDGSMLFRVTINSAAAGSGGSGGSGGSGGSGGSGGSGTSAQVQ
LVESGGGLVQTGGSLRLSCASSGSIAGFETVTWSRQAPGKSLQWVASMTKTNNEIYSDSVKGRF
IISRDNAKNTVYLQMNSLKPEDTGVYFCKGPELRGQGIQVTVSSVDLEHHHHHH

DNA

ATGGCGGCTAGCGTTTTTACCCTGGAAGATTTCGTGGGCGACTGGGAACAGACCGCGGCGTACA
ACCTGGACCAAGTGCTGGATCAAGGTGGCGTGAGCAGCCTGCTGCAGAACCTGGCGGTGAGCGT
TACCCCGATCCAACGTATTGTTCGTAGCGGCGAGAACGCGCTGAAGATCGACATTCACGTGATC
ATTCCGTACGAAGGCCTGAGCGCGGATCAGATGGCGCAAATCGAGGAAGTGTTCAAGGTGGTTT
ACCCGGTTGACGATCACCACTTTAAAGTGATCCTGCCGTATGGTACCCTGGTGATTGACGGCGT
TACCCCGAACATGCTGAACTACTTCGGTCGTCCGTATGAGGGCATCGCGGTTTTTGATGGTAAG
AAAATTACCGTGACCGGTACCCTGTGGAACGGCAACAAAATTATTGATGAGCGCCTGATTACCC
CGGACGGCAGCATGCTGTTTCGTGTGACCATTAATAGCGCGGCCGCTGGGTCCGGCGGTTCAGG
CGGCTCTGGTGGCTCCGGTGGGTCAGGTGGTTCTGGCGGGTCTGGCACTAGTGCACAGGTGCAA
CTGGTTGAAAGCGGTGGCGGTCTGGTGCAAACCGGCGGTAGCCTGCGTCTGAGCTGCGCGAGCA
GCGGTAGCATTGCGGGTTTCGAAACCGTGACCTGGAGCCGTCAGGCGCCGGGCAAGAGCCTGCA
ATGGGTTGCGAGCATGACCAAAACCAACAACGAAATTTACAGCGACAGCGTTAAGGGTCGTTTC
ATCATTAGCCGTGATAACGCGAAAAACACCGTGTACCTGCAGATGAACAGCCTGAAGCCGGAGG
ACACCGGCGTTTATTTTTGCAAAGGTCCGGAACTGCGTGGCCAGGGTATTCAGGTGACCGTTAG
CAGCGTCGACCTCGAGCACCACCACCACCACCAC

PCT2-GSG$_7$-LgBit

Protein

MAASQVQLVESGGGLVEAGGSLRLSCVVTGSSFSTSTMAWYRQPPGKQREWVASFTSGGAIKYT
DSVKGRFTMSRDNAKKMTYLQMENLKPEDTAVYYCALHNAVSGSSWGRGTQVTVSSAAAGSGGS
GGSGGSGGSGGSGGSGTSVFTLEDFVGDWEQTAAYNLDQVLEQGGVSSLLQNLAVSVTPIQRIV
RSGENALKIDIHVIIPYEGLSADQMAQIEEVFKVVYPVDDHHFKVILPYGTLVIDGVTPNMLNY
FGRPYEGIAVFDGKKITVTGTLWNGNKIIDERLITPDGSMLFRVTINSVDLEHHHHHH

DNA

ATGGCGGCTAGCCAGGTGCAACTGGTTGAGAGCGGTGGCGGTCTGGTGGAAGCGGGCGGTAGCC
TGCGTCTGAGCTGCGTGGTTACCGGCAGCAGCTTTAGCACCAGCACGATGGCGTGGTACCGTCA
GCCGCCGGGCAAGCAACGTGAATGGGTGGCGAGCTTCACCAGCGGCGGTGCGATCAAGTACACC
GACAGCGTTAAAGGTCGTTTTACCATGAGCCGTGATAACGCGAAGAAAATGACCTATCTGCAGA
TGGAGAACCTGAAACCGGAAGACACCGCGGTGTACTATTGCGCGCTGCATAACGCGGTTAGCGG
TAGCAGCTGGGGTCGTGGTACCCAAGTGACCGTTAGCAGCGCGGCCGCTGGGTCCGGCGGTTCA
GGCGGCTCTGGTGGCTCCGGTGGGTCAGGTGGTTCTGGCGGGTCTGGCACTAGTGTTTTTACCC
TGGAAGATTTCGTGGGCGACTGGGAACAGACCGCGGCGTACAACCTGGACCAAGTGCTGGAACA
AGGTGGCGTGAGCAGCCTGCTGCAGAACCTGGCGGTGAGCGTTACCCCGATCCAACGTATTGTT
CGTAGCGGCGAGAACGCGCTGAAGATCGACATTCACGTGATCATTCCGTACGAAGGCCTGAGCG
CGGATCAGATGGCGCAAATCGAGGAAGTGTTCAAGGTGGTTTACCCGGTTGACGATCACCACTT
TAAAGTGATCCTGCCGTATGGTACCCTGGTGATTGACGGCGTTACCCCGAACATGCTGAACTAC
TTCGGTCGTCCGTATGAGGGCATCGCGGTTTTTGATGGTAAGAAAATTACCGTGACCGGTACCC
TGTGGAACGGCAACAAAATTATTGATGAGCGCCTGATTACCCCGGACGGCAGCATGCTGTTTCG
TGTGACCATTAATAGCGTCGACCTCGAGCACCACCACCACCACCAT

PCT3-GSG$_7$-LgBit

Protein

MAASQVQLVESGGGLVQTGGSLRLSCASSGSIAGFETVTWSRQAPGKSLQWVASMTKTNNEIYS
DSVKGRFIISRDNAKNTVYLQMNSLKPEDTGVYFCKGPELRGQGIQVTVSSAAAGSGGSGGSGG
SGGSGGSGGSGTSVFTLEDFVGDWEQTAAYNLDQVLEQGGVSSLLQNLAVSVTPIQRIVRSGEN
ALKIDIHVIIPYEGLSADQMAQIEEVFKVVYPVDDHHFKVILPYGTLVIDGVTPNMLNYFGRPY
EGIAVFDGKKITVTGTLWNGNKIIDERLITPDGSMLFRVTINSVDLEHHHHHH

DNA

ATGGCGGCTAGCCAGGTGCAACTGGTTGAAAGCGGTGGCGGTCTGGTGCAAACCGGCGGTAGCC
TGCGTCTGAGCTGCGCGAGCAGCGGTAGCATTGCGGGTTTCGAAACCGTGACCTGGAGCCGTCA
GGCGCCGGGCAAGAGCCTGCAATGGGTTGCGAGCATGACCAAAACCAACAACGAAATTTACAGC
GACAGCGTTAAGGGTCGTTTCATCATTAGCCGTGATAACGCGAAAAACACCGTGTACCTGCAGA
TGAACAGCCTGAAGCCGGAGGACACCGGCGTTTATTTTTGCAAAGGTCCGGAACTGCGTGGCCA
GGGTATTCAGGTGACCGTTAGCAGCGCGGCCGCTGGGTCCGGCGGTTCAGGCGGCTCTGGTGGC
TCCGGTGGGTCAGGTGGTTCTGGCGGGTCTGGCACTAGTGTTTTTACCCTGGAAGATTTCGTGG
GCGACTGGGAACAGACCGCGGCGTACAACCTGGACCAAGTGCTGGAACAAGGTGGCGTGAGCAG
CCTGCTGCAGAACCTGGCGGTGAGCGTTACCCCGATCCAACGTATTGTTCGTAGCGGCGAGAAC
GCGCTGAAGATCGACATTCACGTGATCATTCCGTACGAAGGCCTGAGCGCGGATCAGATGGCGC
AAATCGAGGAAGTGTTCAAGGTGGTTTACCCGGTTGACGATCACCACTTTAAAGTGATCCTGCC
GTATGGTACCCTGGTGATTGACGGCGTTACCCCGAACATGCTGAACTACTTCGGTCGTCCGTAT
GAGGGCATCGCGGTTTTTGATGGTAAGAAAATTACCGTGACCGGTACCCTGTGGAACGGCAACA
AAATTATTGATGAGCGCCTGATTACCCCGGACGGCAGCATGCTGTTTCGTGTGACCATTAATAG
CGTCGACCTCGAGCACCACCACCACCACCAT

SmBit101-GSG$_7$-PCT2

Protein

MAASVTGYRLFEKESAAAGSGGSGGSGGSGGSGGSGGSGTSAQVQLVESGGGLVEAGGSLRLSC
VVTGSSFSTSTMAWYRQPPGKQREWVASFTSGGAIKYTDSVKGRFTMSRDNAKKMTYLQMENLK
PEDTAVYYCALHNAVSGSSWGRGTQVTVSSVDLEHHHHHH

DNA

ATGGCGGCTAGCGTAACAGGATATAGGCTATTTGAAAAAGAGAGCGCGGCCGCTGGGTCCGGCG
GTTCAGGCGGCTCTGGTGGCTCCGGTGGGTCAGGTGGTTCTGGCGGGTCTGGCACTAGTGCACA
GGTGCAACTGGTTGAGAGCGGTGGCGGTCTGGTGGAAGCGGGCGGTAGCCTGCGTCTGAGCTGC
GTGGTTACCGGCAGCAGCTTTAGCACCAGCACGATGGCGTGGTACCGTCAGCCGCCGGGCAAGC
AACGTGAATGGGTGGCGAGCTTCACCAGCGGCGGTGCGATCAAGTACACCGACAGCGTTAAAGG
TCGTTTTACCATGAGCCGTGATAACGCGAAGAAAATGACCTATCTGCAGATGGAGAACCTGAAA
CCGGAAGACACCGCGGTGTACTATTGCGCGCTGCATAACGCGGTTAGCGGTAGCAGCTGGGGTC
GTGGTACCCAAGTGACCGTTAGCAGCGTCGACCTCGAGCACCACCACCACCACCAC

SmBit101-GSG$_7$-PCT3

Protein

MAASVTGYRLFEKESAAAGSGGSGGSGGSGGSGGSGGSGTSAQVQLVESGGGLVQTGGSLRLSC
ASSGSIAGFETVTWSRQAPGKSLQWVASMTKTNNEIYSDSVKGRFIISRDNAKNTVYLQMNSLK
PEDTGVYFCKGPELRGQGIQVTVSSVDLEHHHHHH

DNA

ATGGCGGCTAGCGTAACAGGATATAGGCTATTTGAAAAAGAGAGCGCGGCCGCTGGGTCCGGCG
GTTCAGGCGGCTCTGGTGGCTCCGGTGGGTCAGGTGGTTCTGGCGGGTCTGGCACTAGTGCACA
GGTGCAACTGGTTGAAAGCGGTGGCGGTCTGGTGCAAACCGGCGGTAGCCTGCGTCTGAGCTGC
GCGAGCAGCGGTAGCATTGCGGGTTTCGAAACCGTGACCTGGAGCCGTCAGGCGCCGGGCAAGA
GCCTGCAATGGGTTGCGAGCATGACCAAAACCAACAACGAAATTTACAGCGACAGCGTTAAGGG
TCGTTTCATCATTAGCCGTGATAACGCGAAAAACACCGTGTACCTGCAGATGAACAGCCTGAAG
CCGGAGGACACCGGCGTTTATTTTTGCAAAGGTCCGGAACTGCGTGGCCAGGGTATTCAGGTGA
CCGTTAGCAGCGTCGACCTCGAGCACCACCACCACCACCAC

PCT2-GSG$_7$-SmBit101

Protein

MAASQVQLVESGGGLVEAGGSLRLSCVVTGSSFSTSTMAWYRQPPGKQREWVASFTSGGAIKYT
DSVKGRFTMSRDNAKKMTYLQMENLKPEDTAVYYCALHNAVSGSSWGRGTQVTVSSAAAGSGGS
GGSGGSGGSGGSGGSGTSVTGYRLFEKESVDLEHHHHHH

DNA

ATGGCGGCTAGCCAGGTGCAACTGGTTGAGAGCGGTGGCGGTCTGGTGGAAGCGGGCGGTAGCC
TGCGTCTGAGCTGCGTGGTTACCGGCAGCAGCTTTAGCACCAGCACGATGGCGTGGTACCGTCA
GCCGCCGGGCAAGCAACGTGAATGGGTGGCGAGCTTCACCAGCGGCGGTGCGATCAAGTACACC
GACAGCGTTAAAGGTCGTTTTACCATGAGCCGTGATAACGCGAAGAAAATGACCTATCTGCAGA
TGGAGAACCTGAAACCGGAAGACACCGCGGTGTACTATTGCGCGCTGCATAACGCGGTTAGCGG
TAGCAGCTGGGGTCGTGGTACCCAAGTGACCGTTAGCAGCGCGGCCGCTGGGTCCGGCGGTTCA
GGCGGCTCTGGTGGCTCCGGTGGGTCAGGTGGTTCTGGCGGGTCTGGCACTAGTGTAACAGGAT
ATAGGCTATTTGAAAAAGAGAGCGTCGACCTCGAGCACCACCACCACCACCAC

PCT3-GSG$_7$-SmBit101

Protein

MAASQVQLVESGGGLVQTGGSLRLSCASSGSIAGFETVTWSRQAPGKSLQWVASMTKTNNEIYS
DSVKGRFIISRDNAKNTVYLQMNSLKPEDTGVYFCKGPELRGQGIQVTVSSAAAGSGGSGGSGG
SGGSGGSGGSGTSVTGYRLFEKESVDLEHHHHHH

DNA

ATGGCGGCTAGCCAGGTGCAACTGGTTGAAAGCGGTGGCGGTCTGGTGCAAACCGGCGGTAGCC
TGCGTCTGAGCTGCGCGAGCAGCGGTAGCATTGCGGGTTTCGAAACCGTGACCTGGAGCCGTCA
GGCGCCGGGCAAGAGCCTGCAATGGGTTGCGAGCATGACCAAAACCAACAACGAAATTTACAGC
GACAGCGTTAAGGGTCGTTTCATCATTAGCCGTGATAACGCGAAAAACACCGTGTACCTGCAGA
TGAACAGCCTGAAGCCGGAGGACACCGGCGTTTATTTTTGCAAAGGTCCGGAACTGCGTGGCCA
GGGTATTCAGGTGACCGTTAGCAGCGCGGCCGCTGGGTCCGGCGGTTCAGGCGGCTCTGGTGGC
TCCGGTGGGTCAGGTGGTTCTGGCGGGTCTGGCACTAGTGTAACAGGATATAGGCTATTTGAAA
AAGAGAGCGTCGACCTCGAGCACCACCACCACCACCAC